Investigation into the Human Premature Ageing Disease, Hutchinson Gilford Progeria Syndrome, Using hTERT Immortalised Fibroblasts

A thesis submitted for the Degree of Doctor of Philosophy

By

Gemma Louise Worthington

College of Health and Life Sciences

Brunel University

June 2016

Declaration

I hereby certify that this thesis, has been written by me, and that it is the record of work carried out by me, or principally by myself in collaboration with others as acknowledged, and that it has not been submitted in any previous application for a higher degree.

Gemma Worthington

Acknowledgements

First and foremost, I am extremely grateful to my PhD supervisor, Dr Ian Kill for his training, guidance and kindness. I would like to thank Dr Joanna Bridger for her support and encouragement. I also want to thank Dr David Tree for being my third supervisor. Thank you to the Progeria Research Fund for funding this PhD project.

I would like to thank Dr Evgeny Makarov for his supervision on several areas of this project including the TAT protein development and Quantitative PCR. Thank you to Dr Rhona Anderson and Dr Mehmet Bikul for conducting the mFish experiments and Dr Helen Foster for her collaboration on the Quantitative PCR work. I would also like to thank all the members of our weekly lab meeting for their suggestions on this work.

Thank you to Professor Richard Faragher for the hTERT immortalised HGPS cell lines I have used in this study and thank you to Dr. Christopher Parris for the NB1T cell line. Thank you to Dr Mike Hubank for his collaboration on the whole exome sequencing and Dr Eric Schirmer and team, in particular Dr Peter Meinke for his help with the analysis. Thank you to Professor Susan Michaelis for providing the cDNA templates for molecular cloning. Thank you to Professor Leonhardt's for providing the A Type targeted Nanobody for collaboration in this work.

I want to thank my TGI Fridays Family, especially my "Bar Boys" for their vitality and camaraderie, and the cocktails were pretty good too. I also want to say a massive thank you to Katherine Wilson from Sycamore Counselling, for her amazing guidance. There are times I could not have coped without my fantastic friends at Brunel University, in particular Tolani Enin, who is the greatest supporter. A big thanks to all my wonderful friends especially Samantha Anderson.

For the infinite love and support of my family, both Bourne's and Worthington's, I will never be able to thank you enough. Dad thank you for encouraging me not to give up. Mum "I'm everything I am because you loved me".

Most of all I need to acknowledge the amazing contribution of my husband, Tom, who put up with all the midnight trips to the lab. I am so incredible grateful for his strength and love. Thank You

I would like to dedicate this work to Kimberley, who started this journey.

Abstract

Hutchinson Gilford Progeria syndrome (HGPS) is a rare premature ageing disease affecting children. 80% of "classic" HGPS patients share the same mutation in the *LMNA* gene that gives rise to characteristics similar to normal human ageing and they usually die in their teens from heart attacks or strokes. Cells taken from progeria patients have a short replicative lifespan in culture and this has necessitated the generation of immortalised progeria cell lines with unlimited growth potential. Evaluation of one such immortalised cell line has revealed loss of progeria cell characteristics, such as nuclear shape abnormalities, and a reversion to a normal nuclear morphology. We attributed this reversion to an increased rate of breakdown of the mutant protein, progerin, which normally causes the nuclear abnormalities. Identification of this underlying mechanism has potential therapeutic applications for HGPS patients. Based on this finding this study demonstrates the effect of an A type lamin target nanobody conjugated to an E3 Ubiquitin ligase, as the first step to a nanobody therapy for HGPS. The development of TAT- lamin A and TAT- progerin fusion proteins, which are capable of transducing into human cells at a desired concentration, allow for future investigation into progerin dose effects.

"Atypical" progeria patients have unknown mutations which cause a similar disease but with more varied degrees of severity. The characterisation of an hTERT immortalised cell line, from an "atypical" patient, led to the observation of a genetic instability phenotype, which, in combination with whole exomes sequencing, has enabled the identification of candidate genes within DNA repair and cell cycle regulation. Future identification of another HGPS gene will increase understanding of premature ageing diseases and of normal human ageing.

Abbreviations

3D	3-Dimensional
AD-EDMD	Autosomal dominant Emery-Dreifuss muscular dystrophy
ANTP	*Drosophila* Antennapedia homeotic transcription factor
APD	Accumulated population doublings
APS	Atypical progeria syndrome
AR-EDMD	Autosomal recessive Emery-Dreifuss muscular dystrophy
AWS	Atypical Werner's syndrome
BAF	Barrier-to-autointegration factor
BWA	Burrows-Wheeler Aligner
CDM1A	Cardio myopathy dilated 1A
ChIP	Chromatin imnuno precipitation
CIP	Calf-intestinal alkaline phosphatase
CMT2B1	Charcot-Marie-Tooth disorder type 2B1
DAPI	4', 6-diamidino-2-phenylindole
DCMA1	Dilated cardiomyopathy type 1
DMEM	Dulbecco's Modified Eagle Medium
DMSO	Dimethyl sulfoxide
DNA	Deoxyribonucleic acid
dNTP	Deoxynucleoside-triphosphate
DSB	Double strand breaks
DsRed	Discosoma sp red fluorescent protein
DTT	Dithiothreitol
EDTA	Ethylendiaminetetra-acetic acid
EM	Electron microscopy
ER	Endoplastic reticulum
EZH2	Enhancer Of Zeste Homolog 2
FAM™	6-carboxyfluorescein
FBS	Fetal bovine serum

FISH	Fluorescence in situ hybridization
FITC	Fluorescein isothiocyanate
FPLD	Dunnigan type familial partial lipodystrophy
FTIs	Farnesyltransferase inhibitor
FT/FTase	Farnesyltransferase
g	G force
GATK	Genome Analysis Toolkit
GFP	Green fluorescent protein
GLD	Generalised lipodystraphy
GWAS	Genome wide association study
H3K27me3	Histone H3 containing the trimethylated lysine 27
H3K93Me	Histone H3 lysine 93/ methylation
HAS	HiSeq™ analysis software
HC Abs	Heavy chain antibodies
HGPS	Hutchinson-Gilford Progeria Syndrome
HIV-1	Human immunodeficiency virus
HP DNA	Highly Polymerized Deoxyribonucleic acid
HP1a	Heterochromatin protein 1a
IGF-1	Insulin-like growth factor-1
INM	Inner nuclear membrane
IPTG	Isopropyl β-D-1-thiogalactopyranoside
IVS11+1G>A	intronic variant
kb	Kilobase
kDa	Kilodaltons
LAP2	Lamina-associated polypeptide 2
LAP2b	Lamina-associated polypeptide 2b
LAP2α	Lamina-associated polypeptide 2a
LBR	Lamin B Receptor
LCPS	*LMNA*-associated cardiocutaneous progeria syndrome
LEM	LAP2-emerin-MAN1

LGMD1B	limb girdle muscular dystrophy type 1B
LINC	linker of nucleoskeleton and cytoskeleton
LTR	Long terminal repeat
MAD	Mandibuloacral dysplasia
MB	Methylene blue
Mbp	Mega base pairs
MCS	Multiple cloning site
MEF	Mouse epithelial fibroblasts
mFish	Multiplex fluorescence in situ hybridization
MG132	Carbobenzoxy-Leu-Leu-leucinal
miRNA	Micro ribonucleic acid
miR-9	Micro ribonucleic acid 9
mRNA	Messenger ribonucleic acid
MMCT	Microcell-mediated chromosome transfer
mTOR	Mammalian target of rapamycin
NAC	N-acetyl cysteine
NESPRIN	Nuclear envelope spectrin repeat proteins
NGPS	Nestor-Guillermo Progeria Syndrome
Ni-NTA	Nickel Nitrilotriacetic acid
NLS	Nuclear Localisation Sequence
ORF	Open Reading Frame
PBS	Phosphate-buffered saline
PCR	Polymerase chain reaction
PD	Population doublings
pRB	Retinoblastoma
PTD	Protein-Transduction Domain
QPCR	Quantitative polymerase chain reaction
RD	Restrictive dermopathy
RNA	Ribonucleic acid
RNAi	Ribonucleic acid interference

ROS	Reactive oxygen species
RPM	Rotations per minute
RT-PCR	Reverse transcription - Polymerase chain reaction
SDS	Sodium dodecyl sulphate
SDS-PAGE	Sodium dodecyl sulphate – polyacrylamide gel electrophoresis
shRNAs	Small hairpin ribonucleic acid
SV40	Simian virus 40
TAE	Tris-acetate-Ethylenediaminetetraacetic-acid
TAMRA™	Tetra Methyl Rhodamine
TAT	Transactivator Of Transcription
TAT-BID	TAT – bh3-interacting domain death agonist
TAT-Frataxin	TAT - Friedreich's Ataxia
TMPO	Human Thymopoietin gene
Tri-Me-H3k9	Trimethylated histone H3 lysine 9
tRNAs	Transfer ribonucleic acid
TTP	Thrombocytopenic Purpura
VHH	Heavy-chain immunoglobulins
VP22	Herpes-simplex-virus-1 DNA-binding protein
WRN	Werner's syndrome

Table of Contents

1 Introduction 19

1.1 Hutchinson-Gilford Progeria Syndrome 19

1.1.1 Search for a gene 20

1.1.2 Laminopathies 21

1.2 Lamin Proteins 22

1.2.1 Post-Translational Modifications 25

1.2.2 Nuclear Entry of Lamin Proteins 26

1.2.3 Nuclear Envelope 27

1.3 Progerin 30

1.3.1 Nuclear Structure 30

1.3.2 Nuclear architecture 30

1.3.3 Genome reorganization 31

1.3.4 Gene Expression 31

1.3.5 Proliferation 32

1.3.6 Lamina Dynamics 33

1.3.7 Cell Motility, Nuclear Rigidity and Mechanical Strength 33

1.3.8 Exclusion of Progerin 34

1.4 Current Treatments 35

1.4.1 Clinical Trials 36

1.4.2 Rapamaycin 37

1.4.3 Other Therapy Prospects 38

1.5 Atypical Progeria 39

1.5.1 Non-Progerin producing LMNA mutations 40

1.5.2 Recessive progeria 41

1.5.3 ZMPSTE24 Mutation 41

1.5.4 BANF1 Mutation 41

1.6 Normal Ageing 42

1.6.1 HGPS Cell Phenotype in Normal Human Ageing 43

1.6.2 Progerin Accumulation in Normal Human Ageing 43

1.6.3 Differences between HGPS and Normal Human Ageing 44
1.7 Aims and Objectives 46
2 Materials and Methods 47
2.1 Cell Culture 47
2.1.1 Cell Lines 47
2.1.2 Growth curves 49
2.2 Cell Imaging 49
2.2.1 Indirect Immunofluorescence 49
2.2.2 Computational shape analysis 51
2.2.3 Live Imaging 51
2.2.4 Metaphase preparations 51
2.2.5 Multiplex-FISH 52
2.3 Expression Analysis 53
2.3.1 RT-PCR 53
2.3.2 Quantitative-PCR 55
2.4 Protein analysis 56
2.4.1 Western Blot 56
2.5 Molecular Cloning 58
2.5.1 TAT-Plasmids 58
2.5.2 LMNA Inserts 58
2.5.3 Plasmid Ligation 60
2.5.4 Plasmid Transformation 60
2.5.5 Plasmid Sequencing 60
2.5.6 Protein Purification 61
2.6 Cell Modification 61
2.6.1 Protein transduction 61
2.6.2 Plasmid transformation 61
2.6.3 MG132 62
2.7 Whole exome sequencing 62

3 Characterisation of hTERT Immortalised, Hutchinson Gilford Progeria Syndrome, fibroblast cell lines. 68

3.1 Introduction 68

3.2 Results 70

3.2.1 Growth Potential 70

3.2.2 A-Type Lamins 74

3.2.3 Nuclear Morphology 76

3.2.4 Nuclear Size and Shape 78

3.2.5 DNA Damage 84

3.2.6 Cell Motility 87

3.3 Discussion 93

4 Investigation in to the effect of hTERT immortalisation on Progerin in HGPS Fibroblasts. 96

4.1 Introduction 96

4.2 Results 98

4.2.1 Progerin expression Level 98

4.2.2 Genomic Instability 112

4.2.3 Progerin Protein Level 114

4.2.4 Proteasome Inhibition 117

4.3 Discussion 122

5 Analysis of increased Progerin Degradation in hTERT Immortalised HGPS Fibroblasts. 125

5.1 Introduction 125

5.2 Results 128

5.2.1 Development of TAT-fusion proteins 128

5.2.2 TAT -Lamin A and TAT-Progerin Protein Transduction 144

5.2.3 A-Type Lamin Nanobody Plasmid Transformation 148

5.3 Discussion 151

6 Characterisation of hTERT Immortalised, "Atypical" Progeria Cell line in the Search for a new Causative Genetic Mutation. 155

6.1 Introduction 155

6.2 Results 160

6.2.1 Growth Potential 160

6.2.2 Nuclear Shape 163

6.2.3 Cell Motility 169

6.2.4 Chromosome Number 173

6.2.5 Possibility of Micro-cell mediated chromosome transfer? 175

6.2.6 Candidate Genes 176

6.2.7 Whole Exome Sequencing 180

6.3 Discussion 185

7 Discussion 188

7.1 hTERT immortalisation 188

7.1.1 Progerin 188

7.1.2 Therapeutic Potential 190

7.1.3 Atypical Progeria 191

7.1.4 Normal ageing 191

7.2 Key Findings 192

7.2.1 Future work 192

7.3 Conclusion 193

8 References 194

Table of Figures

Figure 1.1 LMNA Mutations 21
Figure 1.2 LMNA Alternative Splicing 23
Figure 1.3 Schematic Model of Lamin Polymers 24
Figure 1.4 Post-Translational Modifications 26
Figure 1.5 Nuclear Encelope 29
Figure 1.6 Isoprenylation Mevalonate Pathway 35
Figure 2.7 Diagram demonstrating exome enrichment using the Nextra® Rapid Capture Exome kit (Illumina®). 64
Figure 2.8 Diagram showing Next Generation Sequencing Chemistry with the HiSeqTM 2000 Sequencing System (Illumina). 66
Figure 2.9 Exome Sequencing Analysis Workflow 67
Figure 3.10 Growth Potential of hTERT immortalised normal and Hutchinson-Gilford Progeria Fibroblasts 73
Figure 3.11 Localisation of A-Type Lamins in hTERT immortalised normal and Hutchinson-Gilford Progeria Fibroblasts 75
Figure 3.12 Abnormal Nuclear Morphology in hTERT immortalised normal and HGPS Fibroblast cultures 77
Figure 3.13 Thresholding and measuring the nuclei of hTERT immortalised normal and HGPS Fibroblast cultures using ImageJ software 79
Figure 3.14 Computational Analysis of Nuclear Size in hTERT immortalised normal and HGPS Fibroblast cultures 81
Figure 3.15 Computational Analysis of Nuclear Shape in hTERT immortalised normal and HGPS Fibroblast cultures 83
Figure 3.16 DNA Damage Markers in hTERT immortalised normal and HGPS Fibroblast cultures 86
Figure 3.17 Generation of Time Lapse Videos showing Cell Movement in hTERT immortalised normal and HGPS Fibroblast cultures 89
Figure 3.18 Analysis of Cell Movement in hTERT immortalised normal and HGPS Fibroblast cultures 92
Figure 4.19 RT-PCR analysis of Lamin A and Progerin expression within hTERT Immortalised Normal and Hutchinson-Gilford Progeria Fibroblasts 99

Figure 4.20 Diagrammatic representation of experimental design to determine Lamin A and Progerin expression level in a single reaction, using TaqMan® probes 101
Figure 4.21 QPCR experiment schematic for single and dual probe detection of Lamin A and Progerin expression.....103
Figure 4.22 Comparison of single and dual probe QPCR detection methods for the assessment of Lamin A and Progerin expression in hTERT.....105
Figure 4.23 QPCR quantification of Lamin A and Progerin molecules being expressed in Early and Late Passage hTERT HGPS Fibroblasts.....107
Figure 4.24 Relative percentage of Lamin A and Progerin expression in Early and Late Passage hTERT HGPS Fibroblasts using Single and Dual Probe QPCR quantification.....109
Figure 4.25 Ratio of Lamin A and Progerin expression in Early and Late Passage hTERT HGPS Fibroblasts using Single and Dual Probe QPCR quantification 111
Figure 4.26 Chromosome Number Analysis in hTERT immortalised normal and HGPS Fibroblast cultures.....113
Figure 4.27 Analysis of Progerin Levels within hTERT Immortalised Normal and Hutchinson-Gilford Progeria Fibroblasts.....116
Figure 4.28 Treatment of HGPS cells with the proteasome inhibiting drug MG132 119
Figure 4.29 Relative ratio of Lamin proteins in hTERT immortalised HGPS fibroblasts before and after MG132 proteasome inhibition.....121
Figure 5.30 Plasmid maps for pTATv1 and pTATv2 plasmids.....130
Figure 5.31 pTAT plasmid validation using restriction enzyme digestions reactions 131
Figure 5.32 Constructed plasmid maps for pTATv2 with Lamin A and Progerin cDNA inserts.....132
Figure 5.33 PCR amplification of Lamin A and Progerin cDNA inserts 133
Figure 5.34 Treated and purified Lamin A and Progerin cDNA inserts and pTAT plasmids 134
Figure 5.35 Ligation efficiency of Lamin A and Progerin cDNA inserts and pTATv2 plasmid.....135
Figure 5.36 Electropherogram showing sequence variation found in all 4 plasmids sequenced.....136

Figure 5.37 IPTG protein induction 138
Figure 5.38 Analysis of protein purification for TAT- lamin A and TAT- Progerin 140
Figure 5.39 Protein Purification Fractions 141
Figure 5.40 Comparison of run through and protein purification fractions for TAT-lamin A and TAT- Progerin 142
Figure 5.41 Western blot analysis of whole cell extracts before and after IPTG induction using antibody raised against the Histadine tag 143
Figure 5.42 T7 TAG and Lamin A/C Immunofluorescence following TAT-Lamin A and TAT-Progerin protein transduction 145
Figure 5.43 Western blot analysis of whole cell extracts before and after IPTG induction using antibody raised against Lamin A/C 146
Figure 5.44 Western blot analysis of whole cell extracts before and after IPTG induction using antibody raised against the T7 TAG 147
Figure 5.45 pc3236 plamid map 149
Figure 5.46 Fluorescence image analysis of hTERT HGPS cells following transfection of pc3236 encoding A type lamin specific nanobody conjugated to an E3 ubiquitin ligase 150
Figure 6.48 Growth Potential of hTERT immortalised “Atypical” Hutchinson-Gilford Progeria Fibroblasts 162
Figure 6.48 Western Blot analysis of SUN1 and SUN2 proteins in “Atypical” HGPS Fibroblasts 178
Figure 6.49 Western Blot analysis of BAF in “Atypical” HGPS Fibroblasts 179
Figure 6.50 Ingenuity Variant Analysis of whole exome sequencing data for the “Atypical progeria” cell line TAG08466, compared to three unaffected family members 182
Figure 6.51 Ingenuity Variant Analysis software information on the LMNA variation identified in TAG08466 “Atypical” Progeria cell line 183

List of Tables

Table 1 Control and HGPS Fibroblast Cell Lines.....47
Table 2 Summary of Indirect Immunofluorescence Antibodies.....50
Table 3 Components of Reverse Transcription.....53
Table 4 Summary of RT-PCR Reagents.....54
Table 5 Summary of PCR Conditions for the amplification of exon 10-12 LMNA..54
Table 6 Summary of PCR Conditions for the amplification of exons 7-9 ACT4.....54
Table 7 Summary of Western Blot antibodies.....57
Table 8 Summary of Molecular Cloning PCR.....59
Table 9 Summary of Molecular Cloning PCR Conditions.....59
Table 10 M-FISH karyotypes of TAG08466 cells.....xv
Table 11 Occurrence of structural rearrangements in TAG08466 cells.....xvii
Table 12 Occurrence of structural deletions in TAG08466 cells.....xix
Table 13 Occurrence of numerical aberrations TAG08466 cells.....xxi
Table 14 Occurrence of clonal structural rearrangements in TAG08466 cells..... xxiii
Table 15 Occurrence of clonal structural deletions in TAG08466 cells.....xxiv
Table 16 Occurrence of clonal numerical aberrations in TAG08466 cells.....xxv
Table 17 Refind Search.....xxvii
Table 18 Strict Search.....xxxiv

1 Introduction

1.1 Hutchinson-Gilford Progeria Syndrome

Hutchinson-Gilford progeria syndrome is an extremely rare premature ageing disease first described by Jonathan Hutchinson (Hutchinson, 1886a; Hutchinson, 1886b) and Hastings Gilford (Gilford; Gilford, 1904a; Gilford, 1904b) in the late 19th /early 20th century. Today, worldwide there are 135 children diagnosed as having HGPS, however, there may be many more sufferers without a diagnosis (Progeria Research Foundation). The incidence of HGPS is estimated at 1 in 4-8 million live births, with diagnosis primarily based on characteristics (Hennekam, 2006). Symptoms of HGPS first manifest at approximately 1 year of age leading to an average age of diagnosis of 2.9 years. Characteristics of HGPS include a failure to thrive leading to abnormally low weight and height for age, alopecia, lipodystrophy, osteolysis of the distal phalanges and scleroderma of the skin. HGPS patients appear to have a larger than average neurocranium as a result of osteolysis of the visocranium, which results in a small face with a prominent forehead. Osteolysis of the mandible causes micrognathia and teeth overcrowding, while thinning of the skin causes increased visibility of blood vessels especially over the nasal bridge. This group of characteristics give rise to a typical HGPS facial appearance. Patients with HGPS very rarely achieve sexual maturity or experience puberty associated growth spurts. There is however, normal cognitive function in these patients with studies reporting a normal spectrum of intelligence. The incidence of cancer in these patients is, however, below the expected frequency with only two cases of neoplasm, both osteosarcoma, ever being reported (King *et al,* 1978; Shalev *et al*, 2007). As the disease progresses patients suffer increased mobility issues through increased stiffness of the knees, ankles and hips giving rise to a horse-riding stance. Other joints such as the wrists, shoulders and fingers are also affected. The most common causes of death in HGPS patients are heart attacks and strokes caused by atherosclerosis, at a mean age of 13.5 years (Hennekam, 2006).

1.1.1 Search for a gene

The gene responsible for 80% of cases of HGPS was identified simultaneously by two groups in 2003. Eriksson *et al,* 2003 identified two cases of uniparental isodisomy of chromosome 1q in HGPS patients. This concurred with a previous report which had found a balanced inverted insertion involving chromosome 1 resulting in loss of heterozygosity (Brown, 1992). Microsatellite genotyping identified a 5Mbp region comprising of 80 genes in which the HGPS gene must locate (Eriksson *et al,* 2003). One of the genes within that region was the *LMNA* gene. Direct sequencing of 23 patients identified the G608G mutation in exon 11 of the *LMNA* gene (Eriksson *et al,* 2003). De Sandre-Giovannoli *et al,* 2003 also identified the G608G mutation (c.1824C>T) in the *LMNA* gene by comparing HGPS to the phenotypically similar Mandibulo-acral dysplasia which is caused by a mutation in the *LMNA* gene. Both papers concluded that G608G is a de novo mutation which causes activation of a cryptic splice site (Eriksson *et al,* 2003; De Sandre-Giovannoli *et al,* 2003). Eriksson *et al* showed western blot evidence of the production of a 50 amino acid truncated protein named progerin which has a dominant negative effect on cell function. Patients with the G608G mutation have all of the characteristics described above and are termed as having classic HGPS. A clinical review of three patients identified a uniform phenotype arising from the G608G mutation (Mazereeuw-Hautier *et al,* 2007). Classic HGPS can also arise from a mutation at the same nucleotide as the G608G leading to the conservative substitution of glycine to serine G608S. The G608S mutation was found in 1 out of 20 cases of classic HGPS patients and despite the amino acid substitution it caused activation of the cryptic splice site and progerin production in the same way as the G608G mutation (Eriksson *et al,* 2003). Approximately 20% of all patients do not have the G608G mutation and are thus subject to a wider degree of severity of the condition (Eriksson *et al,* 2003). These patients are described as having “Atypical Progeria” for which several genes have already been implicated (Rodriguez and Eriksson, 2010).

1.1.2 Laminopathies

As the majority of cases of HGPS are caused by a mutation to the *LMNA* gene, HGPS joins a group of 9 other disease caused by mutations to *LMNA* called primary laminopathies. There have been over 450 different mutations reported in the *LMNA* gene which give rise to different rare diseases (Torvaldson *et al*, 2015). A similar group of disorders, called secondary laminopathies, are caused by mutations in genes *LMNB1* and *LMNB2*, coding for B-type lamins, *ZMPSTE24* encoding a prelamin A processing protein and genes encoding lamin-binding proteins (*EMD*, *TMPO*, *LBR* and *LEMD3*). Laminopathies can be divided into five subcategories; muscular dystrophies, neuropathies, lipodystrophies, segmental progeroid syndromes and overlapping disorders (McKenna *et al*, 2013). Figure 1.1 shows a diagram of the *LMNA* gene highlighting common mutations and their associated disease.

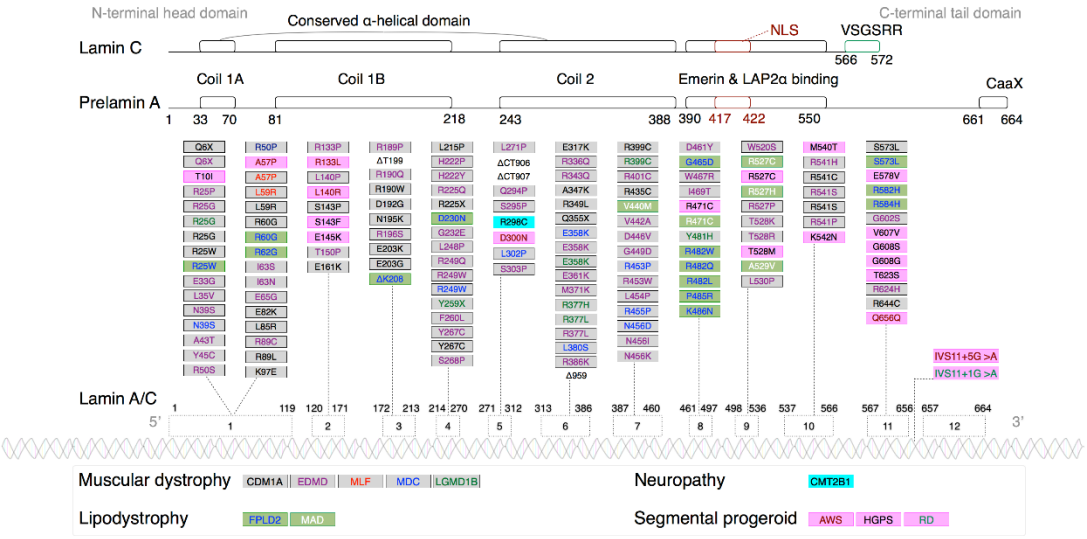

Figure 1.1 LMNA Mutations

Image representing commonly mutated sites within the *LMNA* gene and the disease with which it is associated. CDMA1 - dilated cardiomyopathy type 1, AWS - atypical Werner's syndrome, EDMD Emery-Dreifuss muscular dystrophy, CMT2B1 - Charcot-Marie-Tooth disorder type 2B1, LGMD1B - Limb girdle muscular dystrophy type 1B, FPLD - familial partial lipodystrophy Dunnigan type 2, MAD mandibuloacral dysplasia, HGPS - Hutchinson-Gilford Progeria Syndrome and RD - restrictive dermopathy, MLF - Malouf Syndrome, MDC - Muscular dystrophy, Congenital. Image taken from McKenna *et al*, 2013.

A second premature ageing disease associated with the *LMNA* gene is atypical Werner's syndrome (McKenna et al, 2013). Werner's syndrome is typically caused by mutations in the WRN protein, a RecQ helicase family member involved in DNA repair (Yu *et al*, 1996). Figure 1.1 shows the R133L mutation in exon 2 of the *LMNA* gene. A further three separate mutations within the *LMNA* gene have also been found to cause atypical Werner's syndrome (Chen *et al*, 2003; Doh *et al*, 2009). Like atypical HGPS, atypical Werner's syndrome has similar clinical findings to classic Werner's syndrome including premature aging starting at around 20 years of age, greying hair, scleroderma of the skin, cataracts, atherosclerosis and early onset insulin resistant diabetes. Werner's syndrome is often referred to as adult progeria because of its likeness to HGPS apart from the age of onset. The median age of death is 54 with most resulting from myocardial infarction or cancer (Hisama *et al*, 2011; Hisama *et al*, 2012).

Two other laminopathies with similarities to HGPS are restrictive dermopathy (RD) and mandibuloacral dysplasia (MAD). RD is characterised by an *in utero* growth failure, pulmonary hypoplasia and tight skin. RD is fatal shortly after birth, making it a more sever disease than HGPS (Smigiel *et al*, 2010; Mok *et al*, 1990). MAD has a less severe phenotype than HGPS with characteristics that include short stature, lipodystrophy, alopecia and insulin resistance (Garavelli *et al*, 2009; Zirn *et al*, 2008). An additional *LMNA* mutation c.1620G>A (p.M540I), not shown in figure 1.1, has recently been identified in a foetus from a consanguineous marriage, using *in silico* modelling this homozygous mutation is thought to affect protein structure (Yassaae *et al*, 2016).

1.2 Lamin Proteins

The *LMNA* gene encodes both lamin A and lamin C, which are the main A type lamin proteins found in human cells. Both proteins are produced from the same gene by the process of alternative splicing (See figure 1.2). Lamin C is comprised of only the first 10 exons of the *LMNA* gene, whereas lamin A is made up of 12 exons (Dittmer and Misteli, 2011). The classic HGPS c. 1824C>T mutation results in the activation of a cryptic splice donor site, which results in loss of 50 amino acids from

exon 11 (Eriksson *et al*, 2003; De Sandre-Giovannoli *et al*, 2003). As the HGPS mutation occurs in exon 11, lamin C production is unaffected, whereas a lamin A variant progerin is produced (Figure 1.2). This reduces the cellular level of wildtype lamin A; however, it is the dominant effects of progerin expression that are believed to cause the disease (Reddel and Weiss, 2004). Other A type lamins also encoded by the *LMNA* gene are AΔ10, which is found only in carcinomas and lamin C2 which is specific to male germline cells (Dittmer and Misteli, 2011).

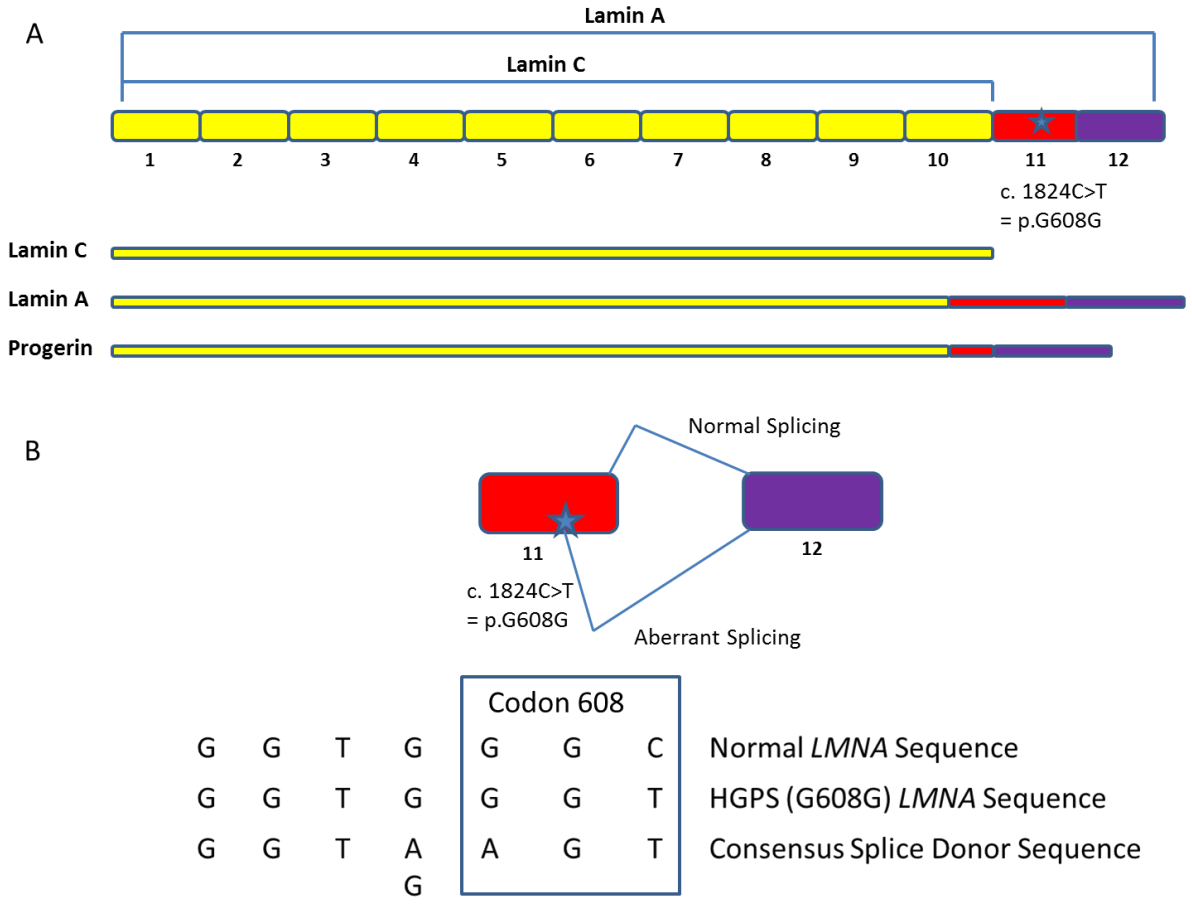

Figure 1.2 LMNA Alternative Splicing

Diagram A shows the two normal proteins produced from the *LMNA* gene, lamin A and lamin C and the mutant protein progerin produced in classic HGPS patients. B demonstrates the activation of the cryptic splice donor site in exon 11 in classic HGPS patients resulting in the loss of last 150 nuclotides of exon 11. B also demonstrates the similarity in sequences between the classic c.1824C>T mutation and the consensus sequence for a splice donor site.

All lamin proteins are type V intermediate filament proteins which form a 10 nm thick filamentous regular meshwork under the inner nuclear membrane, making them a component of the nuclear envelope (Aebi *et al*, 1986). Lamin proteins are comprised of a central helical rod domain that forms parallel dimers giving a coiled coil conformation (Dechat *et al*, 2010). The lamin dimer structure also includes two globular carboxy terminal domains. Dimer formation in these proteins is the first step in polymerisation and the smallest subunit of lamins, as lamins are not believed to exist as monomers (Dechat *et al*, 2010). Figure 1.3 summarises lamin polymerisation to form filaments.

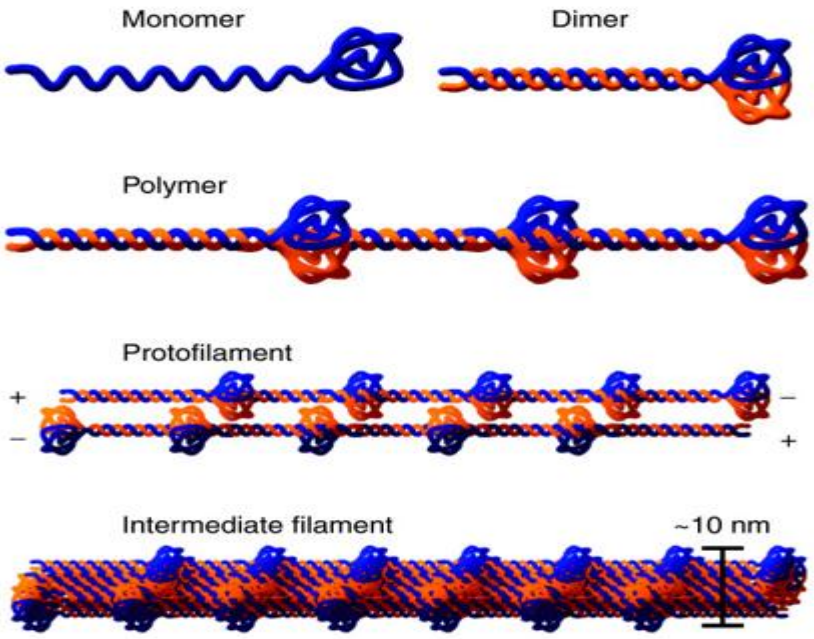

Figure 1.3 Schematic Model of Lamin Polymers

Lamin dimers form from monomers that associate in a parallel, head-to-head manner, forming a coiled coil though the central α-helical domain. Lamin polymers then assemble by association of dimers in a polar head-to-tail manner through a staggered 2 to 4 nm overlap of the highly conserved amino- and carboxy-terminal rod domain ends. Protofilaments are finally produced through anti-parallel association of two lamin polymers. Between three and four protofilaments associate laterally to form an intermediate filament about 10 nm in diameter. Image and legend taken in its entirety from Dittmer and Misteli, 2011.

B-type lamins are a second subgroup of lamin proteins with lamin B1 being encoded by the *LMNB1* gene and lamin B2 and B3 are encoded by *LMNB2*, again through

alternative splicing (Dittmer and Misteli, 2011). Lamin B1 and B2 are expressed at all developmental stages, are believed to be essential for viability and until recently had no known disease associations (Dittmer and Misteli, 2011). Lamin B3 is a B-type lamin variant specific to germline cells (Furukawa *et al*, 1993). Experiments in yeast have shown the ability for A and B type lamins to form heterodimers, however it is not known if these arrangement occur naturally *in vivo* (Ye and Worman, 1995; Georgatos *et al*, 1988). Dimer subunits form fibres in a head to tail arrangement with an essential overlapping region. In Vitro heterodimers have been used to produce mixed polymers, however, it is unclear if this occurs *in Vivo* or if separate A and B type lamin polmers form. The inability to produce 10 nm long fibres *in vitro* has hindered analysis of this matter (Dittmer and Misteli, 2011).

1.2.1 Post-Translational Modifications

Lamin proteins are subject to post-translational modifications and until processed exist as prelamin proteins. Post-translational modifications occur for lamin A, B1 and B2, which all contain a C-terminal CaaX motif. A CaaX motif is made up of a Cysteine residue followed by two aliphatic amino acids and a variable amino acid. CaaX motifs undergo a process of farnesylation, which is the addition of a 15 carbon molecule produced from the isoprenyl pathway, to the cysteine residue (See figure 1.4). The addition of this molecule is believed to anchor proteins to membrane, in this case the inner nuclear membrane. B-type lamins retain their farnesyl group and are permanently anchored to the nuclear membrane. During mitosis these proteins stay associated with the membrane in vesicles. Lamin A, however, is further processed by the endoproteolytic cleavage of the terminal 18 amino acids by ZMPSTE24, removing the farnesylated protein. Lamin A localises to the nuclear membrane but is not anchored and during mitosis is found in a soluble state diffused throughout the cytoplasm. As lamin C does not contain a CaaX motif it is not farnesylated, however, it does associate with the nuclear membrane but shows a similar pattern to lamin A behaviour during mitosis. The mutant lamin A protein, progerin, also contains a CaaX motif and is thus farnesylated. The 50 amino acid region deleted in progerin contains the recognition site for the protease ZMPSTE24 resulting in the inability to remove the farnesyl group from the protein. This results

in the anchoring of progerin to the inner nuclear membrane (Dittmer and Misteli, 2011; Dechat *et al*, 2008; Cau *et al*, 2014).

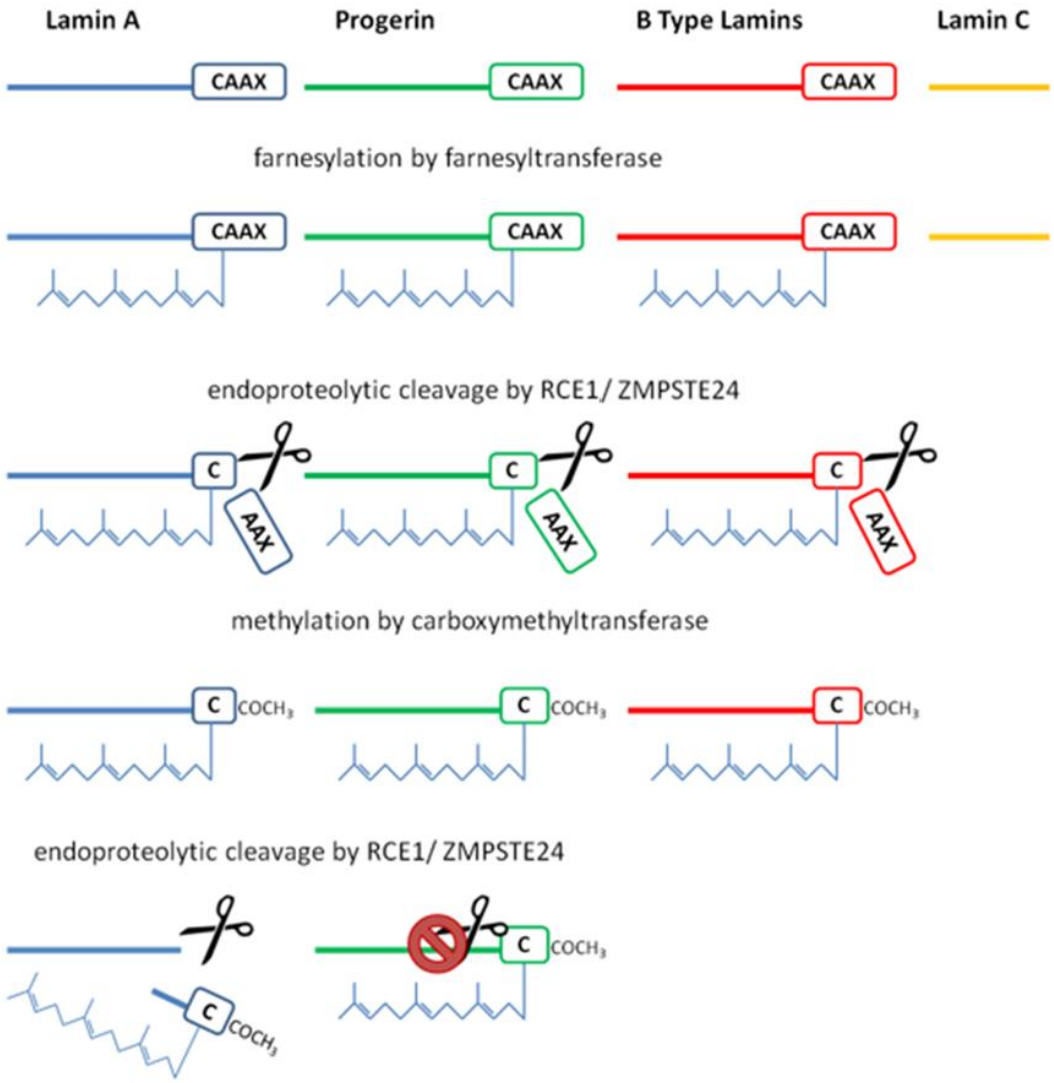

Figure 1.4 Post-Translational Modifications

Diagram depicting the post-translational modifications to lamin A, C, progerin and B type lamins.

1.2.2 Nuclear Entry of Lamin Proteins

The farnesylation of the lamin proteins has been proposed as a method to enable nuclear entry as membrane associated proteins. Conversely the lamin proteins also contain an NLS sequence which would allow for nuclear uptake through the nuclear

pores (Dittmer and Misteli, 2011). For lamins to enter the nucleus as membrane associated proteins farnesylation would have to occur within the cytoplasm. In support of this farnesylation of other proteins has been shown to occur at the endoplasmic reticulum (Winter-Vann and Casey, 2005). This theory suggests that after farnesylation lamins move around the endoplasmic reticulum and enter the inner nuclear membrane around pore complexes. The final cleavage to free lamin A from the membrane would then take place in the nucleus. The second theory suggests that lamins are imported into the nucleus using the NLS where they then become farnesylated and lamin A is then cleaved freeing it from the membrane. The identification of ZMPSTE24s dual location within the nucleus and the ER offers support to the theory of post translational modifications occurring at the ER as this theory requires the initial cleavage prior to farneslyation to occur at the ER and then the second cleavage event to take place in the nucleus (Barrowman *et al*, 2008). Conversely it could be argued that ZMPSTE24s localisation to the ER is to cleave other proteins and that its localisation to the nucleus shows that the whole process can be conducted at the INM. Evidence from studies microinjecting prelamin A into cells shows that nuclear uptake occurs quicker than the appearance of mature lamin A, but as lamin A is not mature until cleaved, these experiments fail to distinguish between the theories (Goldman *et al*, 1992). The most recent evidence comes from Knock out experiments of the NLS in prelamin A and progerin, which result in protein accumulation at the ER. With time lamin A lacking an NLS appears in a soluble state in the cytoplasm. This demonstrates farnesylation and ZMPSTE24 cleavage occurring at the endoplasmic reticulum although does support previous findings that an NLS is required for nuclear uptake of lamin A and progerin (Wu *et al*, 2014). This does lead to the larger question; is farnesylation essential for the formation of a nuclear lamina, despite not being a method for nuclear uptake?

1.2.3 Nuclear Envelope

The nuclear envelope functions to separate the nucleoplasm from the cytoplasm by surrounding nuclear components in a double membrane layer (Cau *et al*, 2014). The nuclear envelope accommodates nuclear pore complexes which allow nuclear uptake of proteins which contain a nuclear localisation sequence (Grossman *et al*, 2012).

The outer nuclear membrane is continuous with the ER again facilitating protein uptake (Cau *et al*, 2014).

The inner nuclear membrane forms attachments with the nuclear lamina. The nuclear lamina, comprised of both A and B type lamin proteins, forms a fibrillar meshwork under the inner nuclear membrane. One function of the nuclear lamina is to offer structural integrity to the nucleus and protect it from strain (Gruenbaum *et al*, 2005). The inner nuclear membrane is comprised of approximately 80 transmembrane proteins, the best characterised of these are the lamin binding proteins, because of their involvement in different diseases (Cau *et al*, 2014). These include the LEM domain proteins; LAP2, Emerin and MAN1, as well as SUN1 and SUN2 (LINC Complex proteins) and Lamin B Receptor (LBR) (Vlcek & Foisner, 2007). LAP2β binding is specific to B type lamins, whereas the splice alternative LAP2α, interacts with A type lamins.

B-type lamins remain anchored to the nuclear membrane, whereas lamin A is also believed to form filaments in the nucleoplasm (Bridger *et al*, 1993). Interactions between LAP2α and lamin A are believed to take place in the nucleoplasm as LAP2α is not membrane associated (Dechat *et al*, 2000). LAP2α binding has been proposed as a mechanism to tether lamin A at intranuclear sites, as well as facilitate interactions with chromatin and transcription factors (Markiewicz *et al*, 2002). BAF, a transcription regulator, has been shown to bind directly to homodomain transcription activators as well as DNA and lamin proteins (Zheng *et al*, 2000; Mansharamani *et al*, 2005). Lamin A is also known to bind pRB, a tumour suppressing transcription factor that regulates apoptosis (Makiewicz *et al*, 2002). Emerin binds lamin A, BAF and chromatin and is thought to have a role in bringing lamin A to the nuclear membrane (Skakaki *et al*, 2001; Goldman *et al*, 2002). Lamin proteins can also bind DNA and histone proteins directly, suggesting a role in nuclear organisation (Zastrow *et al*, 2004; Bridger et al, 2007). A recent study identified 695 genes associated with lamin A of which a majority were transcriptionally silent. Loss of lamin A lead to the relocalisation of these genes to the nuclear periphery however, this did not cause their activation (Kuben *et al*, 2012). Links between the lamina and the cytoskeleton are achieved through Nesprin and SUN proteins (Starr *et al*, 2010), implying a role for the lamina in effecting

changes based on external stimuli (Gruenbaum *et al*, 2005). Figure 1.5 shows the organisation of the nuclear envelope.

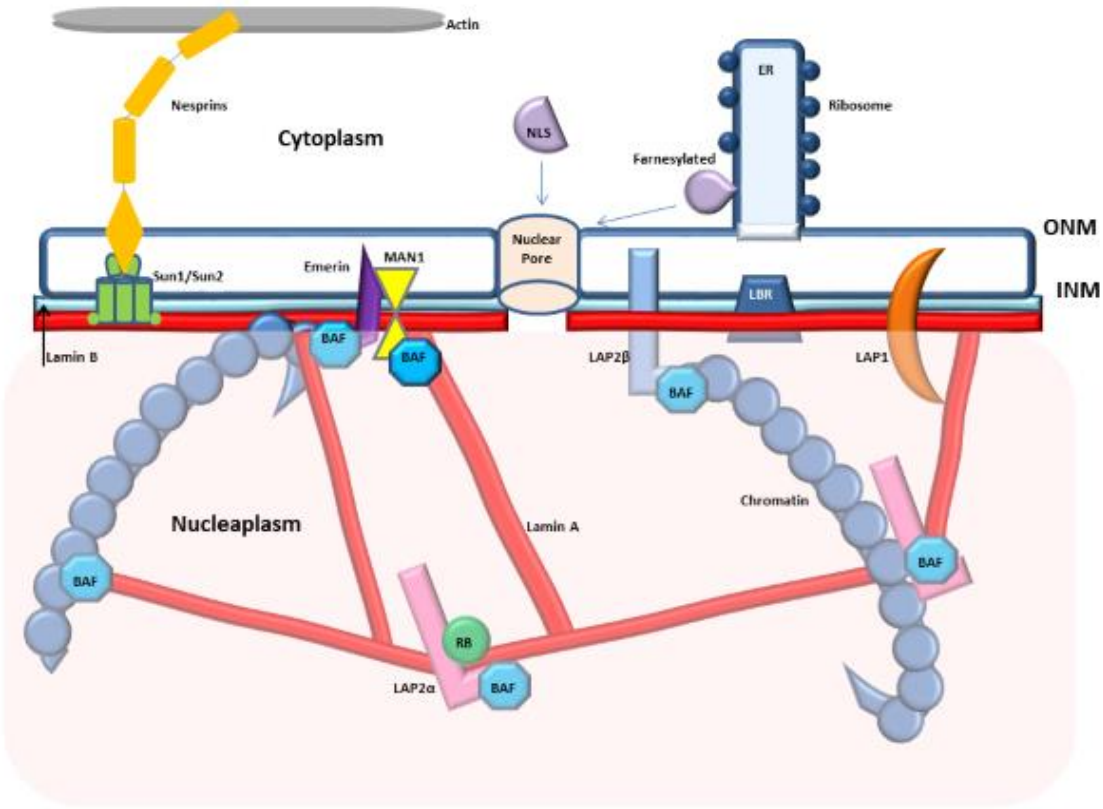

Figure 1.5 Nuclear Encelope

Diagram representing the components of the nuclear envelope, including the nuclear lamina and lamin associated proteins. Also shows two different routes of entry for a protein into the nucleus (NLS or Farnesylated). Image modified from Goldman *et al*, 2002.

The attachments made by lamin A suggests that it is involved in maintaining higher-order chromatin organisation including the anchoring of heterochromain to the nuclear periphery, regulation of gene expression and providing structural integrity to the nucleus. The mutant protein progerin causes much disruption to all three of these functions.

1.3 Progerin

1.3.1 Nuclear Structure

The expression of progerin in HGPS patient cells has been shown to have dramatic effects on nuclear architecture, levels of DNA damage and cell longevity. Eriksson *et al,* 2003 were the first to identify nuclear shape abnormalities in fibroblasts from HGPS patients. These types of abnormalities are also characteristic of other laminopathies such as RD, MAD and atypical Werner's syndrome (Rodriguez and Eriksson, 2010). One study using HGPS fibroblasts found that the number of nuclear lobulations increased as cells aged and the level of progerin increased (Goldman *et al,* 2004). Another study further categorised the nuclear shape abnormalities into blebs, herniations and micronuclei formations and also noted an increase in the number of these nuclei in aged HGPS fibroblasts compared to younger HGPS cultures. This study also identified a change in the distribution of the nuclear lamina from a rim staining pattern observed in young HGPS cells to a lesser rim stain with the appearance of nucleoplasmic speckles in aged HGPS cells (Bridger and Kill, 2004). Electron microscopy has revealed the appearance of a thickened nuclear lamina in HGPS (Goldman et al, 2004), which is believed to result from progerin's permanent anchoring to the nuclear lamina due to its farnesyl group (Dechat *et al*, 2007).

1.3.2 Nuclear architecture

Observed changes to nuclear architecture in HGPS cells include the clustering of nuclear pore complexes (Goldman *et al,* 2004). In most late passage HGPS fibroblasts the nuclear pore complexes were found clustered together usually in association with clefts created by nuclear herniations, leading to stretches of the nuclear envelope depleted of pore complexes. A further change to nuclear architecture is the loss and redistribution of nucleolus associated proteins in the presence of progerin (Mehta *et al,* 2010). Other proteins found to be depleted in HGPS fibroblasts are lamin B and the LAP2 family of proteins. These proteins were depleted from their normal cellular location by up to six fold when compared to

normal control fibroblasts (Scaffidi and Misteli, 2005). LAP2α – telomere association has also been found to be reduced in HGPS cells (Chojnowski *et al*, 2015).

1.3.3 Genome reorganization

A further change to a nuclear envelope associated structure is the loss of peripheral heterochromatin in late passage HGPS fibroblasts (Goldman *et al,* 2004). The protein which acts as an adaptor between lamin A and heterochromatin, HP1α, was found at a twofold lower concentration in HGPS fibroblast when compared to normal controls (Scaffidi and Misteli, 2005). This down regulation was associated with loss of the heterochomatin marker Tri-Me-H3K9. Changes to heterochromatin structure have been shown to predate the appearance of abnormally shaped nuclei during disease progression (Shumaker *et al*, 2006). Other changes to heterochromatin include the loss of H3K27me3, the marker of heterochromatin found on inactivated X chromosomes in female cells and the down regulation of *EZH2* the methyltransferase responsible for this methylation (Shumaker *et al*, 2006). The level of genome reorganisation in the presence of progerin is not limited to heterochromatin as one study showed alterations in the radial position of chromosome territories in cells from HGPS patients (Meaburn *et al,* 2007). The redistribution of chromosomes 13 and 18 to a nuclear interior position resembles the chromosome organisation of non-proliferating control cells (Mehta *et al,* 2007; Mehta *et al,* 2010; Mehta *et al,* 2011).

Global changes in CpG methylation has also been seen in HGPS patients, when compared to normal controls, with changes to transcription factor *MYB* and NF-kappaB associated pathways, providing evidence of epigenetic changes in disease onset (Heyn *et al,* 2013).

1.3.4 Gene Expression

A study using mouse epithelial fibroblasts (MEF) identified global changes in gene expression between control and HGPS models. This study identified lamina-

associated genes for which expression is moderated by progerin (Kubben *et al*, 2012).

Changes in miRNA expression have also been observed in HGPS cells, with one study identifying overexpression of 3 autophagy inhibiting miRNAs, which appears to holt progerin degradation, exacerbating the phenotype (Roll, 2015).

1.3.5 Proliferation

HGPS fibroblasts have also been shown to have a shortened lifespan in culture. The growth of HGPS fibroblasts is characterised by hyperproliferation followed by an abnormally high level of apoptosis. Using the marker of cell proliferation Ki-67 more than 90% of early passage HGPS fibroblasts were found to be proliferative, this is comparable to only approximately 60% of normal early passage fibroblasts. The level of apoptosis was found at more than a 100 folder higher level in early passage HGPS cells compared to normal fibroblasts and increase between 4 and 8 fold through the lifespan (Bridger and Kill, 2004).

One explanation for the reduced lifespan of HGPS cells is a stochastic loss of telomeres. HGPS fibroblasts have been shown to have shorter telomeres than age matched controls (Allsopp *et al,* 1992). A causative relationship between progerin and telomere shortening has been established as hematopoietic cell, which do not express *LMNA,* from HGPS patients were found to have telomere lengths within the normal range (Decker *et al*, 2009). Telomere shortening has been shown to activate DNA damage checkpoints, which result in cells exiting the cell cycle (Campisi *et al,* 2001). As well as telomere shortening HGPS cells have also been found to have higher levels of DNA damage, which could also result in cells exiting the cell cycle. A mouse model of HGPS (*Zmpste24*-/-) revealed that HGPS gives rise to more chromosome aberrations and increased sensitivity to DNA damaging agents (Liu *et al,* 2005). This was determined using the double-strand break DNA damage marker γH2AX. A further study found an increase in the level of aneuploidy in HGPS patient fibroblasts (Mukherjee and Costello, 1998). Similarly it has been observed that HGPS fibroblasts have constitutively active DNA damage checkpoints, which

could lead to early replication arrest (Liu *et al*, 2006). This may in part be due to the interactions between lamin A and the tumour suppressor pRB (Ozaki *et al*, 1994). Entry into S phase is compromised in HGPS fibroblasts, suggesting that mutant lamin A proteins may promote cell senescence by enhancing the activity of pRB (Chen *et al*, 2003). Also it has been demonstrated that prelamin A accumulation in health endothelial cells results in premature senescence (Bonello-Palot *et al*, 2014).

1.3.6 Lamina Dynamics

Using time-lapse analysis the nuclear lamina has been shown to demonstrate dynamic movement, which includes folding and indenting of large areas (Broers *et al*, 1999). Through Fluorescence recovery after photobleaching (FRAP), the proteins of the nuclear lamina were determined to be highly stable, with a low turn-over (Broers *et al*, 1999).

During mitosis progerin was found to co-localise with lamin B and emerin in membrane aggregates. Mislocalisation of progerin during mitosis has been shown to reduce progerins motility and is linked to an increased number of lagging chromosomes and a longer cell cycle (Cao *et al*, 2007; Dechat *et al*, 2007).

1.3.7 Cell Motility, Nuclear Rigidity and Mechanical Strength

HGPS fibroblasts have also been shown to have reduced cell motility and mechanical strength as well as an increased sensitivity to heat stress (Verstraeten *et al*, 2008; Paradisi *et al*, 2005). Cell motility was assessed using a wound healing assay and it was concluded that HGPS fibroblasts had significantly impaired cell migration resulting in a decreased ability for wound closure despite having the ability to proliferate (Verstraeten *et al*, 2008). Similarly it has been shown that nuclear envelope dysfunction in older tissue leads to stronger attachments and abnormal movement (Mellard *et al*, 2011).

Late passage HGPS fibroblasts were found to have increased nuclear stiffness when compared to early passage HGPS cells and all ages of normal fibroblasts

(Verstraeten *et al*, 2008). In HGPS cells a combination of a stiffened nucleoskeleton and softened nuclear interior leads to mechanical irregularities and dysfunction of mechanoresponsive tissues in HGPS patients. The sensitivity to mechanical strain was, however, found in both young and aged HGPS fibroblasts and resulted in an increased level of apoptosis (Verstraeten *et al*, 2008). As vascular tissue is under intense mechanical strain this may explain the prevalence of heart attacks and strokes in these patients. The inability to attenuate wound healing can promote plaque formation, also increasing the risk of heart attacks and strokes.

HGPS cells were also found to have swollen and fragmented mitochondria and a reduction in mitochondrial mobility (Xiong *et al*, 2016). A downregulation of mitochondrial phosphorylation proteins and mitochondrial dysfunction (Rivera-Torres *et al*, 2013; Villa-Bellosta *et al*, 2013) along with elevated levels of ROS has also been observed (Viteri *et al*, 2010; Lattanzi *et al*, 2012).

1.3.8 Exclusion of Progerin

The exclusion of progerin from HGPS cells has been achieved using oligonucleotides that target the cryptic splice site, resulting in only wild type transcripts (Scaffidi and Misteli, 2005). In these cells a reversal of the progeria phenotype was observed, which included restoration of nuclear shape and heterochromatin location, rescue of the distribution of lamin associated proteins and proper expression of previously misregulated genes (Scaffidi and Misteli, 2005). Interestingly, an increase in the nuclear level of lamin A had no effect on this phenotype, suggesting that the effects of progerin cannot simply be diluted out (Scaffidi and Misteli, 2005). One study identified that progeria cell characteristics occur in a progerin dose dependent manner and only become detrimental when a threshold level is reached (Chojnowski *et al*, 2015). This is of particular interest as one potential treatment for progeria would involve promoting the production of lamin C thus reducing the levels of both progerin and lamin A. This is a viable plan as lamin A has been shown not to be essential for viability (Harborth *et al*, 2001), unlike the B type lamins (Vergnes *et al*, 2004).

1.4 Current Treatments

Current treatments for HGPS include statins, bisphosphonates and farnesyltransferase inhibitors. All three of these treatments target the isoprenylation pathway, which is responsible for the farneslyation of lamin A and progerin. This event is believed to permanently anchor progerin to the inner nuclear membrane, causing disease progression (Capell *et al*, 2005), hence its utilization as a target for therapy (Capell and Collins, 2006). Figure 1.6 displays the isoprenylation pathway and the areas targeted by each therapy.

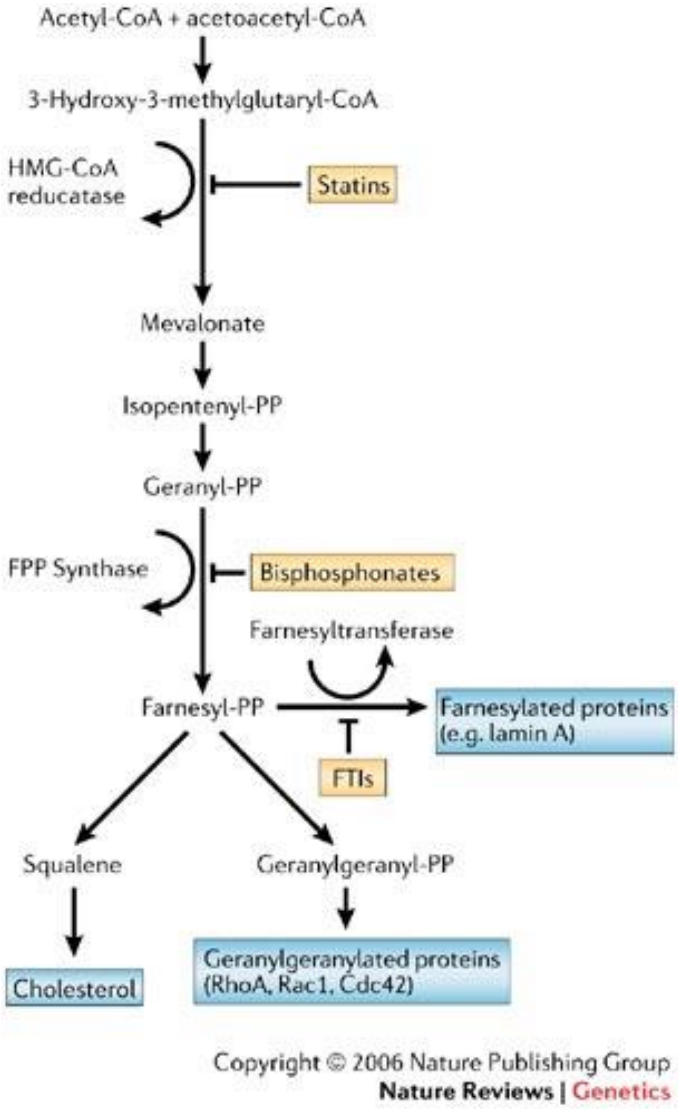

Figure 1.6 Isoprenylation Mevalonate Pathway

Diagram showing the isoprenylation pathway and the stages target by current treatments for HGPS. Image taken from Capell and Collins, 2006.

1.4.1 Clinical Trials

To date there have been four clinical trials for HGPS patients, the first of which began in 2007, just four years after the *LMNA* gene mutation was discovered. Funded by the Progeria Research Foundation in Boston, this clinical trial included 25 classic HGPS patients and used the FTI Lonafarnib (Gordon *et al,* 2012). FTIs are small molecules which reversibly bind farnesyltransferase, inhibiting its ability to produce farnesylated proteins (Figure 1.6)(Capell and Collins, 2006). Pre-commencement of the clinical trial FTIs were shown to improve survival, body weight and bone integrity in murine models of HGPS (Yang *et al,* 2006: Fong *et al,* 2006) as well as improve nuclear shape abnormalities in cultured HGPS fibroblasts (Capell *et al*, 2005; Glynn and Glover, 2005; Toth *et al*, 2005; Mallanpalli *et al*, 2005). Since the commencement of the clinical trial FTIs have also been shown to restore chromosome territory positions to that of normal proliferating cells as well as increase wound healing responses and reduce nuclear stiffness (Mehta *et al,* 2011; Valerie *et al*, 2008). The results of the Lonafarnib clinical trial were mixed for weight gain, a previously predicted marker of successful treatment (Gordon *et al*, 2007), with a great degree of variation found between patients. The trial did suggest improvements in cardiovascular health, mild changes in hearing ability and reported no toxicity to the treatment (Gordon *et al,* 2012). This trial has been criticised for not unequivocally determining the action of lonafarnib on lamin A processing in HGPS patients, despite this requiring a skin biopsy (Couzin-Frankel, 2012). The mixed results found in this clinical trial may result from geranylgeranylation occurring as a result of inhibited farnesylation (see Figure 1.6). In support of this, one mouse study identified prenylated prelamin A and progerin and geranylgeranyltransferase activity despite the addition of FTIs (Varela et al, 2008).

The second clinical trial began in 2008 in France using a combination of statins (pravastatin) and bisphosphonates (Zoledronic Acid). This trial is currently underway, therefore, no data has been published, however, a talk by Prof Nico Levy at the progeria research day at Brunel University in 2011 suggested that patients are experiencing no toxicity and parameters such as weight gain, bone density and cardiovascular health are being examined (Bridger *et al,* 2011). The use of these two drugs in combination was evaluated in a mouse model study which concluded these

drugs effectively inhibit both farnesylation and geranylgeranylation of prelamin A (Varela *et al*, 2008). They also observed increased longevity in a progeria mouse model as well as improvements in weight gain and growth. Similarly improvements in the level of DNA damage and nuclear shape abnormalities have also been reported in response to these drugs (Bridger *et al*, 2011).

Finally the third clinical trial, a continuation of the original trial by the Boston group, began in 2009, this time combining all three drugs, Lonafarnib, pravastatin and Zoledronic Acid. In 2014 it was determined that Lonafarnib treatment extends mean survival by 1.6 years (Gordan *et al*, 2014). This has, however, been subject to criticism, based on lack of a matched cohort and placebo-controlled group (Servick *et al*, 2014). There is now mixed evidence about the significance of farnesylation of progerin in disease progression (Smallwood & Shackleton, 2010), with a mouse model expressing non-farnesylated progerin (*LMNA*$^{nHG/+}$) showing a similar phenotype to mice expressing farnesylated progerin (*LMNA*$^{HG/+}$) (Yang *et al*, 2008). Subsequently, a further non-farnesylated progerin mouse model (*LMNA*$^{csmHG/+}$) was created, where the carboxyl-terminal CSIM motif was changed to CSM, removing the site for farnesylation. These mice did not develop a progeria like disease, having normal body weight and life expectance, leading to the hypothesis that the appearance of disease characteristics in the presence of non-farnesylated progerin is dependent upon the carboxyl-terminal mutation used to eliminate protein prenylation (Yang *et al*, 2011). This brings into question the ultimate efficacy of FTI treatment for HGPS.

1.4.2 Rapamaycin

A further drug for the treatment of HGPS is Rapamycin, the so called “Wonder Drug”. Rapamaycin is a macrolide antibiotic that has been shown to extend life expectancy in yeast (Powers *et al*, 2006), invertebrates (Hansen *et al*, 2007, Bejdov *et al*, 2010) and mammals (Harrison *et al*, 2009, Miller *et al*, 2011). Rapamycin targets the mTOR pathway, which activates the process of autophagy; the recycling of unneeded proteins. One study using fibroblasts from HGPS patients found that treatment with rapamycin restores nuclear structural integrity, heterochromatin

distribution and levels of DNA damage (Cao *et al*, 2011). A second study identified improvements in BAF and LAP2α distribution patterns (Cenni *et al,* 2011). Pre-lamin A and progerin protein have been shown to be degraded through autophagy in response to rapamycin (Graziotto *et al*, 2012), while lamin C protein levels were unaffected (Cenni *et al,* 2011). They also observed an increased life expectancy in these cultures in response to increased degradation of progerin. An increase in *ZMPSTE24* expression was also observed in response to rapamycin treatment (Cenni *et al,* 2011). *LMNA* (-/-) mice also enhanced survival and improved cardiac and skeletal muscle function in response to rapamycin treatment (Ramos *et al*, 2012).

Rapamycin is already used as an immunosuppressant and an anti-cancer drug and is now being proposed as a treatment for HGPS (Cao *et al*, 2011). There are mixed feelings about the suitability of Rapamycin as a treatment for HGPS, however, a phase I/II clinical trial using the rapamycin analogue Everolimus in combination with Lonafarnib is now being conducted by the Progeria Research Foundation in Boston (ClinicalTrials.gov Identifier: NCT02579044, 2015).

1.4.3 Other Therapy Prospects

Other proposed drug treatments are n-acetyl cysteine (NAC), methylene blue (MB), insulin like growth factor 1 (IGF-1) and Remodelin. NACs are ROS scavengers which have been shown to reduce the level of unrepaired DNA damage in HGPS fibroblasts and increase rates of population doublings. It has been proposed that ROS induced DNA damage contributes greatly to poor growth and therefore patients would benefit from a NAC therapy (Richards *et al*, 2011). Similarly treatment with the antioxidant methylene blue was shown to improve mitochondrial defects as well as improved nuclear structure, restored heterochromatin and correction of gene expression in HGPS cells (Xiong *et al*, 2016). Treatment with recombinant IGF-1 was found to increase longevity in a mouse model of HGPS by increasing the previously down-regulated levels of IGF-1 and restoring somatotroph axis function (Marino *et al*, 2010). The small molecule Remodelin shows an improved nuclear shape and decreased markers of DNA damage in HGPS cells through microtubule reorganization (Larrieu *et al,* 2014).

1.5 Atypical Progeria

Approximately 20% of cases of HGPS are not caused by the classic G608G or G608S mutations of the *LMNA* gene. Patients with progeria who do not have these mutations are described as having atypical progeria (APS). These patients are subject to more variation in the clinical phenotype; however, diagnosis is still based on the clinical appearance. Atypical progeria can arise from mutations of the *LMNA* gene at different sites to that which gives rise to classic cases. Currently there are more than 11 other mutations of the *LMNA* gene known to give rise to atypical progeria, three of which result in the production of progerin (McKenna *et al,* 2013).

An intronic variant IVS11+1G>A, found in one patient, was shown to increase the use of the cryptic splice site resulting in higher levels of progerin production than those observed in classic cases. The clinical presentation of this patient was more severe than that of classic patients with abnormalities of the skin first being examined at just 11 weeks of age. This patient experienced rapid development of classic characteristics including joint stiffness, alopecia and micrognathia and subsequently died aged 3.5 years (Moulson *et al*, 2007). A second patient found to have a V607V mutation (c.1821G4A) also showed elevated use of the exon 11 cryptic splice site, which resulted in an extremely severe phenotype that was only conducive to 26 days of life (Moulson *et al*, 2007). Due to the severe nature of this progeriod syndrome it may be classified as a Restrictive Dermopathy (McKenna *et al,* 2013). Analysis of fibroblasts from both these patients revealed abnormally shaped nuclei and treatment of these cells with FTIs suggested that the drug may have been an appropriate treatment for these patients (Moulson *et al*, 2007).

Not all atypical mutations in the *LMNA* gene lead to a more severe phenotype as one atypical patient lived until the age of 45, an age well beyond the average for classic patients (Fukuchi *et al,* 2004). Growth failure was not observed in this patient until approximately 12 years of age, total balding had occurred by age 20 and death resulted from a myocardial infarction. The progeria in this patient resulted from a T623S mutation which caused activation of a cryptic splice site, giving rise to a 35 amino acid truncated protein (Fukuchi *et al,* 2004). The 35 amino acids deleted from

this protein are encompassed within the 50 amino acids deleted in progerin, and like progerin this mutant protein retains its CaaX motif but has no endoproteolytic cleavage site (Fukuchi *et al,* 2004). It remains unclear why deletion of 35 amino acids gives rise to less servere phenotype than progerin.

A further mutation to the tail domain of lamin A is the R644C which alters the endoproteolitic cleaveage site of lamin A (Csoka *et al,* 2004). One study suggested that the use of FTIs for this patient would increase the level of nucleoplasmic unfarnesylated lamin A and reduce the level of abnormally shaped nuclei observed (Toth *et al,* 2005). This patient had many classic progeria attributes and died aged 20 years (Csoka *et al,* 2004), this disorder has subsequently been reclassified as a CDM1A (McKenna *et al*, 2013).

1.5.1 Non-Progerin producing LMNA mutations

Not all mutations in the *LMNA* gene give rise to progerin production, some mutations are found in the early exons and thus affect the rod domains of both lamin A and lamin C. For example one patient has been described as having atypical progeria symptoms such as scleroderma of the skin, growth failure and osteolytic lesions in combination with symptoms of early onset myopathy (Kirschner *et al*, 2005). This patient was found to have a S143F mutation of the *LMNA* gene, which is found in a region close to mutations causing other myopathies (Kirschner *et al,* 2005). Similarly an E145K mutation, which results in atypical progeria, has also been identified (Eriksson *et al*, 2003).

A late onset APS was found to be caused by a mutation in *LMNA* gene at position c.899A>G (D300G), which caused prominent cutaneous and cardiovascular manifestations suggesting this disorder be named *LMNA*-associated cardiocutaneous progeria syndrome (LCPS). This patient also showed a predisposition for cancers in particular basal and squamous cell carcinomas (Kane *et al*, 2013), a phenotype distinct from that of classic HGPS.

1.5.2 Recessive progeria

All the cases described above result from dominant heterozygous mutations which result in disease, however, not all cases of atypical progeria are dominant. One Indian family is described as having 5 out of 7 children diagnosed with atypical progeria (Plasilova *et al*, 2004). The cause of death of one other child remains unclear and one sibling appears healthy. These children are the progeny of a consanguineous marriage which resulted in each affected child being homozygous for the mutation K542N of the *LMNA* gene. This mutation affects both lamin A and lamin C and due to its recessive nature is believed not to interfere with lamin splicing but disrupt lamin A binding. The clinical manifestation of this inherited form of HGPS is similar to that of a classic HGPS patient (Plasilova *et al*, 2004).

1.5.3 *ZMPSTE24* Mutation

As well as alternative mutations in the *LMNA* gene atypical progeria has also been found to arise from mutations in other genes. ZMPSTE24 is the protein responsible for the proteolytic cleavage of the farnesylated terminus of the lamin A protein, a step that cannot be performed on progerin. Mutations in *ZMPSTE24* have also been found to give rise to atypical progeria; one patient was found to be a compound heterozygote for *ZMPSTE24* mutations (c.1085_1086insT and c.794A-G) which resulted in a build-up of prelamin A and abnormally shaped nuclei (Shackleton *et al*, 2005). The clinical manifestation was observed in this patient and encompassed similarities to both MAD and RD. The patient had difficulties in gaining weight, impeded movement of the hips, knees and ankles, reduced subcutaneous fat and osteolysis. The patient died from an infection caused by cracks in the tight sclerotic skin at age 2.9 years (Shackleton *et al*, 2005).

1.5.4 *BANF1* Mutation

A further mutation found to result in atypical progeria (Nestor-Guillermo Progeria Syndrome NGPS) occurs in the *BANF1* gene, which gives rise to the homodimer BAF a binding partner of lamin A (Puente *et al*, 2011). This mutation was identified

in two unrelated relatively long lived atypical patients, one of which resulted from a consanguineous marriage. Both patients were found to be homozygous for the A12T mutation in the *BANF1* gene and had heterozygous unaffected parents and siblings. This mutation has been shown to deplete cellular levels of BAF, due to decreased protein stability, which resulted in abnormally shaped nuclei and mislocalisation of emerin another lamin A binding partner (Puente *et al*, 2011). The identification of a lamin binding partner as a cause of HGPS indicates that other such proteins may also have a role in this disease.

The identification of more genes responsible for atypical forms of this disease would increase our understanding especially if they are lamin binding partners as this may indicate which of lamin A's functions are related to premature ageing.

1.6 Normal Ageing

The resemblance between the pathology of HGPS and normal human ageing has led to much interest in studying the disease as findings may also be applicable to the normal ageing process. Aside from the characteristic resemblance (Merideth *et al*, 2008), other evidence is gathering for the involvement of the nuclear lamina and progerin in normal ageing. The first evidence comes from two invertebrate species, *C. elegans* and *D.melanogaster*, which both have simpler nuclear lamina structures encoded by 1 and 2 genes respectively (Rodriguez and Eriksson, 2010). One study using *C.elegans* found increasing numbers of abnormally shaped nuclei and loss of heterochromatin from the nuclear periphery during normal ageing in all cell types except neurons (Haithcock *et al*, 2005). Furthermore, RNAi knockdown of *CE-LAMIN* caused a significant reduction in lifespan of the worms, but no nuclear morphological abnormalities (Haithcock *et al*, 2005). This shows a link between the nuclear lamina, HGPS cell characteristics and normal ageing in multicelluar organisms. Similarly the size and number of abnormally shaped nuclei was also found to increase with age in drosophila melanogaster (Brandt *et al*, 2008). The development of a drosophila model expressing lamin A and progerin also showed characteristic HGPS nuclear changes (Beard *et al*, 2008). Another study expressed farneslyated forms of the endogenous lamins, *KUGELKERN* and LAMIN B and

observed an earlier decline in locomotor behaviour and a shortened lifespan (Brandt *et al*, 2008). Furthermore, expression of these farnesylated proteins in mammalian cells led to a similar cellular phenotype to that observed in the presence of progerin (Brandt *et al*, 2008).

1.6.1 HGPS Cell Phenotype in Normal Human Ageing

HGPS-like nuclear defects have also been observed in aged human samples. Scaffidi and Misteli, (2006) compared skin fibroblast cell lines from donors aged between 81 to 96 and 3- 11 years for a number of HGPS characteristics. They observed a more rapid increase in the number of abnormally shaped nuclei taken from older donors when compared with younger donor nuclei. Cells from older donors were also found to have a significantly higher number of DNA damage foci compared with younger samples. Disruption of heterochromatin was also observed in cells from aged individuals, with decreased levels of staining for HP1α, H3K93Me and the LAP2 proteins. Between 40 and 90% of cells from older donors showed a reduction in the level HP1α, whereas a reduction was observed in only 20-32% of cells from younger donors. The percentage of nuclei showing a reduction of these heterochromatin markers in aged individuals was similar to the levels observed in HGPS patients; however, in HGPS cells the level of reduction is much higher (Scaffidi and Misteli, 2006). Analysis of 65 signalling pathways identified similarities between those active in HGPS patients samples and those from middle aged and old donors (Aliper *et al*, 2015). The observation of these characteristics in aged individuals shows the similarities between HGPS and normal ageing at a cellular level.

1.6.2 Progerin Accumulation in Normal Human Ageing

There is also mounting evidence for the involvement of progerin in normal human ageing. One study using human fibroblast cells from healthy individuals found evidence of use of the cryptic splice site shown to produce progerin in HGPS (Scaffidi and Misteli, 2006). This study did, however, fail to show an increase in use of this cryptic splice site and subsequent progerin production with age. The use of the HGPS cryptic splice site in normal cells was confirmed by a subsequent

publication which found that progerin is expressed at more than a 160 fold higher level in HGPS compared to age matched controls (Rodriguez *et al*, 2009). Another study also identified progerin in normal fibroblasts and concluded that progerin-induced telomere dysfunction contributes to cellular senescence (Cao *et al,* 2011).

A further *in vitro* study using human skin biopsies again found an increase in the level of the progerin protein, with age in dermal fibroblasts and terminally differentiated keratinocytes (McClintock *et al*, 2007). As this was found not to be caused by an increase in progerin transcripts it is thought to occur through progerin accumulation with age. In support of this, one study examining the cardiovascular pathology of ageing found progerin within coronary arteries of both normal and HGPS samples, although at a much higher level in HGPS. This study concluded that the level of progerin within coronary arteries of normal individuals increased on average by 3.34% per year between the ages of 1 month and 97 years (Olive *et al,* 2010). Therefore, this study also suggests a gradual accumulation of progerin with age.

1.6.3 Differences between HGPS and Normal Human Ageing

Despite the increasing evidence suggesting the roles of the nuclear lamina and progerin in normal human ageing other groups remain sceptical suggesting that the disease mimics ageing but does not encompass all facets of it (NEJM Correspondence 29Th May 2008). That is certainly true with regards to the lack of cognitive decline in these patients and the low incidence of cancer, a well-known age associated disease. The lack of cognitive decline in HGPS patients may result from *LMNA* gene expression not being believed to be involved in brain development as it occurs at a late stage during mouse development (Rober *et al,* 1989). This idea is supported by the fact that no laminopathies result in cognitive neurodegenerative diseases (Capell and Collins, 2006). It has also been hypothesised that neural cells are protected from progerin accumulation in HGPS due to the expression of miR-9 modifying progerin expression (Nissan *et al,* 2012).

Cancer is a disease caused by acquired mutations usually resulting from exposure to the environment. Despite the premature ageing phenotype of HGPS patients they have experienced far less exposure to their environment compared to their rate of ageing. Cells from these patients have also been shown to have a far greater affinity for apoptosis than normal cells and thus opting for this pathway may be cancer protective (Bridger and Kill, 2004). Interestingly ectopic expression of progerin in tumour cells led to multi-nucleation and proliferation arrest (Moiseeva *et al*, 2015).

Ultimately these differences with normal ageing have led to HGPS being termed a segmental progeroid syndrome and it will remain as such unless a causative role of progerin in normal human ageing can be established (Rodriguez and Eriksson, 2010). Although HGPS may not encompass all aspects of normal human ageing the outlined similarities do suggest that greater understanding of the pathology of human ageing could be achieved through studying HGPS.

1.7 Aims and Objectives

The overall aim of this thesis was to investigate the effect of hTERT immortalisation on HGPS patient's fibroblasts, to examine how they responded to immortalisation and assess their suitability for long-term studies of progeria, such as those for drug discovery or for novel disease causing gene identification.
In order to achieve this aim, several objectives were pursued:

1. To identify if continued growth of HGPS fibroblasts in the presence of hTERT would result in a loss of the progeria cell phenotype, including nuclear abnormalities, reduced cell movement and increased DNA damage. The results are described in chapter 3.
2. To identify if the loss of progerin cell phenotype (chapter 3) in hTERT immortalised HGPS fibroblasts occurred through a reduction in the abundance of the mutant protein progerin, either through regulation at the expression level or at a protein level. The results are described in chapter 4.
3. To identify if a reduction in the abundance of progerin in hTERT immortalised HGPS fibroblasts (chapter 5) is caused by an increase in progerin degradation and to determine if this can be exploited for therapy using a novel E3 Ubiquitin Ligase Nanobody raised against A type Lamins. The results are described in Chapter 5.
4. To identify new genes involved in HGPS, by identifying the causative mutation in a cell line derived from an atypical HGPS patient, utilising the growth potential and characteristics resulting from hTERT immortalisation. The results are described in Chapter 6.

Hopefully, the outcome of this research will prove useful in the understanding of the biology of both classic and atypical HGPS and will aid in the future treatment of progeria patients, in particular through nanobody technology.

2 Materials and Methods

2.1 Cell Culture

2.1.1 Cell Lines

All cell lines were cultured in Dulbecco's modified eagle medium (DMEM) GlutaMAX ™ (Gibco®) fortified with 15% Foetal Bovine Serum (FBS) and 5% Penicillin and Streptomycin. Cell lines were passaged twice weekly in 90mm Nunc flasks. A 0.25% trypsin (Gibco®) solution was used to remove cell adhesions to the dish. Cells were grown in a humid 37°C environment with constant CO_2 at 5%. Primary cells were seeded at 2 X 10^5. Immortalised cell lines (hTERT) were set up at 1 in 10 (TAG08466 and NB1T) 1 in 4 (TAG06297 Late) or 1 in 3 (TAG06297 Early) dilutions, depending on growth potential. Table 1 lists all cell lines used in this study.

Table 1 Control and HGPS Fibroblast Cell Lines

Cell Line	HGPS Patient (mutation)	hTERT Immortalised
NB1T	Control	Yes (Dr Christopher Parris unpublished)
TAG06297 Early	Yes (G608G) (Eriksson *et al*, 2003)	Yes (Wallis *et al,* 2004)
TAG06297 Late	Yes (G608G) (Eriksson *et al*, 2003)	Yes (Wallis *et al,* 2004)
TAG08466	Yes (unknown-not G608G) (Professor Nico Levy unpublished communication)	Yes (Wallis *et al,* 2004)
AG08466	Yes (unknown-not G608G) (Professor Nico Levy unpublished communication)	No (Coriell Institute)
AG08468	Control (Mother of AG08466)	No (Coriell Institute)
AG08469	Control (Father of AG08466)	No (Coriell Institute)
AG08470	Control (Sibling of AG08466)	No (Coriell Institute)

The control fibroblast cell line used in this study was established from a healthy new-born foreskin by Drs Fiona Bolland and Ian Kill, Brunel University London, in 2005. The NB1 cell line was subsequently hTERT immortalised by Dr Christopher Parris, Brunel University London, establishing the NB1T cell line.

The TAG06297 cell line was established through hTERT immortalisation of the primary HGPS cell line AG06297, by Professor Richard Faragher's group at Brighton University (Wallis *et al*, 2004). The AG06297 cell line (Coriell Institute) was established in 1972 from a 46XY patient with the classic 2036C>T mutation in the *LMNA* gene. Progerin production in this patient has previously been confirmed by Western Blot analysis (Clements *et al*., in revision). This patient had all the classical progeria characteristics and died at age 14 of congestive heart failure. "TAG06297 Early" is derived from cells shortly after the establishment of the hTERT culture, whereas the "TAG06297 Late" cells are derived from cultures with more than two years continual growth.

AG08466, is a primary fibroblast cell line, established in 1985 from an ante-mortem skin biopsy from a 46XX patient with "Atypical HGPS" (Coriell Institute). Patient was described as having some classic characteristics of HGPS such as loss of subcutaneous fat, osteoarthritis and venous prominence; however, the patient experienced no alopecia and developed some Marfan syndrome like characteristics (Coriell Institute). The underlying causative genetic mutation responsible for HGPS has yet to be established. Primary fibroblasts from the Mother (AG08468), Father (AG08469) and sibling (AG08470) of AG08466 were utilised (Coriell Institute).

AG08466 cell line was hTERT immortalised, by Professor Richard Faragher's group at Brighton University (Wallis *et al*, 2004) and subsequently renamed TAG08466 to indicate its immortalisation status.

2.1.2 Growth curves

At each cell passage the number of population doublings achieved was calculated based on haemocytometer readings, using the equation Population doublings = 3.32[log(number of cells harvested) – log(number of cells seeded)]. This was determined for each hTERT immortalised cell line over a 46 day period in culture.

2.2 Cell Imaging

2.2.1 Indirect Immunofluorescence

Cultures were grown for 3-4 days on 0.1 mm thick glass coverslips. Cell were fixed using 3.74% formaldehyde and permeabilized using an ice cold 1:1 methanol: acetone solution. Blocking was achieved using a 0.1% FBS 1x phosphate buffered saline (PBS) Solution. Indirect immunofluorescence was performed by the sequential incubation of cells with a primary and secondary antibody in a moist chamber. Primary antibodies were raised against the protein of interest and secondary antibodies contained a fluorophores for visualisation. Table 2 summarises all antibodies used in this study. Coverslips were mounted on Snowcoat® slides using a Mowiol mountant containing the fluorescent DNA stain DAPI (4',6-Diamidino-2-Phenylindole).

Table 2 Summary of Indirect Immunofluorescence Antibodies

Protein	Primary Antibody (Dilution)	Secondary Antibody (Dilution)
Ki-67	Anti-Ki-67 Rabbit monoclonal (Dako A0047) (1:30)	anti-Rabbit TRITC (Dako R0156 Swine polyclonal) (1:25)
Lamin A	Anti-Lamin A mouse monoclonal (abcam® ab8980) (1:50)	anti-Mouse Goat Polyclonal FITC (Sigma® F9006) (1:64)
Lamin A/C	NCL-LAM-A/C (Novocastra™ mouse monoclonal) (1:30)	anti-Mouse Goat Polyclonal FITC (Sigma® F9006) (1:64)
γH2AX	Anti-phospho -H2A.X (Upstate 07-164 (1:100)	anti-Mouse Goat Polyclonal FITC (Sigma® F9006) (1:64)
Progerin	Anti-Progerin Mouse monoclonal (Enzo 13A4) (1:50)	anti-Mouse Goat Polyclonal FITC (Sigma® F9006) (1:64)
T7 Tag	Anti-T7 Tag rabbit polyclonal (abcam ac117486) (1:200)	anti-Rabbit TRITC (Dako R0156 Swine polyclonal) (1:25)

In most cases cells were visualised under the 40x or 100x objective, of a fluorescence Axioscope 2 (Zeiss) microscope. Images were taken using a ProgRes®C12 plus camera (Jenoptic) using the ProgRes Capture Pro 2.5 software. For transfection analysis slides were viewed using the 100X objective of the HF14 Leica DM4000 microscope and images captured using the Leica DFC365 FX camera using Las AF software. 3D fluorescence microscopy was achieved by taking Z stacks using the Elipse Ti microscope (Nikon) and deconvolution using NIS-Elements Advanced Research Software. Unless otherwise stated, a minimum of 250 nuclei per coverslip were analysed when using indirect immunofluorescence and all staining was performed in triplicated.

2.2.2 Computational shape analysis

Slides were prepared as described in section 2.2.1, without the addition of primary or secondary antibodies, allowing for visualisation of DNA using DAPI mountant. Cells were visualised and imaged as described in section 2.2.1, using a 40x objective. Using the particle analysis tool on ImageJ 1.37c software a threshold level was set to incorporate all the nuclei in one image. The highlighted shapes were then analysed based on: area, perimeter, major and minor axis, circularity (4π(area/perimeter2) and aspect ratio (major axis/minor axis). A minimum of 650 nuclei were examined per cell line.

2.2.3 Live Imaging

Semi-confluent dishes of cells were selected and put on the inverse mounted, Axiovert 200M (Zeiss) microscope. Cells were maintained at 37^{o}C with 5% CO_2 using the incubator attachment and heated stage of the cell observer microscope. Phase contrast images were taken every 5 minutes for an 8 hour period. Images were opened in ImageJ 1.37c software and converted to a stack, which allowed fluid movement through all images, making a video. The manual tracking plugin was used to track the position of the nucleus of a specific cell at each time point, giving a list of XY coordinates for each frame. The hypotenuse was then calculated to give the distance moved between each frame. The sum of the entire hypotenuse for the 8 hour period was calculated to give the total distance moved by the cell. A minimum of 30 cells were tracked per cell line.

2.2.4 Metaphase preparations

Metaphase preparations were created by incubating, approximately 70% confluent dishes per cell line, with 1µg of Colcemid (Gibco® 15210-040) in DMEM, for 30 minutes. Cells were then harvested from the dish using 0.25% trypsin and pelleted by centrifugation at 1000rpm for 5 minutes. The pellets were re-suspended drop-wise with agitation in a 0.075M hypotonic solution to cause cell swelling. A series of pelleting and re-suspending steps, using 3:1 methanol: acetic acid, were used to fix the cells (protocol as described by Anderson, 2010). After the final re-suspension,

cells were dropped from height onto Snowcoat® slides and incubated in a warm environment until dry.

Slides were selected for analysis based on the mitotic index and lack of cytoplasm around chromosomes. Large rectangular glass coverslips were placed over the cells and secured with a DAPI containing Mowiol mountant. Images of metaphase spreads were captured using an Axioplan 2 automated microscope (Zeiss), using Metafer, the automated slide scanning and imaging platform. Images were captured using Metasystems camera using MSearch software. Up to eight slides were secured into the automated stage and the regions containing the cells were mapped out. The focus level was then set, before the software scanned the slide and captured images of chromosome spread. After the removal of any unusable images, such as unfocused or incomplete spreads, the number of chromosomes were counted for at least 100 images for each cell line.

2.2.5 Multiplex-FISH

Multiplex-FISH was performed by Dr Rhona Anderson, Brunel University London, the method for which is discussed in "Multiplex fluorescence in situ hybridization (M-FISH)" (Anderson, 2010). M-FISH is a three-step process employed for studying complex interchromosomal rearrangements, by creating a 24-colour karyotype. Each homologous pair of chromosomes is uniquely labelled, by combining the limited numbers of spectrally distinct fluorophores. The superimposing of images, captured through different band-pass filters, by M-FISH software enable each chromosome to be identified based on its combination of fluorophores. Finally, analysis of these Karyotypes can be performed, enabling observation of any structural or numerical abnormalities.

2.3 Expression Analysis

2.3.1 RT-PCR

Confluent 90 mm dishes of cells were harvested using 0.25% trypsin (Gibco®) solution and pelleted. RNA was extracted using Nucleospin® RNA II (MACHEREY-NAGEL) extraction columns. The RNA concentrations were determined using the NanoDrop^{TM} spectrophotometer.

For every 1µg of RNA, 100 ng concentration of d(N)6 primers (Invitrogen) were added and allowed to anneal through a 40 second incubation at 90^{o}C (tetrard). The reverse transcription reaction was set up as described in table 3 and incubated at 50^{O}C for 1 hour.

Table 3 Components of Reverse Transcription

Components of Reverse Transcription
RNA + d(N)6 primers
1ST Strand Buffer
0.5 mM dNTPs (Bioline)
DTT
DNase Out
RT Superscript III enzyme (Invitrogern)

The reverse transcription products were used as the template cDNA for a PCR reaction, using primers designed previously (Dr Evgeny Makarov), which amplify exons 10-12 of the *LMNA* gene. Forward primer (Ex10f1) GAA GTG GCC ATG CGC AAG CTG. Reverse Primer (Ex12r2) GGT GAG GAG GAC GCA GGA AG. Primers that amplify exons 7-9 of *ACT4* were used as an endogenous control. Forward primer (Ex7f1) CGA CCC TGT CAC CAA CCT GGA C. Reverse Primer (Ex9r1) GGC CAG CTT CTC GTA GTC CTC C. Table 4 summarises the components of RT-PCR. Table 5 summaries PCR conditions for amplification of

exons 10-12 of the *LMNA* gene. Table 6 summaries the PCR conditions for amplification of exons 7-9 of *ACT4.*

Table 4 Summary of RT-PCR Reagents

Components of PCR
Forward Primer (0.5µM)
Reverse Primer (0.5µM)
FINNZYMES Buffer (1.5mM Mg^{2+})
dNTPs (Bioline) 200µM
cDNA (1:25 Dilution of RT product)
FINNZYMES DyNAzyme^{TM} (NEB).
H20

Table 5 Summary of PCR Conditions for the amplification of exon 10-12 LMNA

Temperature	Duration/ Cycles	
94ºC	2 minutes	
94ºC	30 seconds	30 Times
62ºC	30 seconds	
72ºC	1 minute	
72^{O}C	5 minutes	

Table 6 Summary of PCR Conditions for the amplification of exons 7-9 ACT4

Temperature	Duration/ Cycles	
94ºC	2 minutes	
94ºC	30 seconds	30 Times
57ºC	30 seconds	
72ºC	1 minute	
72^{O}C	5 minutes	

PCR products were run on 2% Agarose TAE buffer gels with a 0.5 μg/Ml concentration of Ethidium Bromide. Agarose gels were visualised using the Gel Doc EZ Imager (Bio-Rad). DNA markers used for agarose gels were DNA HyperLadder I (Bioline) and DNA Hyperladder II (Bioline).

2.3.2 Quantitative-PCR

Quantitative-PCR probes and primers are the intellectual property of Dr Evgeny Makarov and are, therefore, not described in this work. Primer and probe binding regions are shown in figure 4.20. qPCR was performed using the Quantstudio™ 7 Flex Real – Time PCR System (Applied Biosystems™) and data analysis performed using the Quantstudio™ Real-Time PCR software Version 1:1 (Applied Biosystems™).

F1 and F2 are the names given to the pJET1.2 cloning vector plasmids which contain a copy of the lamin A and progerin amplicons respectively. The purified plasmid was quantified using NanoDrop™ spectrophotometer and the number of molecules calculated using Avogadro's constant.

bp (size of double strand product)(330 daltons * 2 nt/bp)	g/molecule
Avagadro's Constant (6.023 x 10^{23} Molecules/moles)	

bp size of double strand product for lamin A = 3641
bp size of double strand product for progerin = 3491
This was used to make known concentration points for the calibration curve ranging from 1F1/F2 (10 molecules) up to 8F1/F2 (100000000 molecules).

2.4 Protein analysis

2.4.1 Western Blot

Western blot samples were established by cell scrapping from a confluent dish on the day of passage. A sister dish, set up at the same time, was used to determine the cell number by a haemocytometer count. The cell number was used to determine the volume of 3x sample buffer containing SDS which should be added to the dish to give a final concentration of $2x10^5$ cells per 10 µl of sample.

Equivalent cell numbers were loaded to 10% precast polyacrylamide gels (Mini-PROTEAN® TGX™ Precast Gel Bio-Rad). Western blot was performed as described by Towbin *et al,* 1979. Gels were run, at a constant voltage of 75V until condensed and then 150V until the marker exited the gel. Table 7 shows a summary of all antibodies used for western blot analysis in this study.

Table 7 Summary of Western Blot antibodies

Protein	Primary Antibody (Dilution)	Secondary Antibody (Dilution)
Lamin A/C	NCL-LAM-A/C (Novocastra™ mouse monoclonal) (1:200)	anti-Mouse Goat polyclonal IRDye® 800CW (LI-COR 926-32210)
Lamin A/C	NCL-LAM-A/C (Novocastra™ mouse monoclonal) (1:200)	anti-Mouse Rabbit polyclonal Horseradish Peroxidase (Dako P0448) (1:10,000)
T7 Tag	Anti-T7 Tag rabbit polyclonal (abcam ac117486) (1:1000)	anti-Rabbit Goat polyclonal Horseradish Peroxidase (Sigma® A0545) (1:20,000)
SUN1	Anti-SUN1 (Abcam ab124916 Rabbit monoclonal) (1:1000)	anti-Rabbit Goat polyclonal Horseradish Peroxidase (Sigma® A0545) (1:20,000)
SUN2	Anti-SUN2 (Abcam ab124916 Rabbit monoclonal) (1:1000)	anti-Rabbit Goat polyclonal Horseradish Peroxidase (Sigma® A0545) (1:20,000)
BANF1	Anti-BANF1 (Abcam ab88464 mouse monoclonal) (1:1000)	anti-Mouse Rabbit polyclonal Horseradish Peroxidase (Dako P0448) (1:10,000)
Histidine Tag	Anti-histidine tag (Qiagen Mouse monoclonal) (1:1000)	anti-Mouse Rabbit polyclonal Horseradish Peroxidase (Dako P0448) (1:10,000)

Horseradish Peroxidase conjugated secondary antibodies were visualised via the chemiluminescence generated by catalysed oxidation of Luminol, using the Molecular Imager® ChemiDoc™ XRS+ (Bio-Rad) using Image Lab™ software. Exposure times were set based on the level of illumination on individual membranes.

IRDye® 800CW fluorophore conjugated secondary antibodies were visualised using the Odyssey®Sa Infrared Imaging System (LICOR) using Imaging Studio v3.1 Software (LICOR).

2.5 Molecular Cloning

2.5.1 TAT-Plasmids

pTATv1 and pTATv2 plasmid were obtained from Professor Steven Dowdy. Plasmids were purified from DH5α bacterial cultures using the NucloeSpin® Plasmid purification kit (MACHEREY-NAGEL). Plasmids were confirmed using restriction digestions with NotI (Fermentas) in Buffer 0 (Fermentas) and EcoNI (New England Biolabs) in NEB4 Buffer (New England Biolabs). Restriction digestion products were run on 0.8% Agarose TAE buffer gels with a 0.5 μg/Ml concentration of Ethidium Bromide. Agarose gels were visualised using the Gel Doc EZ Imager (Bio-Rad). DNA markers used for agarose gels were DNA HyperLadder I (Bioline) and DNA Hyperladder II (Bioline).

BamHI and NotI restriction sites were selected for directional cloning. Double digest reactions was performed on both plasmids, using BamHI (Fermentas) and NotI (Fermentas), in BamHI buffer (NEB). A further double digestion reaction, to reduce re-ligation, was performed using SacI (NEB) and SalI (NEB), for which the recognition site are in between NotI and BamHI. The vectors were then treated with Calf Intestine alkaline phosphatase (CIP- NEB 0450804) again to reduce the likelihood or re-ligation of the plasmids without taking up an insert. The plasmids were then purified using the Wizard® SV Gel and PCR Clean-Up System (Promega A9282).

2.5.2 *LMNA* Inserts

Lamin A and progerin cDNA sequences were obtained from Professor Susan Michaelis, Johns Hopkins University, in plasmids pMM45-1 and pMM46-2 respectively, see Appendix i. PCR amplification was used to add NOTI and BAMHI

restriction sites to dictate the orientation of insertion into the plasmid. Forward PCR primer containing BamHI B-LAMorf.f1 CaggatCCGTCCCAGCGGCGCGC and reverse PCR primer containing NotI N-LAMorf.r1 gtgcggccgcCATGATGCTGCAGTTCTGGG.

Table 8 Summary of Molecular Cloning PCR

Components of PCR
B-LAMorf.f1 Forward Primer (0.5µM)
N-LAMorf.r1 Reverse Primer (0.5µM)
FINNZYMES Buffer (1.5mM Mg^{2+})
dNTPs (Bioline) 200µM
FINNZYMES DyNAzyme^{TM} (NEB).
(1ng/10ng) DNA
H20

Table 9 Summary of Molecular Cloning PCR Conditions

Temperature	Duration/ Cycles	
94°C	1 minute 30 seconds	
94°C	30 seconds	35x
62°C	30 seconds	
72°C	1 minute 20 seconds	
72°C	3 minutes	

Double digest reactions were performed on both lamin A and Progerin inserts, using BamHI (Fermentas) and NotI (Fermentas), in BamHI buffer (NEB). The inserts were then purified using the Wizard® SV Gel and PCR Clean-Up System (Promega A9282).

Plasmid and insert concentrations were estimated using 0.8% Agarose TAE buffer gel electrophoresis with a 0.5µg/Ml concentration of Ethidium Bromide. Agarose gels were visualised using the Gel Doc EZ Imager (Bio-Rad). DNA markers used for agarose gels were DNA HyperLadder I (Bioline) and DNA Hyperladder II (Bioline).

2.5.3 Plasmid Ligation

Ligation was performed as outlined in the fermentas T4 DNA Ligase protocol. Three times the amount of insert was mixed with plasmid and incubated in the presence of T4 DNA ligase (NEB).

2.5.4 Plasmid Transformation

Transformation into rubidium chloride competent DH5α cells was induced through heatshock. LB medium was inoculated with cells post-ligation and selected using Kanamycin resistance agar plates. A control plate was set up where no insert had been added to the ligation mix. Numerous colonies were observed on both the lamin A and progerin plates. No colonies were present on the control plate suggesting a successful transformation. Four colonies from each insert were used to inoculate 2ml overnight cultures. The plasmids were then purified using the NucloeSpin® Plasmid purification kit (MACHEREY-NAGEL) and a sample was digested with BamHI (Fermentas) and NotI (Fermentas). Colonies with an insert were identified by 0.8% Agarose TAE buffer gel electrophoresis with a 0.5µg/Ml concentration of Ethidium Bromide. Agarose gels were visualised using the Gel Doc EZ Imager (Bio-Rad). DNA markers used for agarose gels were DNA HyperLadder I (Bioline) and DNA Hyperladder II (Bioline).

2.5.5 Plasmid Sequencing

Plasmids were sequenced by Beckman Coulter Genomics using two of their universal primers, T7P (TAA TAC GAC TCA CTA TAG GG) and T7 term (CTA GTT ATT GCT CAG CGG). The sequenced region covered the insert and approximately 100bp either side of the insertion site. The sequences were aligned to the reference sequence, taken from the in silico plasmid maps, using DNASTAR® software.

2.5.6 Protein Purification

Plasmids selected from sequencing analysis were transformed into rubidium chloride competent Rosetta™ cells (Novagen), a BL21 variant which contains tRNAs (recognise AGG, AGA, AUA, CUA, CCC, GGA codons) specific for the production of human proteins. The Rosetta™ cells also contain a plasmid that confers chloramphenicol resistance. 0.5mM Isopropyl β-D-1-thiogalactopyranoside (IPTG) was used to induce the production of the proteins under the control of the T7 promoter. A sample of the culture before and after induction was run on a 10% precast polyacrylamide gels PAGE (Mini-PROTEAN® TGXTM Precast Gel Bio-Rad). This gel was then stained for proteins using Coomassie® Blue.
Protein were purified from Rosetta™ cultures as described by Becker-Hapak et al, 2001 using Ni- NTA Agarose (Qiagen) resin in a batch method. 20mM, 50mM, 100mM and 250mM concentrations of imidazole were used to elute the proteins from the column.

2.6 Cell Modification

2.6.1 Protein transduction

TAT-Fusion proteins were desalted using PD-10 desalting column and added directly to media of ~70% confluent cells at a final concentration of 10ug/ml. Indirect immunofluorescence (2.1) was performed after 30 minutes.

2.6.2 Plasmid transformation

Plasmid pc3236 (Figure 5.45) was obtained from Professor Heinrich Leonhardt Munich University and transfected into DH5α cells. Purified plasmids were transfected into 40-50% confluent fibroblast cultures using X-tremeGENE™ HP DNA Transfection Reagent (Sigma-Aldrich®) to a final concentration of 1µg/ml.

2.6.3 MG132

MG132 (Sigma M7449-200UL) was added directly to cell media at a final concentration of 10 µM. DMSO was added as a loading control, to untreated cells, in the same manner. MG132 treated cells were harvested for western blot analysis as described in 4.1 at 2, 5, 8 and 24 hour time points.

2.7 Whole exome sequencing

DNA extraction was performed using the QIAamp DNA Mini Kit (Qiagen 51304) and quantified using the Nanodrop^{TM} 2000c Spectrophotometer (Thermo Scientific). Exon enrichment was performed using the Nextra Rapid Capture Exome Kit (Illumina) 50ng DNA protocol, as illustrated in figure 2.7.

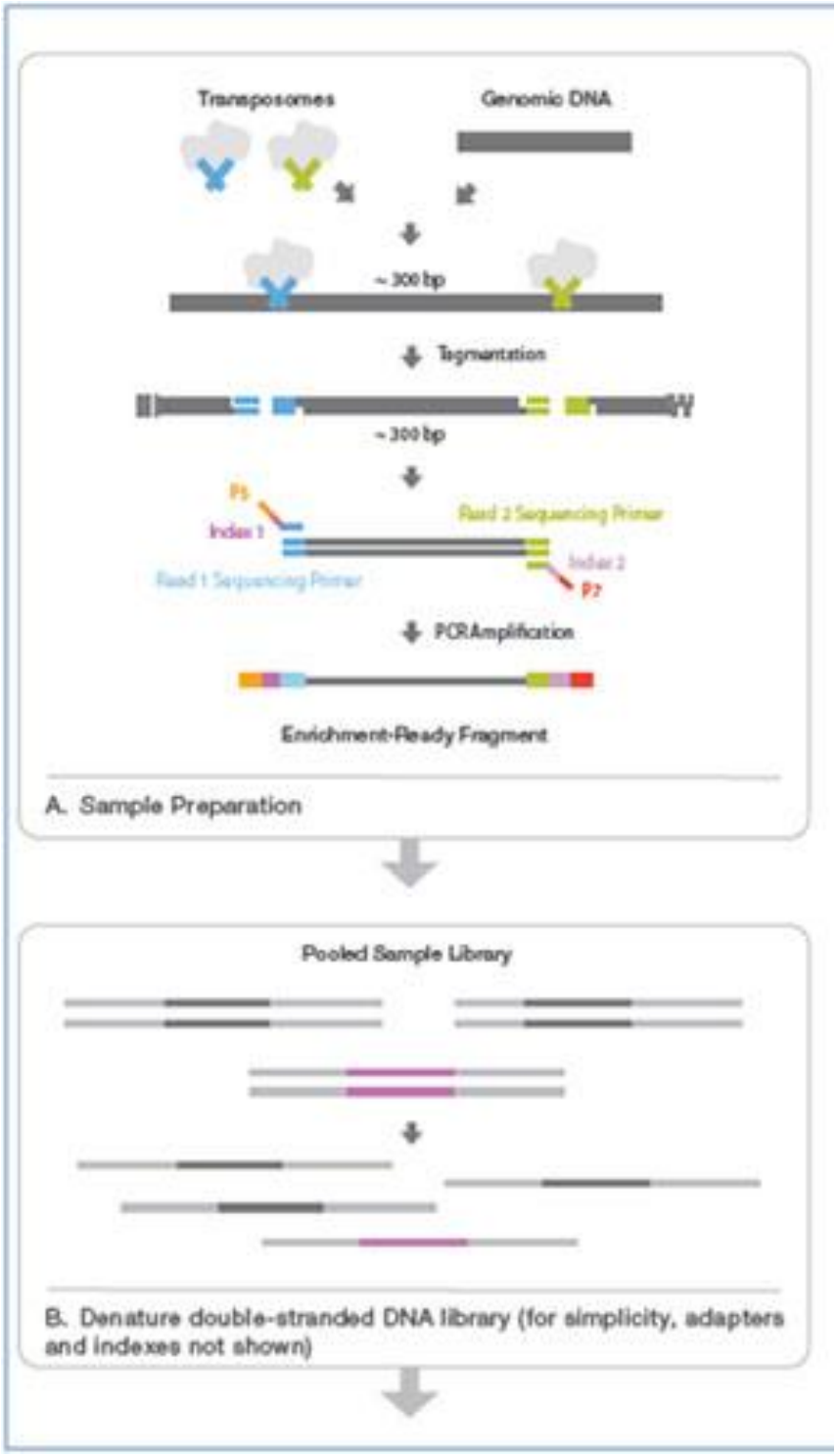
Transposomes
Genomic DNA
~ 300 bp
Tagmentation
~ 300 bp
P5
Index 1
Read 2 Sequencing Primer
Index 2
P7
Read 1 Sequencing Primer
PCR Amplification
Enrichment-Ready Fragment
A. Sample Preparation
Pooled Sample Library
B. Denature double-stranded DNA library (for simplicity, adapters and indexes not shown)

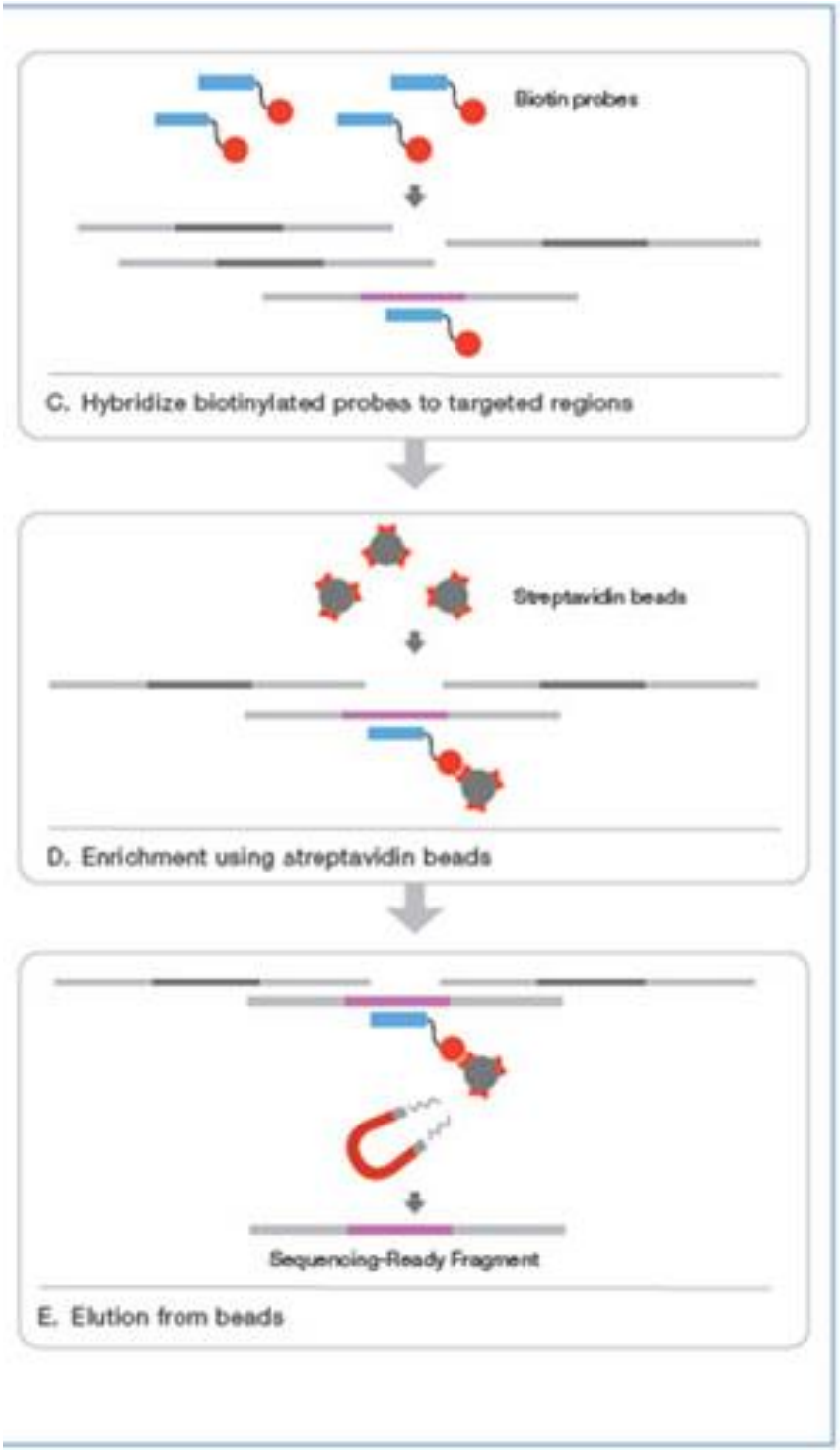

Figure 2.7 Diagram demonstrating exome enrichment using the Nextra® Rapid Capture Exome kit (Illumina®).

Image taken from the Nextra Rapid Capture Exomes Datasheet DNA sequencing (Illumina).

Exome sequencing was performed using the HiSeq™ 2000 Sequencing System (Illumina) as outlined in figure 2.8.

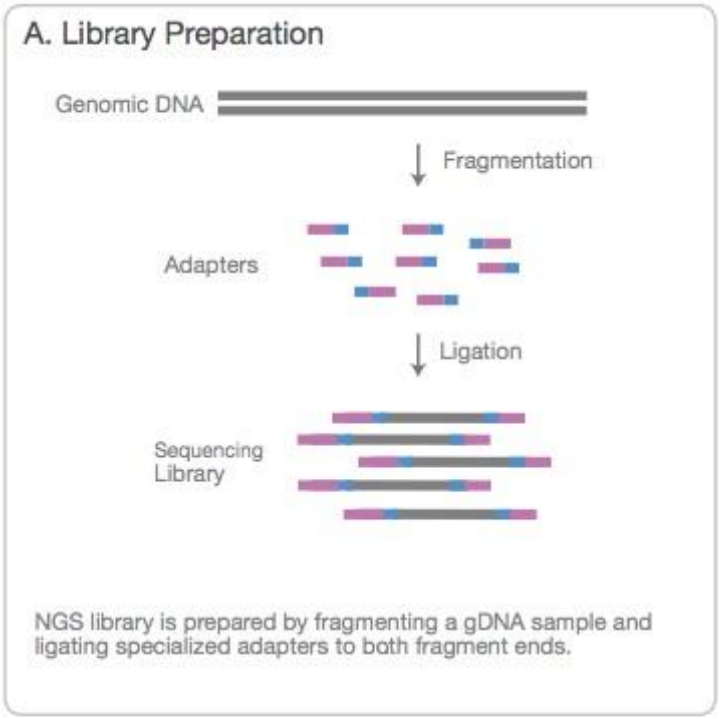
A. Library Preparation
Genomic DNA
Fragmentation
Adapters
Ligation
Sequencing
Library
NGS library is prepared by fragmenting a gDNA sample and ligating specialized adapters to both fragment ends.

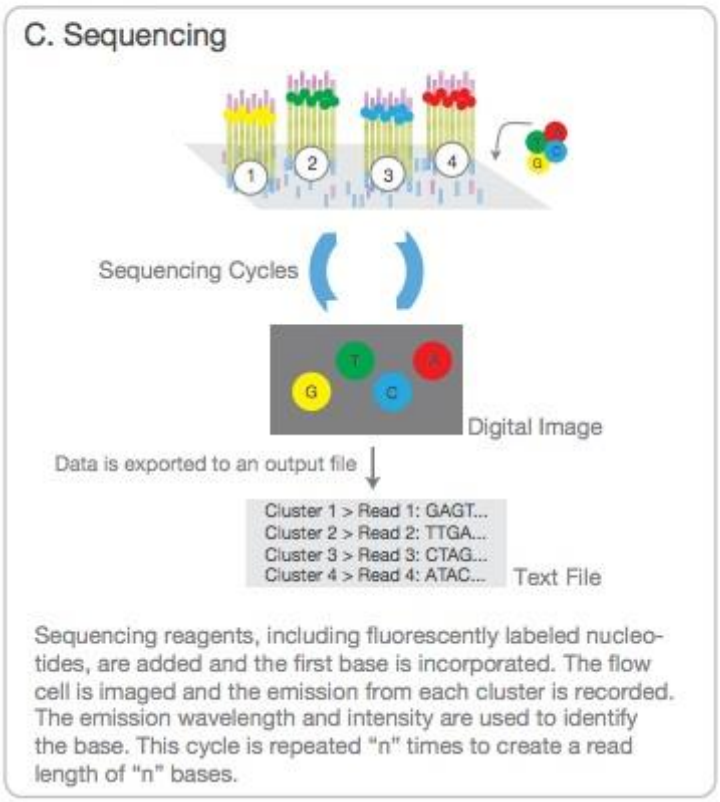
C. Sequencing
1
2
3
4
Sequencing Cycles
T
A
G
C
Digital Image
Data is exported to an output file
Cluster 1 > Read 1: GAGT...
Cluster 2 > Read 2: TTGA...
Cluster 3 > Read 3: CTAG...
Cluster 4 > Read 4: ATAC...
Text File
Sequencing reagents, including fluorescently labeled nucleotides, are added and the first base is incorporated. The flow cell is imaged and the emission from each cluster is recorded. The emission wavelength and intensity are used to identify the base. This cycle is repeated "n" times to create a read length of "n" bases.

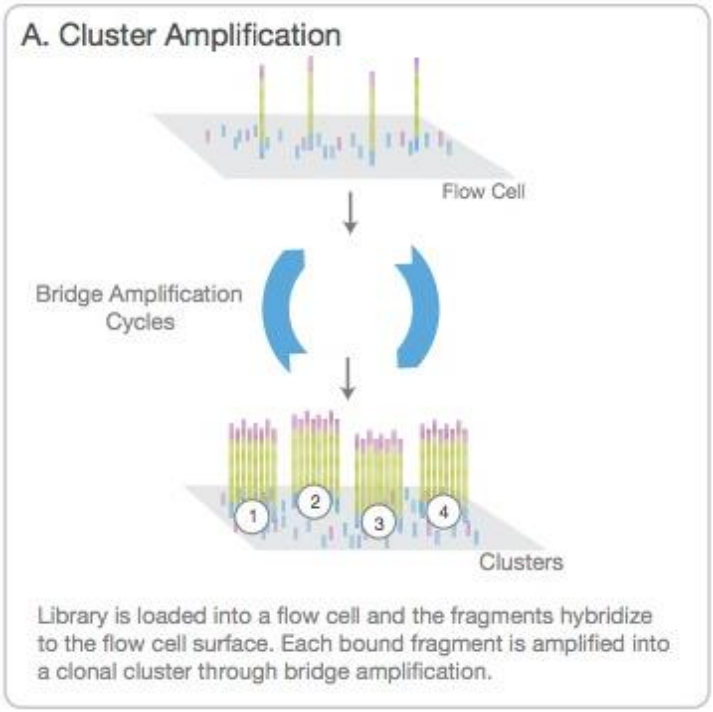

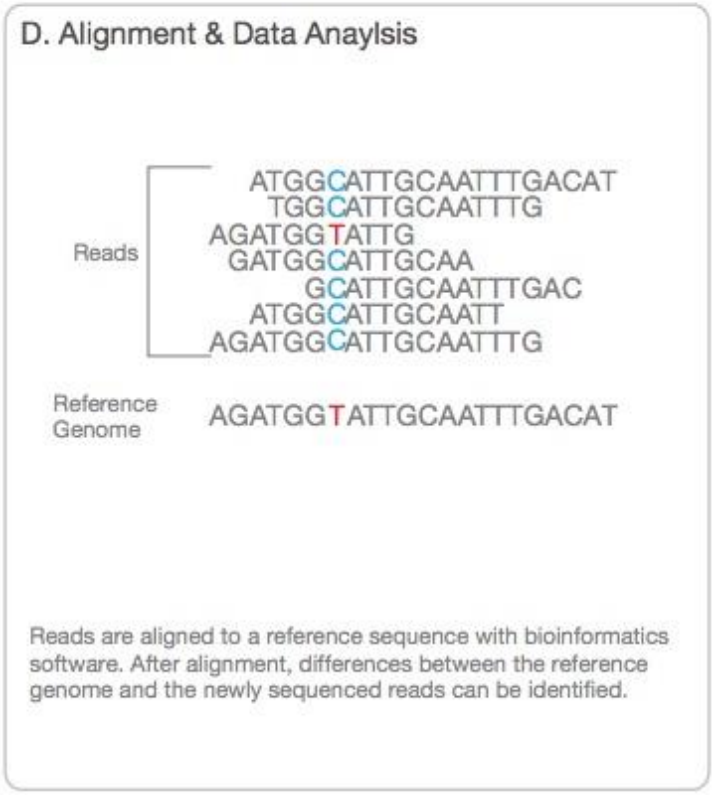

Figure 2.8 Diagram showing Next Generation Sequencing Chemistry with the HiSeqTM 2000 Sequencing System (Illumina).

Image taken from "An Introduction to Next Generation Sequencing" (Illumina).

Exome sequencing data was analysed using the HiSeq™ analysis software (HAS). Reads were aligned to the human hg19 Genome using the Burrows-Wheeler Aligner (BWA). Genome Analysis Toolkit (GATK) software was used to identify variants and realign any sequences that were out of place due to insertions or deletions (Indel Realigner). Figure 2.9 outlines this process.

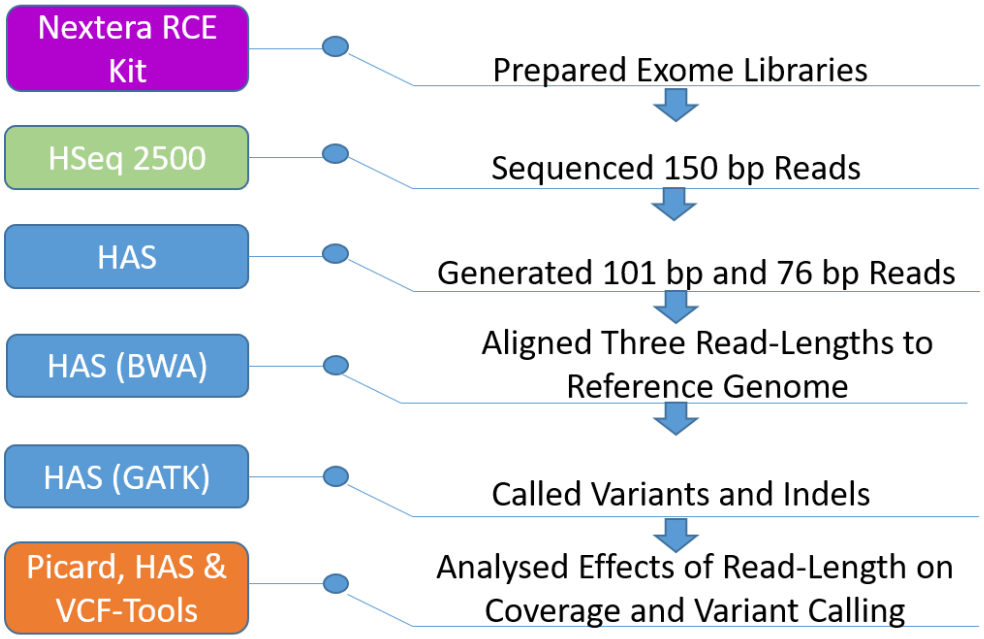

Figure 2.9 Exome Sequencing Analysis Workflow

Image taken from the Nextra Rapid Capture Exomes Datasheet DNA sequencing (Illumina).

Exome sequences were analysed for potentially deleterious variants using Ingenuity® Variant Analysis Software™ (Qiagen) as outlined in the Ingenuity® Variant Analysis™ Quick-Start Guide (Qiagen).

3 Characterisation of hTERT Immortalised, Hutchinson Gilford Progeria Syndrome, fibroblast cell lines.

3.1 Introduction

The stable transfection of hTERT, which encodes the reverse transcriptase subunit of human telomerase, has been shown to lengthen telomeres and bypass replicative senescence in human cells (Bodnar *et al,* 1998). This results in limitless replicative potential, whilst seemingly having no effect on cell phenotype or differentiation markers (Lee *et al*, 2004). It has been shown, that unlike other methods for cell immortalisation (SV40), ectopic hTERT expression increases replicative lifespan without transforming cells or triggering genomic instability (Morales *et al,* 1999; Jiang *et al*, 1999; Pirzio *et al*, 2004). The benefit of hTERT immortalization *in vitro* is a stable cell resource that allows long-term investigations to be carried out.

The short replicative lifespan of HGPS cells in culture, characterized by increased levels of apoptosis and premature replicative senescence (Bridger &Kill, 2004; Benson *et al*, 2010), reduces their viability for *in vitro* study. With only a small number of HGPS patients world-wide, there are few cells lines available, driving the need for a stable cell resource.
Since 2000, several stable hTERT HGPS cells lines have been produced that show lengthened telomeres and increased replicative lifespans (Benson *et al*, 2010; Kudlow *et al*, 2008; Ouellette *et al*, 2000; Wallis *et al*, 2004). The study by Wallis *et al, 2004* resulted in successful immortalization for several clones, however, a significant proportion of clones were found to be resistant to immortalization. Out of 15 clones, isolated from 3 different donors, 5 continued on to senescence despite the expression of hTERT, something not observed in any controls. This suggests that the lengthening of telomeres alone is not sufficient to negate replicative senescence in HGPS cells, questioning what changes may have occurred between clones that immortalized and those that showed resistance.

With shortened telomeres and progerin both being identified as factors for replicative senescence (Allsopp *et al*,1992; Decker *et al,* 2009), telomerase and progerin may act as opposing forces within cells, suggesting a need to modulate progerin to achieve immortalization. A link has since been established between down-regulation of progerin expression, in normal fibroblasts, in response to immortalized with hTERT (Cao *et al,* 2011). One hypothesis is that a reduction in progerin expression, in response to hTERT, is a key factor to permit immortalisation in the HGPS cell lines (Cao *et al*, 2011).

A second study, however, identified no changes in progerin expression in response to hTERT but they did observe a reduction in telomere related DNA damage (Benson *et al*, 2010). This led to the theory that hTERT negates the progerin-induced telomere dysfunction that leads to replicative arrest and premature senescence in HGPS cultures (Benson *et al,* 2010).

Despite hTERT immortalization being described as having no effect on phenotype (Lee *et al,* 2004), if it is modifying progerin within cells, this may have a dramatic effect on HGPS cell characteristics. Conversely, a study analysing nuclear shape abnormalities, in cells retrovirally transduced with progerin, showed no improvement in response to hTERT immortalization, despite having the same growth potential as controls and cells transduced with Lamin A (Kudlow *et al*, 2008). This makes it optimistic that hTERT immortalized cells may be useful for the study of a disease characterized by increased cell senescence.

The primary aim of this chapter is to provide a thorough analysis of the effects of hTERT immortalisation on HGPS cell phenotype and assess the viability of this cell line for further studies. Using one of the strains created by Wallis *et al*, 2004, TAG06297, several properties will be investigated including; growth potential, nuclear abnormalities, nuclear shape, cell movement, DNA damage and protein localisation. Details of progeria cell phenotype are outlined in chapter 1.3.

It has also been suggested that hTERT immortalised cultures, with difficulty in cell cycle regulation can result in out-growths of a variant population, indicating HGPS

hTERT cell lines may have a stability shelf-life (vanWaarde-Verhagen et al, 2005). Therefore, analysis of progeria cell characteristics will be undertaken for both an Early (shortly after immortalization) and Late (+2 years growth) passage TAG06297 culture.

3.2 Results

The AG06297 fibroblast cell line, originating from patients with the classic G608G form of the syndrome, was immortalized using hTERT (TAG06297) by Professor Richard Faragher (Wallis et al, 2004). Unlike other HGPS cell line all, all four colonies from AG06297 immortalised normally (Wallis et al, 2004).

AG06297 primary cells were shown to be relatively long-lived amongst HGPS cultures achieving just over 40 population doublings at their maximum replicative lifespan (Bridger & Kill, 2004). Analysis of the nuclear morphology of primary AG06297 cells showed that primary cells from this cell line do display typical HGPS nuclear abnormalities. Early passage cells were found to have 29.2% of nuclei with a nuclear abnormality and this rose to above 70% in late passage primary cells. Unfortunately, AG06297 cells available from Coriell Cell Repository are at the end of their replicative lifespan and as such failed to grow in culture, causing no further characterisation of these primary cells to be carried out.

3.2.1 Growth Potential

Cells taken from progeria patients display a diverse but relatively short replicative lifespan in culture, which has been characterized by hyperproliferation and increased levels of apoptosis (Bridger & Kill, 2004).

To determine the effect of hTERT immortalisation on the TAG06297 cell line, separate cultures from two points in the cell line's history were analysed. "TAG06297 Early" is derived from cells shortly after the establishment of the hTERT culture, whereas the "TAG06297 Late" cells are derived from cultures with more than two years continual growth. To investigate the growth rate and potential

of both cultures, growth curves were produced (Figure 3.10A). Cell passage was carried out twice weekly to avoid confluence. A fibroblast culture from a healthy individual (NB1T), also immortalized with hTERT was used as a control (Unpublished Data, see Chapter 2.1.1). At each passage the cell number was counted using a haemocytometer and used to calculated the number of Population Doublings achieved (3.32 [log(harvested)-log(seeded)]). Cells grown on glass coverslips were used to estimate the proportion of proliferating cells, using indirect immunofluorescence with an antibody for the proliferation marker Ki-67 (Figure 3.10B). Despite little understanding of Ki-67 function, it is widely used as a marker for proliferation, as it is exclusive to the nucleus of proliferating cells (Kill *et al*, 1996). Figure 3.10C shows representative images of the staining pattern observed for Ki-67.

A

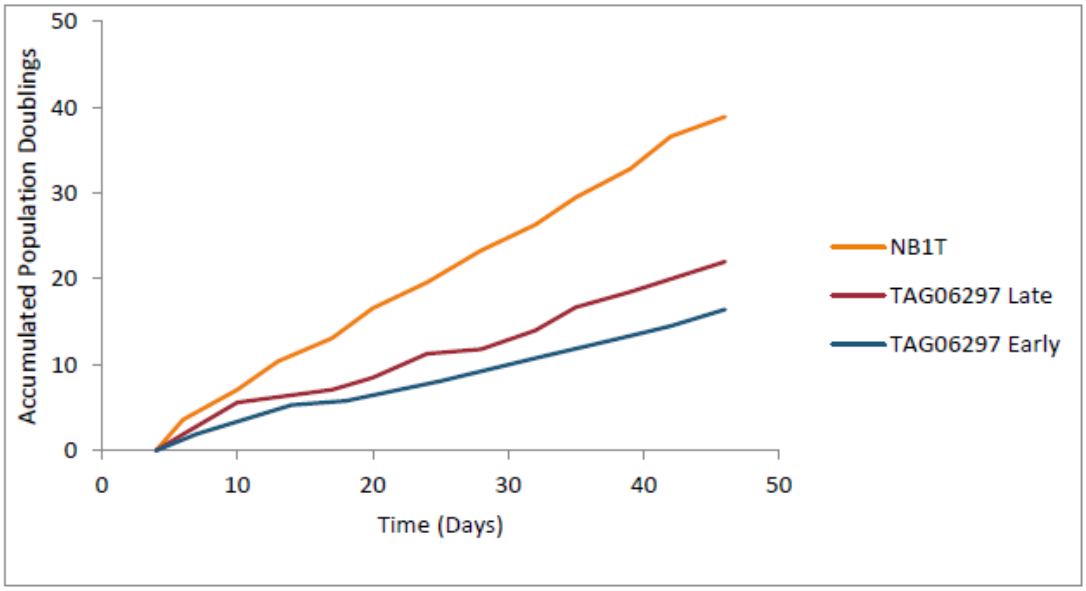

B

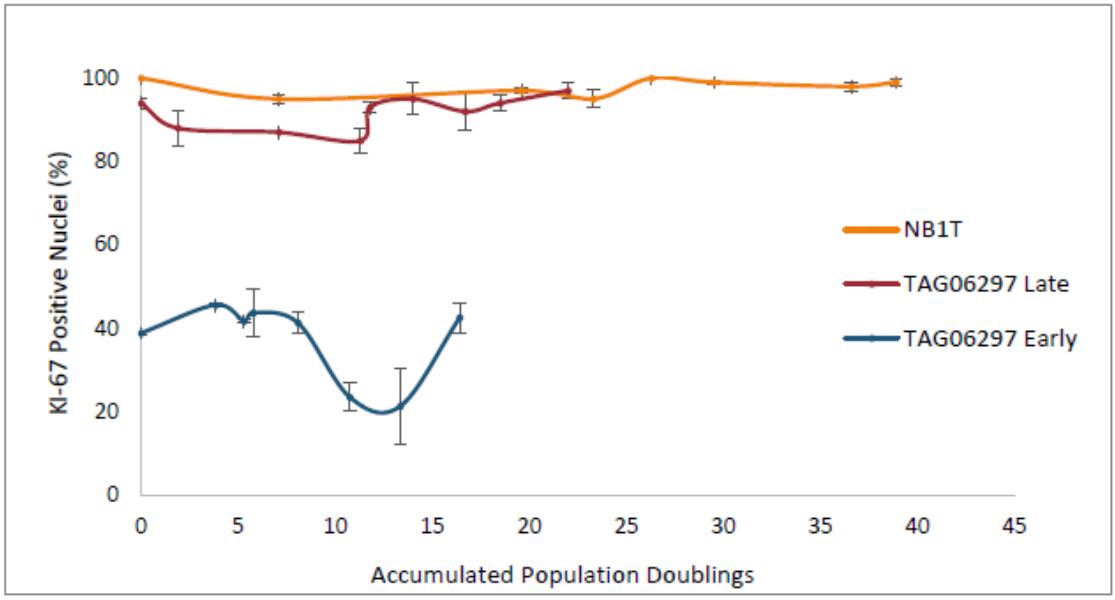
100
80
60
40
20
0
Ki-67 Positive Nuclei (%)
0
5
10
15
20
25
30
35
40
45
Accumulated Population Doublings
NB1T
TAG06297 Late
TAG06297 Early

C

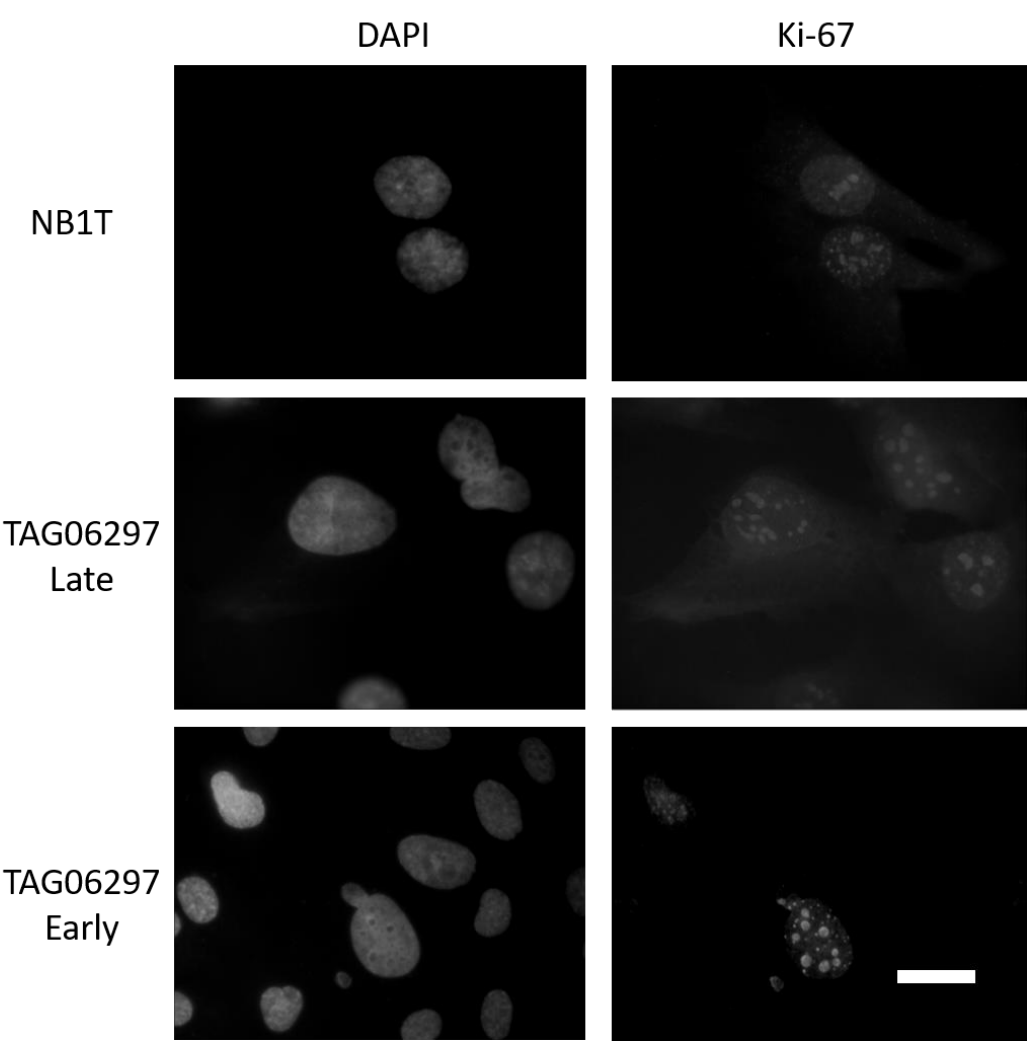
DAPI
Ki-67
NB1T
TAG06297 Late
TAG06297 Early

D

Cell Line	Average PD	APD	Slope	Average Ki-67 +VE Nuclei (%)
NB1T	3.21±0.13	38.9	0.91	98±0.7
TAG06297 Early	1.81±0.27	16.4	0.36	37±3.3
TAG06297 Late	2.23±0.35	22	0.5	91±1.3

Figure 3.10 Growth Potential of hTERT immortalised normal and Hutchinson-Gilford Progeria Fibroblasts

(A) Compares the number of population doublings (PD) achieved by a normal hTERT immortalized fibroblast cell line (NB1T) and Early and Late passage cell lines of the HGPS derived TAG06297, both of which are immortalised with hTERT. Growth curves were constructed from data gathered over a 46 day period and the number of population doublings was calculated using the formula 3.32 [log(harvested)-log(seeded)]. (B) Shows the fraction of proliferating cells within each culture, determined using the proliferation marker ki-67, plotted against the accumulated population doublings (APD) achieved within 46 days. Error bars represent Standard Error of the mean. (C) Representative images displaying how proliferating cells were identified by positive staining for ki-67. Scale bar =10µm. (D) table summarising the growth of each cell line in the 46 day period.

There are observable differences in the growth curves of all three hTERT cell lines, the slopes of which varying from 0.91 to 0.36 APD/Time, with NB1T achieving the most Population Doublings in the time frame. There is a visible difference between the slope of the growth curves for TAG06297 Early and Late, with the TAG062697 Late passage cell line achieving more APDs placing it closer to that achieved by NB1T (Figure 3.10A). The difference of 0.43 PD on average per passage, between the two TAG06297 cell lines, had a notable effect in culture. The higher rate of growth in the TAG06297 Late cell line made it a more viable asset for gaining cell numbers.

When comparing Ki-67 levels within the cultures, both NB1T and TAG06297 Late show a high fraction of proliferating cells, whereas TAG06297 Early has less than half of the cells within the culture contributing to growth (Figure 3.10D). This difference is statistically significant with T-TEST (two tailed) values of $1x10^{-11}$ and

$1.1x10^{-11}$ for NB1T and TAG06297 Late respectively. This difference in proliferating cell fractions may explain the differences in the growth curves and the rate of growth observed in culture between TAG06297 Early and Late. The difference between NB1T (98%) and TAG06297 Late (91%), for Ki-67 positive fraction, is also significant, with a T-TEST (two tailed) value of 0.00047. This demonstrates that continued growth, following immortalisation with hTERT, results in an increased number of proliferative cells within a culture and therefore increase growth. This suggests that changes have occurred within the culture as a result of long-term hTERT expression.

NB1T and TAG06297 Late show less variation in their percentage proliferative cells, suggesting a stability not seen in the TAG06297 Early culture. Analysis of variance within the cultures using F-TESTS, showed no significant difference between NB1T and TAG06297 Late (F-TEST 0.061), however, both showed significantly less variation than TAG06297 Early (F-TEST 0.00031 and 0.016 respectively). The effect of hTERT on Progeria cells appears varied within the TAG06297 Early culture, supporting the hypothesis that hTERT and Progerin act as opposing forces within cells. Despite growth differences, the growth curves for all three cell lines show no indication of levelling off, signifying a stable hTERT immortalisation.

3.2.2 A-Type Lamins

One of the first described characteristics of HGPS fibroblasts is the thickened nuclear rim (Goldman *et al,* 2004). Using electron microscopy the thickness of the lamina is able to be accurately measured and was determined to be significantly thicker in HGPS fibroblasts than controls (Goldman *et al,* 2004). This is a characteristic that can also be observed by immunofluorescence. As progerin is a mutant form of lamin A, unless specifically designed not to, antibodies that target lamin A also visualize progerin. To determine if continued growth in hTERT has any effect on the localisation of A-type lamins to the nuclear envelope or the thickened nuclear rim phenotype, indirect immunofluorescence using antibodies for Lamin A and Lamin A/C was performed (Figure 3.11).

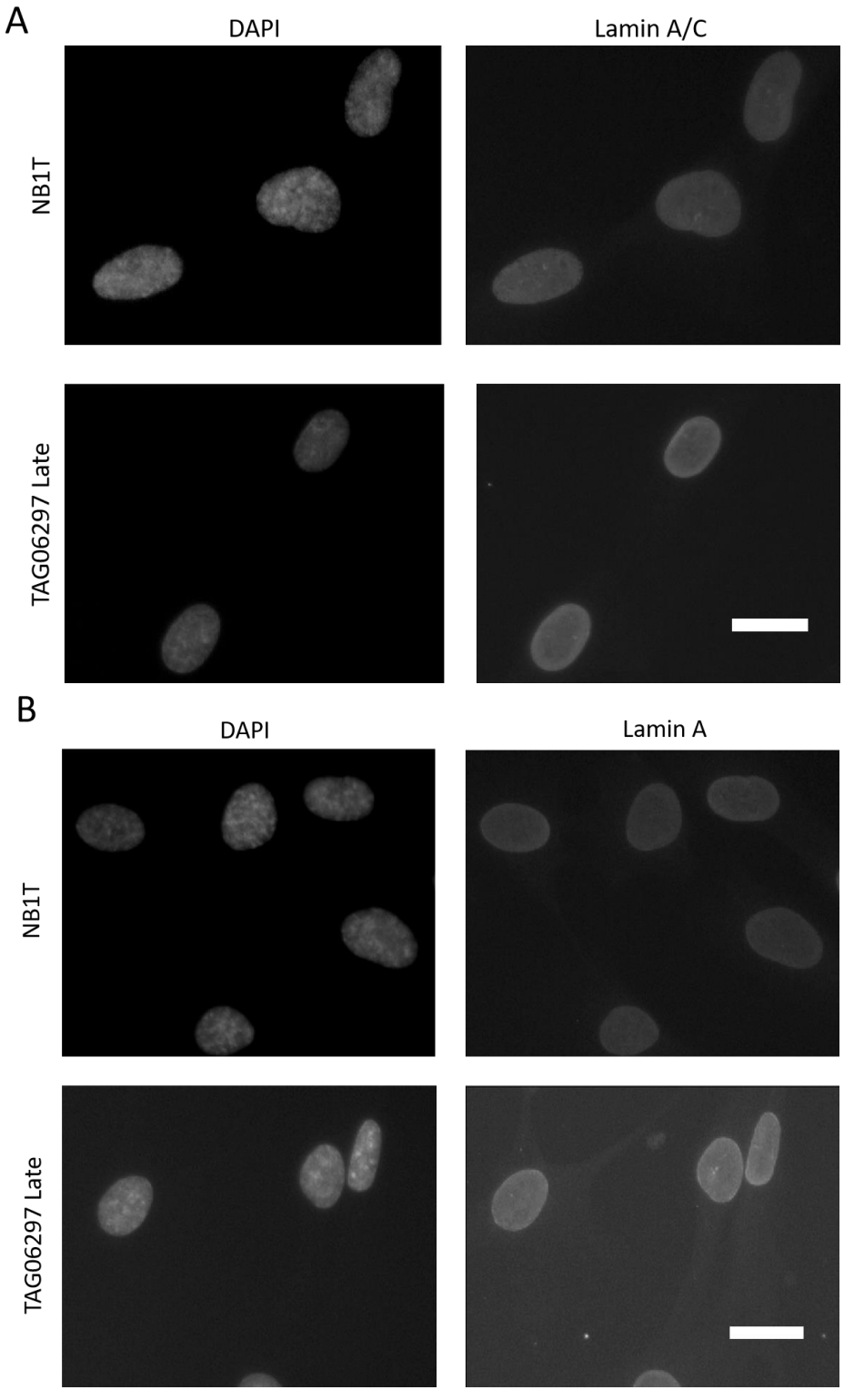

Figure 3.11 Localisation of A-Type Lamins in hTERT immortalised normal and Hutchinson-Gilford Progeria Fibroblasts

Indirect immunofluorescence of hTERT immortalized control fibroblast cell line (NB1T) and Late passage HGPS derived TAG06297 cells, grown on glass coverslip and formaldehyde fixed, using antibodies for Lamin A/C shown in (A), Lamin A shown in (B). Nucleus visualized using DAPI. Scale bar =10 µm.

There are observable differences in the staining pattern of Lamin A and Lamin A/C, for NB1T and TAG06297 Late, in the HGPS cell line a slightly thickened nuclear lamina can be observed. This was significant enough to allow differentiation of these cell lines down the microscope. This is supported by both Lamin A and Lamin A/C antibodies conferring the same staining Pattern. This suggests that hTERT immortalisation does not affect the localisation of A type lamins to the nuclear envelope and suggests a level of progerin within the culture.

3.2.3 Nuclear Morphology

One of the most striking effects of progerin expression within cells is the resulting changes in nuclear morphology. Primary HGPS fibroblasts have been shown to accumulate significantly higher fractions of cells with nuclear membrane blebs, invaginations, micronuclei formation and other abnormal morphologies (Bridger & Kill, 2004; Goldman *et al,* 2004). Since it seems likely that accumulation of gross nuclear abnormalities could have a profound effect on cell cycle events, such as mitosis, we wished to determine how progeria cells coped with increased levels of growth following immortalization with hTERT. Nuclear morphology was analysed in the TAG06297 Early and Late cultures as well as the control cell line NB1T. Cells were cultured on glass coverslips, fixed and mounted in DAPI for nuclear visualisation. The slides were analysed manually and the nuclei showing variation from a smooth elliptical nucleus resulted in a score of abnormal morphology. Figure 3.12A shows examples of normal and abnormal nuclear morphology, the table in Figure 3.12B sumerizes the findings within these cultures.

A

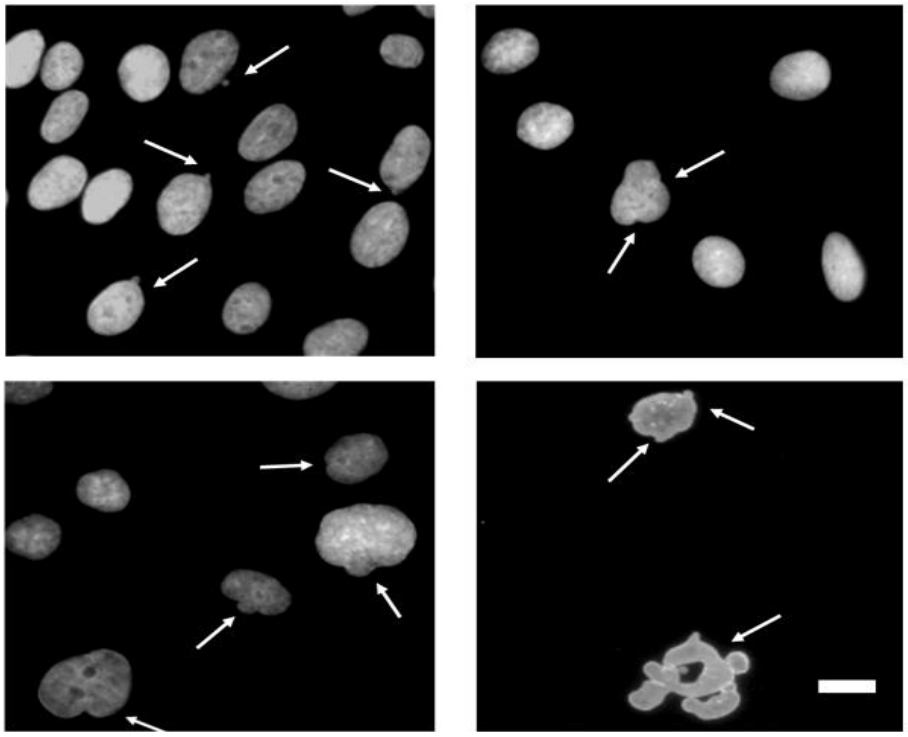

B

Cell Line	% Replicative Lifespan complete	% of Abnormally Shaped Nuclei
NB1T	-	12.9±1.73
TAG06297 Early	-	72.4±1.06
TAG06297 Late	-	14.7±3.12
NB1*	96.2	17.9± 2.0
AG06297*	96.9	70.3 ±4.2

Figure 3.12 Abnormal Nuclear Morphology in hTERT immortalised normal and HGPS Fibroblast cultures

Nuclear morphology was revealed using the DNA stain DAPI and was analysed for shape abnormalities such as, folds or crevices, herniations, lobules and micronuclei. (A) Arrows indicate nuclei identified as having nuclear morphology abnormalities. Scale bar = 10µm. The table in (B) shows the percentage of abnormal nuclear morphology identified in NB1T and Early and Late passage strains of the hTERT HGPS cell line TAG06297 (n=750). Representitative images shown are the TAG06297 Late cell line. *Data for primary cultures is the previously published work of Bridger and Kill, 2004.

NB1T and TAG06297 Late demonstrate a statistically similar fraction of abnormal nuclei within the culture (T-TEST two tailed 0.44). This level of nuclear abnormality is comparable to that of a high percentage replicative lifespan NB1 primary fibroblast culture and much reduced on a high percentage replicative lifespan AG06297 primary culture (T-TEST two tailed $2.5x10^{-4}$). This demonstrates that after a continued period of growth, as a result of hTERT, the fraction of abnormal nuclei in TAG06297 Late cultures is more comparable to that of control cells than to progeria cells. Comparisons made to low percentage replicative lifespan primary NB1 cells show fewer abnormal nuclei 2.3± 0.8%, whereas AG06297 still show a significantly higher level 29.2±2.1. TAG06297 Early, however, demonstrate a level of nuclear abnormality statistically alike to that of AG06297 primary fibroblasts (T-TEST two tailed 0.44). This dramatic change in nuclear morphology between the two TAG06297 cell lines (T-TEST two tailed $7.1x10^{-6}$) suggests a change in progeria cell phenotype, when grown in the presence of hTERT, which results in a higher fraction of cells with a healthier nuclear morphology than that seen in young primary progeria fibroblasts.

3.2.4 Nuclear Size and Shape

To further investigate the effect of continued growth, in the presence of hTERT, image analysis of nuclear size and shape was performed on digital images of cultures. Images of cells grown and fixed on glass cover were analysed using ImageJ software as described in material and methods 2.1.2. By setting the threshold to encompass the nuclear region stained with DAPI, measurements of nuclear size (area and perimeter) and shape (aspect Ratio and Circularity) could be produced. Figure 3.13A gives an example of setting the threshold to encompass the whole DAPI stained region and the table summarises the measurements collected.

A

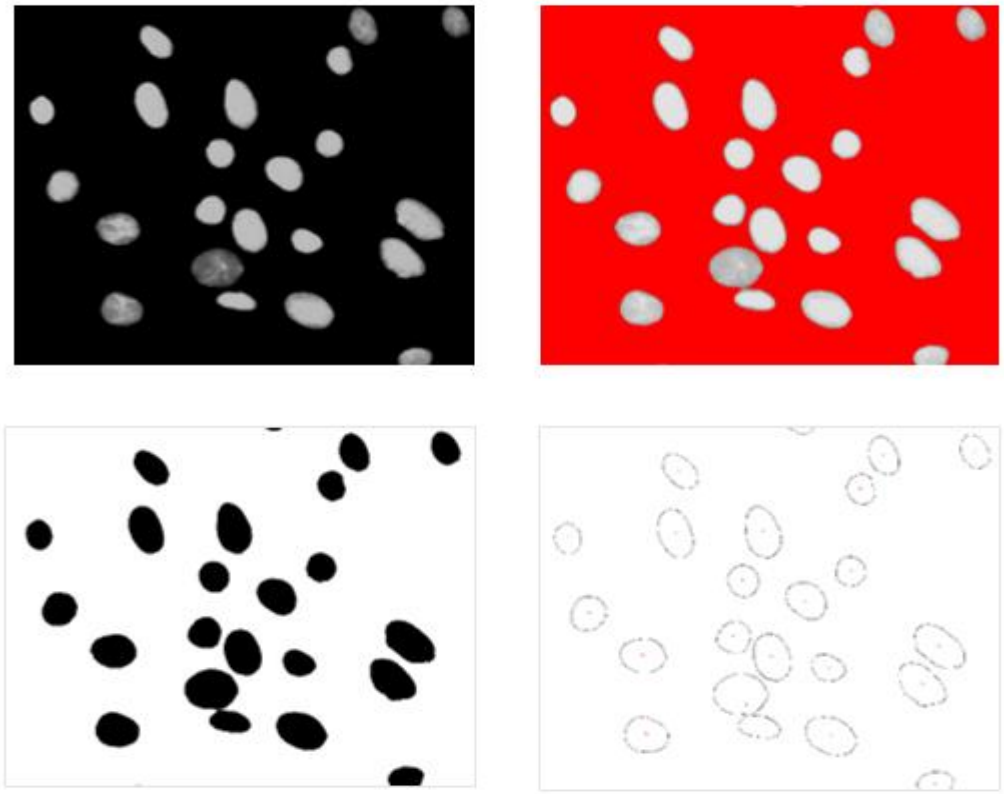

B

Parameter	Description
Area	Contained within Threshold
Perimeter	Length of Outer Edge
Circularity	$C = \frac{4\pi Area}{Perimeter^2}$
Aspect Ratio	$AR = \frac{Major\ Axis}{Minor\ Axis}$

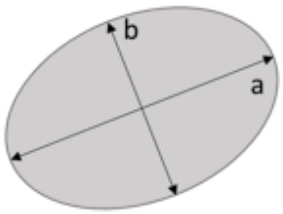

a = Major Axis
B = Minor Axis

Figure 3.13 Thresholding and measuring the nuclei of hTERT immortalised normal and HGPS Fibroblast cultures using ImageJ software

Cells grown on cover slips were formaldehyde fixed and mounted in DAPI. Images of the nucleus were captured and analysed using ImageJ particle analysis software. The nuclear regions were defined by adjusting the pixel threshold (red) then converted to numbered outlines corresponding to the measurements (A). The table in (B) summarizes the measurements collected using this software.

Figures 3.14 and 3.15 show data presented as both frequency distributions and box plots, in order to sufficiently display variations in the distribution of nuclei observed in a culture as well as making comparisons between the means. Data was collected for both NB1T (control) cell line as well as TAG06297 Late cells.

A

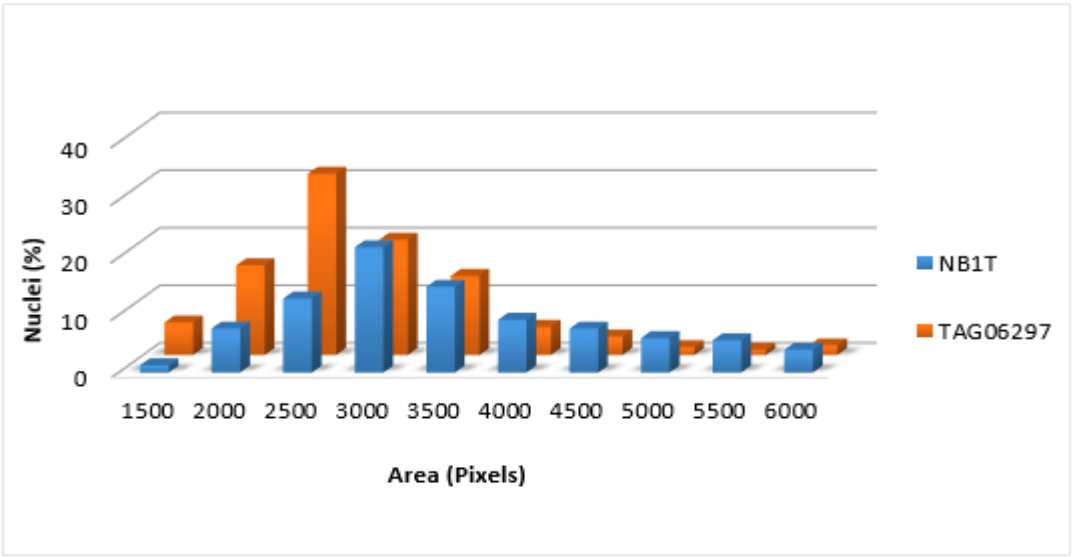

B

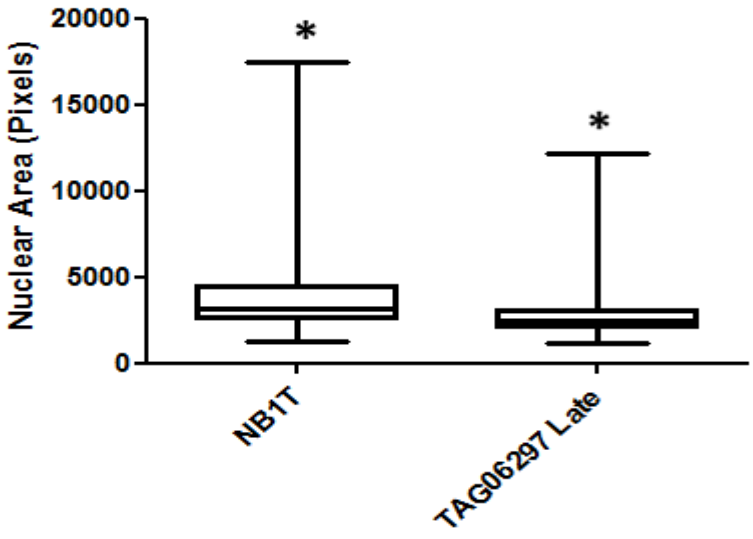

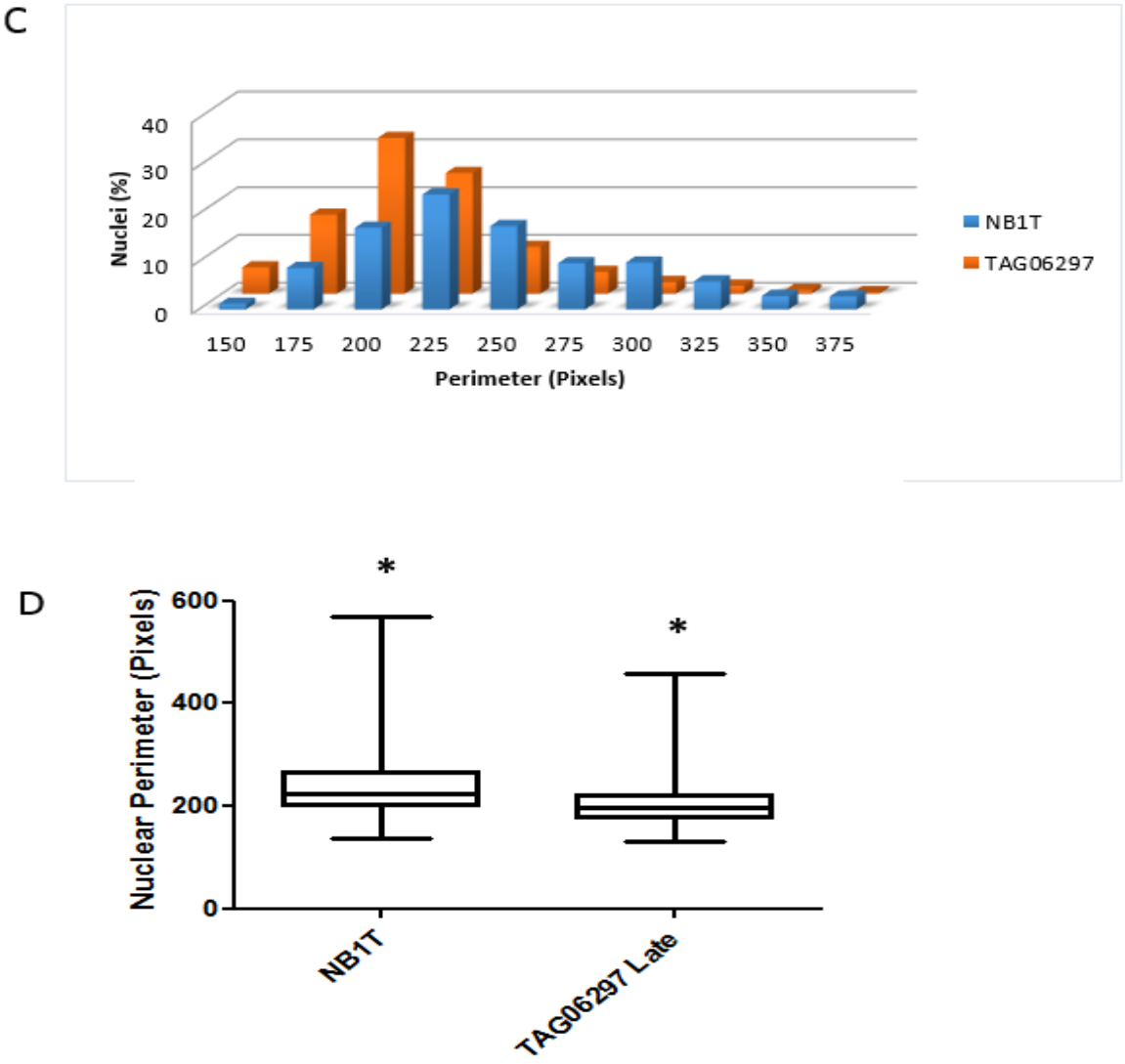

Figure 3.14 Computational Analysis of Nuclear Size in hTERT immortalised normal and HGPS Fibroblast cultures

NB1T is a normal fibroblast cell line that has been immortalised with hTERT and TAG06297 Late is HGPS derived and hTERT immortalised. Analysis using ImageJ software to measurements nuclear area, displayed as a frequency distribution (A) and a box plot (B) and nuclear perimeter displayed as a frequency distribution (C) and a box plot (D). * identifies statistically significant differences between the two cell lines.

A

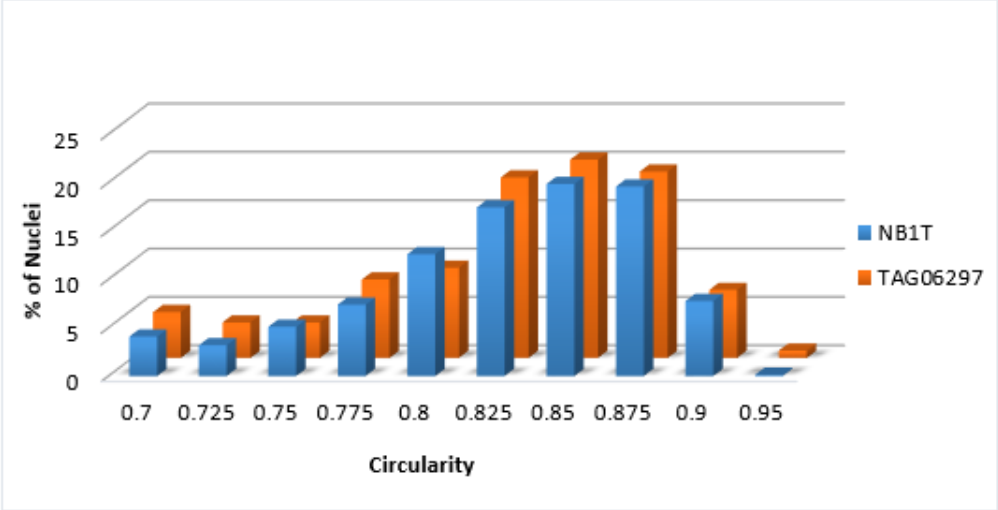
25
20
15
10
5
0
% of Nuclei
0.7
0.725
0.75
0.775
0.8
0.825
0.85
0.875
0.9
0.95
Circularity
NB1T
TAG06297

B

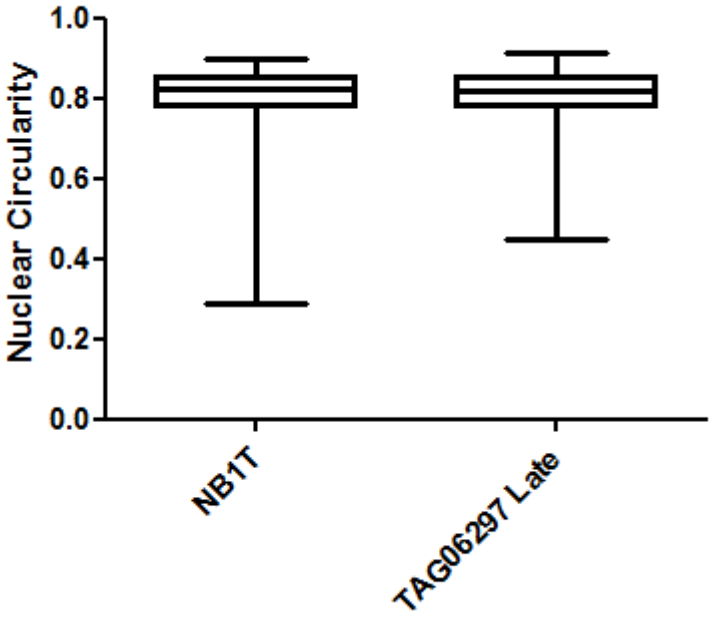
1.0
0.8
0.6
0.4
0.2
0.0
Nuclear Circularity
NB1T
TAG06297 Late

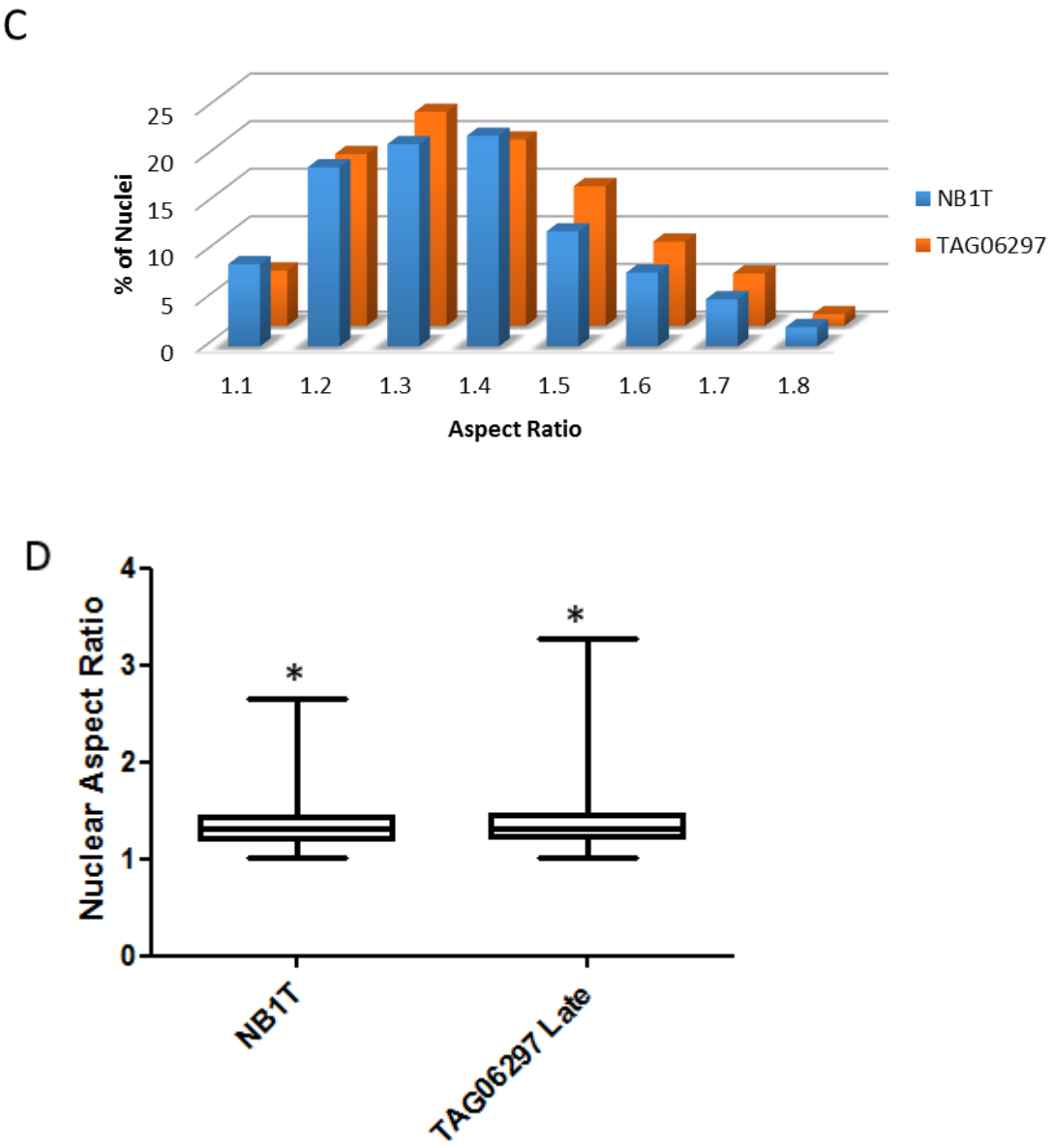

Figure 3.15 Computational Analysis of Nuclear Shape in hTERT immortalised normal and HGPS Fibroblast cultures

NB1T is a normal fibroblast cell line that has been immortalised with hTERT and TAG06297 Late is HGPS derived and hTERT immortalised. Analysis using ImageJ software to measurements nuclear Circularity and displayed as a frequency distribution (A) and a box plot (B) and nuclear Aspect Ratio displayed as a frequency distribution (C) and a box plot (D). * identifies statistically significant differences between the two cell lines.

Comparisons between NB1T and the TAG06297 Late cultures reveal statistically significant differences in nuclear size, as defined by area (T-TEST two tailed

<0.0001) and perimeter (T-TEST two tailed <0.0001). In accordance with previous findings for primary HGPS fibroblasts, the TAG06297 Late cells were found to have smaller nuclei (Choi *et al*, 2011). This suggests that hTERT expression in HGPS cells does not modify nuclear size.

Aspect ratio and Circularity (Figure 3.15) measurements were both used to examine nuclear shape. Previous reports show HGPS fibroblasts to have, on average, a higher fraction of circular nuclei than those observed in healthy controls (Choi et al 2011). Using the same calculation of Circularity, no significant difference was identified between NB1T and TAG06297 Late cell lines (T –TEST two tailed 0.6410) with even the distribution of nuclei appearing similar. Furthermore, Aspect ratio was found to be statistically significantly higher for TAG06297 Late than NB1T (T-TEST two tailed 0.0171), suggesting that cell of this line do not have a more circular appearance but instead have ellipsoid nuclei, such as that observed in healthy cells. This shift in nuclear shape supports the hypothesis that hTERT expression modifies the phenotype of HGPS cells, resulting in a healthier appearance.

3.2.5 DNA Damage

Another characteristic of HGPS cells is the increased level of double strand DNA breaks, which are thought to contribute to replicative arrest (Liu *et al*, 2005). In order to investigate the potential effect of hTERT on DNA damage levels in HGPS cells, both TAG06297 Early and Late and NB1T were stained using an antibody against the double strand break DNA damage marker γH2AX. Figure 3.16A-C shows the staining observed using γH2AX and the table in Figure 3.16D summarizes the proportions within each culture.

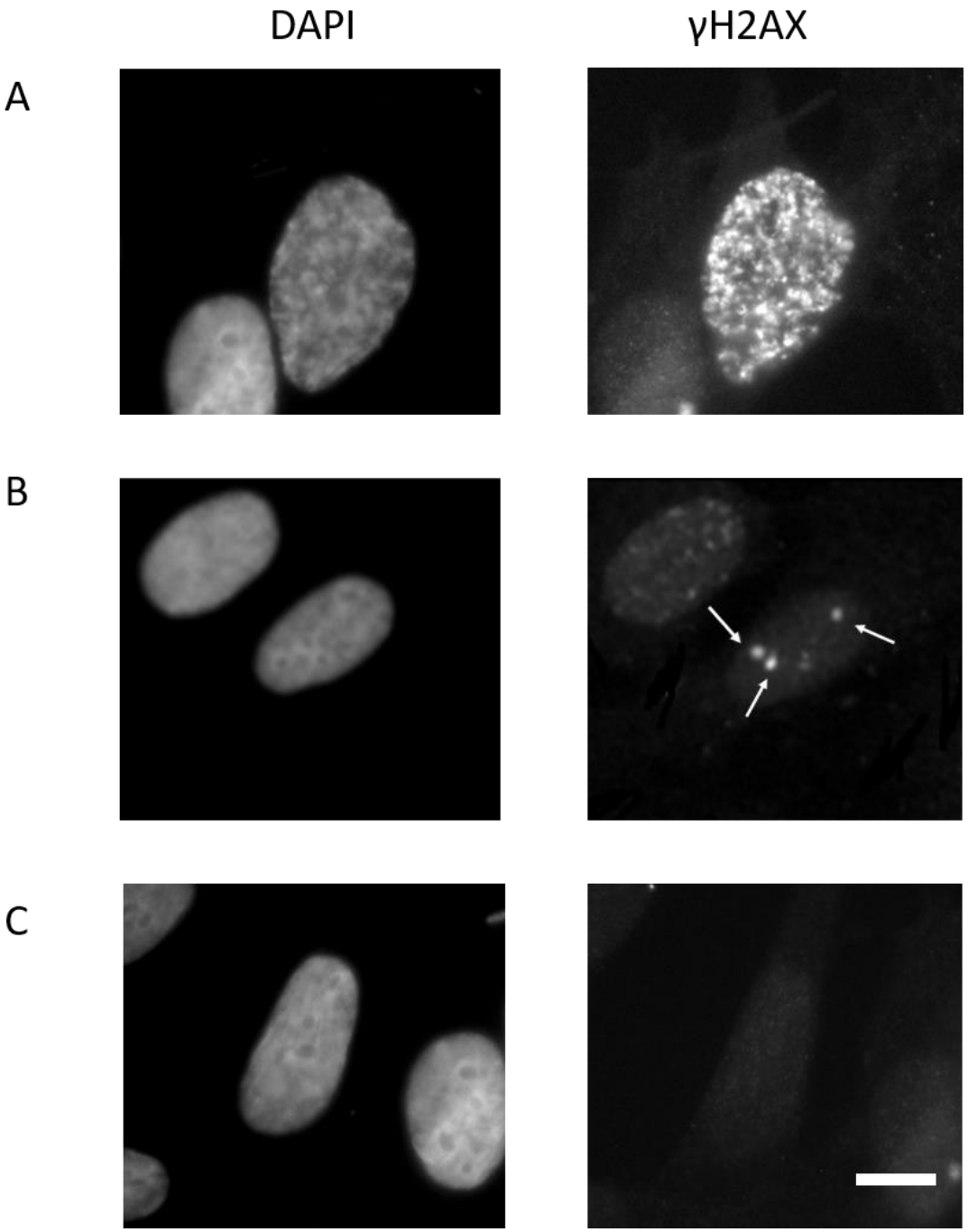
DAPI
γH2AX
A
B
C

Cell Line	Speckles	Discrete Foci	No Foci
NB1T	0.5±0.5	6.6±1	92.5±1.3
TAG06297 Early	81.6±4.2	11.1±5.6	7.2±2.6
TAG06297 Late	26.4±2.5	7.9±2.6	65.7±4.1
T Test (Early vs Late)	$3.95X10^{-5}$*	0.42	0.001*

Figure 3.16 DNA Damage Markers in hTERT immortalised normal and HGPS Fibroblast cultures

Presence of DNA damage was analysed using an antibody against the DNA damage marker γH2AX. Two distinct staining patterns were identified (A) shows the presence of many speckles and (B) shows the discrete foci. γH2AX negative cells are shown in (C). Scale bar = 10μM. (D) summarizes the percentage composition of a normal fibroblast culture immortalised with hTERT and Early and Late strains of the HGPS hTERT fibroblast cell line TAG06297. *indicates statistically significant (T-TEST two tailed) shift from no foci to speckles between the Late and Early passage TAG06297 cultures.

When analysing the cell lines for the marker γH2AX, two staining patterns were identified. One staining pattern includes cells that contained one or several large foci within the nucleus (Figure 1.6A), likely correlating to individual or low amounts of double strand DNA break sites (Löbrich *et al*, 2010). The proportion of cells displaying this type of staining was consistent between all three cell lines (T-TEST two tailed >0.24), highlighting this as a typical level of DNA damage within a hTERT culture. The second pattern revealed a great number of small speckles of γH2AX throughout the nucleus (Figure 1.5B). This pattern was observed in both HGPS cultures although the TAG06297 Early had a statistically significantly higher proportion of nuclei with this pattern (T-TEST two tailed $3.95X10^{-5}$). This pattern correlates with higher levels of DNA damage within the cells, which could result in them exiting the cell cycle (Liu *et al*, 2005). This speckled appearance may in fact correspond to increased levels of DNA damage as a consequence of progerin expression, as this staining pattern was virtually unidentified in the control cell line.

Cells were also observed with no positive staining for γH2AX (Figure 3.16C) consistent with no detectable double stranded DNA damage within that cell. The majority of NB1T (control) cells, showed no staining for γH2AX. A shift from a speckled appearance to more nuclei with no foci can be observed in the TAG06297 Late culture (Figure 3.16D). This reduction in DNA damage between TAG06297 Early and TAG06297 Late, suggested that continued growth in the presence of hTERT does affect progeria cell characteristics. It is reasonable that a reduction in the level of DNA damage would enable cells to continue progressing through the cell cycle.

3.2.6 Cell Motility

Despite having the ability to proliferate, primary HGPS fibroblasts have been shown to have reduced cell motility, which leads to a decreased ability to heal wounds in culture (Verstraeten *et al*, 2008). In order to investigate whether hTERT has any effect on progeria characteristics not directly linked to cell proliferation, cell movement was analysed using live imaging. Time lapse videos, with five minute intervals, were produced over an eight hour period, for TAG06297 Early and Late and NB1T. Once all of the images had been captured they were converted into a stack in ImageJ software and the Manual Tracking Pluggin was used to follow an individual cell through each image. By following the nucleus of the cell through each frame, coordinates were generated that could then be plotted on a graph. Figure 3.17A shows an example of one cell in the first and the last frame of the stack and the yellow line represents the route travelled by that cell. Figure 3.17B-D shows all the individual cell tracks for each cell line plotted on separate graphs. It is apparent from these graphs that NB1T (Figure 3.17B) travelled further in the 8 hour period, as demonstrated by the longer track lines. This is a result of both TAG06297 cell lines remaining in the same position between several frames therefore not adding any travel to their tracks. Although, TAG06297 Late (Figure 3.17D) does show a higher amount of movement than TAG06297 Early (Figure 3.17C), when comparing the two graphs. This is consistent with observations made by visual inspection of the time lapse videos.

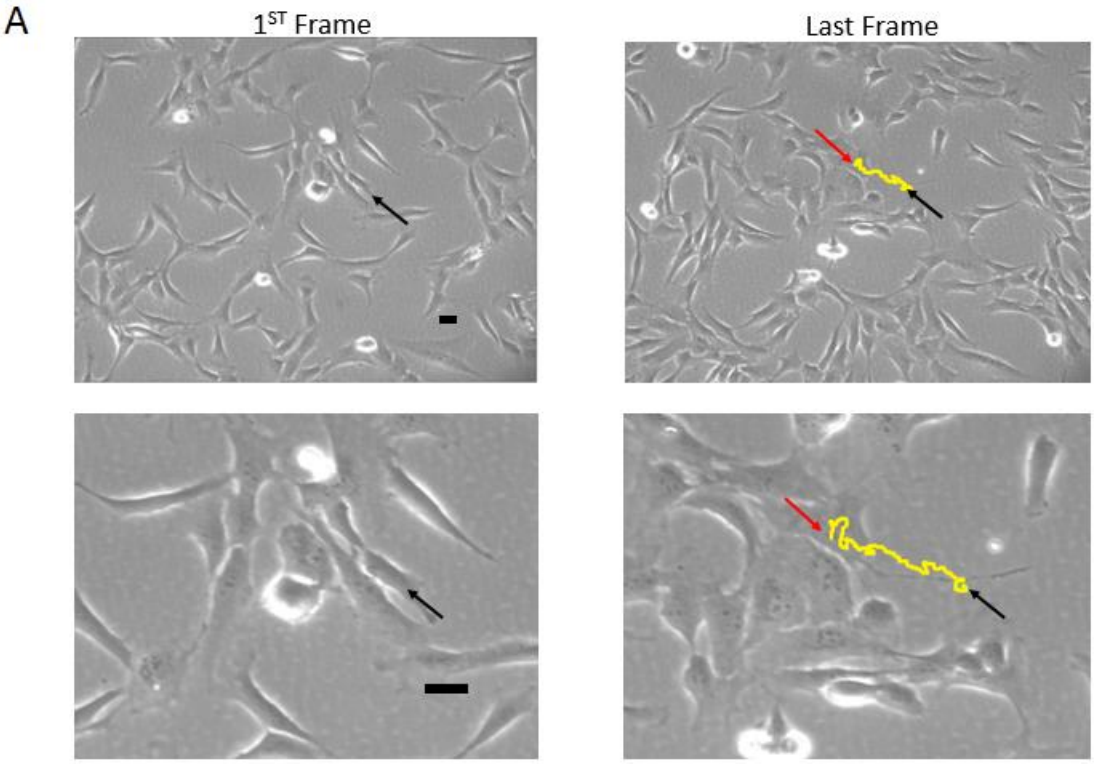
A
1ST Frame
Last Frame

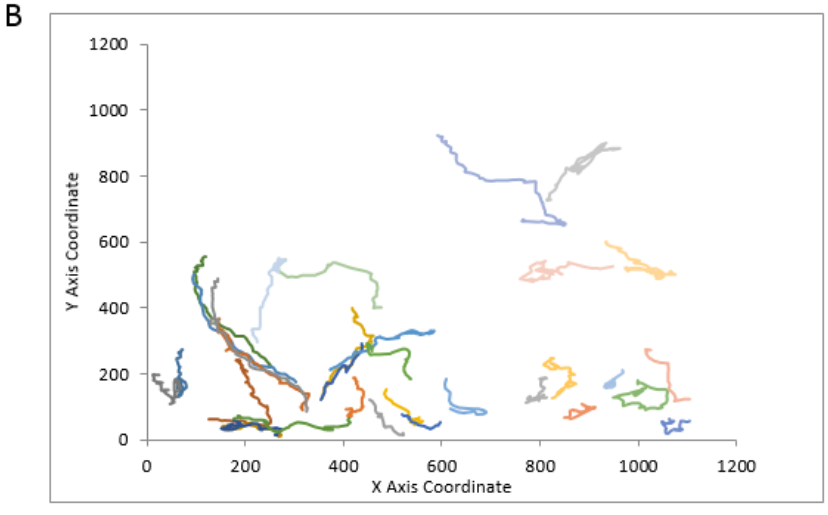
B
1200
1000
800
600
400
200
0
Y Axis Coordinate
0
200
400
600
800
1000
1200
X Axis Coordinate

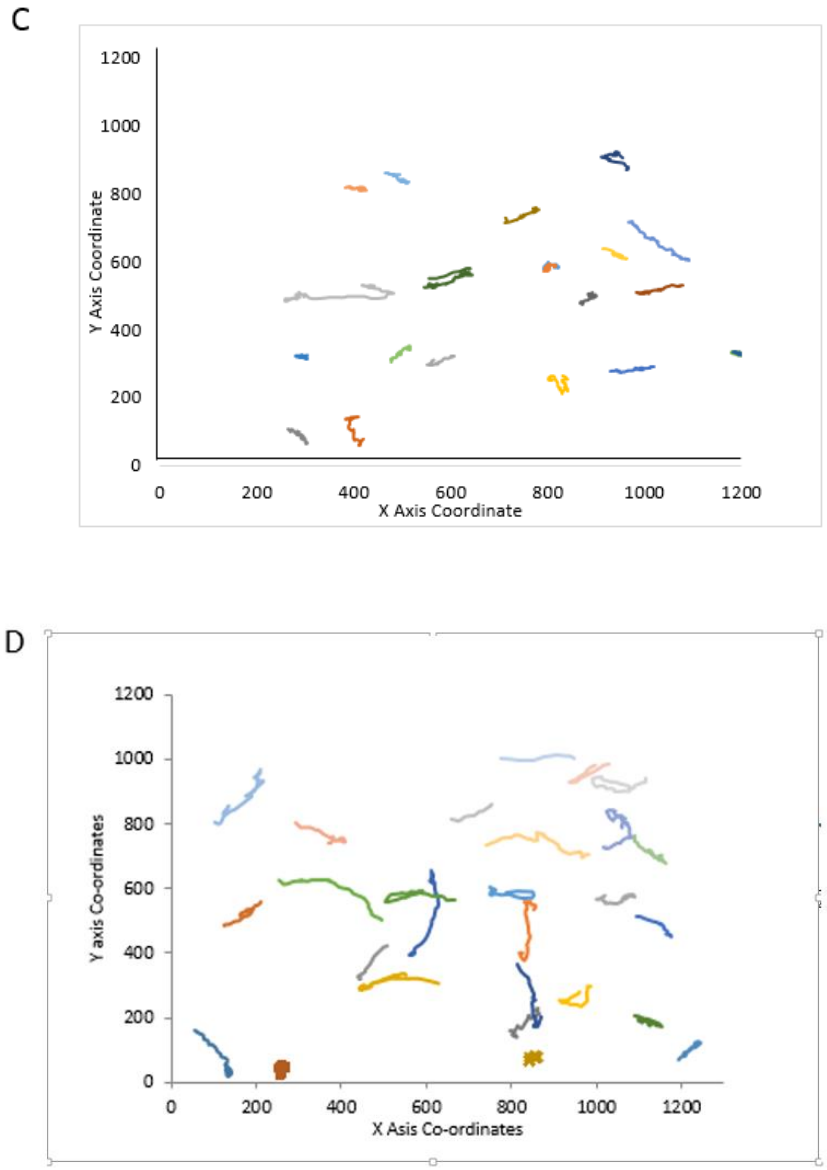

Figure 3.17 Generation of Time Lapse Videos showing Cell Movement in hTERT immortalised normal and HGPS Fibroblast cultures

Time lapse images were taken every 5 minutes for an 8 hour period. Using the Manual Tracking Plugin on ImageJ software, individual cells were given X and Y axis co-ordinates and their movement was tracked through all 96 images. (A) shows the first image taken and the black arrow highlights the start position for an individual cell and the 96th Image taken, where the black arrow indicates the start position of the cell and the red arrow shows the end position. The yellow line shows the track of the cell movement between the start and end point. Scale bars = 10 µm. The coordinates for each cell were plotted on a graph, where each line represents a single cell's movement. (B) shows the cell movement for a normal fibroblast cell line that has been immortalised with hTERT (NB1T). (C) shows Early and (D) shows Late passage strains of the HGPS derived TAG06297, immortalised with hTERT.

In order to further analyse the time lapse videos all cell tracks were centred to the middle of the graph, allowing comparison form a standardized start point (Figure 3.18A-C). The average total distance and displacement (distance from start point to end point) have been marked on the graphs. The black circles, represent the average total distance achieved by cells in that culture. NB1T achieved the greatest distance moved (Figure 3.18A), which was statistically higher than both TAG06297 Early and Late cell lines (T-TEST two tailed $5.5x10^{-6}$ and 0.0006 respectively). The TAG06297 cell lines differed statistically from each other (T-TEST one tailed 0.026) with TAG06297 Late cells on average moving a greater distance.

A

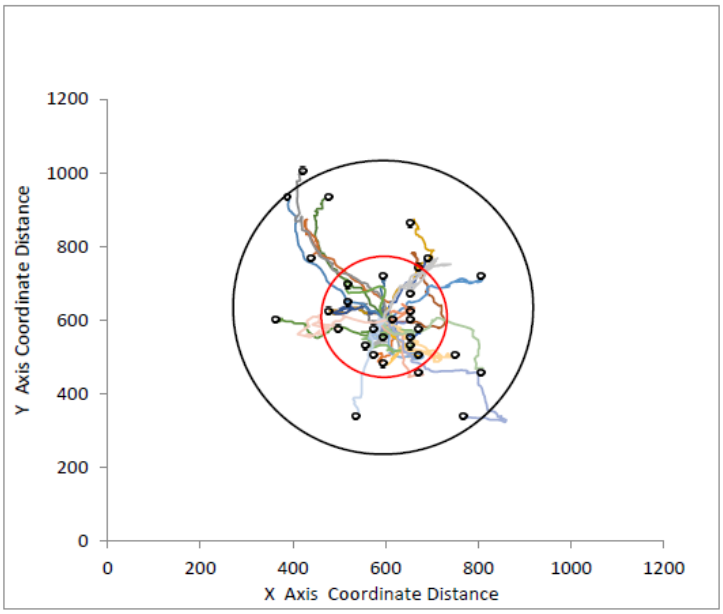

B

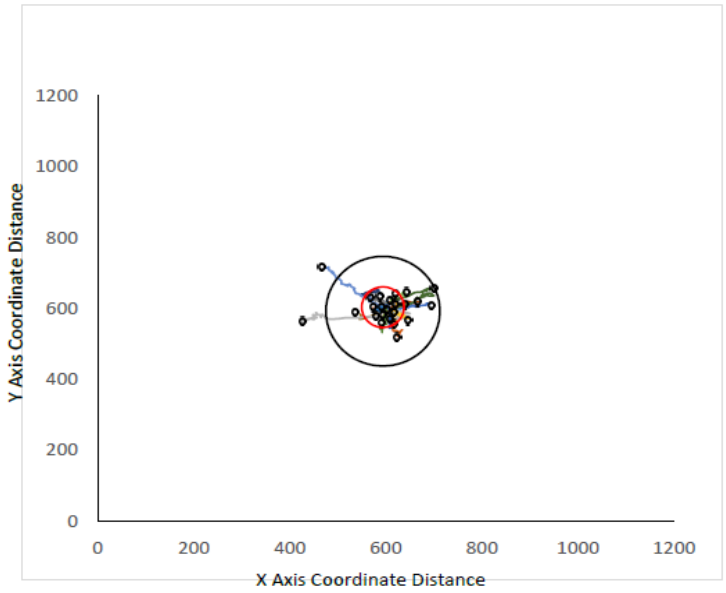
1200
1000
800
600
400
200
0
Y Axis Coordinate Distance
0
200
400
600
800
1000
1200
X Axis Coordinate Distance

C

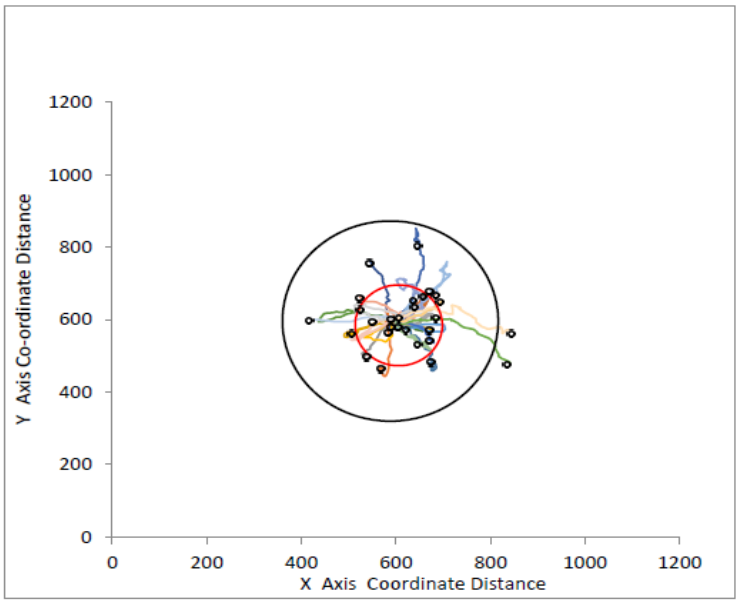
1200
1000
800
600
400
200
0
Y Axis Co-ordinate Distance
0
200
400
600
800
1000
1200
X Axis Coordinate Distance

D

Cell Lines	Cell Average Total Distance (µm)	Cell Average Total Displacement (µm)	Cell Average Velocity (µm/sec)	Meanderings Ratio
NB1T	238.27±17.01	109.24±12.60	29.78±2.1	0.46±0.03
TAG06297 Early	125.29±12.36	31.04±5.56	15.66±1.54	0.24±0.02
TAG06297 Late	159.69±12.07	66.63±8.81	19.96±1.51	0.43±0.03

Figure 3.18 Analysis of Cell Movement in hTERT immortalised normal and HGPS Fibroblast cultures

Time lapse images taken every 5 minutes for an 8 hour period were used to produce X and Y axis co-ordinates for individual cells through all 96 images. The coordinates for each cell were centred and plotted on a graph, where each line represents a single cell's movement. The black circle represents the average total distance moved in 8 hours and the red circle shows the average displacement (the difference between start and end locations). (A) shows the cell movement for a normal fibroblast cell line that has been immortalised with hTERT (NB1T). (B) shows Early and (C) shows Late passage strains of the HGPS derived TAG06297, immortalised with hTERT. (D) Summaries the average movement made by each cell line including the velocity and the meandering ratio (total displacement/total distance).

In order to analyse the type of movement made by each cell line the Meanderings Ratio was determined, by dividing the displacement by the distance (Figure 3.18D). This identifies if cells are moving round in circles or whether they show greater directionality to their movements. The Meanderings Ratios show that NB1T and TAG06297 Late demonstrate the same pattern of movement (T-TEST two tailed 0.62), with a tendency to more linear advances, whereas the TAG06297 Early appear to move within a small area. The movement displayed by TAGO6297 Early differs significantly from that of both NB1T and TAG06297 Late (T-TEST two tailed $3.95x10^{-5}$ and 0.003 respectively).

In order to heal wounds effectively cells must move forward into the available space (Verstraeten *et al*, 2008), this suggests that the meandering ratio of NB1T and TAG06297 Late is more ideal for this task. The ability to heal wounds is also affected by rate of movement (Verstraeten *et al*, 2008), therefore, the average cell velocity was also calculated for each cell line. NB1T cells demonstrated a statistically significantly faster velocity compared to both TAG06297 cell lines (T-

TEST two tailed 0.0006). The rate of velocity (Figure 3.18D) is also increased in the TAG06297 Late compared with the Early (T-TEST one tailed 0.026) culture bringing it closer to that of the control, yet still statistically less. This suggests that the presence of hTERT within HGPS cells has affected the type of movement and increased cell velocity, both of which would enable better wound healing, demonstrating characteristics of a healthier cell phenotype.

3.3 Discussion

The aim of this study was to determine if hTERT immortalisation of HGPS cells resulted in a loss of progeria cell phenotype, which would significantly reduce their wide-spread usability in research. From the results it is evident that several differences between TAG06297 Early and Late have been observed in response to hTERT expression. The continued growth and limitless replicative potential is advantageous and in line with previous studies successfully showing lengthened telomeres and increased lifespan, including the paper describing the immortalisation of this cell line (Benson *et al*, 2010; Kudlow *et al*, 2008; Ouellette *et al*, 2000; Wallis *et al*, 2004).

The fraction of cells contributing to the growth is also in line with previous findings, which showed the lack of the senescence marker β-galactosidase in over 80% of hTERT HGPS cell (Benson *et al*, 2010). Here we observe more than 80% of cells from the TAG06297 Late culture as positive for the proliferation marker Ki-67. The previous study however, reported immediate changes in response to hTERT as soon as 14 days later, whereas here we see TAG06297 Early cells have only around 30% contributing to growth, with the assumption that the other 70% are senescent. This finding supports previous work that suggesting that HGPS cells can still senesce despite hTERT expression and suggests an outgrowth of cells not telomerase resistance (Wallis *et al*, 2004). This explains the differences observed between the Early and Late cultures.

When comparing nuclear abnormalities, a similar proportion of nuclei were observed to have abnormalities as to be proliferatively inactive. Although this study does not

make a direct link between these two properties, the changes observed between the Early and Late TAGO6297 cultures does provide evidence for a link between senescence bypass and healthy cell phenotype. This contradicts previous findings where no improvement in nuclear shape was observed (Kudlow *et al*, 2008). As the improvement in nuclear shape was only observed in the Late culture it is possible that this reduction was not determined in the previous study as cells were not grown for the same time period. This again provides evidence for an outgrowth of immortalized HGPS cells from a senescent background and indicates that the mechanism by which these cell bypass senescence has impacts on the whole progeria phenotype.

The reduction in DNA damage observed in the TAG06297 Late culture is also in line with previous findings, which identified a more than 80% reduction in DNA damage specifically associated with telomeres (Benson *et al*, 2010). Again, however, this study identified these changes as rapidly as 7 days after immortalisation, whereas in the Early TAG06297 cultures we see a large proportion of cells with a level of DNA damage similar to that described for primary cultures. This again suggests an outgrowth of cells with a more healthy phenotype, brought about by hTERT, that are able to continue through the cell cycle likely due to a reduction in DNA damage.

In this study we have identified a reduction in nuclear abnormalities, a similar nuclear shape as control cells, a reduction in DNA damage, an increase in cell motility and an increase in the proliferative active proportion of culture between Early and Late passage cells. This overall suggests that hTERT immortalization of HGPS cells does have long-term effects on progeria cell characteristics, which results in a more normal and healthy cell phenotype. This limits the usability of this cell line to study HGPS with several of the most common and easily observable markers of the disease cell phenotype being rectified to nearly undeterminable from a healthy cell population.

Similar results to those observed in this study, have been achieved by RNA interference, using shRNAs to reduce the expression of progerin by 26%. This reduction in progerin in HGPS fibroblasts improved nuclear morphology, increased cell proliferative lifespan and reduced the premature senescence of HGPS cultures

(Huang *et al*, 2005). A second study using splicing correction to eliminating the use of the cryptic splice site also observed correction of the HGPS phenotype (Scaffidi & Misteli, 2005). This led to the conclusion that gene therapy could be employed to rectify progeria cell characteristics and therefore, treat HGPS. By directly reducing the level of progerin within HGPS cells these studies achieved the same result as the natural outgrowth of hTERT immortalised HGPS cells.
This cell line does present a rare opportunity to investigate the changes that have taken place over time, in response to hTERT, that have ultimately been able to rectify many consequences of progerin production. As previously stated, one hypothesis is that telomere length is an upstream regulator of progerin, which inversely effect its production (Cao *et al*, 2011). This would suggest that the immortal TAG06297 cells have decreased progerin expression and thus progerin protein, resulting in improved cell phenotype. The other theory is that telomere length is a key factor in triggering DNA damage-induced by progerin and by artificially lengthening the telomere the ability for progerin induced senescence is reduced (Benson *et al*, 2010).

By further understanding the mechanism by which these cells have negated premature senescence in response to hTERT, this pathway could be exploited for drug development. Current efforts focus on the reduction of progerin by upstream processing inhibitors (FTI's) (Capell and Collins, 2006) or general increase in protein turn-over (Rapamycin) to remove the mutant progerin (Cao et al, 2011). The use of these drugs *in vitro* has yielded similar improvements in progeria cell characteristics as those observed in this study, including nuclear shape (Capell et al, 2005; Glynn and Glover, 2005; Toth et al, 2005; Mallanpalli et al, 2005; Cao et al, 2011), DNA damage (Cao *et al*, 2011), cell motility (Valerie *et al*, 2008) and increased lifespan in culture (Cao et al, 2011). So although this cell line may have little use for the study of long-term effects of these drugs, it opens up new possibilities for identifing new targets in the treatment of HGPS.

4 Investigation in to the effect of hTERT immortalisation on Progerin in HGPS Fibroblasts.

4.1 Introduction

The identification of loss of progeria cell phenotype in the hTERT immortalised HGPS cell line TAG06297 late (Chapter 3), has raised questions about the abundance of the mutant protein progerin within these cells. Progerin has been described as having a dominant negative effect (De Sandre-Giovannoli *et al*, 2003; Eriksson *et al*, 2003), where ectopic expression of progerin in control cells has resulted in a progeria cell phenotype (Fong *et al*, 2009; Luo *et al*, 2014). The exclusion of progerin from HGPS cells has been achieved using oligonucleotides that target the cryptic splice site, resulting in only wild type transcripts (Scaffidi and Misteli, 2005). In these cells a reversal of the progeria phenotype was observed (Scaffidi and Misteli, 2005). This suggests that the improvement in progeria cell phenotype in the TAG06297 Late cell line, in response to hTERT immortalisation, is linked to a reduction in the toxic mutant protein progerin.

A reduction in Progerin expression in response to hTERT immortalisation of HGPS cells has previously been observed (Cao *et al*, 2011). Using Quantitative PCR, one study identified an up to 10 fold reduction in progerin expression relative to total *LMNA* transcription in response to hTERT immortalisation (Cao *et al*, 2011). A total lack of progerin expression was also observed in hTERT immortalised controls cells, whereas progerin was detectable in primary control cell lines, albeit at a 50 fold lower concentration than in HGPS fibroblasts (Cao *et al*, 2011). This study concluded that lengthened telomeres acts as an upstream signal for regulating progerin production in both HGPS and normal cells (Cao *et al*, 2011).

The method used to detect *LMNA* expression in this study was QPCR using SYBR® Green (Cao *et al*, 2011). Though this method is often used, largely due to economic considerations, several limitations have been observed with the use of SYBR®

Green, in particular the inability to determine if the product of interest is really being amplifed (Bustin *et al*, 2009). This is of particular relevance when comparing the abundance of lamin A and progerin, that are generated through alternative splicing (Eriksson *et al*, 2003), and therefore share a great deal of sequence homology. False positives have been observed in probe-based assays using SYBR® Green, where the presence of primer dimers has reduced PCR efficiency (Bustin *et al*, 2009). The study in question identified as much as 15% of *LMNA* expression products being progerin in a control cell and a 5 times higher number of progerin molecules than lamin A being expressed in HGPS fibroblasts (Cao *et al*, 2011). This suggests that the use of SYBR® Green to assess *LMNA* expression has led to the over representation of progerin within these cells.

A second study using SYBR® Green to quantify lamin A and progerin expression determined substantially less progerin expression in control cells, with progerin being identified as accounting for only 1% of *LMNA* transcripts (Scaffidi & Misteli, 2006). No increase in this value was seen even when examining control cells from elderly donors, and it was concluded that progerin is expressed at a 50x higher level in HGPS cells than all controls (Scaffidi & Misteli, 2006). One weakness in the experimental design of this QPCR, is the need to induce 3 sequence mutations in order to differentiate been lamin A and progerin transcripts (Scaffidi & Misteli, 2006). This again calls into question the specificity of this approach.

Rodriguez *et al*, designed a TaqMan® probe method for QPCR analysis of *LMNA* transcription products. This study used 9 HGPS primary cell lines, including AG06297 cell line, from which the TAG06297 cell line originates, and found that progerin is expressed 160 fold more in cells from HGPS patients than from aged matched controls (Rodriguez *et al*, 2009). They identified an increase in progerin expression with age in both HGPS and control fibroblasts (Rodriguez *et al*, 2009). This study demonstrates to date, the most robust method for the quantification of *LMNA* expression, however, the placement of the forward primer 4 nucleotides from the probe has been criticised. This methodology again demonstrates a potential bias for the over representation of progerin.

With limitations in all previous attempts to establish progerin expression, this identifies the need for a new QPCR design, capable of reliably distinguishing and estimating *LMNA* transcripts. A new system would also enable more accurate estimation of progerin involvement in normal human ageing.
The aim of this chapter is to identify the effects of hTERT immortalisation on *LMNA* expression and progerin abundance within TAG06297 Late cells. We wish to determine if the loss of progeria cell characteristics in the TAG06297 cell line is resulting from a reduction in the amount of mutant protein Progerin. This will involve the use of a novel QPCR design to quantify *LMNA* expression and Western blot and indirect immunofluorescence analysis to examine progerin at the protein level. Through understanding how hTERT immortalisation led to an improved cell phenotype in HGPS fibroblasts (Chapter 3), potential avenues for therapy could be identified.

4.2 Results

4.2.1 Progerin expression Level

The first step in determining progerin expression in the TGA06297 Late cells was using RT-PCR. Primers designed over the exon 11 – exon 12 junction distinguish between lamin A and progerin transcripts. For primer details see methods and materials 2.3.1 Figure 4.19 shows the resulting agarose gel, following RT-PCR.

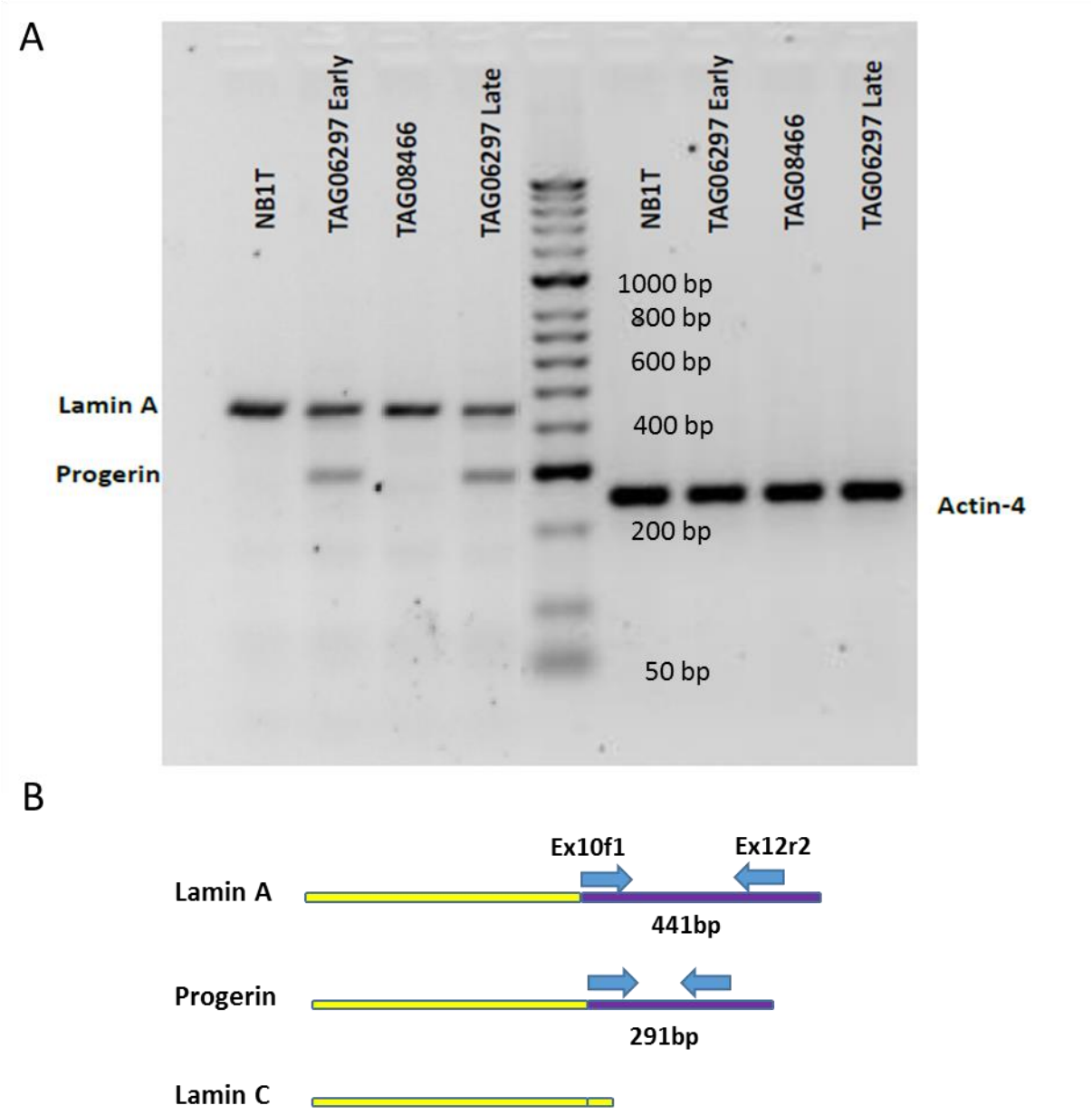

Figure 4.19 RT-PCR analysis of Lamin A and Progerin expression within hTERT Immortalised Normal and Hutchinson-Gilford Progeria Fibroblasts

Agarose gel image shows RT-PCR produced from NB1T, a hTERT immortalised fibroblast cell line and two strains of the HGPS fibroblasts TAG06297 Early and Late passage. The lanes on the left of the ladder contain cDNA amplified using primers for lamin A and progerin. B identifies the primer placement for the forward primer Ex10f1 in exon 10 of *LMNA* and the reverse primer Ex12r2 in exon 12 of *LMNA*. Yellow Bars represent the region of sequence homology, whereas the purple bar identifies the sequence unique to Lamin A and with the 150 nucleotide deletion in progerin. The lanes on the right of the ladder in A show the loading control using primers for exons 7 to 9 of the actin gene. TAG08466 is a hTERT immortalised "Atypical" HGPS cell line, with an unknown genetic mutation, although thought not to result from progerin expression (see chapter 6).

Using RT-PCR, progerin expression is clearly visible in both TAG06297 Early and Late cell lines, whereas no band corresponding to progerin is identified in the NB1T controls or the “Atypical” (non –G608G) HGPS cell line, TAG08466. This confirms the continued expression of progerin in the TAG06297 Late cell line, despite the transition from a “progeria cell” phenotype to a more normal cell phenotype previously described (Chapter 3).

The next step is to accurately quantify any changes in the expression level of progerin between TAG06297 Early and Late cell lines which could account for the observed changes at the cellular level (Chapter 3). With several criticisms being made of the established QPCR methods used to quantify lamin A/ progerin expression level, we opted to employ a novel QPCR design using TaqMan® probes. The TaqMan® Probes are the intellectual property of Dr Evgeny Makarov and are, therefore, not described in this work. The probe placement and experimental design is, however, summarised in figure 4.20.

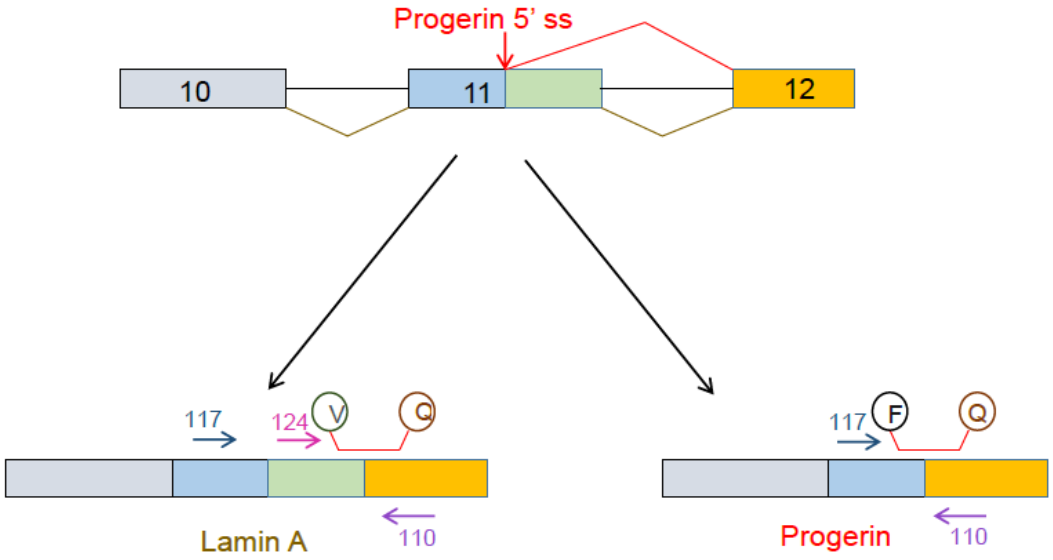

Figure 4.20 Diagrammatic representation of experimental design to determine Lamin A and Progerin expression level in a single reaction, using TaqMan® probes

Diagram represents the exon 11 – exon 12 junction, where lamin A and progerin transcripts are distinguished through use of the cryptic splice site. 117 and 124 represent the positions of the two different forward primers and 110 shows the position of the reverse primer. V shows the position of the VIC® dye labelled TAMRA™ probe for lamin A including the quencher (Q) and F shows the position of the FAM™ dye labelled TAMRA™ probe for progerin including the quencher (Q). Image provided by Dr Evgeny Makarov.

Figure 4.20 shows the exon 11 – exon 12 junction, where activation of the cryptic splice site gives rise to progerin (Eriksson *et al*, 2003). QPCR design uses two separate TaqMan® Probes, VIC® dye labelled TAMRA™ for lamin A and FAM™ dye labelled TAMRA™ for progerin, positioned over the unique exon junctions in these transcripts. The same forward (117) and reverse (110) primers can, therefore, be used to quantify both lamin A and progerin transcripts. The additional forward primer 124 has been added to negate any potential bias, caused by primer 117 being further away from the probe in lamin A transcripts, which could lead to underestimation of lamin A from the *LMNA* gene. The aim of this design is to effectively quantify both Lamin A and Progerin within a single reaction.

For effective validation of this novel QPCR method, single and dual probe detection was used to quantify lamin A and progerin, in TAG06297 Early and Late cells. Figure 4.21 shows an experimental schematic where lamin A and progerin are detected separately and together, using just primers 117 and 110 and with the addition of primer 124.

ABI Taqman Gene Expression 24-11-15 HF

	1 2	3 4	5 6	7 8	9 10	3	11 12	
A	3F1+3F2	4F1+4F2	5F1+5F2	6F1+6F2	7F1+7F2		8F1+8F2	LAM-VIC-TAMRA 124+110
B	3F1+3F2	4F1+4F2	5F1+5F2	6F1+6F2	7F1+7F2		8F1+8F2	PR0-FAM TAMRA 117+110
C	3F1+3F2	4F1+4F2	5F1+5F2	6F1+6F2	7F1+7F2		8F1+8F2	LAM-VIC-TAMRA 117+110
D	3F1+3F2	4F1+4F2	5F1+5F2	6F1+6F2	7F1+7F2		8F1+8F2	LAM-VIC + PR0-FAM 124 + 117 + 110
E	NB1T	T06L	T08	T06E	1972		NTC1	LAM-VIC-TAMRA 124+110
F	NB1T	T06L	T08	T06E	1972		NTC2	PR0-FAM TAMRA 117+110
G	NB1T	T06L	T08	T06E	1972		NTC3	LAM-VIC-TAMRA 117+110
H	NB1T	T06L	T08	T06E	1972		NTC4	LAM-VIC + PR0-FAM 124 + 117 + 110

A+E

Q-PCR Reagents		Mastermix	
Components	1x (µl)	26x (µl)	
ABI Taqman Gene Expression Master mix	10	260	
LAM-VIC-TAMRA (10µM)	0.3	7.8	(Final conc. of probe is 150 nM)
Primer 124 (10µM)	0.6	15.6	(Final conc. of primer is 300 nM)
Primer 110 (10µM)	1.2	31.2	(Final conc. of primer is 600 nM)
cDNA	4	104	
Water	3.9	101.4	
Sum	16	416	

B+F

Q-PCR Reagents		Mastermix	
Components	1x (µl)	26x (µl)	
ABI Taqman Gene Expression Master mix	10	260	
PRO=FAM-TAMRA (10µM)	0.6	15.6	(Final conc. of probe is 300 nM)
Primer 117 (10µM)	0.6	15.6	(Final conc. of primer is 300 nM)
Primer 110 (10µM)	1.2	31.2	(Final conc. of primer is 600 nM)
cDNA	4	104	
Water	3.6	93.6	
Sum	16	416	

C+G

Q-PCR Reagents		Mastermix	
Components	1x (µl)	26x (µl)	
ABI Taqman Gene Expression Master mix	10	260	
LAM-VIC-TAMRA (10µM)	0.3	7.8	(Final conc. of probe is 150 nM)
Primer 117 (10µM)	0.6	15.6	(Final conc. of primer is 300 nM)
Primer 110 (10µM)	1.2	31.2	(Final conc. of primer is 600 nM)
cDNA	4	104	
Water	3.9	101.4	
Sum	16	416	

D+H

Q-PCR Reagents		Mastermix	
Components	1x (µl)	26x (µl)	
ABI Taqman Gene Expression Master mix	10	260	
LAM-VIC-TAMRA (10µM)	0.3	7.8	(Final conc. of probe is 150 nM)
PRO-FAM-TAMRA (10µM)	0.6	15.6	(Final conc. of probe is 300 nM)
Primer 124 (10µM)	0.6	15.6	(Final conc. of primer is 300 nM)
Primer 117 (10µM)	0.6	15.6	(Final conc. of primer is 300 nM)
Primer 110 (10µM)	1.2	31.2	(Final conc. of primer is 600 nM)
cDNA	4	104	
Water	2.7	70.2	
Sum	16	416	

F1:F2 mixes (1:1) made - add 4µl per well

Thermal Cycle: STANDARD

Temp	Time	Cycles
50°C	2 min	1
95°C	10 min	1
95°C	15 sec	50 cycles
62°C	1 min	

Figure 4.21 QPCR experiment schematic for single and dual probe detection of Lamin A and Progerin expression

Image shows the 96 well plate set up for the assessment of expression level of Lamin A and Progerin in: NB1T a control cell line, TAG08466 (T08) an "Atypical" HGPS cell line, 1972 a primary HGPS cell line and Early (T06E) and Late (T06L) passage versions of theTAG06297 HGPS cell line. Apart from where specified all cell lines are hTERT immortalised. Blue highlighting indicates the use of VIC® dye labelled TAMRA™ for lamin A using primers 124+110 and green highlighting shows wells for the detection of Lamin A, with VIC® dye labelled TAMRA™, using primers 117+110. Pink highlighting shows the use of FAM™ dye labelled TAMRA™ probe for the detection of Progerin. Grey highlighting shows the use of both VIC®TAMRA™ and FAM™-TAMRA™, with all three primers 124+117+110, for the assessment of both Lamin A and Progerin expression in a single reaction. F1 and F2 are the calibration curve template plasmids which contain amplification fragments for lamin A and progerin respectively. Calibration curve range from 1000 (3F1/3F2) – 100,000,000 (8F1/8F2) copies per well. NTC = Non Template Control. Experiment and schematic designed by Dr Helen Foster and Dr Evgeny Makarov.

F1 and F2 are the names given to the pJET1.2 cloning vector plasmids which contain a copy of the lamin A and progerin amplicons respectively. The purified plasmid was quantified using NanoDrop™ spectrophotometer and the number of molecules calculated using Avogadro's constant. This was used to make known concentration points for the calibration curve ranging from 1F1/F2 (10 molecules) up to 8F1/F2 (100000000 molecules). For each experiment a 6 point calibration curve was used, putting the sample concentration within the calibrated range. The addition of the non-corresponding probe to the amplicon resulted in no signal detection, demonstrating the probe specificity. The percentage of each transcript, for TAG06297 Early and Late, is summarised in figure 4.22 for both single and dual probes with both primer sets.

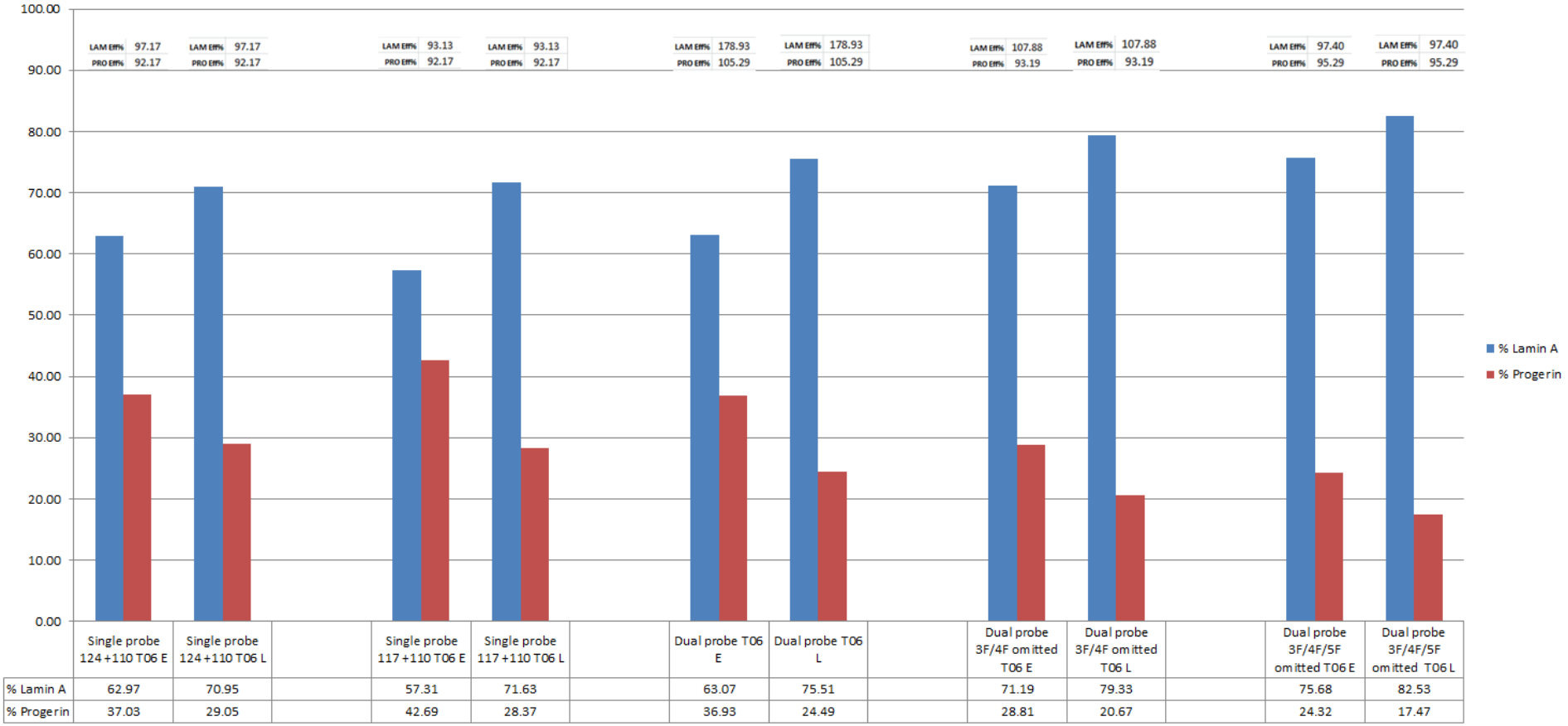

	Single probe 124 +110 T06 E	Single probe 124 +110 T06 L		Single probe 117 +110 T06 E	Single probe 117 +110 T06 L		Dual probe T06 E	Dual probe T06 L		Dual probe 3F/4F omitted T06 E	Dual probe 3F/4F omitted T06 L		Dual probe 3F/4F/5F omitted T06 E	Dual probe 3F/4F/5F omitted T06 L
% Lamin A	62.97	70.95		57.31	71.63		63.07	75.51		71.19	79.33		75.68	82.53
% Progerin	37.03	29.05		42.69	28.37		36.93	24.49		28.81	20.67		24.32	17.47

Figure 4.22 Comparison of single and dual probe QPCR detection methods for the assessment of Lamin A and Progerin expression in hTERT

Lamin A and Progerin expression levels shown as a percentage of total expression. Bar charts from left to right Comparison of use of primers 124 and 117 on Lamin A detection in single reactions. Comparison of single and dual probe QPCR detection. Effect of improved QPCR efficiency by omission of specific points in the standard curve. Experiment and analysis performed by Dr Helen Foster and Dr Evgeny Makarov.

From the various experiments in figure 4.22, the additional use of primer 124 does not appear to affect the percentage of lamin A and progerin detected for either TAG06297 Early or Late. This suggests that despite the position of primer 117 making the lamin A transcript significantly longer, it is not causing a bias for the higher detection of the smaller product, progerin. This means that primers 117 + 110 are sufficient for the accurate detection of both lamin A and progerin. The QPCR efficiencies (figure 4.22) are within an acceptable range with and without primer 124. The use of both probes in a single reaction does, however, show an undesirable QPCR efficiency of around 170%, something which is remedied by manipulation of the calibration curve (figure 4.22). This does however, increase the percentage of lamin A and decrease that of progerin in both TAG06297 cell lines, while not eliminating the difference between cell lines. This suggesting the need for both single and dual probe detection, in order to validate the findings. Further optimisation of the dual probe approach to get accurate results from a single reaction would be significant for the study of HGPS and the role of progerin in normal human ageing.

With this in mind both single and dual probes reactions were used for the quantification of lamin A and progerin expression in TAG06297 Early and Late sample. Figure 4.23 shows the average number of molecules of Lamin A and progerin detected in each sample.

A

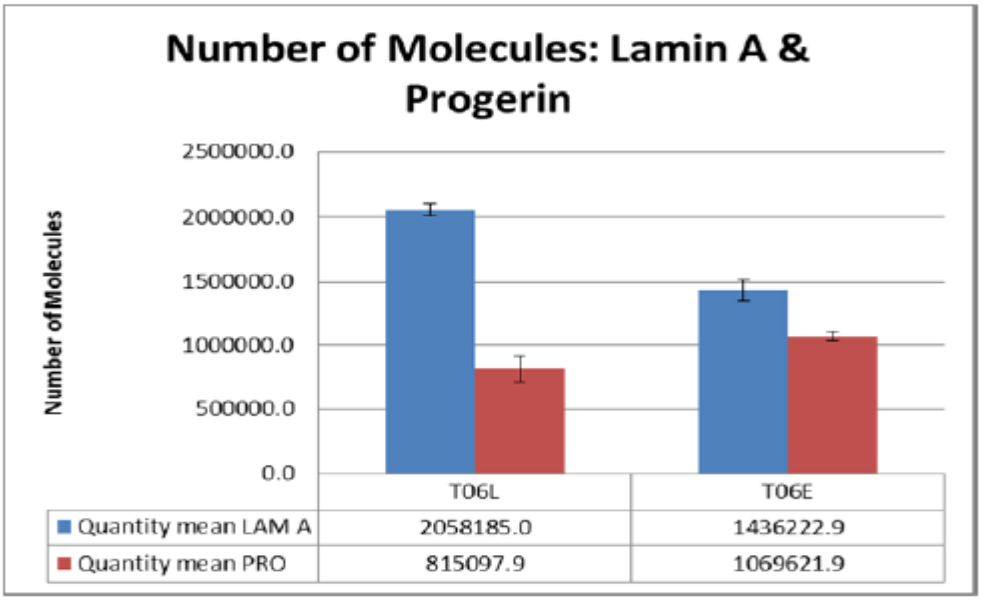

B

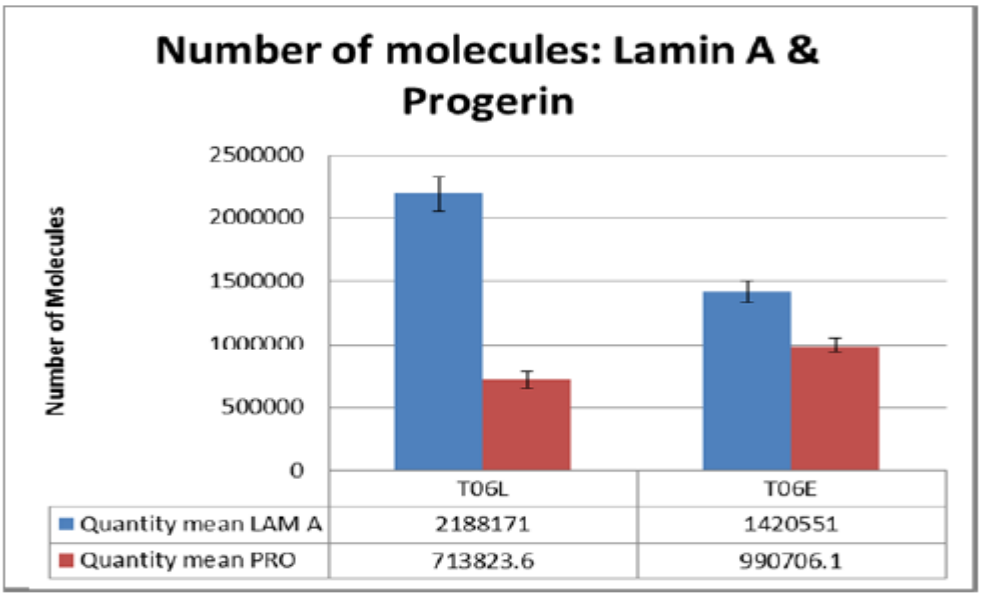

Figure 4.23 QPCR quantification of Lamin A and Progerin molecules being expressed in Early and Late Passage hTERT HGPS Fibroblasts

Number of molecules of Lamin A and Progerin detected in TAG06297 Late (T06L) and TAG06297 Early (T06E) cell lines. Quantity of each protein shown as the mean of all three repeats. A shows separate quantification using single probe reactions, whereas, the data in B was gathered using dual probes for the detection of both lamin A and progerin in one reaction. Experiment and analysis performed by Dr Helen Foster and Dr Evgeny Makarov.

QPCR efficiencies for the single probe quantification reactions were 93% for lamin A and 92.2% for progerin. Using the dual probe the QPCR efficiencies were 105.9%

for lamin A and 88.5% for progerin. Both QPCR methods identify a statistically significant higher number of lamin A molecules than progerin with T-TEST (two tailed) P values of $9.95 \text{ X } 10^{-05}$ for TAG06297 Late and 0.0013 for TAG06297 Earlies. Figure 4.24 shows the percentage of each transcript in both cell lines.

A

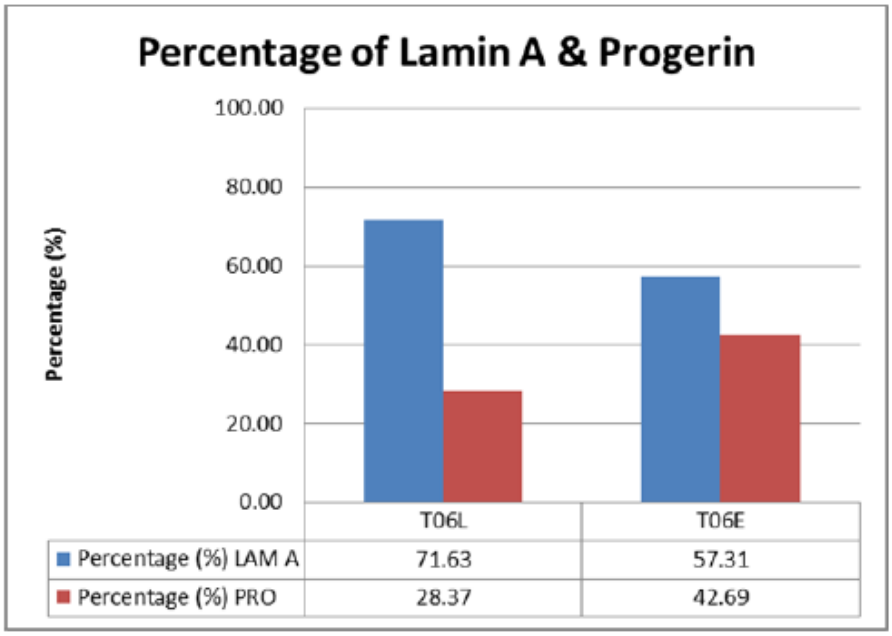

B

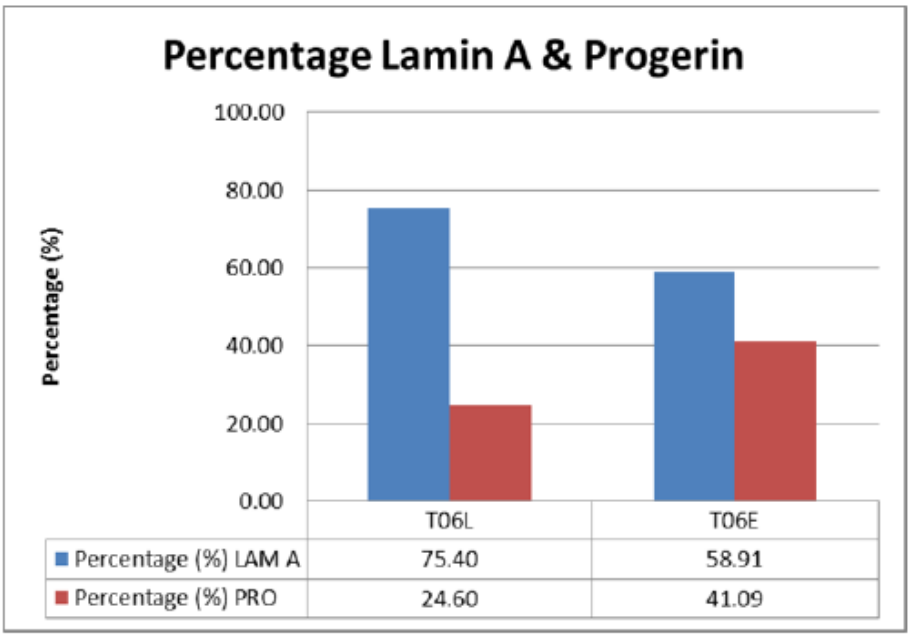

Figure 4.24 Relative percentage of Lamin A and Progerin expression in Early and Late Passage hTERT HGPS Fibroblasts using Single and Dual Probe QPCR quantification

Percentage of lamin A and progerin detected in TAG06297 Late (T06L) and TAG06297 Early (T06E) cell lines. Lamin A and progerin expression levels are shown as a percentage of total expression. A shows separate quantification using single probe reactions, whereas, the data in B was gathered using duel probes for the detection of both lamin A and progerin in one reaction. Experiment and analysis performed by Dr Helen Foster and Dr Evgeny Makarov.

Single probe quantification identifies a 60:40 split between lamin A and progerin in the TAG06297 Early cell line, whereas, a 70:30 split of *LMNA* expression products is identified in the TAG06297 Late cell line. The difference in the percentages of lamin A and progerin expression between TAG06297 Early and Late is statistically significant, whether using either single or dual probes for quantification (T-TEST two tailed 0.009076 and $5.65x10^{-05}$ respectively). This suggests that changes have occurred in the expression level of progerin in response to prolonged growth in the presence of hTERT. Figure 4.25 shows the relative ratio of lamin A to progerin in both TAG06297 cell lines.

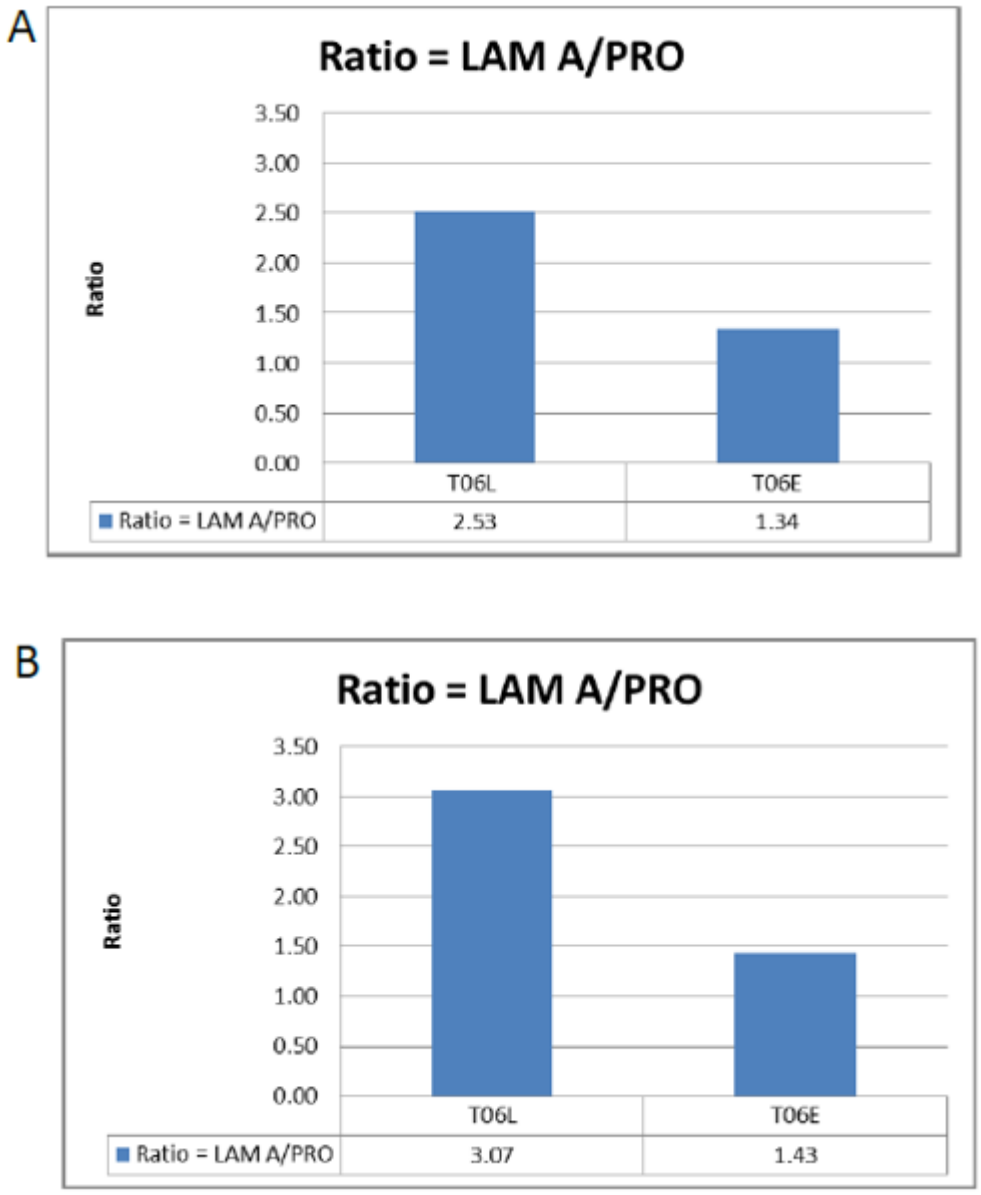

Figure 4.25 Ratio of Lamin A and Progerin expression in Early and Late Passage hTERT HGPS Fibroblasts using Single and Dual Probe QPCR quantification

Ratio of lamin A and progerin detected in TAG06297 Late (T06L) and TAG06297 Early (T06E) cell lines. A shows separate quantification using single probe reactions, whereas, the data in B was gathered using dual probes for the detection of both lamin A and progerin in one reaction. Experiment and analysis performed by Dr Helen Foster and Dr Evgeny Makarov.

The 2 fold decrease in the ratio of lamin A to progerin observed between the TAG06297 Late and Early cells shows a trend to decrease progerin expression in response to hTERT. This is consistent with previous findings (Cao *et al*, 2011),

which used a different QPCR methodology. The extent of the repression of progerin transcription in response to hTERT is, however, not as great as 10 fold reduction previously reported (Cao *et al*, 2011). The tendency is to express more lamin A than progerin in both TAG06297 cell lines. A 1.2:1 expression ratio has previously been observed in primary AG06297 cells (ratio created with data pooled from 8 HGPS cell lines) (Rodriguez *et al*, 2009), which is comparable to the 1:3.1 for lamin A to progerin in the TAG06297 Early cell line, signifying no real difference in expression ratio between Early and primary cells. The 3:1 ratio identified in TAG06297 Late cells, demonstrates the change in response to protracted growth following hTERT immortalisation. This, however, is not a substantial enough reduction to bring the TAG06297 Late cells in line with control cells, where a ratio of >240:1 was previously determined (Rodriguez et al, 2009). With approximately 30% of *LMNA* transcripts being progerin in the TAG06297 Late cell line, changes purely at the transcription level may not account for the "healthy" cell phenotype observed in this cell line. With a cell phenotype more similar to controls, where no progerin was detected (data not shown), it is likely that the TAG06297 Late cell line has adopted an alternative route to modulate progerin in order to cope with hTERT growth pressure.

4.2.2 Genomic Instability

HGPS cell lines have previously been described as having high levels of genomic instability with progerin causing a potential loss of lagging chromosomes during mitosis (Cao *et al*, 2007; Dechat *et al*, 2007). Primary cells from the TAG06297 patient have been described as having a normal 46XY karyotype (Coriell Institute). In order to determine if the moderate changes in expression level of the *LMNA* gene in response to hTERT are caused by general genomic instability in this cell line, chromosome number analysis was performed. For NB1T controls and TAG06297 Late cells metaphase preparations were identified using Metafer software and the number of chromosomes were counted. Figure 4.26 gives examples of metaphase preparations and summarises the established chromosome number for each cell line.

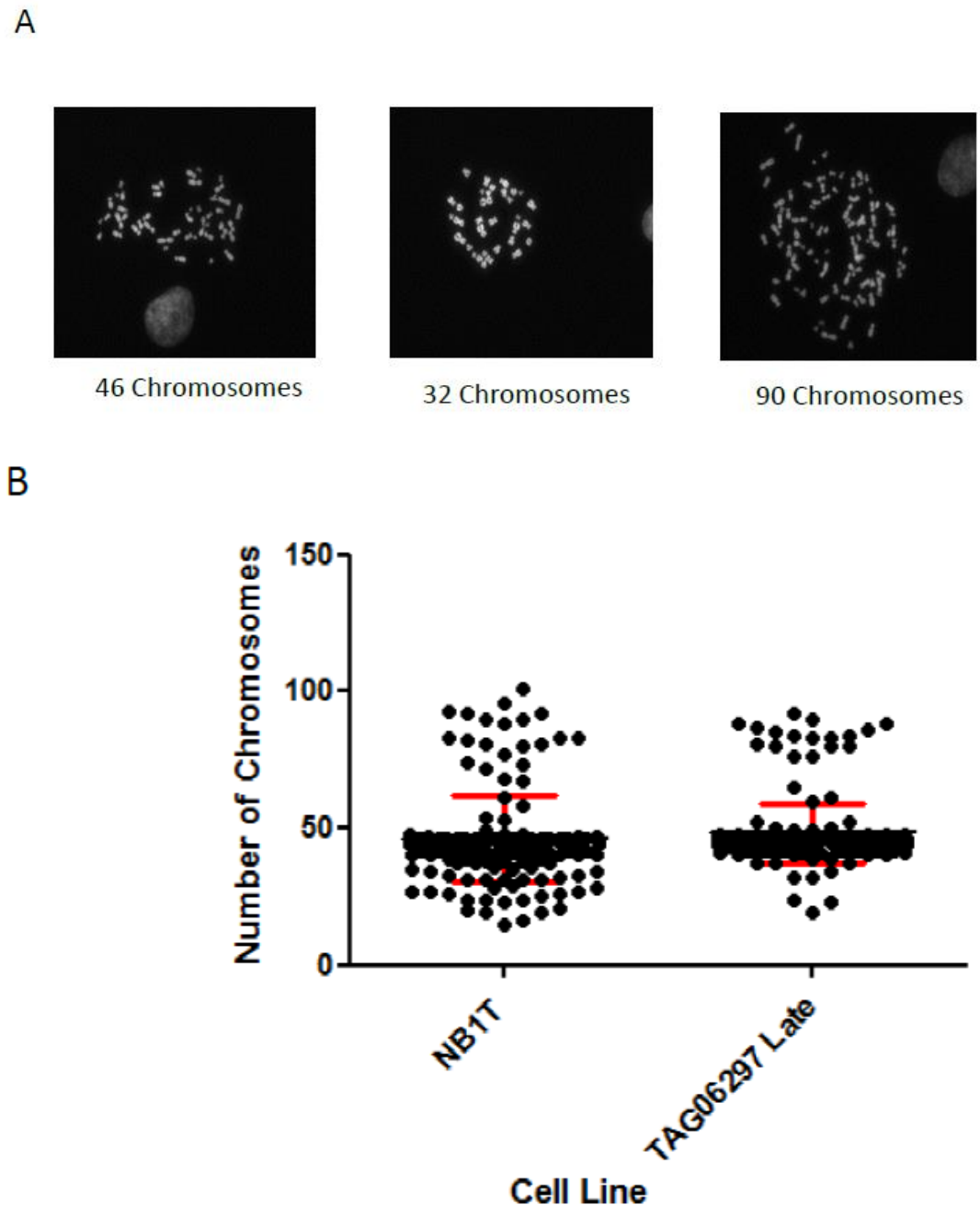

Figure 4.26 Chromosome Number Analysis in hTERT immortalised normal and HGPS Fibroblast cultures

Metaphase preparations were visualised with DAPI and images captured using Metafer software. (A) shows a metaphase images containing different numbers of chromosomes. The number of chromosomes per metaphase were determined for NB1T a normal fibroblast cell line that has been immortalised with hTERT and a hTERT immortalised Late passage strains of the HGPS derived TAG06297 (B). For NB1T 180 Metaphases were analysed and for TAG06297 the number analysed was 224.

A T-Test (two-tailed) showed no significant difference in chromosome number for NB1T and TAG06297 Late cells, with a P Value = 0.096, where both cell lines had a median of 46 chromosomes. This suggests that no broad changes in chromosome number have occurred in the TAG06297 Late cell line, despite forced growth of a premature ageing diseased cell type where genomic instability is predicted. This again, identifies improvement in progeria cell characteristics in response to growth in the presence of hTERT (Chapter 3). It also raises questions about the progerin protein level within this cell line, where progerin associates with membranes during mitosis has been identified as key factor in aneuploidy (Cao *et al*, 2007; Dechat *et al*, 2007). Simple analysis of chromosome number, does suggest relative genomic stability, although a more comprehensive karyotype using M-FISH would identify any specific changes in chromosome 1 (*LMNA* locus). The observed changes in progerin expression level in TAG06297 Late cells, however, do not occur due to global genomic instability of this cell line.

4.2.3 Progerin Protein Level

With moderate increase in the ratio between lamin A and progerin expression being demonstrated in the TAG06297 Late compared to the Early cell line, we needed to determine the effect at the protein level. Reduction in progerin protein has previously been shown to result in improved progeria cell characteristics (Scaffidi & Misteli, 2005), such as those described in chapter 3. Western blot analysis was used to compare progerin abundance between control and TAG06297 Early and Late cell lines (figure 4.27C).

A

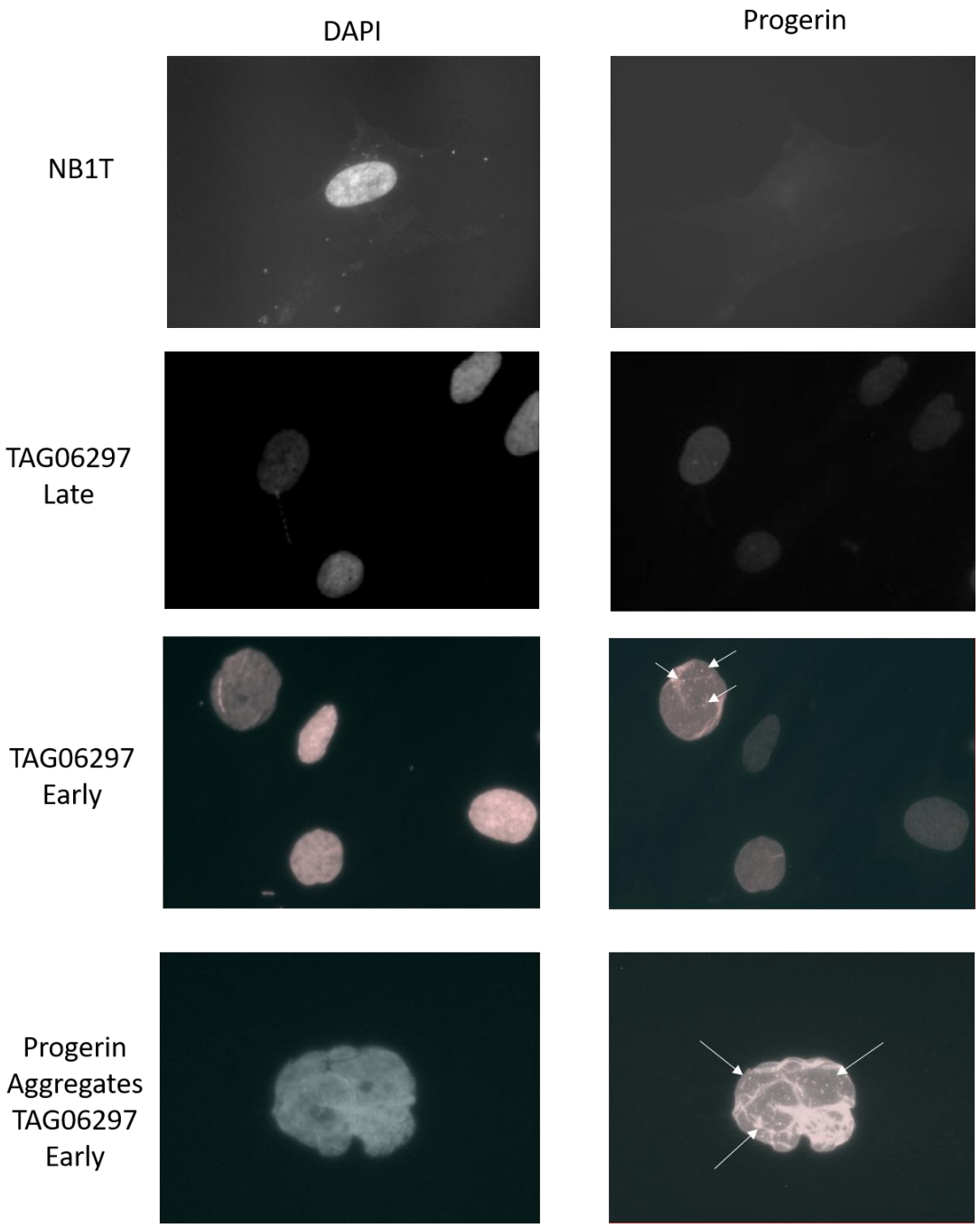

B

Cell Lines	Progerin Nuclear Rim (%)	Progerin Aggregates (%)	Progerin Negative (%)
NB1T	0	0	100
*TAG06 Early	74.8±0.8	25±0.4	0.2±0.3
*TAG06 Late	92.3±0.7	4.9±0.8	2.8±1.6
T Test*	0.0006	0.0004	0.3

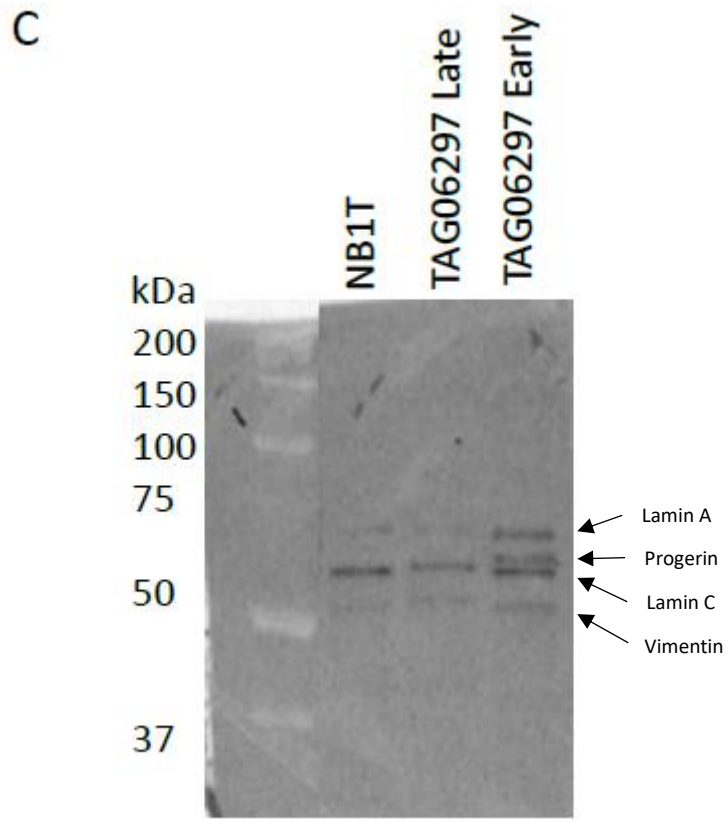

Figure 4.27 Analysis of Progerin Levels within hTERT Immortalised Normal and Hutchinson-Gilford Progeria Fibroblasts

Indirect immunofluorescence using an anti-Progerin antibody revealed two different staining patterns (A) Nuclear Rim stain and Nuclear Aggregates. Table (B) summerizes the proportion of each staining pattern found within NB1T, A hTERT immortalised fibroblast cell line and two strains of the HGPS fibroblasts TAG06297 Early and Late passage. (C) Western Blot analysis using an anti- Lamin A/C antibody identifies the levels of Lamin A, C and progerin.

Using chemiluminescence and loading an equal cell number for each cell line, no progerin was detected in the TAG06297 Late cell line, whereas, a band at ~65 kDa confirming progerin is observable for the TAG06297 Early cell line. This preliminary result identifies a substantial change at the protein level of the abundance of progerin between these two cell lines.

Using immunofluorescence with an anti-progerin antibody the cellular location of progerin was identified (figure 4.27A). For the control cell line, NB1T, no progerin protein was detected. Interestingly, progerin staining did give a positive nuclear rim stain in 92% of TAG06297 Late cells analysed (figure 4.27B). This is significantly higher (T-TEST two tailed $3.6x10^{-5}$) than TAG06297 Early cells, where a statistically significantly higher proportion of nuclei (25%) were found to have progerin nuclear aggregates (T-TEST two tailed $2.7x10^{-5}$). The nuclear aggregate staining pattern categorises a great build-up of progerin looking to be a catastrophic level, with this typically found in cells with extreme nuclear shape abnormalities. Progerin is clearly present in the TAG06297 Late cells although at a much lower level than in the early cell line. The inability to detect progerin in the TAG06297 Late cells with Western blot may be due to it being below the level of detection for chemiluminescence with only $1x10^5$ cells loaded per sample. This does sugest a significant difference between TAG06297 Early and Late cell lines which in all likelihood gives rise to the reduction in progeria cell phenotype in the TAG06297 Late cell line, however the western blot results require verification and quantification with densitometry.

4.2.4 Proteasome Inhibition

The observed reduction in protein level does not appear to marry up with the moderate changes in expression ratio between lamin A and progerin. This suggests that progerin is being regulated at the protein level, leading to the improved progeria phenotype previously described for the TAG6297 Late cell line (Chapter 3).

Poly-ubiquitination of proteins has been identified as a signal for protein degradation through proteasomal machinery and autophagic clearance (Dikic *et al,* 2009). Two sites for the poly-ubiquitination have been identified (Tan *et al*, 2008; Belzile *et al,* 2010) and one study determined preferential use of K63 for progerin (Graziotto *et al*, 2012), which promotes autophagic clearance of aggregated proteins (Tan *et al*, 2008). K48 poly-ubiquitination is believed to promote protein degradation through the proteasome (Belzile *et al,* 2010). Further evidence suggests that nuclear envelope proteins are not substrates for proteasomal degradation under normal cell conditions

(Chen *et al*, 2002; Dino-Rockel & von Mikecz, 2002; von Mikecz, 2006). Equally there is evidence suggesting proteasomal degradation of Emerin, in cells lacking A-type lamins, credibly not normal cell conditions (Muchir *et al*, 2006). To further investigate if hTERT expression in TAG06297 Late cells had resulted in abnormal cellular conditions, which increases the rate of progerin degradation through the proteasome, this was examined using the proteasome inhibiting drug MG132.

MG132 is a cell permeable, reversible inhibitor of proteolytic activity of the 26S proteasome complex. MG132 has previously been used for the purposes of determining protein degradation, whereby monitoring the build of a protein post proteasomal inhibition gives insight into the rate of protein degradation (Wu *et al*, 2009). Figure 4.28A shows the resulting Western blot analysis of TAG06297 Late cells at various time points following 10 µm MG132 treatment.

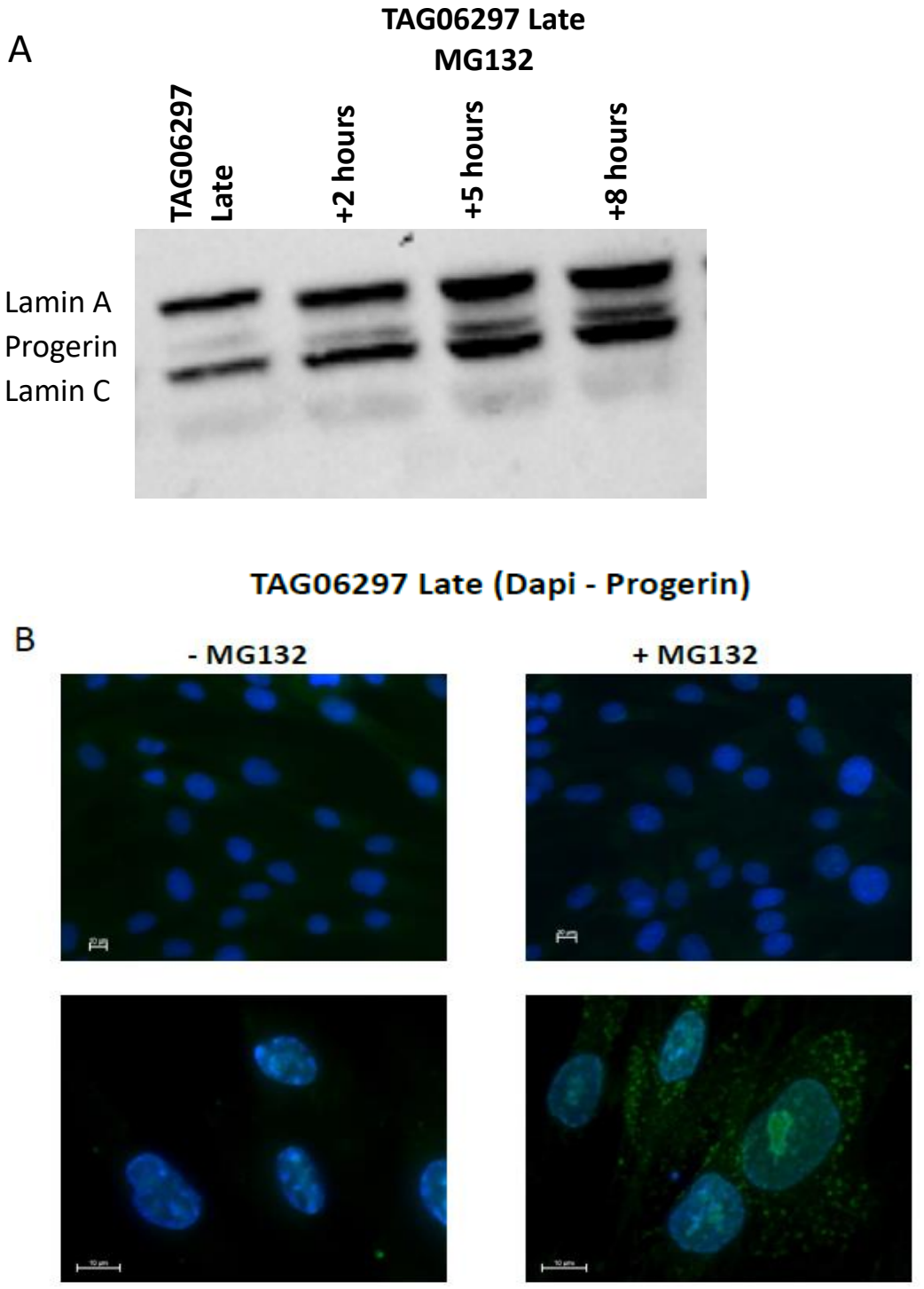

Figure 4.28 Treatment of HGPS cells with the proteasome inhibiting drug MG132

TAG06297 Late cells, a HGPS patient derived cell line immortalised with hTERT, were treated with 10 µm concentration of MG132. (A) Western Blot analysis using an anti-Lamin A/C specific antibody shows the build-up of progerin at incremental time-points. The sub-cellular location of the build-up of progerin 8 hours after inoculation is shown in (B), visualised using an anti-progerin specific antibody. Scale bar = 10 µm

With the same number of cells loaded for each time-point following MG132 proteasome inhibition, this preliminary result shows the internal build-up of protein. The accumulation of progerin, lamin A and lamin C demonstrate that inhibition of the proteasome results in a cellular increase in these proteins. This does suggest a link between proteasome activity and Lamin stability although this a preliminary result in need of further investigation. The proteasome was previously not identified as the method of degradation for these proteins (Graziotto *et al*, 2012) and further investigation may suggest proteasome degradation through the poly-ubiquitination of K48 (Belzile *et al*, 2010).

2 hours post-incubation with MG132 progerin is no longer below the level of detection for chemiluminescence of $1x10^5$ cells. The build-up progerin and lamin A and C is observed at 5 and 8 hours post MG132 treatment. A 24 hour time point following MG132 inoculation was also examined, however, total cell death was observed, resulting in no Western blot analysis. A DMSO loading control showed no effect on cell viability after 24 hours.

The location of progerin build up in response to MG132 proteasome inhibition was identified using immunofluorescence and is shown in figure 4.28B. 8 hours post MG132 treatment progerin is located in cytoplasmic aggregates, a cellular location not previously identified for this nuclear lamina anchored protein (Capell *et al*, 2005). This coincides with the known sub-cellular location of proteasomal activity (Peters *et al*, 1994) and adds further evidence to the effective inhibition of the proteasome using MG132 and suggests that progerin is degraded via the proteasome. Nuclear build-up of progerin is also observed 8 hours after MG132 proteasome inhibition, a location where proteasome activity has also been observed (Peters *et al*, 1994).

To examine the rate of protein degradation in this cell line, immunofluorescence was used as a detection method for Western blot analysis. With fluorescence output being linear to sample concentration, comparisons in band intensity can be used to quantify protein levels within samples. Figure 4.29 shows the resulting Western blot image and the band intensity for each protein.

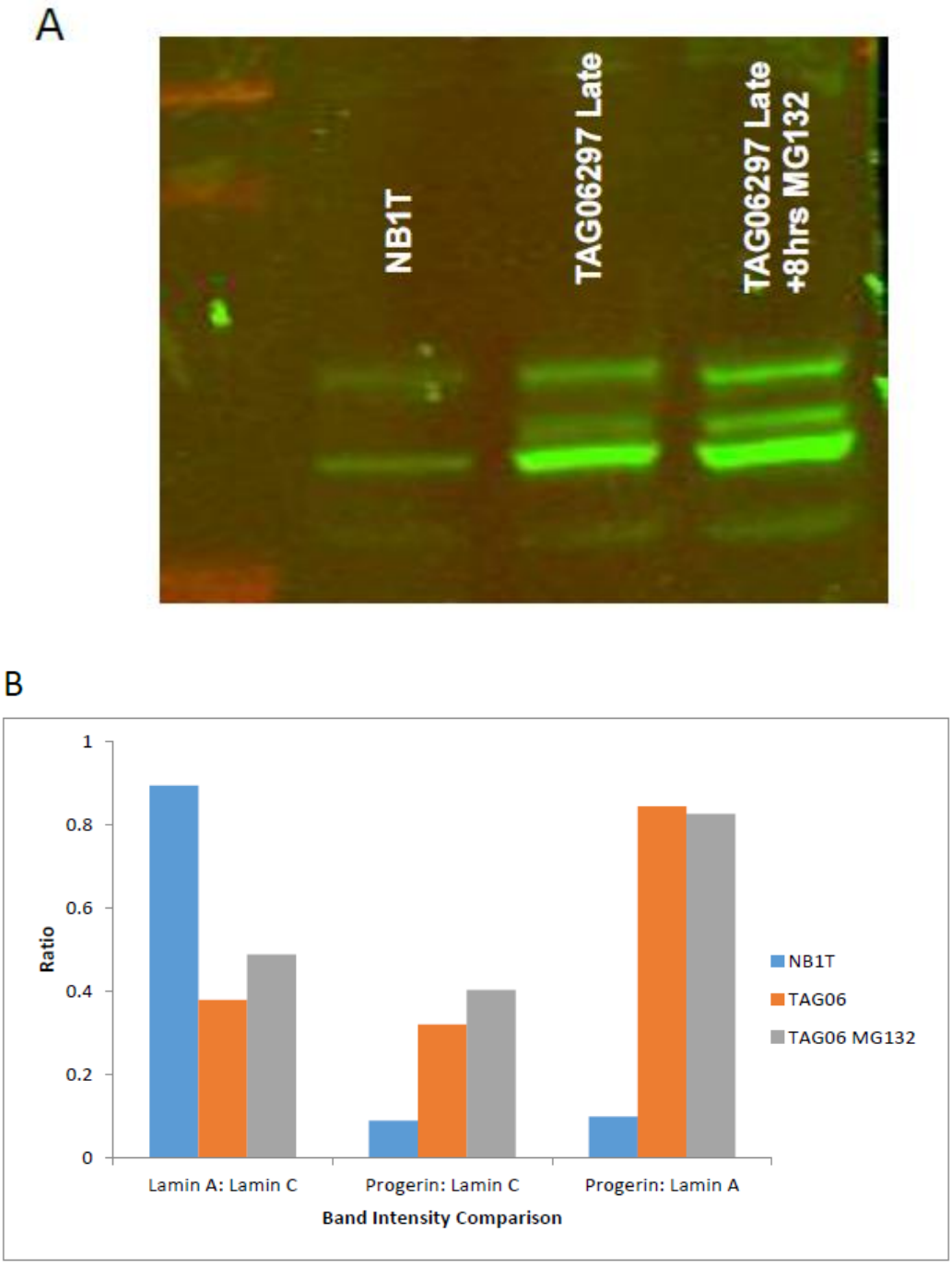

Figure 4.29 Relative ratio of Lamin proteins in hTERT immortalised HGPS fibroblasts before and after MG132 proteasome inhibition

TAG06297 Late cells, a HGPS patient derived cell line immortalised with hTERT, were treated with 10µm concentration of MG132. (A) Western Blot analysis using an anti-Lamin A/C specific antibody, visualised using fluorescent secondary antibodies shows the build-up of progerin post 8 hour incubation with MG132. (B) Compares the ratios of band intensities between control NB1T cell line and the HGPS cell line TAG06297 before and after MG132 treatment.

Through fluorescence detection, progerin is visible in $1x10^5$ cells, determining what was previously postulated that progerin is present in the TAG06297 Late cell line, albeit at a level below detection using chemiluminescence.

From analysing the band intensity in each lane the ratio of proteins has been determined (figure 4.29B). NB1T cells demonstrate a near 1:1 ratio for lamin A: lamin C whereas TAG06297 Late shows less than half that ratio. This is not surprising as progerin is produced from activation of cryptic splice site within lamin A sequence and does not affect lamin C transcripts (De Sandre-Giovannoli et al, 2003; Eriksson et al, 2003). The totalling of progerin and Lamin A proteins is more comparable to lamin A: lamin C ratio observed in the control cell line.

MG132 treatment of TAG06297 Late cells alters the ratios between both lamin A and Progerin relative to lamin C. The increase in these ratios shows that both proteins are being broken down at a rate quicker than lamin C, as determined by an increased build-up. This is similar to the finding using the autophagy promoting drug Rapamycin, where rates of progerin degradation were seen at a higher rate than Lamin C (Cao *et al*, 2011). No difference in the ratio between lamin A: progerin post drug treatment show that these proteins are building up at a similar rate. This provisional result suggests that improvements in progeria cell phenotype previously identified for the TAG06297 Late cell line (chapter 3) may result from the increased proteasomal degradation of both lamin A and progerin but not lamin C.

4.3 Discussion

In this study we demonstrate the effective use of a novel QPCR design, for the estimation of *LMNA* expression in a single reaction, using dual probes for the separate detection of lamin A and progerin. The estimation of progerin relative to Lamin A is more in line with previous attempts at quantification using Taqman® (Rodriguez *et al*, 2009), confirming a relative ratio of 1.3:1 Lamin A: progerin expression. The moderate difference observed in ratios between AG06297 primary fibroblasts (Rodriguez *et al*, 2009) and TAG06297 Early cells is likely an artefact of QPCR design whereby the previous study showed a slight bias to over-represent

progerin transcript abundance due to primer placement (Rodriguez *et al*, 2009). This is slight when compared to attempts to quantify using SYBR® Green, where 5x more progerin was detected than Lamin A (Cao *et al*, 2011). This suggests the need to use this dual method to repeat work which examined progerin transcription in normal human fibroblast and identified its involvement in normal human ageing (Scaffidi & Misteli, 2006).

QPCR expression analysis is in agreement with cell characterisation work, which identified TAG06297 Early cells as showing hallmarks of a classic progerin cell phenotype (Chapter 3), which results from the dominant negative effect of progerin (Scaffidi and Misteli, 2005). TAG06297 Late cells show an improved cell phenotype in response to hTERT immortalisation (Chapter 3), something previously suggested to occur through downregulation of progerin expression (Cao *et al*, 2011). QPCR data from this study is in agreement with previous findings, which suggest downregulation of progerin expression, in response to hTERT immortalisation (Cao et al, 2011). This was postulated to occur through telomere length acting as an upstream signals in regulating progerin production (Cao *et al*, 2011). A previous study used a 25-mer morpholino oligonucleotide (exo11) to effectively block use of the cryptic splice site, reducing progerin expression and improving cell phenotype (Scaffidi and Misteli, 2005). This has been suggested as a potential therapy, using a small molecule inhibitors to modify splicing. The observed 2 fold decrease in response to hTERT immortalisation is significantly less than the 10 fold change previously observed (Cao *et al*, 2011). This moderate change is more difficult to interpret when trying to determine the impact on cell function. TAG06297 Late cell have been characterised as similar to control fibroblasts for several parameters, including nuclear shape (Chapter 3), suggesting a significant reduction in progerin protein abundance.

The ratio of progerin to Lamin A protein in TAG06297 Late cells differs from the expression ratio determined using QPCR. There are number of reasons for this including mRNA stability and translation efficiency (Gingold and Pilpel, 2011). Another consideration is that the increased protein degradation observed in the TAG06297 Late cells through MG132 proteasome inhibition, is reducing the

expression in a negative feedback loop. This system has previously been described (Graziotto *et al,* 2012). Through TAG06297 Late QPCR and proteasome inhibition, it is possible that improvement in progeria cell phenotype caused by hTERT immortalisation, result from a combination of increased protein degradation and reduced progerin expression, which may or may not be linked through a negative feedback loop.

The suggestion of proteasomal degradation of lamin A and progerin, likely through poly-ubiquitination of k48 (Belzile *et al,* 2010), offers new therapeutic avenues. Increased progrein degradation is already being considered as an avenue for therapy using rapamycin, a drug to increase general autophagy (Cao *et al,* 2011; Graziotto *et al,* 2012). Rapamycin treatment on fibroblasts in culture has resulted in improvements in progeria cell phenotype similar to those described in response to hTERT immortalisation (Cao *et al,* 2011; Graziotto *et al,* 2012). It is possible that increased progerin degradation has been achieved in this cell line through preferential poly-ubiquitination as a result of either increased E3 ligase abundance or changes to progerin sequence increasing its ubiquitin ligase affinity (Fu *et al,* 2004). To further investigate this, other drugs target specific machinery of the 26S proteasome could be employed for example; clasto-Lactacystin β-Lactone an inhibitor of the 20S proteasome, Epoxomicin an inhibitor of Z catalytic subunits of the proteasome (Meng *et al,* 1999) and Calpeptin an inhibitor of calpain 2. Identification of specific E2/E3 ligase combinations and sites on progerin would be essential for exploitation of proteasome degradation as therapy for HGPS (Marblestone *et al,* 2013).Comparisons of sequence between Early and Late TAG06297 cells may also offer insight into changes in response to hTERT that have improved progeria cell phenotype. With serious criticisms of the impending clinical trial using rapamycin as a treatment for HGPS (personal communication with Dr Joanna Bridger), understanding the changes in response to hTERT immortalisation, which have yielded a similar outcome, may offer less risky therapeutic avenues for HGPS in the future.

5 Analysis of increased Progerin Degradation in hTERT Immortalised HGPS Fibroblasts.

5.1 Introduction

It has previously been suggested that HGPS fibroblasts show an increase in progerin degradation following long term growth in the presence of hTERT (Chapter 4). It is thought that this reduction in the level of the toxic protein progerin results in a loss of progeria cell characteristics and a more healthy phenotype than previously observed (Chapter 3). Further experiments are needed to demonstrate the causative link between reduction in progerin level and reinstatement of a healthy cell phenotype. Two separate methods have been employed to determine this relationship: TAT mediated protein transduction to quantify the rate of progerin degradation and Nanobodies targeted to A type Lamins and conjugated to a ubiquitin ligase to confirm that Lamin A and Progerin are broken down through ubiquitination and proteasomal degradation.

The Transactivator of Transcription protein (TAT) from the HIV-1 virus was first shown to transduce across a plasma membrane in 1988 (Green & Loewenstein 1998, Frankel & Pabo, 1988). TAT was shown to penetrate cells, enter into the nucleus and perform its normal biological function of activating a viral LTR promoter (Dayton *et al*, 1986; Fisher *et al*, 1986). The transduction properties of this protein are believed to help viral infection by transducing into uninfected cells and changing the expression profile (Elliott *et al*, 1997; Hawiger *et al*, 1999). The Protein-Transduction Domain (PTD) of TAT has since been identified as the 11 amino acid sequence Tyr-Gly-Arg-Lys-Lys-Arg-Arg-Gln-Arg-Arg-Arg found at residues 47-57 of the protein (Schwarze *et al*, 2000). The method by which the TAT PTD crosses the plasma membrane has been shown to be through a process of micropinocytosis (Wadia *et al*, 2004), although some debate still remains about whether TAT can also directly penetrate across the plasma membrane (Palm-Apergi *et al*, 2012). TAT is not the only protein containing a cell penetrating peptides or PTD, others include *Drosophila* Antennapedia homeotic transcription factor (ANTP) and the herpes-

simplex-virus-1 DNA-binding protein (VP22) (Schwarze *et al*, 2000). The availability of expression vectors containing the sequence for these amino acids (Becker-Hapak *et al*, 2001) and the ability to transport proteins as large as β-galactosidase across the plasma membrane have made TAT a preferential choice for protein transduction (Fawell *et al*, 1994).

Numerous TAT- fusion proteins have been produced, achieving successful transduction both *in vitro* and *in vivo* (Wadia & Dowdy, 2005). The production of TAT-fusion proteins holds great therapeutic value with studies examine their ability to targeting cancer cells, for example with TAT-BID (Orzechowska *et al*, 2014) and TAT-FOXO3^{TM} (Esaffi *et al*, 2011). They have also been of interest for their potential therapeutic application for mitochondrial diseases (Lin & Kao *et al*, 2015), for instance in Friedreich's Ataxia, where a TAT-Frataxin fusion protein was injected into a mouse model, which resulted in successful compensation for the missing protein (Vyas *et al*, 2012).

One of the main advantages of using protein transduction over conventional transformation of genetic material is the control of protein concentration. Using TAT mediated protein transduction the concentration of protein added to the cells can be controlled, as cells take up protein in a concentration dependent manner. The concentration of protein produced following transformation is dependent on factors such as position of incorporation into the genome. This can also cause a large amount of variation between cells, whereas, TAT mediated protein transduction has been shown to achieve a high level of uniformity. A further advantage of TAT-mediated protein transduction is that cell penetration occurs as quickly as within 5 minutes (Becker-Hapak *et al*, 2001).

The aim of this research is to develop TAT-lamin A and TAT- progerin fusion proteins, in order to accurately address the issue of increased protein degradation in TAG06297 Early cell line. Through protein transduction the rate of degradation of exogenous proteins can be determined and comparisons between TAG06297 Early and Late cultures can be drawn. These fusion proteins will also be useful in determining the level at which progerin elicits a detrimental effect on cell function,

something equally interesting from the perspective of therapy and the role of progerin in normal human ageing.

Nanobodies have been identified as a unique component of sera from the camelid family of mammals, namely Llamas and Alpacas (Hamers-Casterman *et al,* 1993). Camelids were found to produce conventional heteroteterameric antibodies, but also functional heavy chain antibodies (HC Abs) which fail to incorporate a light chain (Hamers-Casterman *et al,* 1993). The VHH (variable domain of heavy chain antibodies) or single antigen-binding domain of these antibodies is the smallest antigen recognising fragment at approximately 15kDa, cornering the name Nanobody (Muyldermans *et al,* 2013). One explanation regarding the evolution of these newly-discovered naturally occurring single antigen binding domains is that they enable binding to otherwise inaccessible epitopes, which proved of selection value (Flajnik *et al,* 2011).

The small size, high specificity, straightforward expression and increased stability in varying temperatures and pH have made Nanobodies an exciting resource both commercially and therapeutically (Muyldermans *et al*, 2013, Rothbauer *et al*, 2008). The generation of GFP conjugated Nanobodies or Chromobodies has allowed for the real-time tracking of endogenous proteins in live cells (Rothbauer *et al,* 2006). This technology has now been used to capture the localization dynamics of cytoskeltetal components, at various stages of development, in a living vertebrate organism (Panza *et al*, 2015). Nanobodies, however, are more than just tools for observing protein function and can effect change. Nanobodies have been shown to modulate endogenous proteins in living cells, making them useful for therapeutic targeting (Kirchhofer *et al,* 2010), with 8 clinical trials currently underway. One such phase II clinical trial has reported positive findings for the treatment of Acquired Thrombotic Thrombocytopenic Purpura (TTP) with a Nanobody target to inhibit the reaction between blood platelets and Ultralarge von Willebrand Factor Multimers (Peyvandi *et al*, 2016).

The aim of this work is to use Nanobodies to enhance the rate of A type lamin degradation in the TAG06297 Early cell line. The hypothesis is that an A type lamin

specific Nanobody conjugated to a E3 ubiquitin ligase will be capable of mimicking the increased degradation observed in the TAG06297 Late cell line (Chapter 4) in response to prolonged hTERT expression. This will hopefully replicate the improvements observed in progeria cell characteristics, virtually restoring a normal cell phenotype. This offers great therapeutic opportunities for HGPS, using a technology already going through clinical development.

5.2 Results

5.2.1 Development of TAT-fusion proteins

In order to create lamin A and progerin TAT fusion proteins, a recombinant construct was first created through molecular cloning. Two plasmid constructs were available from Professor Steven Dowdy's lab, the pioneer of this technology. The two plasmids, called pTATv1 and pTATv2 both contain the genetic sequence for the 11 amino acids of the TAT protein, controlled under a T7 promoter. The constructs also contain multiple cloning sites allowing for the insertion of the desired sequence, in this case lamin A or progerin cDNA. Both plasmids also confer Kanamycin resistance and contain histidine tags to allow for protein purification. One difference between the two plasmids is that pTATv1 contains a histidine tag at both the beginning and the end of the open reading frame, whereas pTATv2 has only one histidine tag at the C terminus of the protein. The pTATv2 construct also contains a T7 tag sequence, for which there are commercially available antibodies. Figure 5.30 shows the plasmid maps for pTATv1 and pTATv2.

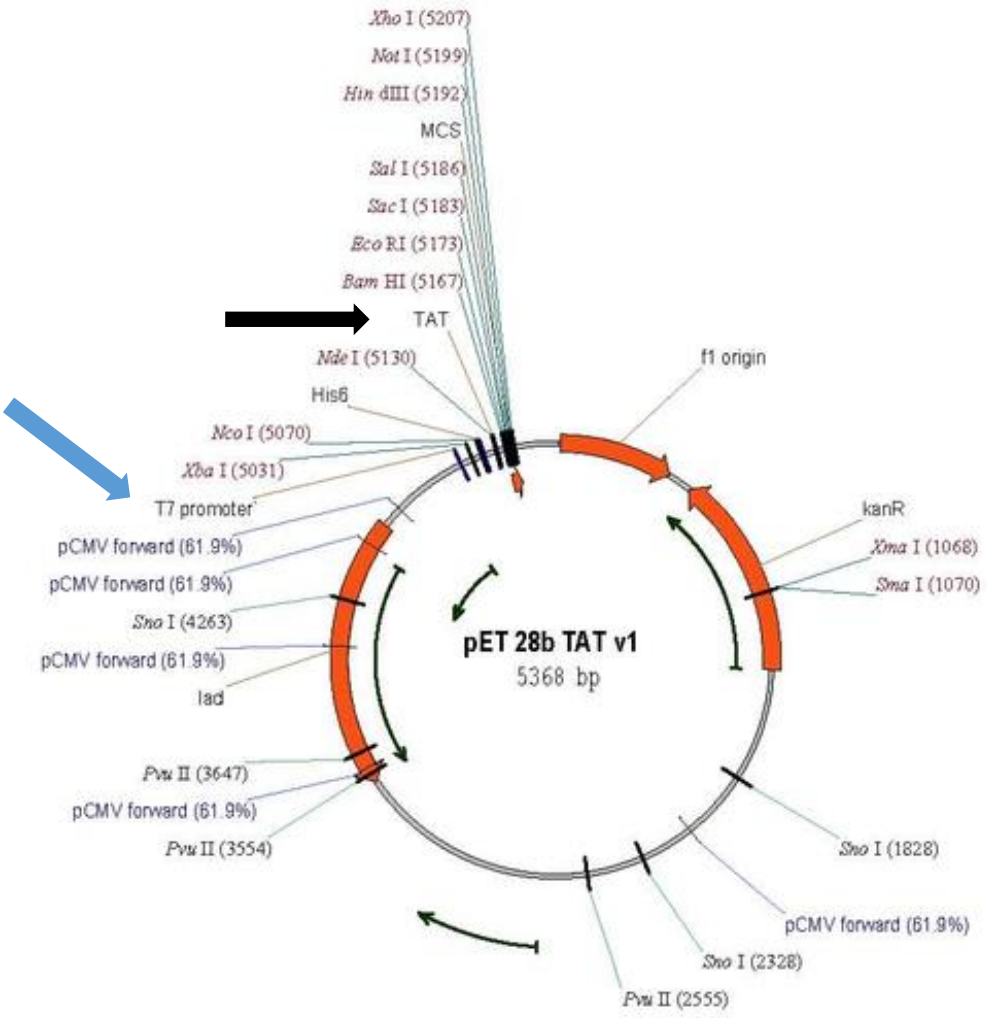
Xho I (5207)
Not I (5199)
Hin dIII (5192)
MCS
Sal I (5186)
Sac I (5183)
Eco RI (5173)
Bam HI (5167)
TAT
Nde I (5130)
His6
Nco I (5070)
Xba I (5031)
T7 promoter
pCMV forward (61.9%)
pCMV forward (61.9%)
Sno I (4263)
pCMV forward (61.9%)
lacI
Pvu II (3647)
pCMV forward (61.9%)
Pvu II (3554)
f1 origin
kanR
Xma I (1068)
Sma I (1070)
pET 28b TAT v1
5368 bp
Sno I (1828)
pCMV forward (61.9%)
Sno I (2328)
Pvu II (2555)

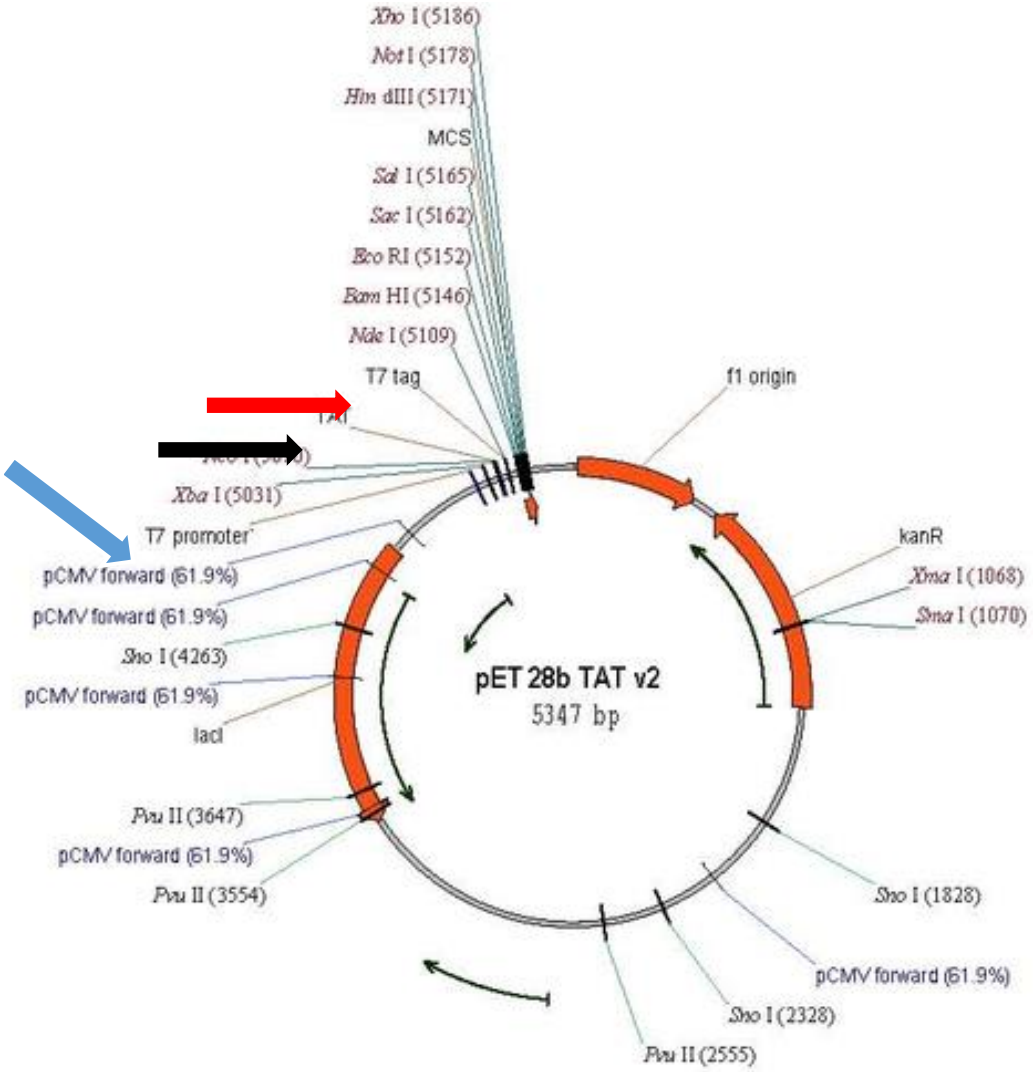

Figure 5.30 Plasmid maps for pTATv1 and pTATv2 plasmids

Black arrows indicate the TAT sequence and the blue arrows show the T7 promoter. The red arrow indicates the only difference between the plasmids, the presence of a T7 tag on pTATv2. Kanamycin resistance and various restriction enzyme sites are also labelled. Both plasmids based on pET cloning vector backbone. MCS stands for multiple cloning site. Plasmid maps for pTATv1 and pTATv2 taken from the addgene website (http://www.addgene.org/35620/).

Restriction digestion reactions were used to validate the identity of the pTAT plasmids. Both plasmids were linearised with a *NotI*, enzyme digestion, for which both pTATv1 and pTATv2 contain a single recognition site. With both pTAT

plasmids containing two recognition sites for the restriction enzyme *EcoNI*, two fragments of 3680bp and 1688bp, were expected. Figure 5.31 shows the agarose gel image where the fragments from the digestion reactions were visualised.

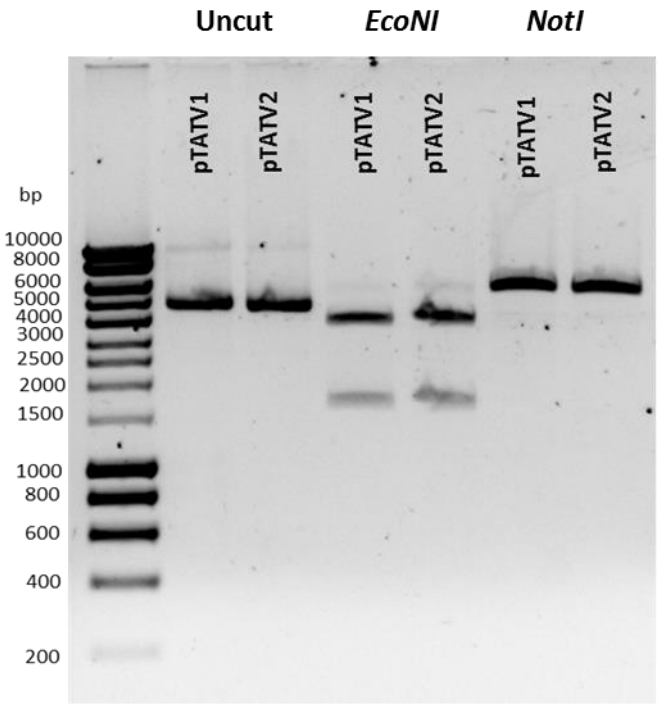

Figure 5.31 pTAT plasmid validation using restriction enzyme digestions reactions

Image of a 0.8% agarose gel showing the DNA fragments following *EcoNI* and *NotI* restriction enzyme digests of pTATv1 and pTATv2 plasmids. The marker is DNA HyperLadder I.

As the expected pattern was observed following the *NotI* and *EcoNI* digestion reactions, the plasmids were purified from cultures of competent *E.coli* DH5α cells, using kanamycin resistance as a selection marker.

The recombinant constructs were first designed *in silico* using DNASTAR® software. In order to have the correct orientation of the lamin A and progerin inserts directional cloning was used by selecting two different restriction sites. *BamHI* was selected based on its extensive use as a restriction enzyme for molecular cloning. *NotI* was the second enzyme selected based on its terminal location and small alanine recognition site, hoping to create an open structure at the end of the protein,

allowing easy access to the histidine tag. The resulting constructs are mapped in figure 5.32.

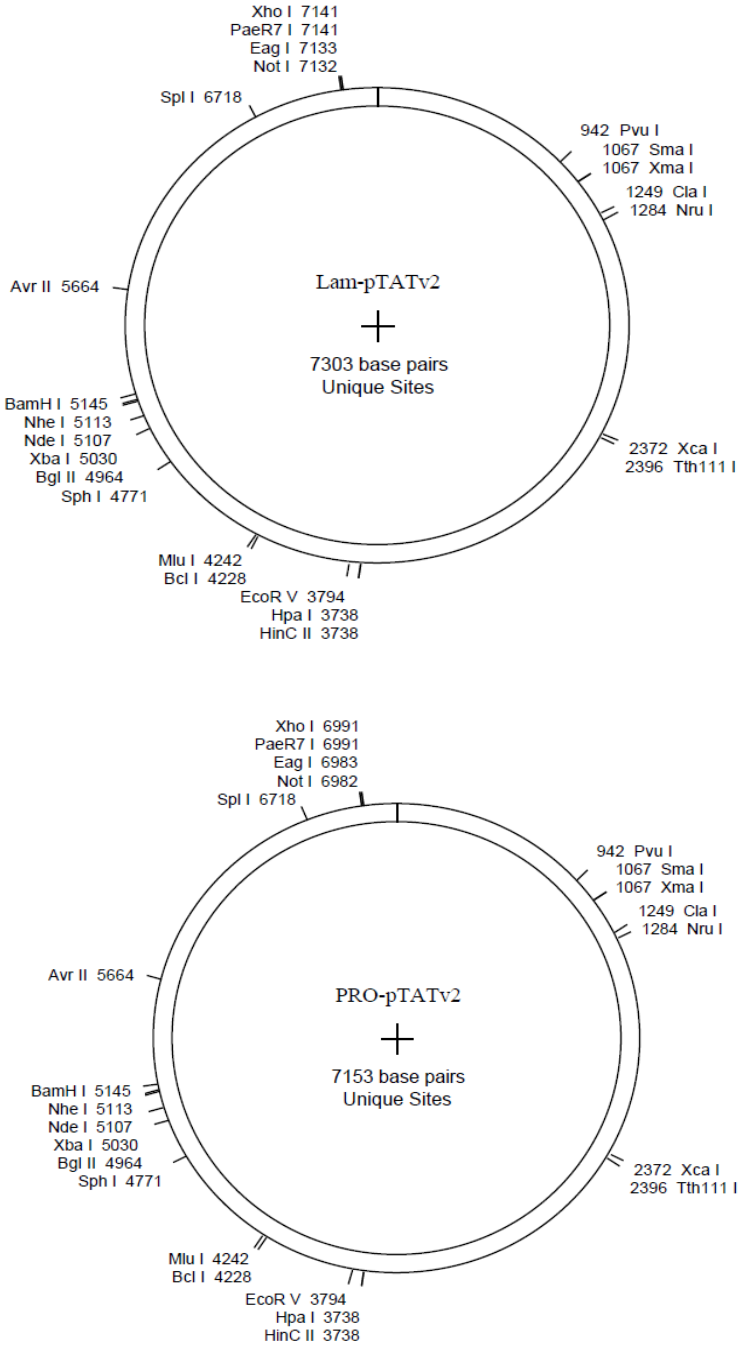

Figure 5.32 Constructed plasmid maps for pTATv2 with Lamin A and Progerin cDNA inserts

A shows the pTATv2 plasmid with the 1935bp lamin A cDNA insert, making a total plasmid size of 7303bp. B shows the pTATv2 plasmid with the progerin cDNA insert of 1785bp. The 150bp size difference reflects the 50 amino acid deletion in the progerin protein. Maps show use of *BamHI* and *NotI* restriction sites. Plasmid maps were constructed using DNASTAR® software.

Lamin A and progerin cDNA Insert sequences were prepared from template plasmid constructs (Appendix i) obtained as a kind gift from Professor Susan Michaelis, Johns Hopkins University. A PCR reaction was used to amplify the desired insert, using primers with adaptors containing the restriction enzyme recognition sequences. The forward primer contained the recognition sequence for *BamHI* and the reverse primer contains a *NotI* recognition sequence, both were designed using DNASTAR® software (see methods and materials 2.2.1.) Figure 5.33 shows an image of the PCR products after gel electrophoresis using 1% agarose.

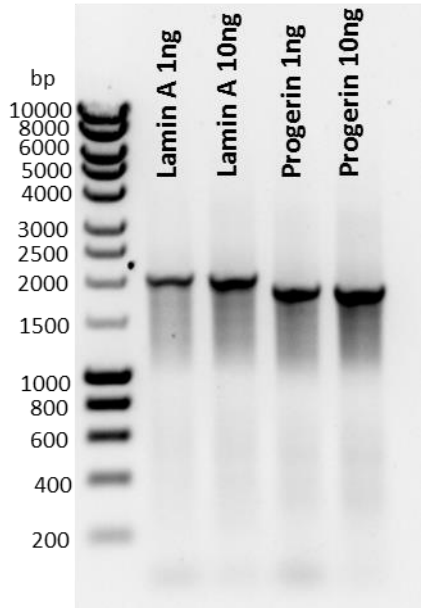

Figure 5.33 PCR amplification of Lamin A and Progerin cDNA inserts

Agarose gel image showing PCR amplification of lamin A and progerin cDNA insert sequences. For both cDNA sequences 1ng and 10ng of template DNA were used for the PCR reaction. The marker on the gel is DNA HyperLadder I and was visualised using the Gel Doc EZ Imager. The 150bp size difference between the two cDNA inserts cofirms the progerin deletion.

The gel image in figure 5.33 shows bands of expected sizes for both the lamin A and progerin sequences. As the template used to make the inserts was cDNA construct, post-splicing, the 150bp size difference between the two inserts apparent in the gel, equates to the 50 amino acid deletion in progerin resulting from activation of the cryptic splice site.

Double digest reactions were then performed on both the plasmids and the insert sequences, using *BamHI* and *NotI* restriction enzymes. A further double digestion reaction was performed on the plasmids using *SacI* and *SalI* restriction enzymes. Both these enzymes have unique cut sites inbetween the *BamHI* and *NotI* recognition sites. This digestion was performed inorder to reduce the possibility of religation of the plasmid. Calf Intestine alkaline phosphatase (CIP) treatment was used to remove the 5' phosphate group meaning no phosphodiester bonds could be formed. As this treatment was not performed on the insert sequences they are still capable of forming such bonds with the vectors. Following these treatments a sample of both plasmids and inserts were run a 0.8% agarose gel. Figure 5.34 shows an image of this gel.

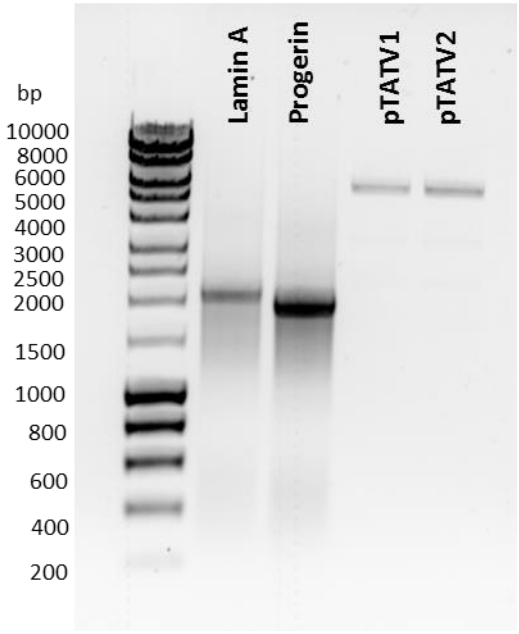

Figure 5.34 Treated and purified Lamin A and Progerin cDNA inserts and pTAT plasmids

1% agarose gel showing fragments for each cDNA insert following *NotI* and *BamHI* restriction digestion and fragments for both plasmids following *NotI*, *BamHI*, *SaII*, *SacI* digestion and CIP treatment. The marker on the gel is DNA HyperLadder I. The gel was visualised using the Gel Doc EZ Imager.

The gel image shown in figure 5.34 was used to estimate each fragmen's concentration, in order to determine what volumes should be taken for the ligation

reaction. Based on the advantage of having a T7 tag within the construct, the pTATv2 plasmid was selected for molecular cloning. Three times the number of insert was mixed with pTATv2 plasmid and incubated in the presence of T4 DNA ligase.

Competent DH5α cells were transformed with pTATv2 plasmids with either lamin A or progerin inserts. Following successful transformation, where numerous colonies were observed on both the lamin A and progerin plates but none were found on control plates (no insert), the plasmids were purified from eight separate colonies from each of lamin A and progerin. A sample of each plasmid was digested with BamHI and NotI . Figure 5.35 shows the products from the digestion reaction run on a 1% agarose gel.

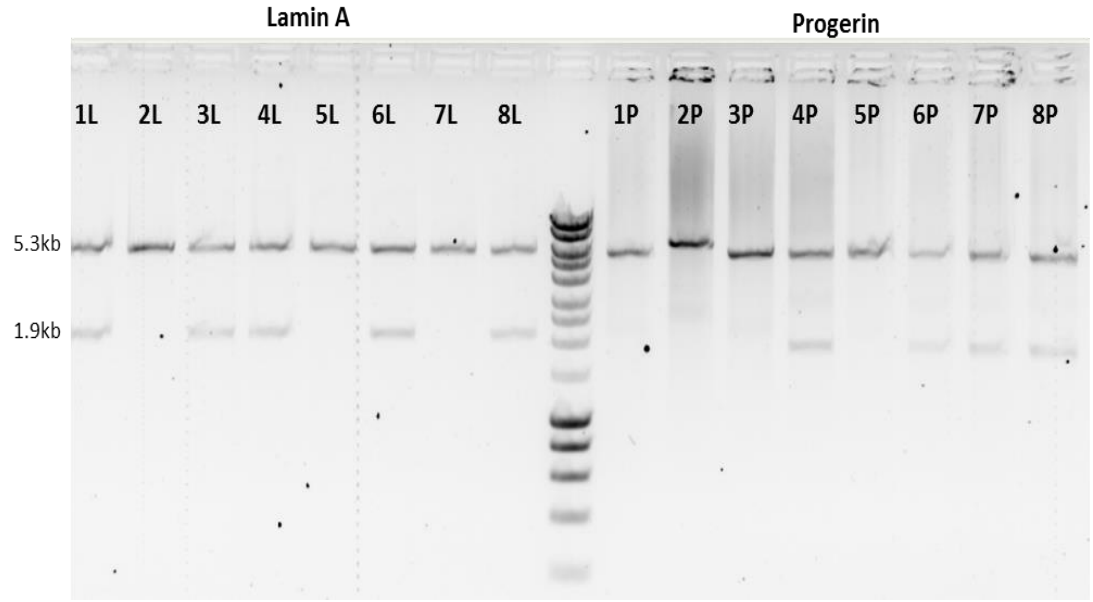

Figure 5.35 Ligation efficiency of Lamin A and Progerin cDNA inserts and pTATv2 plasmid

The top band seen in all lanes confirm pTATv2. The smaller band confirms the presence of the cDNA insert 1L-8L from Lamin A ligation and 1P-8P from progerin ligation. Lanes with two bands show colonies which have taken up a plasmid containing the respective cDNA insert. The marker on the gel is DNA HyperLadder I . The gel was visualised using the Gel Doc EZ Imager.

The plasmids which had taken up an insert were identified in figure 5.35. Two of these plasmids for each insert were selected for DNA sequencing. Plasmids were sequenced by Beckman Coulter Genomics using two of their universal primers, T7P (TAA TAC GAC TCA CTA TAG GG) and T7 term (CTA GTT ATT GCT CAG CGG). The sequenced region covered the insert and approximately 100bp either side of the insertion site. The sequences were aligned to the reference sequence, taken from the *in silico* plasmid maps, using DNASTAR® software. The same base pair change was found in all four inserts, suggesting that this variation was present in the original template DNA. Figure 5.36 shows electropherograms and sequence alignment for the sequence variation.

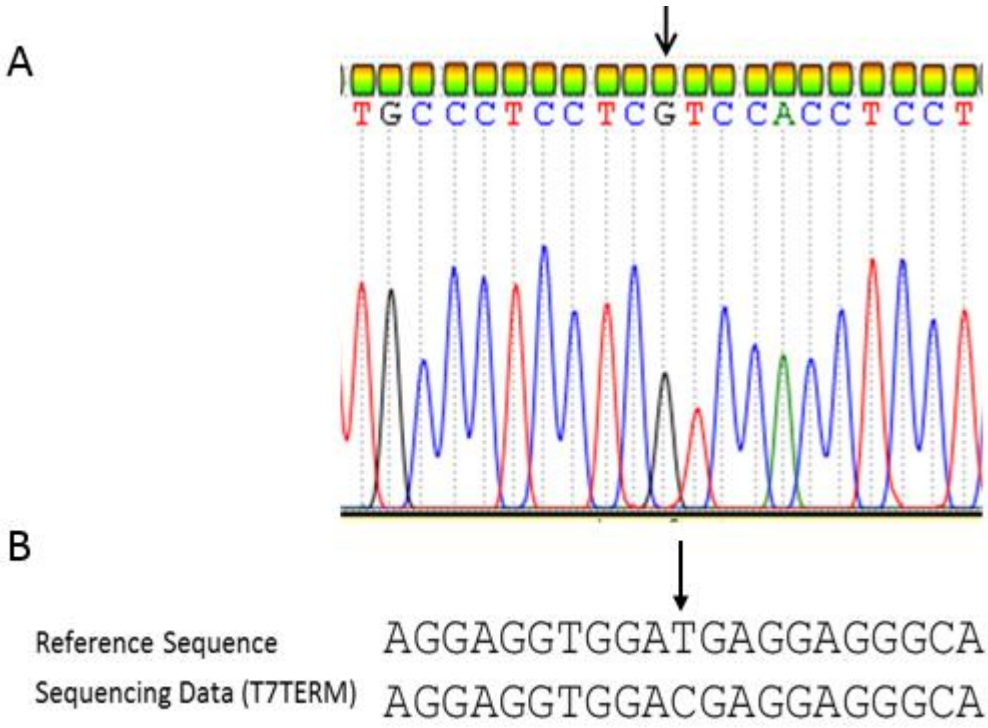

Figure 5.36 Electropherogram showing sequence variation found in all 4 plasmids sequenced

Graph shows the sequences reads obtained using the T7 term reverse primer. Arrow indicates the sequences variation. Image B shows the reference sequence aligned to the complimentary T7 term read once it had been inverted.

The sequence variation shown in figure 5.36, GAT>GAC at nucleotide 1495, is a silent mutation which does not change the amino acid, aspartic acid, at position 441 of these protein. As it is believed this variation was present in the template DNA, plasmids containing this sequence variation could continue to be used. This was the only sequence variation found in the 3L plasmid, however, 6L contained several sequence changes. Therefore, 3L was selected as the plasmid to be used to produce the TAT- lamin A protein. Plasmid 4P was identified as having a variation which altered the amino acid sequence of progerin making it unsuitable to use for protein production. 8P was found to contain a second synonomous mutation of AAT>AAC at nucleotide 1575. As this does not change the amino acid, asparagine, 8P was selected for protein production. See Appendix ii for all sequencing data.

The 3L and 8P plasmids were transformed into rubidium chloride competent Rosetta^{TM} cells (Novagen), a BL21 variant which contains tRNAs (recognise AGG, AGA, AUA, CUA, CCC, GGA codons) specific for the production of human proteins. The Rosetta^{TM} cells also contain a plasmid that confers chloramphenicol resistance. 0.5mM Isopropyl β-D-1-thiogalactopyranoside (IPTG) was used to induce the production of the proteins under the control of the T7 promoter. A sample of the culture before and after induction was run on a 10% SDS PAGE. This gel was then stained for proteins using coomassie blue. Figure 5.37 shows an image of the gel.

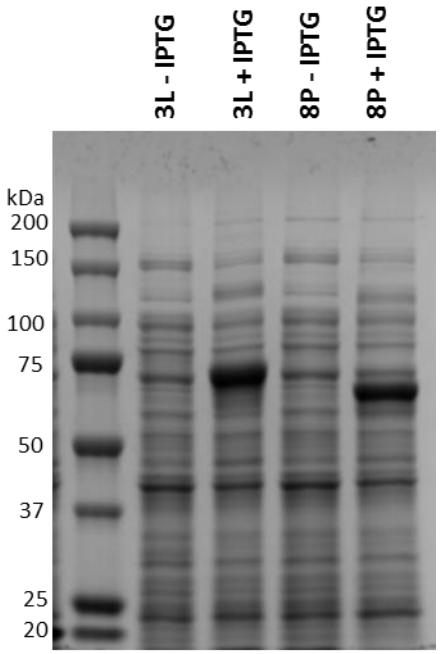

Figure 5.37 IPTG protein induction

Image of a 10% SDS PAGE showing proteins found in Rosetta™ cell before and after protein induction using IPTG. The additional bands in the +IPTG are at the expected molecular weights for TAT-Lamin A (75 KDa) and TAT-Progerin (70 KDa) respectively. The ladder is the Precision Plus Protein™ standard (Bio-Rad). The image was taken using the Gel Doc EZ Imager (Bio-Rad).

The addition of the TAT domain to proteins is believed to add between 5-10 kDa to the observed molecular weight, therefore TAT-lamin A is expected to have a molecular weight of 75 kDa and TAT-progerin of 70 kDa. IPTG induction caused the production of proteins of expected sizes, shown by the appearance of thick bands on the gel in figure 5.37. The 50 amino acid difference between these two proteins can be observed on the gel in figure 5.37. After protein induction was confirmed, protein purification was attempted using the histidine tag found on the fusion proteins.

Protein purification was performed as outlined by Becker-Hapak *et al*, 2001. Total cell extract was produced by incubation with Buffer Z, which contains 8M Urea and causes cell lysis and sonication to break open inclusion bodies and shear DNA. Centrifugation at 16,000G was enough to separate total cell extract into either pellet

(DNA) or supernatant (Proteinaceous). 20mM imidazole was used to increase binding efficiency of the supernatant to the Ni- NTA Agarose (Qiagen) resin. The unbound proteins (run-through) were removed and elution of proteins from the column was attempted with increasing concentrations of imidazole.

Analysis with a Bradford assay identified that no protein was eluted from the column in any fractions. Figure 5.38 shows an SDS PAGE analysis of the total cell extract, pellet, supernatant and run-through, and was used to determine the stage at which the protein was lost.

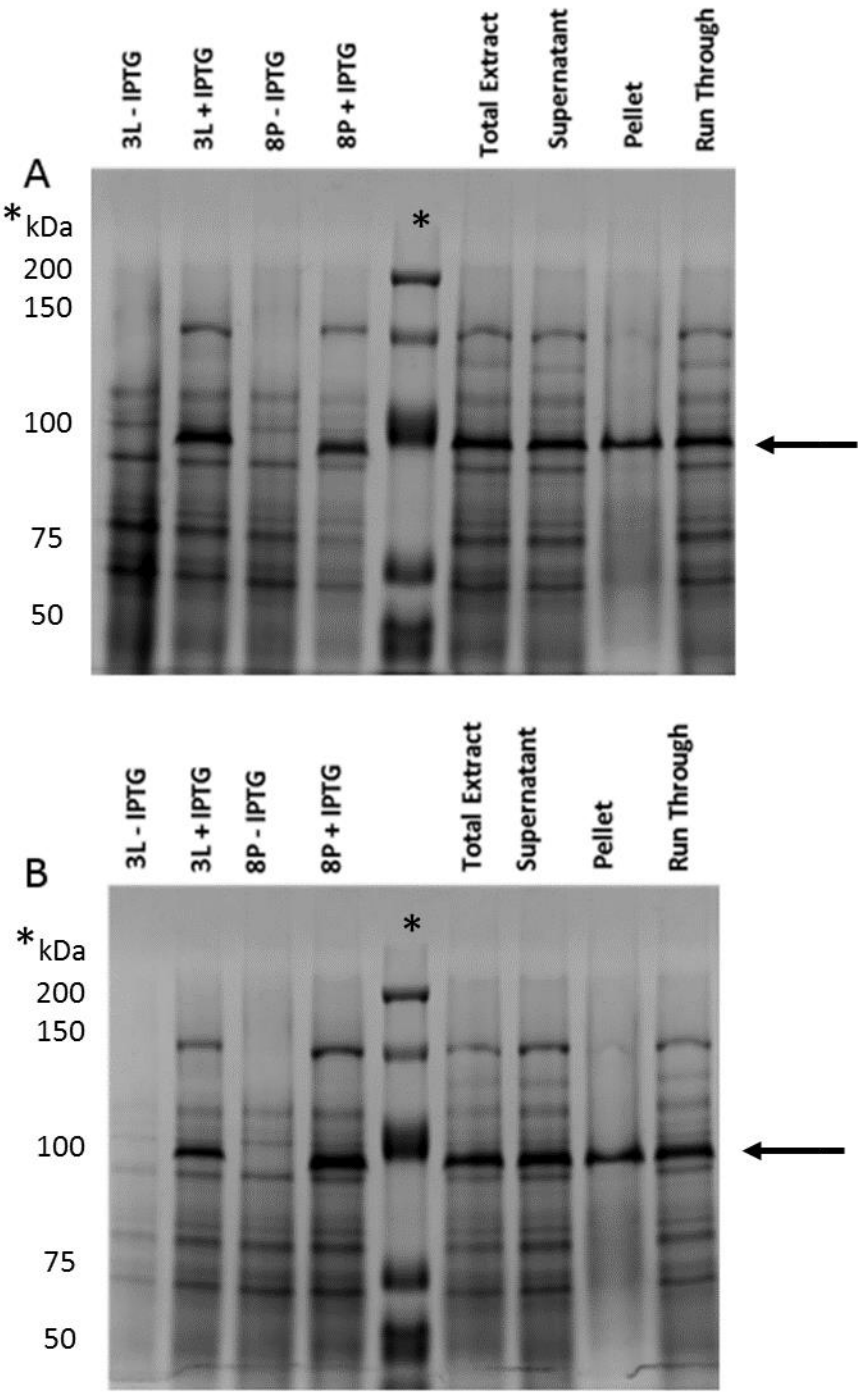

Figure 5.38 Analysis of protein purification for TAT- lamin A and TAT- Progerin

10% SDS PAGE gels showing before and after IPTG induction for both TAT-Lamin A and TAT- Progerin. Image A shows the proteins found in the total cell extract, supernatant, pellet and run through for the TAT-Lamin A protein. Image B shows the same for the TAT-Progerin protein. Three times the volume of re-suspended pellet was loaded onto the gel compared with all other sample. The ladder in both gels is the Precision Plus Protein^{TM} standard. The images were taken using the Gel Doc EZ Imager.

Since the protein was present in the total cell extract and supernatant it was not affected by sonication and not much was lost into the pellet. Unfortunately, the presence of the desired proteins in the run through shows that the protein did not bind to the column. In order to remedy this, a lower final concentration of imidazole (10 mM) was added to the supernatant. Under these conditions a relatively low yield of protein was purified. Figure 5.39 shows the purified fractions which contain lamin A (Figure 5.39A) and progerin (Figure 5.39B).

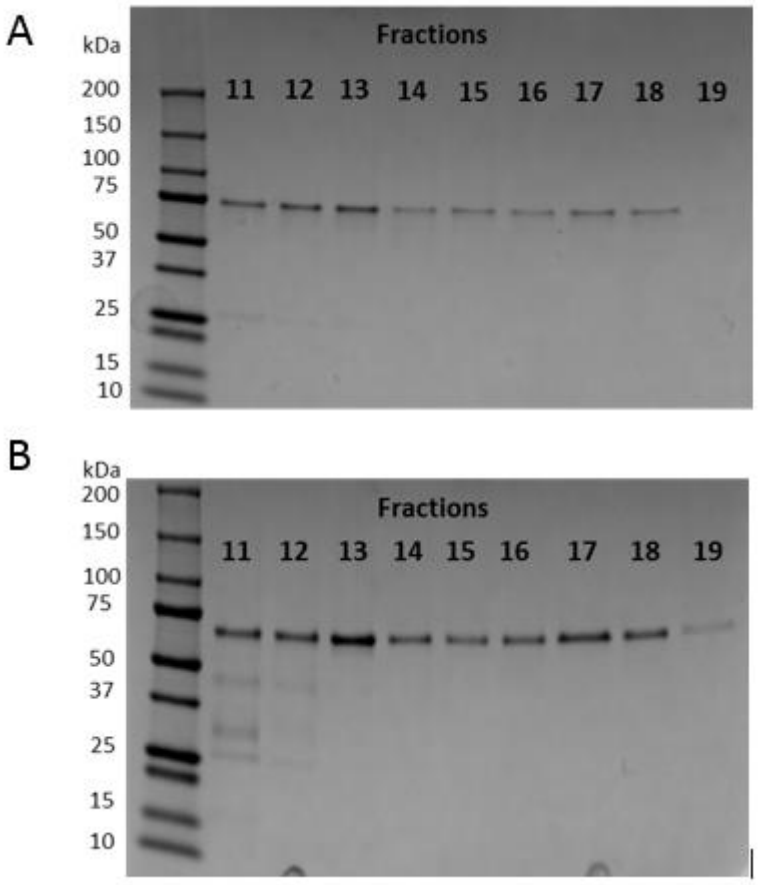

Figure 5.39 Protein Purification Fractions

10% SDS PAGE gels showing purified fractions of TAT-lamin A (A) and TAT-progerin (B). The ladder in both gels is the Precision Plus Protein^{TM} standard. The images were taken using the Gel Doc EZ Imager.

Despite the purification of the desired protein a considerable amount of this protein was still found in the run-through. Figure 5.40 shows analysis of the fractions for the purification attempt using the lower concentration of imidazole.

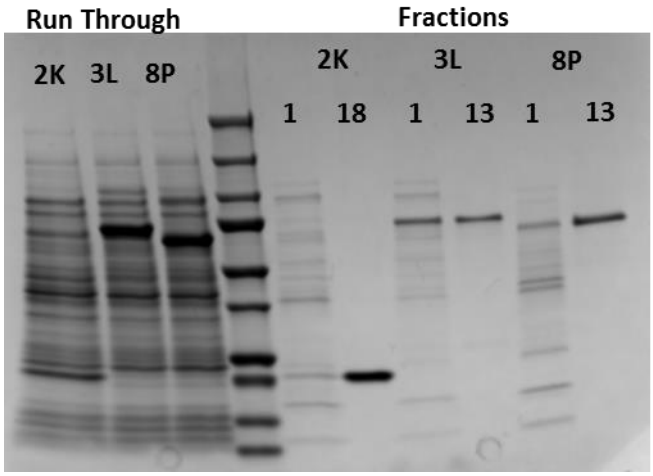

Figure 5.40 Comparison of run through and protein purification fractions for TAT- lamin A and TAT- Progerin

SDS PAGE gel stained with coomassie blue showing the run through and peak purified fragment for both TAT-Lamin A, TAT-Progerin and for a TAT-p16 fusion protein (2K) which has a good protein yield and was purified simultaneously with the two other proteins. The gel also shows the run-through, first fraction eluted from the column (1) and the peak purified fraction for Lamin A and Progerin this is fraction 13, wheras 2K is fraction 18. The image was taken using the Gel Doc EZ Imager.

The SDS PAGE in figure 5.40 shows the run through and fractions for 3L, 8P and a TAT-p16 fusion protein for comparison. After incubation with the resin the level of TAT-p16 (2K) is minimal within the run-through, with the majority of protein being found in the purified fractions. The reverse can been seen for the TAT-Lamin A and TAT-Progerin proteins, suggesting that the nature of the proteins, in particular their filamentous structure, may be involved in their low binding efficiency. Further optimisation, including increasing incubation times and reducing temperatures all failed to increase the binding efficiency.

To determine if the poor binding ability of the proteins to the column is as a result of a lack of a histidine tag, western blot analysis was performed on whole cell lysate post IPTG protein production. An anti-histidine tag antibody was used in combination with a horseradish peroxidase conjugated secondary antibody and

visualised using chemiluminescence. An image of the resulting membrane is shown in figure 5.41.

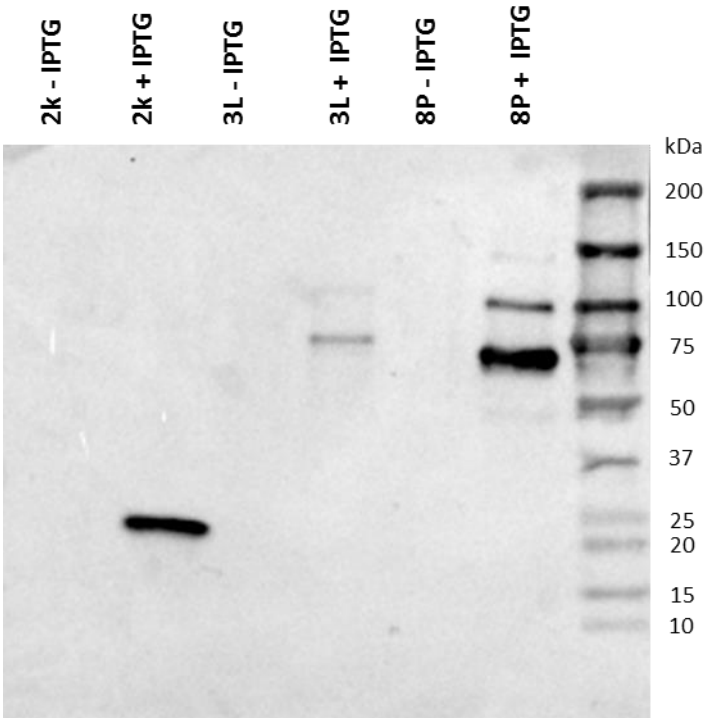

Figure 5.41 Western blot analysis of whole cell extracts before and after IPTG induction using antibody raised against the Histadine tag

Image showing a western blot membrane probed with a histidine tag antibody, identifying the presence of proteins with a histadine tag post- IPTG protein induction, namely, TAT-p16 (2K), TAT-Lamin A (3L), TAT-Progerin (8P). The marker is the Precision Plus Protein™ standard and membrane was visualised under chemiluminescence using the Molecular Imager® ChemiDoc™ XRS+ using Image Lab™ software.

The image in figure 5.41 shows that the proteins produced do contain a histidine tag and should, therefore, bind to the Ni-NTA Agarose column. Under the SDS conditions we see that the histidine tag is detectable both for TAT-lamin A, TAT-progerin and as a control TAT-p16. For control, TAT-p16 a single band is visible and at the expected molecular weight of 25 kDa. For TAT-lamin A and TAT-progerin, the main band in each lane is the expected molecular weight and likely indicates the fusion protein, however, several bands revealing larger proteins are also visible for both fusion proteins. This suggests that more than one transcription

product is being produced from the plasmid and the interaction between these proteins is undetermined.

5.2.2 TAT -Lamin A and TAT-Progerin Protein Transduction

TAT-mediated protein transduction was attempted with the small amount of purified fusion-proteins. 2DD primary fibroblasts, grown on glass cover slips, were incubated with the fusion protein for a 30 minute period. After this time cells were fixed and stained using antibodies against the T7 tag and lamin A/C, as described in section 2.2.1. Representative Images of the staining pattern observed using these two antibodies is shown in figure 5.42.

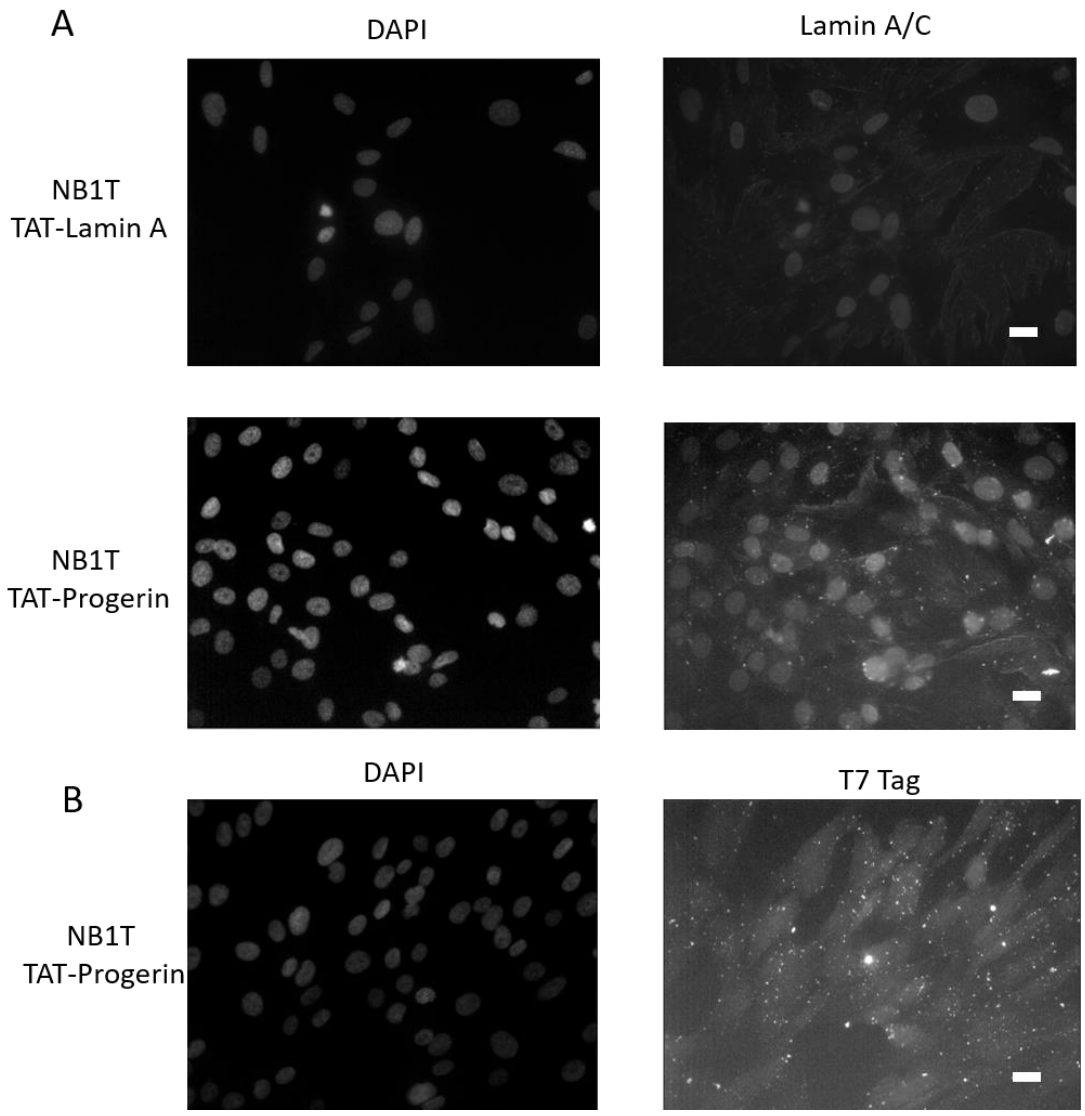

Figure 5.42 T7 TAG and Lamin A/C Immunofluorescence following TAT-Lamin A and TAT-Progerin protein transduction

Images showing the staining pattern observed after protein transduction using lamin A/C (A) and T7 tag (B) antibodies and DAPI.

The staining patterns shown in figure 5.42 suggests that the proteins have not penetrated the plasma membrane and may have formed aggregates outside of the cells. To increase the likelihood of cell penetration the 8M urea was removed from the buffer before transduction. This was performed using a PD-10 desalting column. The use of this column resulted in a successful transduction for the p16-TAT protein. The TAT-Lamin A and TAT-progerin proteins both gave the same staining pattern as that observed before the desalting step (data not shown).

To determine that the antibodies were recognising the correct proteins western blot analysis was performed using lamin A/C and T7 tag antibodies. The before and after IPTG induction samples were run on 10% gels and probed as described in section 4.2.4. Images of the western blot membranes probed with lamin A/C and T7 tag antibodies are shown in figures 5.43 and 5.44 respectively.

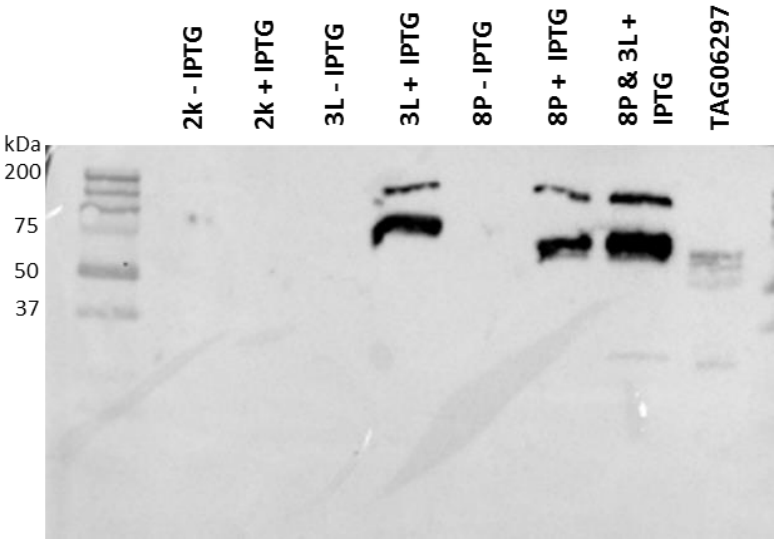

Figure 5.43 Western blot analysis of whole cell extracts before and after IPTG induction using antibody raised against Lamin A/C

Image showing a western blot membrane probed with a lamin A/C antibody, identifying the production of Lamin A/C proteins post- IPTG protein induction. Bands at 75 kDa confirm TAT- Lamin A (3L) and at 70 kDa (8P) show TAT-Progerin. Larger than expected bands are also observed in both 3L and 8P. No bands are detected in 2k as plasmid encodes a TAT-p16 protein and no lamin proteins. TAG06297 is a hTERT immortalised HGPS fibroblast cell line. The marker is the Precision Plus Protein™ standard (Bio-Rad) and membrane was visualised under chemiluminescence using the Molecular Imager® ChemiDoc™ XRS+ using Image Lab™ software.

The gel in figure 5.43 shows the proteins are of expected size when compared to the sample prepared from hTERT HGPS fibroblast cell line TAG06297. The larger proteins visualised using the histadine Tag antibody are also visualised with Lamin A/C antibody, identifying them as a larger transcript from the pTATv2 plasmid. As

expected no bands were identified in the control TAT-p16 sample, also showing that the lamin A/C antibody is not interacting with any endogenous bacterial proteins.

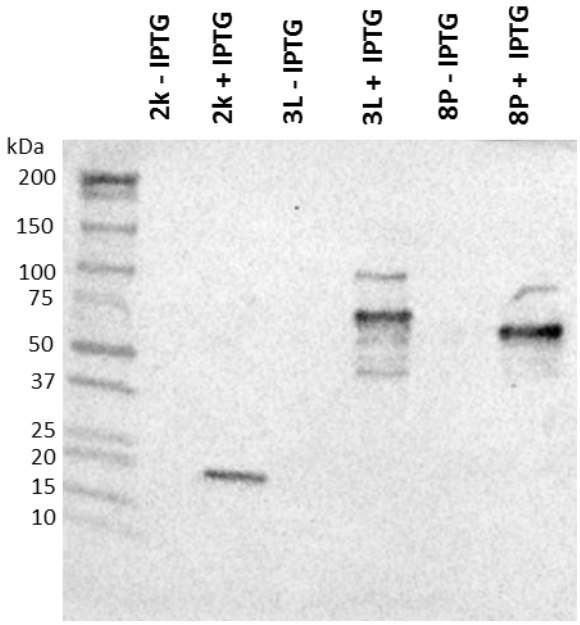

Figure 5.44 Western blot analysis of whole cell extracts before and after IPTG induction using antibody raised against the T7 TAG

Image showing a western blot membrane probed with a T7 TAG antibody, identifying the production of proteins containing T7 TAG post- IPTG protein induction. Bands at 75 kDa confer TAT- Lamin A (3L) and at 70 kDa (8P) show TAT-Progerin. Larger than expected bands are also observed in both 3L and 8P. Bands are detected in 2k as the plasmid encodes a TAT-p16 protein with a T7 TAG. TAG06297 is a hTERT immortalised HGPS fibroblast cell line. The marker is the Precision Plus Protein™ standard and membrane was visualised under chemiluminescence using the Molecular Imager® ChemiDoc™ XRS+ using Image Lab™ software.

Figure 5.44 shows the western blot using an antibody raised against the T7 tag. The inclusion of this tag within our fusion protein was aimed to allow differentiation between endogenous and transduced proteins within the HGPS cells. For TAT-Lamin A, TAT-progerin and TAT-p16 bands are visualised at the correct molecular weight. For both TAT-Lamin A and TAT-progerin, however, the same 100 kDa band, presumed a larger undesired transcription product, and also several smaller bands are also visible. The presence of additional transcription products, low

purification yield and aggregation upon protein transduction hindered the progression of this work.

5.2.3 A-Type Lamin Nanobody Plasmid Transformation

As several issues arose with the use of TAT-lamin A and TAT-progerin fusion proteins, as a method for the validation of increase progerin degradation in response to growth in the presence of hTERT, a second method using Nanobody technology was attempted. An A type lamin targeted nanobody with a conjugated E3 ubiquitin ligase was designed by Professor Heinrich Leonhardt's laboratory, the pioneers of this technology. The aim of this work was to recreate the process that we believe occurred naturally within the TAG06297 cultures in response to hTERT expression. By targeting A-type lamins and bringing them into close proximity to an E3 ubiquitin ligase, an increase in the rate of A-type lamin degradation through polyubiquitination was expected. It is hypothesised that through a reduction in the level of progerin in HGPS fibroblasts, a similar loss of progeria cell characteristics could be observed as that seen in the TAG06297 Late culture in chapter 3. The pc3236 plasmid was provided by Professor Leonhardt's group and a map of this plasmid is shown in figure 5.45.

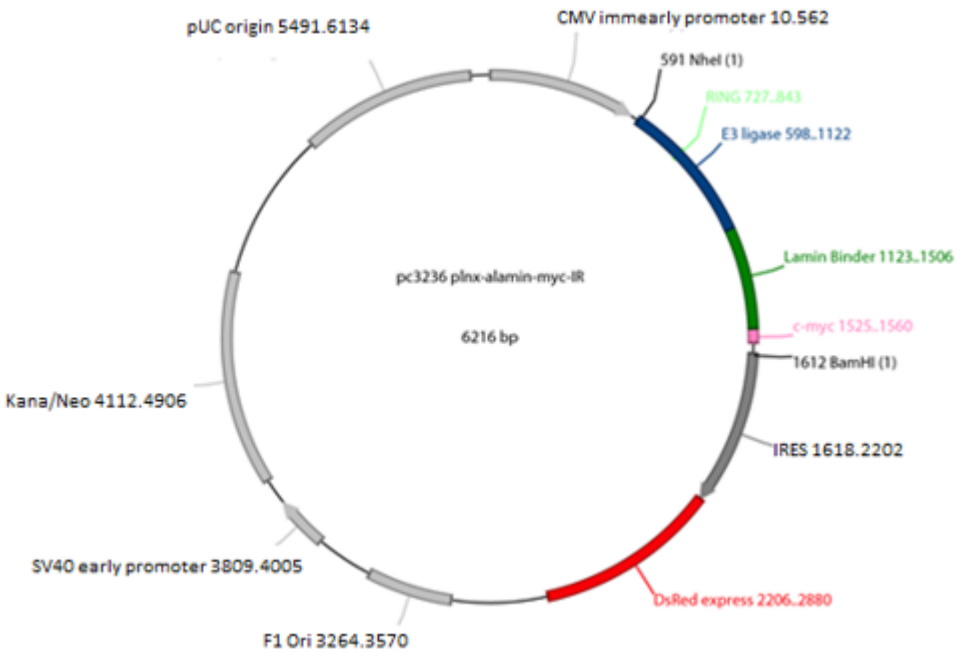

Figure 5.45 pc3236 plamid map

Plasmid map showing the E3 ligase coding sequence in blue, next to the A type lamin recognition sequence shown in green. Shown in red is the red fluorescent protein DsRed. Map provide by Professor Leonhardt's group.

Pc3236 was transiently transfected into NB1T hTERT control fibroblast cultures as well as TAG06297 early and late hTERT HGPS cultures. Transfected cells were cultured for 24 and 48 hour periods followed by fixation and visualisation using fluorescence microscopy. A plasmid expressing GFP was used as a negative control. No antibodies were needed as cells expressing pc3236 were expressing DsRed and were therefore distinguishable. The transfection efficiency for the control GFP plasmid was 30% and for pc3236 was 10%. Data was gathered and analysis performed by Dr Joanna Bridger.

Analysis of cells 24 hours post transfection show nuclear morphology changes detected using DAPI staining. Control NB1T fibroblasts show elongated nuclei in 100% of cells positive for DsRed as compared to elliptical structure of non-transfected cells. In NB1T cells expressing the pc3236 plasmid clumping of chromatin was also visible which is reminiscent of chromocentres. Similarly

TAG06297 Late cell also show an elongated nuclear morphology in response to the A type Lamin nanobody. They also show the presence of bright foci accumulation and a tendency to form multinuclei. The TAG06297 Early cells, however, seem less affected by the pc3236 plasmid with <40% of DsRed positive cells showing changes to nuclear morphology and chromatin aggregation. Figure 5.46 shows representative images of the DAPI staining in response to transfection with pc3236. Very few changes to nuclear morphology were observed following transfection with the GFP control plasmid.

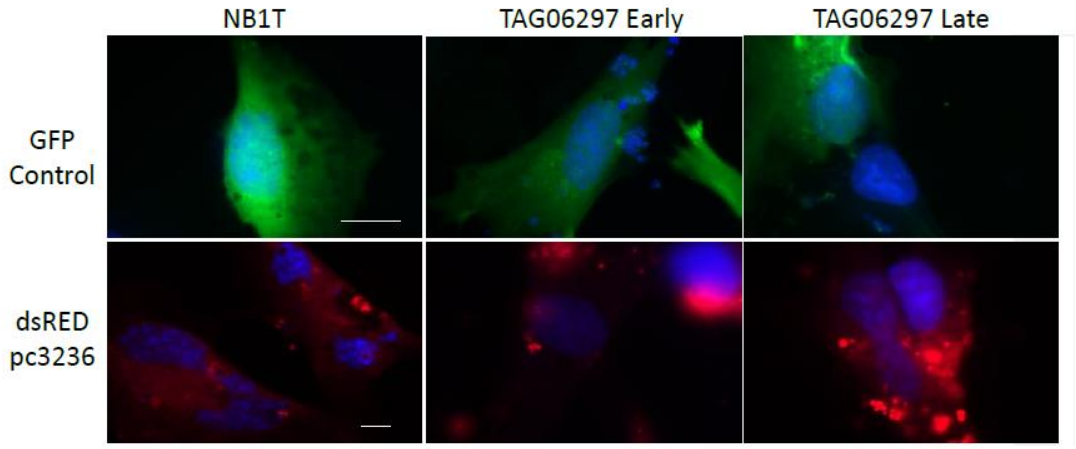

Figure 5.46 Fluorescence image analysis of hTERT HGPS cells following transfection of pc3236 encoding A type lamin specific nanobody conjugated to an E3 ubiquitin ligase

Pc3236 expression shown in red by the expression of DsRed. Control plasmid encoding GFP shown in green. Nuclei stained with DAPI and visualised using fluorescent microscopy. Transfection performed on an early passage and late passage version of the TAG06297 HGPS fibroblast cell line immortalised with hTERT. Images captured and analysed by Dr Joanna Bridger. Scale bar = 10µm.

The difference in effect of the A type lamin targeted Nanobody on TAG06297 Early and Late can be explained by the difference in level of A type lamin proteins within these cells. Loss of progeria cell characteristics (as described in chapter 3) has been attributed to an increase in protein degradation of both lamin A and progerin (as described in chapter 4) resulting in less toxic A type lamins and therefore, explaining

the similarity in response of both control (NB1T) cells and the TAG06297 Late cultures.
The TAG06297 Early culture still demonstrate the negative effects of progerin expression and ultimately benefit in the short term from the reduction of A type lamin proteins. 48 hours after transfection, however, cell loss, thought to be through apoptosis, is observable in all three cell lines, inhibiting the gathering of data from these slides. Cell death in TAG06297 Early cells was observed at a slower rate, again providing tentative support to the hypothesis.

Ultimately this finding suggests that targeting A-type lamins through pc3236 does not support cell viability. The Nanobody recognition sequence binds to all A-type lamins, knockdowns of which have previously been shown to reduce viability in mice (Sullivan *et al*, 1999). This supports the observation that cells were undergoing the early stages of apoptosis 24 hours after the Nanobody transfection. Further information would be better gathered using a Nanobody specific to Lamin A and progerin as neither of these are essential for cell survival, with an entirely health lamin C only mouse model having been created (Fong *et al*, 2006).

5.3 Discussion

In this work we have shown the production of TAT- lamin A and TAT- progerin fusion proteins. The next step in the development of these proteins is to optimise the purification protocol. The 8M Urea should be ample to denature the proteins and open up their structure. Through western blot analysis we know the histidine tag is present in these fusion proteins, yet is unable to bind to the Ni-NTA column. With the difficulty previously observed in immunoprecipitation of these filament proteins (Herrmann, 2004), this could suggest that even in denaturing conditions they are forming secondary structures masking the histidine tag. One option to overcome this would be to use the pTATv1 plasmid as this contains two histidine sequences (see figure 5.30), hopefully increasing the purification efficiency. Screening with three different antibodies (Lamin A/C, Histidine tag and T7 tag) all reveal the production of several proteins of increased molecular weight. Though the majority of the protein produced is of the correct molecular weight, the effect of these contaminating

proteins is unknown and pure product is required for protein transduction. The plasmids were selected based on low levels of genetic variation from the reference sequences and as no splicing occurs in bacteria cells one protein product was expected. With optimisation of the purification process, greater stringency by increased imidazole concentration, may enable the selection of pure protein products. Once proteins of the correct size have been purified TAT-mediated protein transduction can be attempted. It is possible that the nature of these filaments affinity for dimer formation (Dechat *et al*, 2010) is also inhibiting the transduction process, in particular as no improvement was seen following desalting, a step known to increase transduction efficiency for other TAT fusion proteins (Becker-Hapak *et al*, 2001). Successful protein transduction and incorporation into the nuclear lamina must be observed before further experiments can be conducted using the TAT proteins.

The aim of developing these TAT-fusion proteins was to determine the rate of progerin degradation in HGPS fibroblasts and show an increased rate of degradation in response to long term growth in the presence of hTERT. Progerin degradation, in response to Rapamycin treatment of HGPS fibroblast, has previously been explored using radiolabelled- pulse chase experiments followed by immunoprecipitation, which showed an increase in breakdown of the soluble fraction of progerin compared to lamin C (Cao *et al*, 2011). This technique could also be employed to look at the effects of hTERT.

Another potential use of these transducing proteins is to determine at what level progerin causes an effect on cell function. Small levels of progerin have been detected in cells and skin from elderly donor (Scaffidi & Misteli, 2006; Rodriguez *et al*, 2009; McClintock *et al*, 2007), however, it is not known if this is a cause of ageing or if it is a by-product. In order to investigate this, increasing concentrations of TAT- progerin could be added to control cells until it is determined it has elicited a detrimental effect, by the appearance of progeria cell characteristics.

It would be interesting to determine if only a small amount of progerin is required to harm cell function or if there is a critical level at which progerin can no longer be

tolerated. If this is the case therapeutic efforts, such as the proposed rapamycin treatment (Cao *et al*, 2011), can be put into reducing progerin to below the critical level. It could also be that the ratio between progerin and lamin A is the key factor, therefore, transduction of lamin A would restore cell function. In this case future treatments of HGPS could involve increasing cellular levels of lamin A. This would be in contradiction to previous findings, however, which suggest that the toxic effect of progerin is not negated by Lamin A abundance (Scaffidi & Misteli, 2005).
A further use of the TAT fusion proteins is to investigate how progerin and lamin A enter the nuclear lamina. There is much confusion about how lamin A and progerin are incorporated into the nuclear lamina (Dittmer & Misteli, 2011).

Immunofluorescence analysis at time points after protein transduction could add clarity to this matter. The fusion proteins can also be used to identify lamin A and progerin binding partners using a ChIP type method. The addition of the histidine tag to these proteins will allow easy purification for the ChIP like assay. This would add insight into the differences between lamin A and progerin within the nuclear lamina. It could also determine whether lamin A and lamin B co-polymerise (Ye & Worman, 1995; Georgatos *et al*, 1988; Dittmer & Misteli, 2011).

The use of Nanobodies targeted to A type lamins, conjugated to a E3 ubiquitin ligase, was aimed at replicating the natural occurring events observed in response to prolonged growth in the presence of hTERT, whereby TAG06297 Late cells had reduced their progerin and improved cell phenotype (Chapter 4). By transfecting a plasmid encoding an A type lamin target Nanobody conjugated to an E3 ligase it was thought that TAG06297 Early cells would begin to present like TAG06297 Late cells.

We observed that the A type Lamin target Nanobody -E3 ubiquitin ligase did elicited an effect, it is unfortunate that by targeting both Lamin A and Lamin C cell death occurred. It is not surprising that increasing the breakdown of all of these proteins led to cell death, but it does demonstrate the potency of this approach. A Nanobody designed to specifically increase the degradation of Lamin A and Progerin, would better mimic the effects observed in the TAG06297 Late cell line,

offering possibilities for therapy. With potential therapies, such as rapamycin treatment (Cao *et al*, 2011), already exploring the option of increased protein degradation, Nanobodies offer a more specific approach than increased autophagy. With many concerns about the suitability of Rapamycin it may be a case of the right approach but the wrong method. Nanobodies are already being employed therapeutically (Peyvandi *et al*, 2016) and may be the right method.

The production of TAT-lamin A and TAT-progerin offer a novel approach to investigating HGPS. The proteins offer the opportunity to investigate the cell biology underlying HGPS as well as the potential to identify new genes and therapeutic targets for this disease. Although in their infancy TAT-Lamin A and TAT-progerin fusion proteins are an exciting and useful tool in studying HGPS. The first experiments using Nanobodies conjugated to an E3 ubiquitin ligase in HGPS cells show therapeutic promise for the treatment of this so far incurable disease.

6 Characterisation of hTERT Immortalised, "Atypical" Progeria Cell line in the Search for a new Causative Genetic Mutation.

6.1 *Introduction*

Identification of new genes involved in the progeriod process will give a better understanding of the underlying mechanisms of HGPS. One of the main aims of this research is to identify new genes responsible for the rare "Atypical" form of HGPS. Several uncommon gene mutations have already been reported (see section 1.5), which alter lamin A binding partners and proteins involved in lamin A processing. This highlights the importance of lamin A and nuclear envelope proteins in this disease, suggesting potential candidate genes may be proteins that form lamin A interactions.

The rare nature of this disease means there are a limited number of patients and thus cell lines available. One available cell line, AG08466 (Coriell Institute), is a fibroblast cell line, established in 1985, originating from an 8 year old girl with "Atypical HGPS". The skin biopsy used to establish the cell line was taken ante-mortem and information about the longevity of this patient is unavailable. The patient had a normal 46, XX karyotype and some classic characteristics of HGPS such as loss of subcutaneous fat, osteoarthritis and venous prominence; however, the patient experienced no alopecia and developed some Marfan syndrome like characteristics (Coriell Institute). The underlying mutation in this patient has yet to be established. Sequence analysis has revealed a normal genotype for nucleotide c.1824C in the *LMNA* gene (Personal communications Professor Nico Lévy). Further sequencing analysis, performed at Brunel University London, showed no mutation in the lamin A binding partners *emerin* and *LAP2α* (Godwin, 2010).

The low incidence of this disease makes normal methods of disease gene identification more challenging, as for instance there are not enough patients to

perform a genome wide association study (GWAS). It is difficult because some mutations are found only in a small number of patients or may be specific to an individual.

Micro-cell mediated chromosome transfer (MMCT) is one proposed method for identifying the underlying mutation in the AG08466 cell line. This technique allows the removal of genetic material from a cell line (donor) and subsequent incorporation of this chromosome into a second cell line (recipient) (Fournier & Ruddle, 1977). This is a well-established technique that was first developed in the 1970's and has proved an effective tool for gene discovery, especially in the cancer field (Anderson & Stanbridge, 1993; Yoshida et al, 2000; Meaburn et al, 2005). Most notably p53 and pRB were identified using this method (Stanbridge 1992). The breakthrough in this technique came when an entire human genome library was created in a mouse cell background (Cuthbert et al, 1995). Each chromosome from a healthy individual was transferred into separate mouse cells. The easy removal of the human chromosome from the mouse background allowed for complementation studies, which have led to the identification of a large number of tumour suppressor genes (Meaburn et al, 2005). Chromosomes from the mouse library are transferred into tumour cells and if complementation occurs loss of neoplastic characteristics such as growth in soft agar can be observed. This indicates that a tumour suppressor gene, which has been inactivated in the tumour cell, is encoded within the transferred chromosome. Upon transfer of the chromosome, it is incorporated into its normal nuclear location and thus has a normal expression profile (Tindall et al, 1998). One method that has been employed to determine the specific locus of the tumour suppressor gene within the chromosome involves transferring chromosome fragments that have been produced by exposure to γ- irradiation, in a deletion mapping type exercise (Dowdy et al, 1990). For example the colorectal cancer tumour-suppressor gene has been mapped to a 900-kilobase region on the short arm of chromosome 8 through MMCT of chromosome fragments (Flanagan et al, 2004). This technique has also been applied to identify senescence associated genes, by first identifying chromosomes with the ability to allow immortalised cells to senesce (Meaburn et al, 2005).

MMCT has been used to identify a large number of disease associated genes, all of which have been recessive, and identified through complementation. A novel application of this technique was theorised for this research, where MMCT would be used to identify a dominant disease causing gene. The Majority of cases of HGPS result from de novo mutations that alter one copy of a gene giving rise to a disease phenotype (Eriksson et al, 2003; De Sandre-Giovannoli et al, 2003). With this in mind and the fact there is no history of a consanguineous marriage in the case of AG08466 (Coriell Institute), it is likely that the underlying mutation is dominant. By transferring single chromosomes from the AG08466 cell line into a control cell line the aim is to identify which chromosome contains the gene mutation. This will be determined by the appearance of a diseased phenotype in the control cells, which contain the chromosomes with the gene mutation. As this is a novel application of this technique the proof of principle would be to transfer chromosome 1 from a classic G608G progeria cell into a control cell, and observe changes to a disease phenotype. Figure 6.47 summarises the proposed use of MMCT.

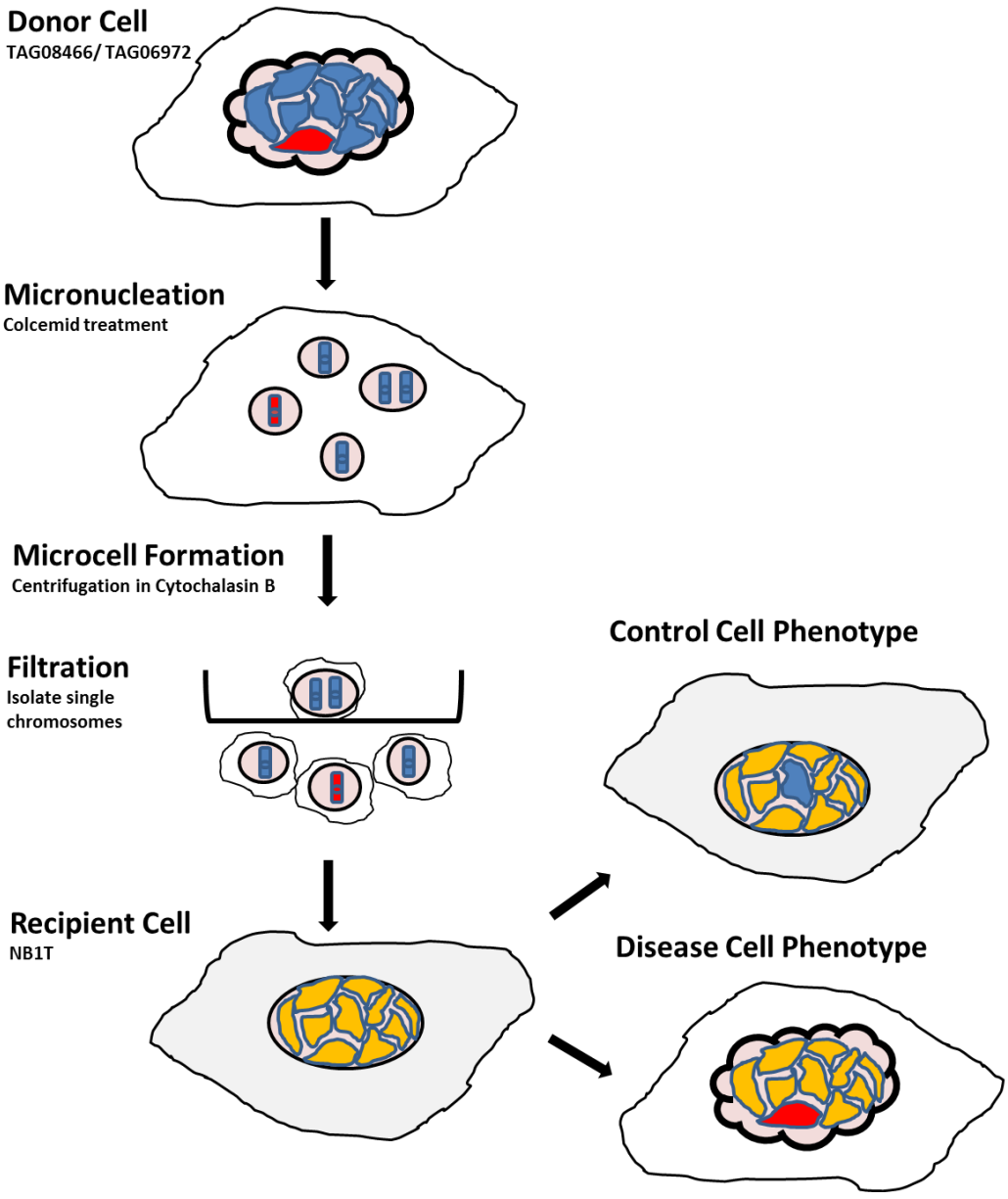

Figure 6.47 Diagrammatic representation of Microcell Mediated Chromosome Transfer

A diagram summarising the process of microcell mediated chromosome transfer for the identification of a chromosome containing a progeria causing mutation. Image adapted from Meaburn et al, 2005.

The AG08466 cell line is one of a few HGPS cell lines to be successfully hTERT immortalised (Wallis *et al*, 2004) and it is anticipated that offers new opportunities for cell characterisation and gene discovery. Through hTERT immortalisation the projected increased cell number offers opportunities to use, previously successful methods for gene discovery, that require a large cell number such as Micro-cell Mediated Chromosome Transfer.

Through characterisation with the hTERT immortalised TAG08466 cell line and the classic G608G cell line TAG06297, it is postulated that further insight into the underlying mechanism will also be gained and a list of potential candidate genes generated.

Whole Exome Sequencing, is another potential method for gene identification for the TAG08466 cell line, with cells available from three unaffected relatives for comparison (Coriell Institute). Whole exome sequencing has already been effectively used for the identification of a *BANF1* mutation in two patients with "Atypical" progeria (Puente *et al*, 2011). Our knowledge of how these cells behave in the presence of hTERT can be used to aid in the bioinformatics of gene discovery and help hypothesis about any potential causative mutations mode of action.

The aim of this chapter is to identify new genes involved in HGPS, by identifying the causative mutation in a cell line derived from an "Atypical" progeria patient. By identifying further causes of the disease greater understanding of the disease pathology will be achieved. Knowledge about premature ageing disease can also add greater understanding to the processes behind normal human ageing.

6.2 Results

6.2.1 Growth Potential

Cells taken from progeria patients display a diverse but relatively short replicative lifespan in culture, which has been characterized by hyperproliferation and increased levels of apoptosis (Bridger & Kill, 2004). The AG08466 fibroblast cell line, originating from an "Atypical" progeria patient with an as yet unknown causative genetic mutation, was immortalized using hTERT (TAG08466) by Professor Richard Faragher (Wallis et al, 2004). AG08466 primary cells were shown to be relatively long-lived amongst HGPS culture achieving just over 45 population doublings at their maximum replicative lifespan, more than the classic HGPS cell line AG06297(Bridger & Kill, 2004).

To investigate the growth rate and potential of the "Atypical" TAG08466 cells, growth curves were produced and compared to the hTERT immortalised classic HGPS cell line TAG06297 (Figure 6.47). Cell passage was carried out twice weekly to avoid confluence. A fibroblast culture from a health individual (NB1T), also immortalized with hTERT was used as a control (Unpublished Data, see Chapter 2.1.1). At each passage the cell number was counted using a haemocytometer and used to calculated the number of Population Doublings achieved (3.32 [log(harvested)-log(seeded)]). Cells grown on glass coverslips were used to estimate the proportion of proliferating cells, using indirect immunofluorescence with an antibody for the proliferation marker Ki-67 (Figure 6.47). Despite little understanding of Ki-67 function, it is widely used as a marker for proliferation, as it is exclusive to the nucleus of proliferating cells (Kill *et al*, 1996). Figure 6.48 shows representative images of the staining pattern observed for Ki-67. TAG06297 cells are defined as TAG06297 Late to coinside with previous chapters, TAG08488 and NB1T are also late passage cultures with more than 2 years continued growth in culture.

A

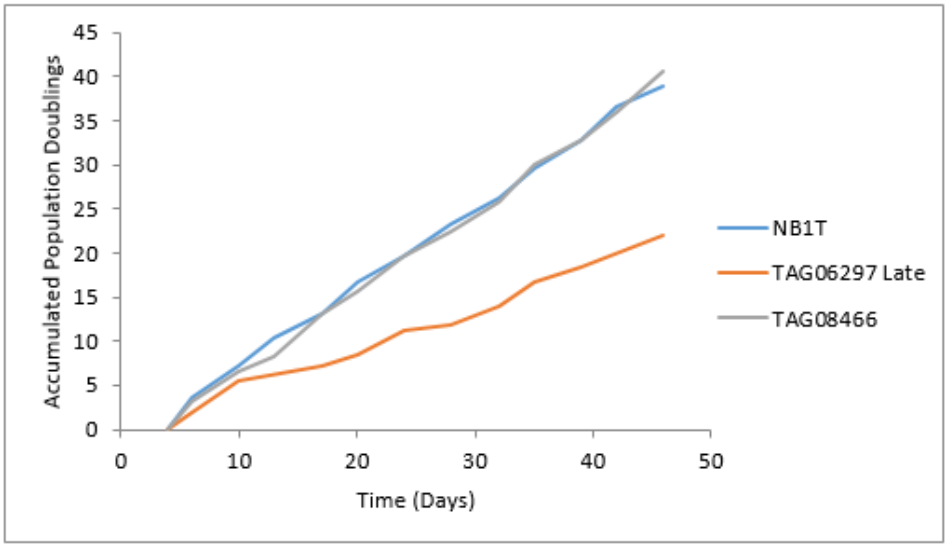
Accumulated Population Doublings
Time (Days)
NB1T
TAG06297 Late
TAG08466

B

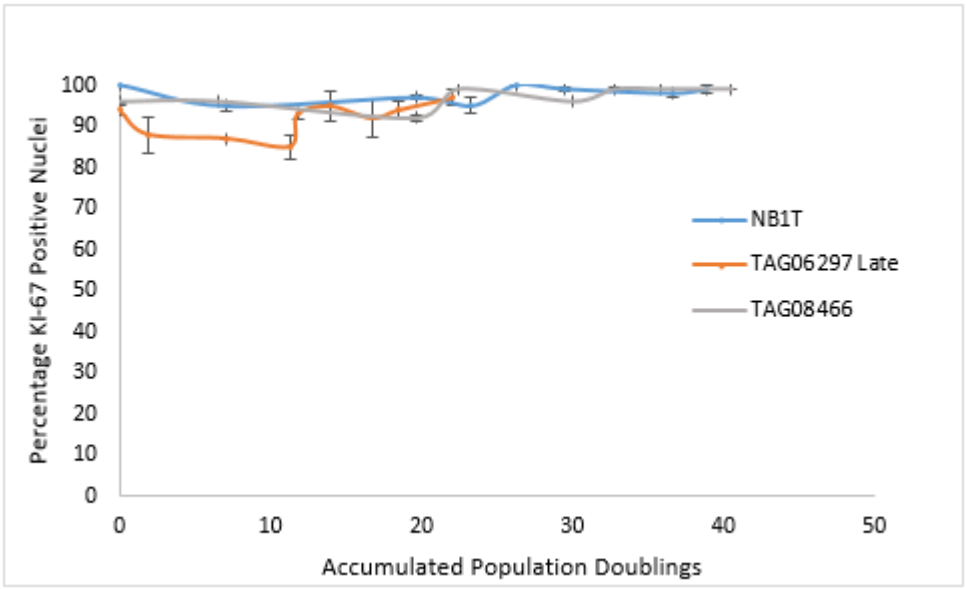
Percentage KI-67 Positive Nuclei
Accumulated Population Doublings
NB1T
TAG06297 Late
TAG08466

C

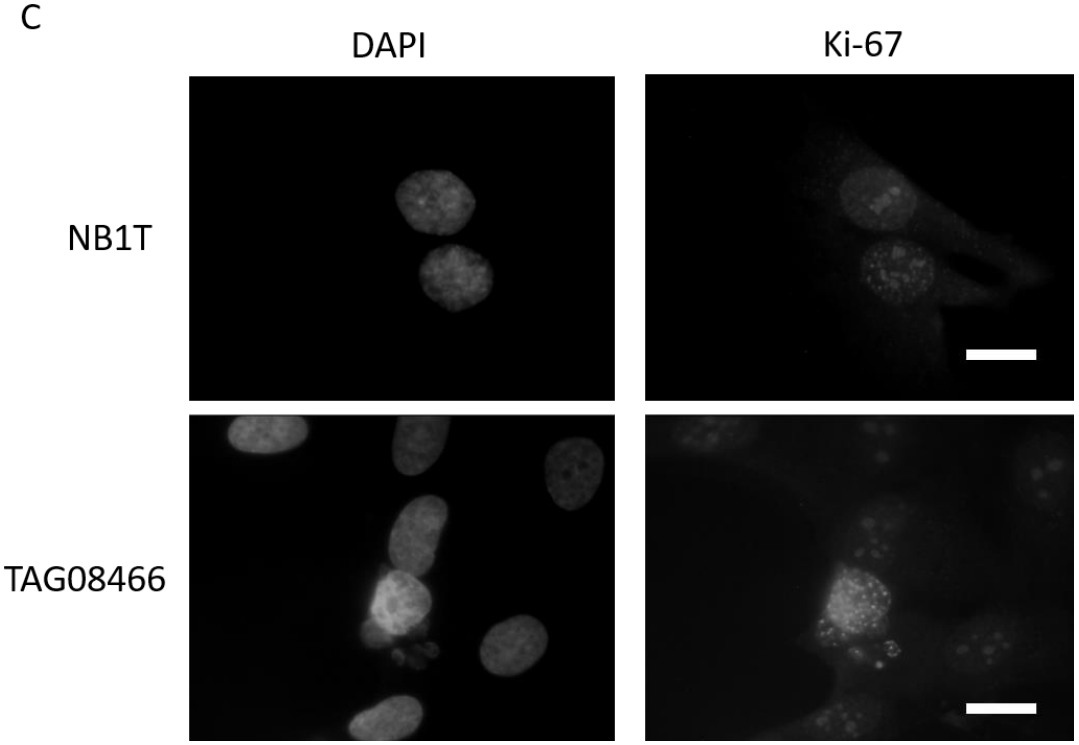

D

Cell Line	Average PD	APD	Slope	Average Ki-67 +VE Nuclei (%)
NB1T	3.21±0.13	38.9	0.91	98±0.7
TAG08466	3.4±0.3	40.5	0.93	97±0.9
TAG06297 Late	2.23±0.35	22	0.5	91±1.3

Figure 6.478 Growth Potential of hTERT immortalised "Atypical" Hutchinson-Gilford Progeria Fibroblasts

(A) Compares the number of population doublings (PD) achieved by a hTERT immortalized Atypical progeria cell line TAG08466, with control fibroblast cell line NB1T and classic HGPS derived TAG06297, all of which are immortalised with hTERT. Growth curves were constructed from data gathered over a 46 day period and the number of population doublings was calculated using the formula 3.32 [log(harvested)-log(seeded)]. (B) Shows the fraction of proliferating cells within each culture, determined using the proliferation marker ki-67, plotted against the APD achieved within 46 days. (C) Representative images displaying how proliferating cells were identified by positive staining for ki-67. Scale bar =10μm. (d) table summarising the growth of each cell line in the 46 day period.

There are observable differences in the growth curve of “Classic” (TAG06297) and “Atypical” (TAG08466) hTERT cell lines, the slopes of which varying from 0.5 to 0.93 APD/Time, with TAG08466 achieving the most population doublings in the 46 day period. The difference of 1.17 PD on average per passage, between TAG06297 and TAG08466 cell lines, had a substantial effect in culture. The higher rate of growth in the TAG08466 cell line makes it a very practical asset for gaining cell numbers. Interestingly, there is no statistically significant difference between the growth rate (T- TEST two tailed 0.59) of TAG08466 and the NB1T control cell line, demonstrating the practical value of this cell line as a resource for progeria cells.

When comparing Ki-67 levels within the cultures, all three cell lines show a high fraction of proliferating cells, with more than 90% of cells within the culture contributing to the growth. Again, there is no significant difference between TAG08466 and NB1T cell lines with T-TEST (two tailed) P value of 0.46. The difference between for Ki-67 positive fraction of TAG06297 (91%) compared to NB1T (98%) and TAG08466 (97%), is significant, with a T-TEST (two tailed) values of 0.00047 and 0.00591 respectively. This difference in proliferating cell fractions may explain the differences in the growth curves and the rate of growth observed in culture between the two HGPS cell lines. This does suggest a difference in response to hTERT immortalisation between the classic G608G mutated cells and the “Atypical” cell line with the unknown mutation, pondering the influence the underlying mutation may have played in this extremely successful immortalisation.

6.2.2 Nuclear Shape

One of the most observable effects of progerin expression within cells is the resulting changes in nuclear morphology. Primary classic HGPS fibroblasts nuclei have been shown to accumulate significantly higher fractions of cells with nuclear membrane blebs, invaginations, micronuclei formation and other abnormal morphologies (Bridger & Kill, 2004). The TAG08466 cell line does not contain the G608G mutation (Bridger & Kill, 2004) and no progerin expression or protein has been detected in this cell line (See Chapter 4). Primary AG08466 cells were found not to have a significantly higher percentage of abnormal nuclei than controls at low

a percentage of their replicative lifespans (T-TEST two tailed 0.12), however, an increase was observed when comparing cells with a high (T-TEST two tailed 0.024) percentage replicative lifespan (Bridger & Kill, 2004). The primary AG08466 showed significantly lower levels of nuclear abnormalities than primary AG06297s, however, at both stages of the cultures lifespan (T-TEST two tailed 0.002 and 0.008 respectively). As the underlying mutation in the AG08466 cell line is unknown, the cause of the increased number of nuclear abnormalities is not understood. Since it seems likely that accumulation of gross nuclear abnormalities could have a profound effect on cell cycle events, such as mitosis, we wished to determine how the TAG08466 cells coped with increased levels of growth following immortalization with hTERT.

Nuclear morphology was analysed in TAG08466 and TAG06297 cultures as well as the control cell line, NB1T. Cells were cultured on glass coverslips, fixed and mounted in DAPI for nuclear visualisation. The slides were analysed manually and the nucleus that showed variation from a smooth elliptical nucleus resulted in a score of abnormal morphology. Figure 6.48A shows examples of normal and abnormal nuclear morphology, the table in Figure 6.49 summarizes the findings within these cultures.

A

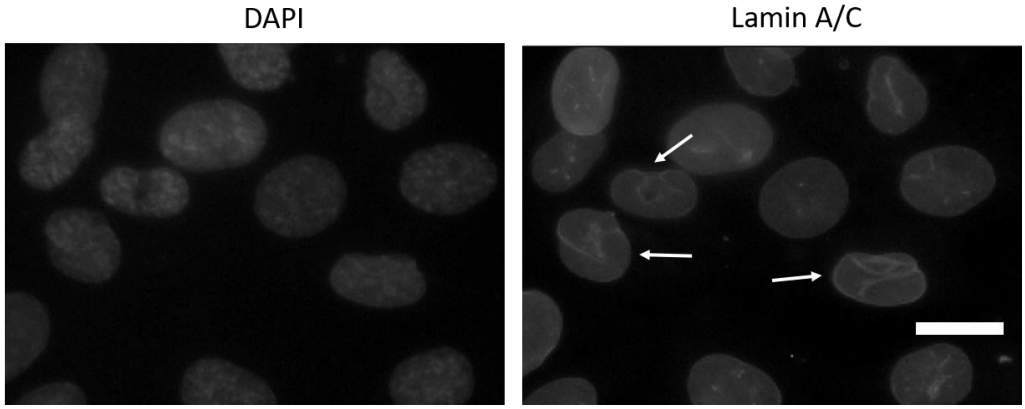

Cell Line	% of Abnormally Shaped Nuclei
NB1T	12.9±1.73
TAG08466	80.2±2.9
TAG06297 Early	72.4±1.06
TAG06297 Late	14.7±3.12

Figure 6.49 Abnormal Nuclear Morphology in hTERT immortalised "Atypical" HGPS Fibroblast cultures

Nuclear morphology was revealed using the DNA stain DAPI and was analysed for shape abnormalities such as, folds or crevices, herniation's, lobules and micronuclei. (A) Arrows indicate nuclei identified as having nuclear morphology abnormalities. Scale bar = 10μm. The table in (B) shows the percentage of abnormal nuclear morphology identified in; NB1T – a normal fibroblast culture, TAG06297 - a classic HGPS cell line and TAG08466 a cell line from an "Atypical" HGPS patient (n=750). All three cell lines have been immortalised with hTERT.

Upon visual inspection of the DAPI stained nuclei, TAG08466 cells were observed as having a "wrinkly" nucleus unlike that observed in either the TAG06297 or NB1T cultures (Figure 6.48A). NB1T and TAG06297 Late demonstrate a statistically similar fraction of abnormal nuclei within the culture (T-TEST two tailed 0.44). TAG08466 cells, with the appearance of the "wrinkly" nucleus, showed statistically significantly higher percentages of nuclear abnormalities than the late passage TAG06297 cells (T-TEST two tailed 0.00002) and NB1T cells (T-TEST value of

two tailed 0.000009). The percentage of nuclear abnormalities observed for the TAG08466 cell line is more comparable to that of the TAG06297 Early cell line (T-TEST two tailed 0.023) two tailed, before the increase in progerin degradation and subsequent loss of progeria cell characteristics (Chapter 3 & 4). The percentage is also more comparable to classic G608G primary fibroblasts with high percentage replicative lifespan (T-TEST two tailed 0.099), than the primary counterparts of the TAG08466. This demonstrates that hTERT immortalisation does not improve progeria cell characteristics, in a cell line not expressing progerin and despite the increased growth potential has exacerbated a common progeria cell characteristic. This again adds interest to the nature of the underlying mutation and its role in nuclear structure and how that leads to HGPS patient phenotype.

To further investigate the effect of continued growth, in the presence of hTERT, image analysis of nuclear size and shape was performed on digital images of cultures. Images of cells grown and fixed on glass cover were analysed using ImageJ software as described in material and methods 2.2.2. By setting the threshold to encompass the nuclear region stained with DAPI, measurements of nuclear size (area and perimeter) and shape (aspect Ratio and Circularity) could be produced. Figure 6.50 shows data presented as frequency distributions for NB1T (control) TAG06297 and TAG08466 cells.

A

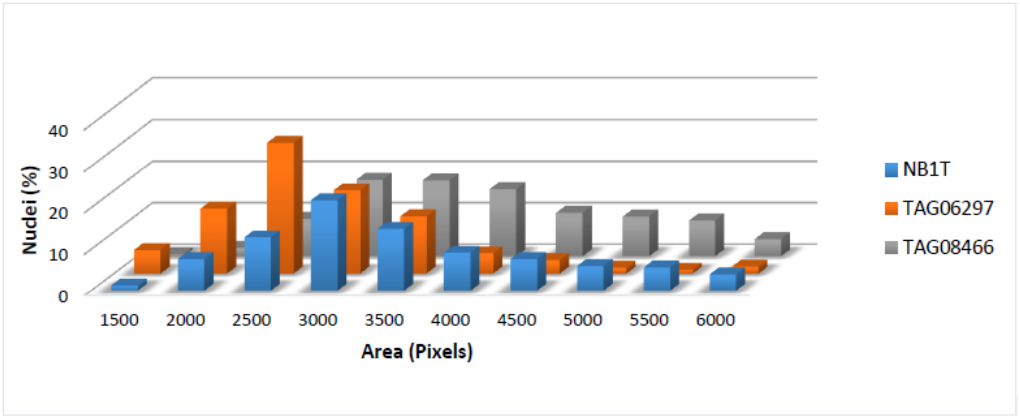
Nudei (%)
40
30
20
10
0
1500
2000
2500
3000
3500
4000
4500
5000
5500
6000
Area (Pixels)
NB1T
TAG06297
TAG08466

B

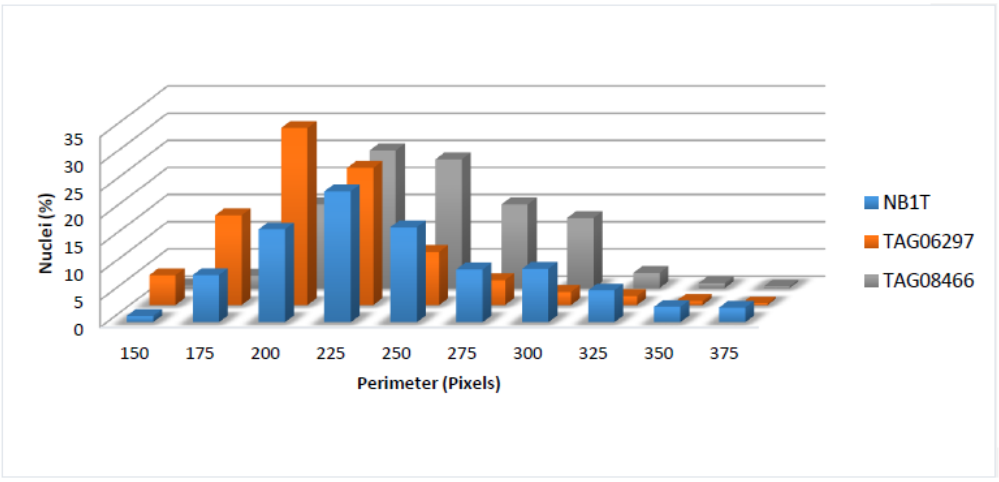
Nuclei (%)
35
30
25
20
15
10
5
0
150
175
200
225
250
275
300
325
350
375
Perimeter (Pixels)
NB1T
TAG06297
TAG08466

C

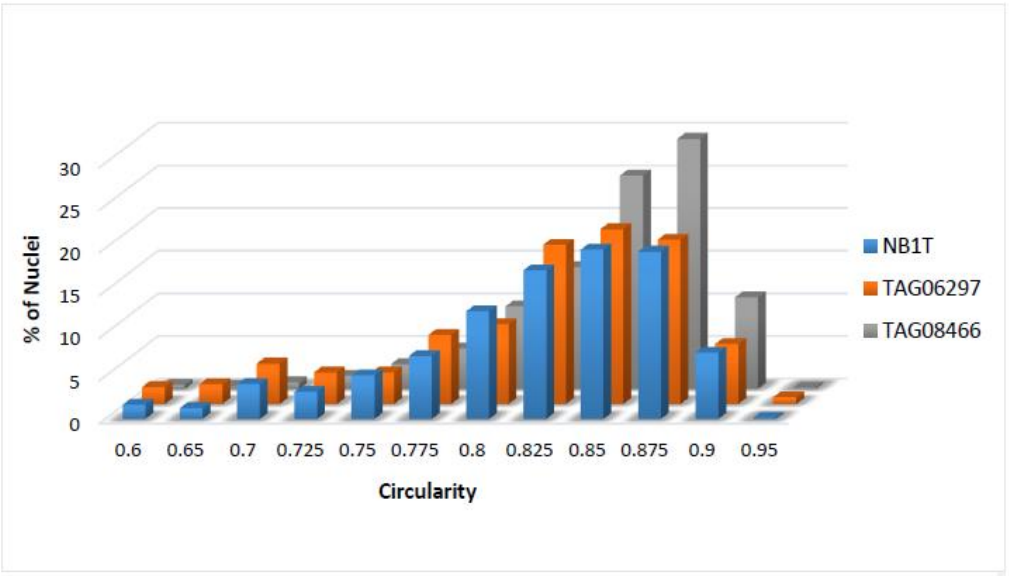
% of Nuclei
30
25
20
15
10
5
0
0.6
0.65
0.7
0.725
0.75
0.775
0.8
0.825
0.85
0.875
0.9
0.95
Circularity
NB1T
TAG06297
TAG08466

D

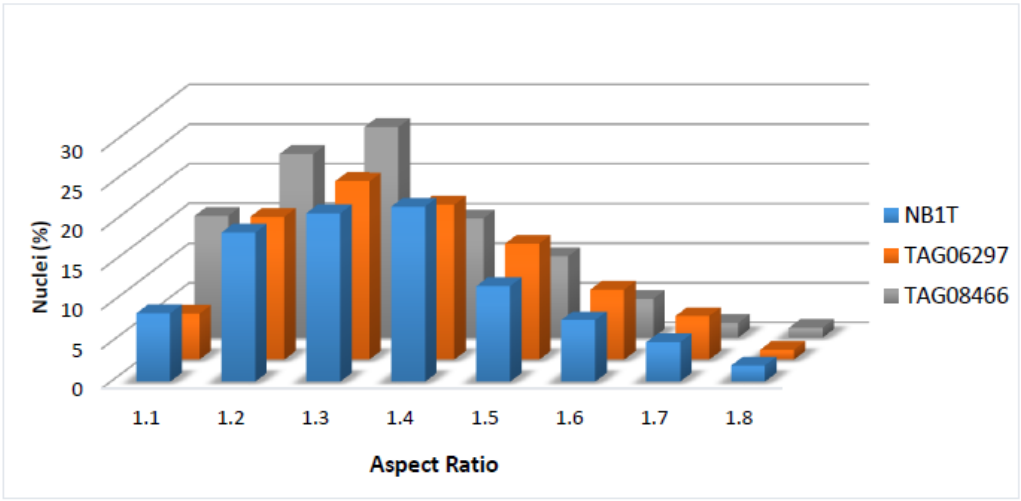

Figure 6.50 Computational Analysis of Nuclear Size and Shape in hTERT immortalised "Atypical" HGPS Fibroblast cultures

Cells grown on cover slips were formaldehyde fixed and mounted in DAPI. Images of the nucleus were captured and analysed using Image J particle analysis software. The nuclear regions were defined by adjusting the pixel threshold. Nuclear regions were analysed for (A) Area, (B) Perimeter, (C) Circularity (4pi(area/perimeter)) and (D) Aspect Ratio (major axis/minor axis). TAG08466 cell line originates from a patient with Atypical HGPS, TAG06297 Late is derived from a classic HGPS patient and NB1T is a healthy control fibroblast cell line. All three cell lines have been immortalised with hTERT.

Comparisons between NB1T and the TAG06297 Late cultures reveal statistically significant differences in nuclear size, as defined by area (T-TEST two tailed <0.0001) and perimeter (T-TEST two tailed <0.0001). In accordance with previous findings for primary HGPS fibroblasts, the TAG06297 Late cells were found to have smaller nuclei (Choi *et al*, 2011). TAG08466 cells were found to have nuclei of a similar size to NB1T cells (T-TEST two tailed area 0.3070 and perimeter 0.8437) that were statistically significantly larger than TAG06297 (T-TEST two tailed <0.0001 area and perimeter).

Aspect ratio and Circularity (Figure 6.50) measurements were both used to examine nuclear shape. Previous reports show HGPS fibroblasts to have, on average, a higher fraction of circular nuclei than those observed in healthy controls (Choi et al 2011). Using the same calculation of Circularity, no significant difference was identified between NB1T and TAG06297 Late cell lines (T –TEST two tailed 0.6410) with the

distribution of nuclei appearing similar. TAG08466 cells, however, showed a statistically significant higher number of circular nuclei than both NB1T and TAG06297 (T-TEST two tailed <0.0001). Furthermore, the measurement of Aspect Ratio also identified rounder nuclei in TAG08466 cell line than either NB1T (T-TEST two tailed <0.0001) or TAG06297 (T-TEST two tailed <0.0001). The identification of larger, rounder and more "wrinkly" nuclei in response to hTERT immortalisation is the opposite effect to that observed in a cell line with the classic G608G mutation. Although a large amount of growth has been observed in the TAG08466 culture, cells appear worse than the classic G608G cell, where less growth was witnessed. This raises the question of how the underlying mutation, which differs from progerin, has affected the cells response to hTERT.

6.2.3 Cell Motility

Despite having the ability to proliferate, classic primary HGPS fibroblasts have been shown to have reduced cell motility, which leads to a decreased ability to heal wounds in culture (Verstraeten *et al*, 2008). With the unknown mutation in the TAG08466 and a less well characterised cell phenotype, it is not known if this cell line exhibits a reduced cell motility. On visual inspection of the culture, however, TAG08466 cell can be seen to grow in colonies or patches rather than spreading throughout the dish, suggesting an issue with cell motility.

Cell motility in this cell line was investigating using live cell imaging. Time lapse videos, with five minute intervals, were produced over an eight hour period, for TAG06297 Early and Late passage, TAG08466 and NB1T. Once all of the images had been captured they were converted into a stack in ImageJ software and the Manual Tracking Pluggin was used to follow an individual cell through each image. By following the nucleus of the cell through each frame, coordinates were generated that could then be plotted on a graph (see chapter 3.2.6). Cell coordinates were centred to the middle of the graph, allowing comparison form a standardized start point (Figure 6.51).

A

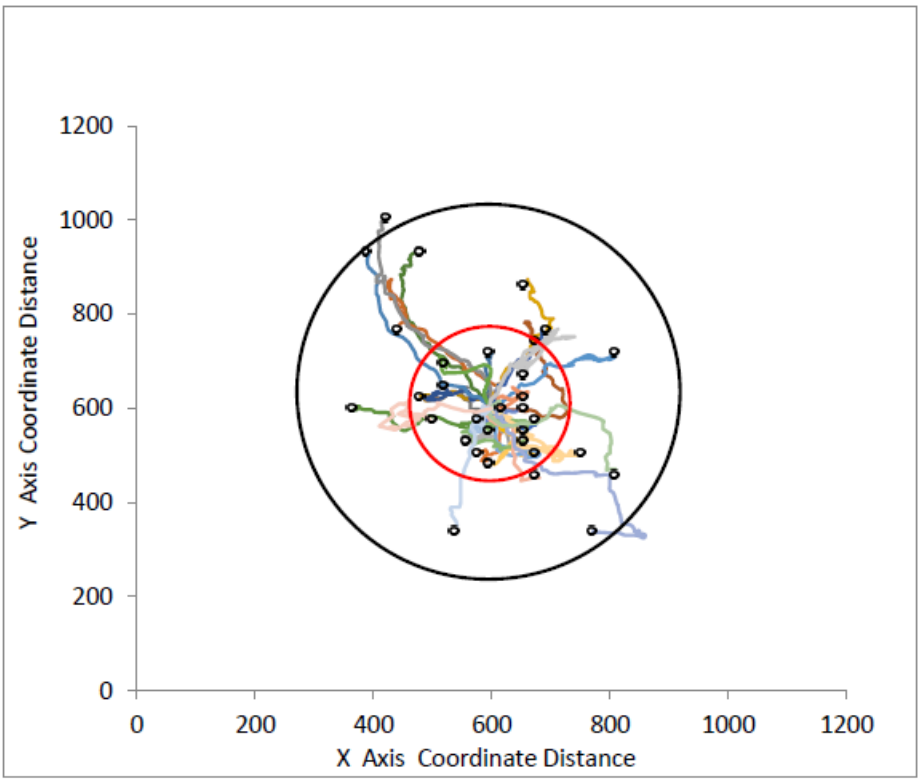
1200
1000
800
600
400
200
0
Y Axis Coordinate Distance
0
200
400
600
800
1000
1200
X Axis Coordinate Distance

B

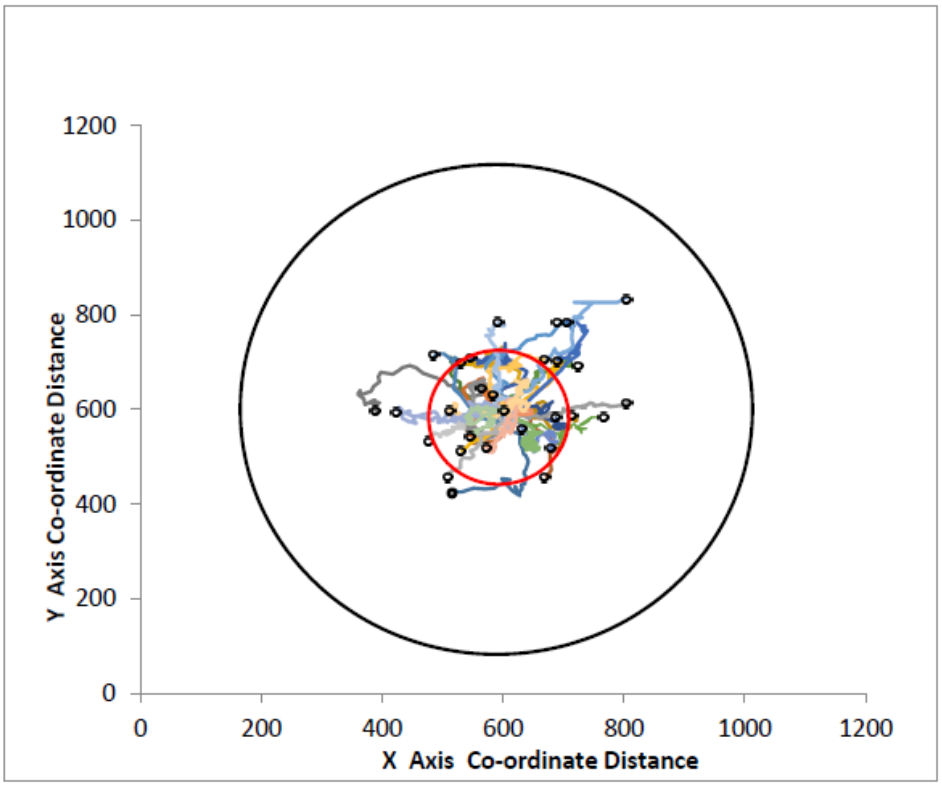
1200
1000
800
600
400
200
0
Y Axis Co-ordinate Distance
0
200
400
600
800
1000
1200
X Axis Co-ordinate Distance

C

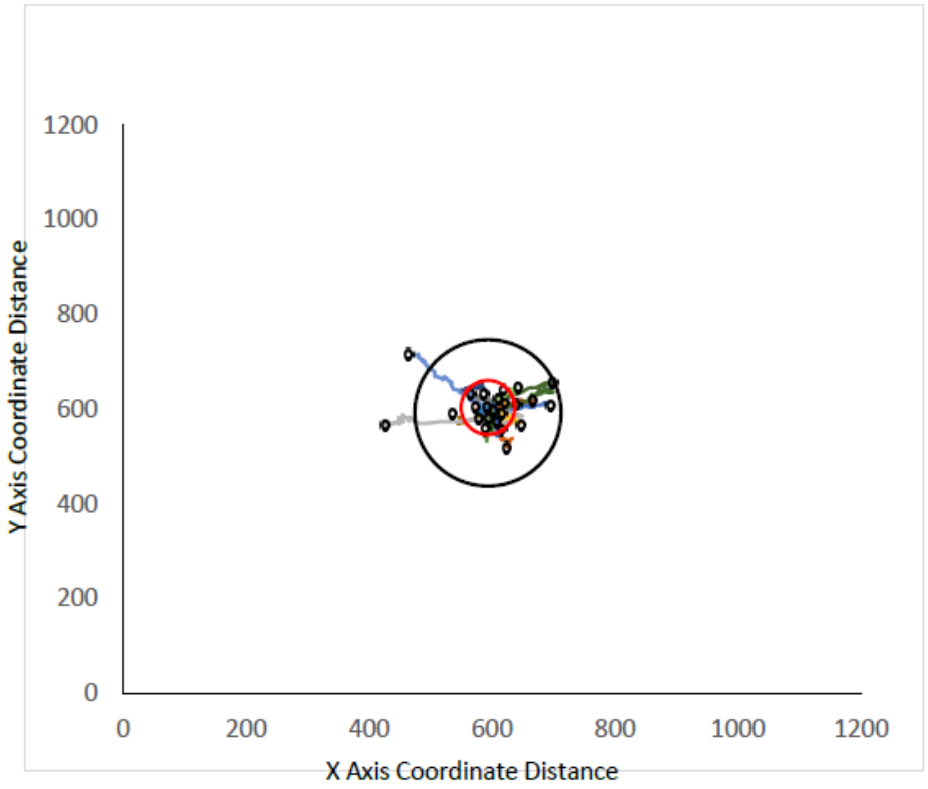
1200
1000
800
600
400
200
0
Y Axis Coordinate Distance
0
200
400
600
800
1000
1200
X Axis Coordinate Distance

D

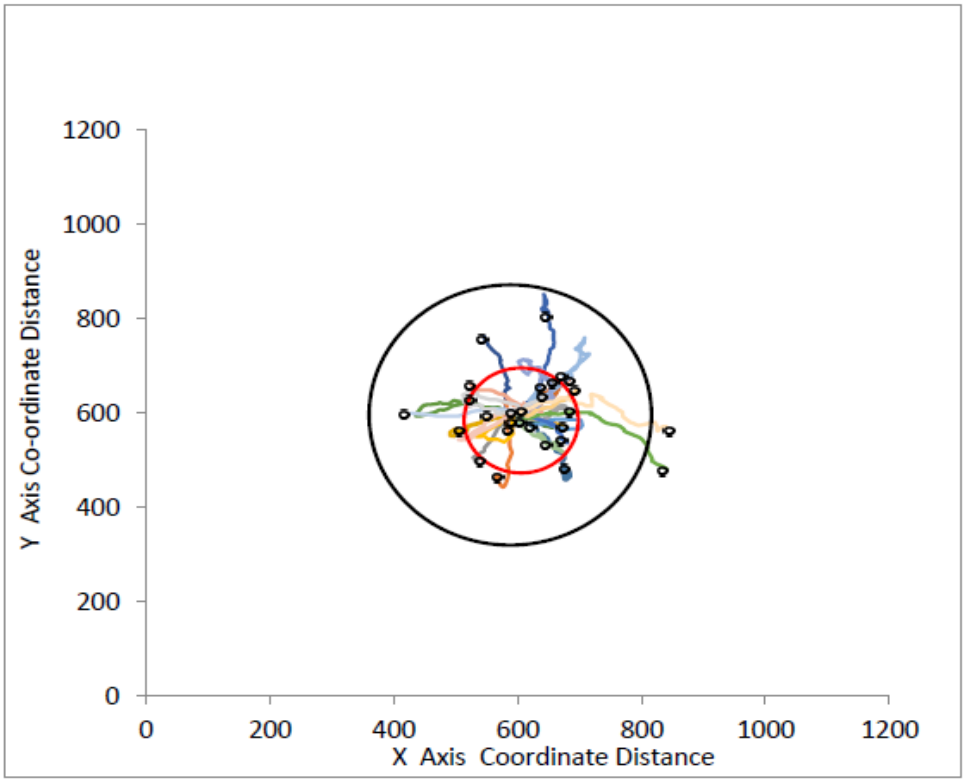
1200
1000
800
600
400
200
0
Y Axis Co-ordinate Distance
0
200
400
600
800
1000
1200
X Axis Coordinate Distance

Cell Lines	Cell Average Total Distance (µm)	Cell Average Total Displacement (µm)	Cell Average Velocity (µm/sec)	Meanderings Ratio
NB1T	238.27±17.01	109.24±12.60	29.78±2.1	0.46±0.03
TAG08466	316.96±15.5	88.04±7.71	39.62±1.9	0.29±0.02
TAG06297 Early	125.29±12.36	31.04±5.56	15.66±1.54	0.24±0.02
TAG06297 Late	159.69±12.07	66.63±8.81	19.96±1.51	0.43±0.03

Figure 6.51 Time Lapse Video analysis of Cell Movement in hTERT immortalised "Atypical" HGPS Fibroblast cultures

Time lapse images were taken every 5 minutes for an 8 hour period. Using the Manual Tracking Plugin on Image J software, individual cells were given X and Y axis co-ordinates and their movement was tracked through all 96 images. The coordinates for each cell were centred and plotted on a graph, where each line represents a single cell's movement. The black circle represents the average total distance moved in 8 hours and the red circle shows the average displacement (the difference between start and end locations). (A) shows the cell movement for a normal fibroblast cell line NB1T. (B) shows the cell movement for the "Atypical" HGPS fibroblast culture TAG08466. (C) shows Early and (D) shows Late passage strains of the classic HGPS derived TAG06297. All cell lines are hTERT immortalised. (E) Summaries the average movement made by each cell line including the velocity and the meandering ratio (total displacement/total distance).

The average total distance and displacement (distance from start point to end point) has been marked on the graphs. The black circles, represent the average total distance achieved by cells in that culture. TAG08466 achieved the greatest distance moved (Figure 6.51B), which was statistically higher than both TAG06297 Early and Late cell lines (T-TEST two tailed 1.41×10^{-10} and 1.15×10^{-12} respectively) and NB1T (T-TEST two tailed 0.0012). The TAG08466 cell line, therefore, also achieved the fastest cell velocity, which was significantly greater than the other three cell lines (T-TEST two tailed <0.0012). As the TAG08466 showed a significantly higher velocity and distance moved than the TAG06297 Early cells, the most representative of a classic G608G mutation, this suggests that this cell line is not affected, with the same reduction in rate of cell movement as that observed in classic progeria cells.

In order to analyse the type of movement made by each cell line the Meanderings Ratio was determined, by dividing the displacement by the distance (Figure 6.51D).

This identifies if cells are moving round in circles or whether they show greater directionality to their movements. The Meanderings Ratios show that NB1T and TAG06297 Late demonstrate the same pattern of movement (T-TEST two tailed 0.62), with a tendency to more linear advances.

TAG08466, however, demonstrates a movement statistically similar to theTAG06297 Early (T-TEST two tailed 0.17), where they appear to move within a small area. As the TAG08466 cells have a greater velocity they achieved a greater distance in the 8 hour time period, all be it moving in a small area. This pattern of movement does explain the patchy growth observed in culture and would do little to aid wound healing *in Vivo*. The progeria like movement pattern observed in the TAG08466 cell line, along with the "wrinkly" nuclear shape, put forward the involvement of the cytoskeleton in this case of progeria, with the interaction between lamins and SUN proteins having been previously established as occurring through the LINC complex (Gruenbaum *et al,* 2005; Haque *et al,* 2006; Haque *et al,* 2010).

6.2.4 Chromosome Number

Genome instability has previously been reported to occur in classic HGPS cells, with one study identifying the inclusion of progerin in membranes during mitosis leading to lagging chromosomes and loss of genetic material (Cao *et al,* 2007). TAG06297 Late cells were shown to have a similar level of genomic instability to the hTERT immortalised controls NB1T with a median chromosomes number per cell of 46 (Chapter 4). As the TAG08466 cell line does not express progerin, the effect of the unidentified mutation on genomic stability is unknown, however, the primary cell line was karyotyped by Coriell Cell Repository and described as 46 XX. In order to determine genomic stability, fixed metaphase preparations were assayed by DAPI staining, captured using Metafer software. Figure 6.52 contains a box plot displaying the number of chromosome per metaphase analysed for TAG08466, TAG06297 and NB1T.

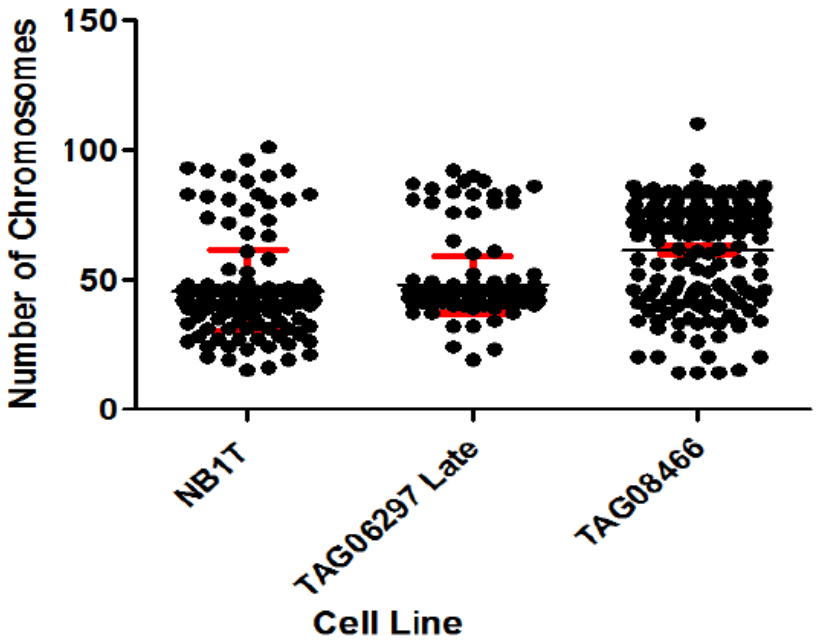

Figure 6.52 Chromosome Number Analysis in hTERT immortalised "Atypical" HGPS Fibroblast cultures

Metaphase preparations were visualised with DAPI and images captured using metacyte software. The number of chromosomes per metaphase were determined for NB1T a normal fibroblast cell line that has been immortalised with hTERT and a hTERT immortalised Late passage strains of the HGPS derived TAG06297. For NB1T 180 Metaphases were analysed, for TAG06297 the number analysed was 224 and for TAG08466 167 Metaphases were analysed.

A T-test revealed no significant difference in the chromosome number of NB1T and TAG06297 (two tailed P value 0.096), with both cell lines having a median chromosome number of 46. TAG08466, however, was found to have a median chromosome number of 69, which differs statistically from NB1T (T-Test two tailed <0.001) and TAG06297 Late (T-Test two tailed <0.001). As the TAG08466 cell line was observed as having a median chromosome number of 69, further analysis of the karyotype of this cell line was performed by Dr Rhona Anderson and Dr Mehmet Bikkul, using M-FISH. Figure 6.53 shows all the chromosomes of one TAG08466 cell aligned to their chromosome number.

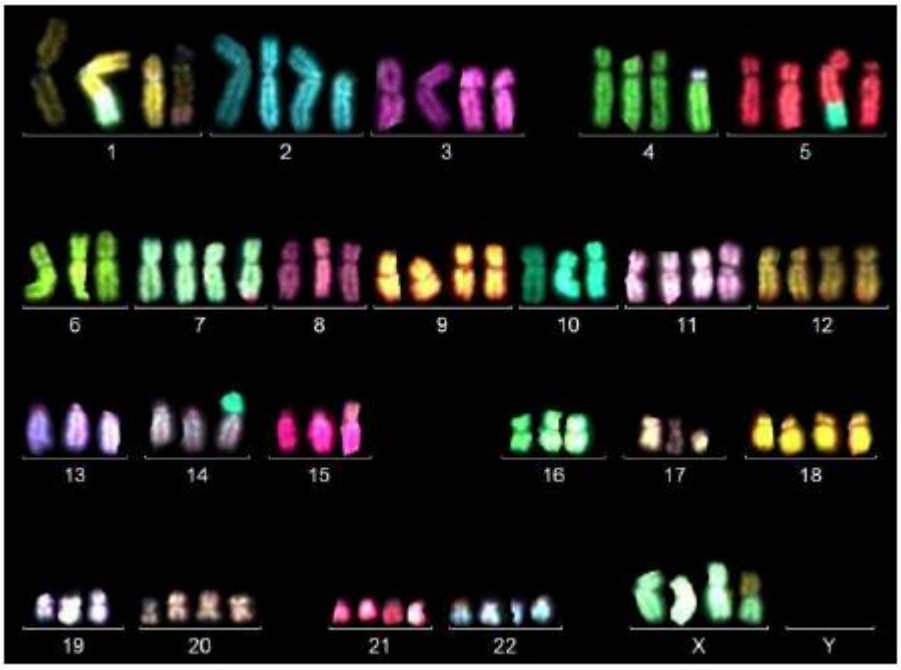

Figure 6.53 Representative M-FISH karyotype of the "Atypical" HGPS fibroblast culture TAG08466

Cell 21 showing
83,XXX,t(X;1),ins(1;14),der(1)t(14;1;17),del(2p),del(3p),der(4)t(4;19),der(5)t(5;10), del(5p),-6,der(7)t(7;21),-13,-14,der(14)t(10;14),-15,der(15)t(8;15),-16,del(17q). M-FISH carried out by Dr Rhona Anderson and Dr Mehmet Bikkul.

Analysis of 17 metaphase spreads identified the TAG08466 cells as having a near tetraploid (XXXX) karyotype with a large amount of aneuploidy and genomic instability. For a full karyotype of all cells analysed see Appendix iii. This near tetraploid karyotype is in complete contrast to the relative stability of the TAG06297 cell line previously observed (Chapter 3). With hTERT cultures a level of genomic instability may be expected (van Waarde-Verhagen et al, 2005), but the TAG08466 demonstrate this at a significantly higher level than controls (T-TEST two tailed <0.001).

6.2.5 Possibility of Micro-cell mediated chromosome transfer?

Through characterisation of both hTERT immortalised progeria cell lines, with growth curves, increased replicative potential has been determined (Figure 6.47).

This would enable a higher number of donor cells to be grown for micronucleation and ultimately increase the yield of hybrid colonies. In order to perform the chromosomes transfer an assay to distinguish between control and diseased cell phenotype must be identified. Several well established hallmarks of progeria cells were characterised for the “Atypical” TAG08466 cell line and tested for suitability as an assay. With a statistically significant difference in nuclear shape having been observed between NB1T controls and TAG08466 cells, it provides a logical assay for differentiation between healthy and disease cells. Cell motility was also able to distinguish between diseased and control cells, however, its low throughput approach make it less ideal assay.

Further characterisation of these cell lines has, however, revealed genomic instability and a near tetraploid karyotype for the TAG08466 cell line. The increased chromosomes number has the potential to dilute the statistical power of the chromosome transfer. More colonies would need to be generated in order to have a full panel of hybrids containing each chromosome from the TAG08466 cells. With the complex Karyotype and genomic instability (figure 6.52 & 6.53), there would be no guarantee that all genetic information had been transferred. This instability of the immortalised cell lines has highlighted their unsuitability as donors for the MMCT. MMCT is only made viable with use of immortalised cell lines to act as both donor and recipients to increase the potential yield and negate the low replicative potential of primary progeria cells. This causes the need for a new method to identify the causative mutation in the “Atypical” HGPS cell line TAG08466.

6.2.6 Candidate Genes

With MMCT ruled out as a method for determining the underlying mutation in TAG08466 cell line, a list of candidate genes was drawn up. From analysis of the characterisation data, it was apparent that the TAG08466 cell line demonstrated an unusual pattern of movement (figure 6.54). This led to interest in the proteins linking the lamina and the cytoskeleton. SUN1 and SUN2 provide a link between the Nesprin proteins and the nucleus through attachments with the nuclear lamina (Haque *et al,* 2006; Haque *et al,* 2010). Nesprin proteins bind to actin filaments and

are believed to form a link between the nucleus and the extracellular matrix (Gruenbaum *et al*, 2005). Work performed by Dr Derek Warren's group shows that Nesprin dysfunction in older tissue lead to stronger attachments and abnormal movement (Mellard *et al*, 2011). Therefore, a mutation in the Nesprin or SUN proteins could also be the underlying cause of progeria in the TAG08466 cell line. As there are several Nesprin isoforms, first investigating the SUN proteins would prove a logical step in identifying the underlying mutation in the TAG08466 cell line. Interestingly, SUN1 and SUN2 mutations have been identified as causes for several muscle dystrophies, another disease type typically associated with *LMNA* mutations, through disruption of the nuclear-cytoplasmic connection (Meinke et al, 2014). Western blot analysis was initially performed in order to determine the abundance of SUN1 and SUN2 in the TAG08466 cell line. Figure 6.54 shows the western blot results for both proteins

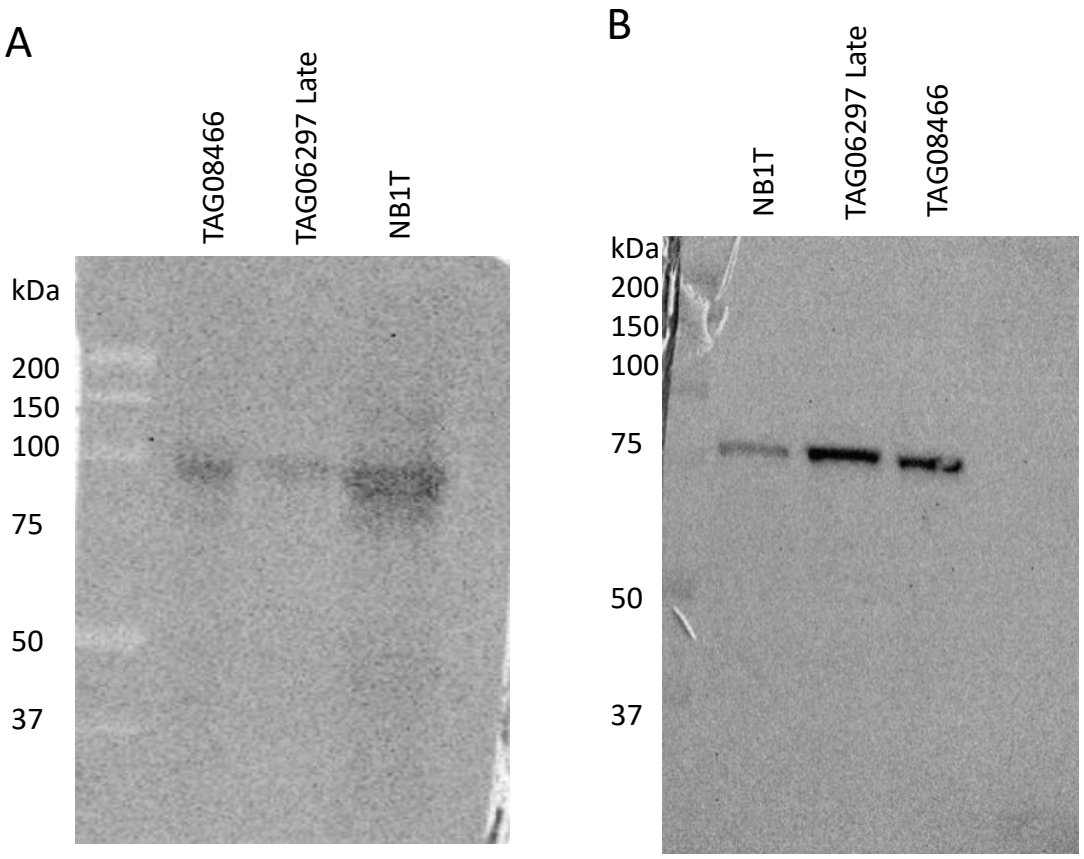

Figure 6.48 Western Blot analysis of SUN1 and SUN2 proteins in "Atypical" HGPS Fibroblasts

Image A shows a western blot membrane probed with an anti-SUN1 antibody. Image B depicts a western blot membrane probed with an anti-SUN2 antibody. Both antibodies were used in conjunction with horseradish peroxidase secondary antibodies and visualised under chemiluminecence on the Bio-Rad gel dock system. The ladder in both gels is the Precision Plus Protein^{TM} standard (Bio-Rad). NB1T is a normal fibroblast culture, TAG06297 is a classic HGPS cell line and TAG08466 a cell line from an "Atypical" HGPS patient. All three cell lines have been immortalised with hTERT.

Through western blot analysis it can been seen that both SUN1 and SUN2 are present in the TAG08466, although in particular for SUN1 no conclusions can be drawn about its abundance due to the poor nature of the antibody. The sensitivity of western blot analysis does not allow for the determination of small changes to the proteins, which could affect their function despite a stable protein level.

The only known progeria causing mutation not yet ruled out for the TAG08466 cell line is the *BANF1* mutation, which has been shown to cause a dramatic reduction in its encoded homodimer protein BAF (Puente *et al*, 2011). Figure 6.55 shows the Western blot membrane probed with an anti-BAF antibody.

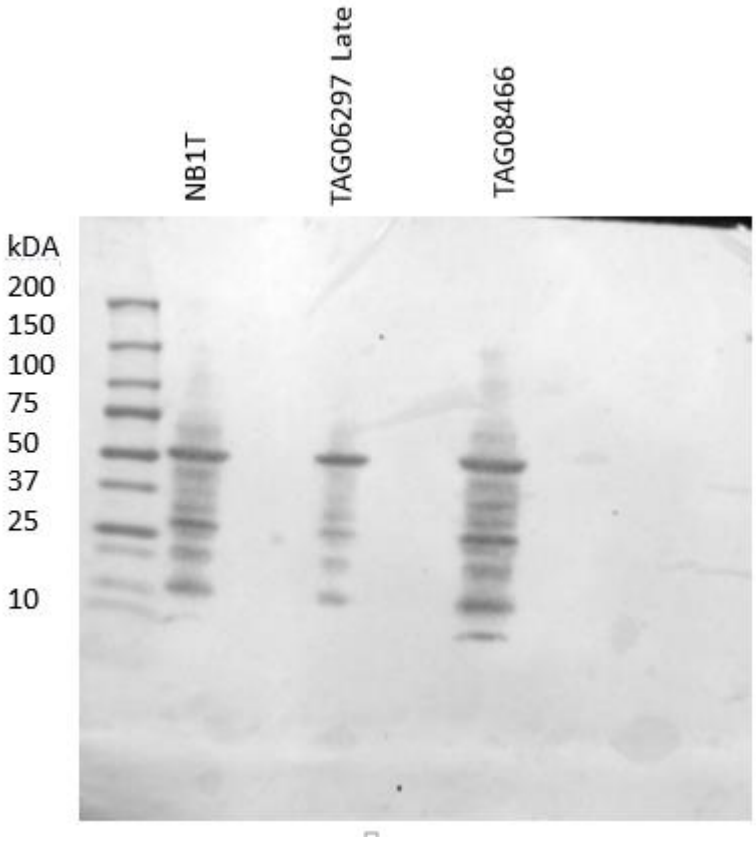

Figure 6.49 Western Blot analysis of BAF in "Atypical" HGPS Fibroblasts

Image shows a western blot membrane probed with an anti-BAF antibody used in conjunction with horseradish peroxidase secondary antibodies and visualised under chemiluminecence on the Bio-Rad gel dock system. The ladder is the Precision Plus Protein^{TM} standard (Bio-Rad). NB1T is a normal fibroblast culture, TAG06297 is a classic HGPS cell line and TAG08466 a cell line from an "Atypical" HGPS patient. All three cell lines have been immortalised with hTERT.

The results of this western blot do not show a loss of the band corresponding to BAF at 10 kDa in any of the three cell lines, indicating that the previously described *BANF1* mutation is not the underlying cause for progeria in TAG08466. This again does not rule out a different mutation within the *BAMF1* gene, with a different effect on the BAF protein, from being the genetic cause of HGPS in the TAG08466 cell line.

A more appropriate approach would be to sequence a list of candidate genes, including lamin A binding partners. The problem with this technique is that lamin A is believed to interact with a large number of proteins, many of which may have not yet been identified (Gruenbaum *et al*, 2005, Cau et al, 2014).

6.2.7 Whole Exome Sequencing

Whole genome sequencing or exome sequencing is becoming more available with next generation sequencing technologies. Although a relatively costly option, it may be appropriate for the identification of progeria causing variants in the AG08466 cell line, with the availability of cell lines from three direct relatives. The *BANF1* mutation was identified in two unrelated patients predominantly due to a consanguineous marriage pointing to a recessive inheritance of the disease (Puente *et al*, 2011). Several other laminopathies have been identified using WES and pedigree information for instance a servere cardiomyopathy (Roncarati et al, 2013) and a cardiac conduction disorder (Lai et al, 2013). The likely mode of inheritance and genetic information from three unaffected direct relatives made exome sequencing possible. In the majority of cases de novo mutations have been found as the underlying cause, resulting in a dominant disease effect. Therefore, the use of sequencing would be required to identify SNPs in the patient not found in direct relatives, which would most likely give a more extensive list than the four homozygous recessive mutations only identified in the *BANF1* mutation patient. In order to achieve this, whole exome sequencing of the patient, both parents and a sibling was performed. Primary cell lines were obtained from the Coriell Cell Repository and DNA was exon enriched using the Nextra® Rapid Capture All Exome Kit. Sequencing was performed on the Illumina HiSeq2500 at University College London, in collaboration with Dr Mike Hubank. Figure 6.56 shows the filter cascade used to sort through identified variants, in order to identify those of interest.

A

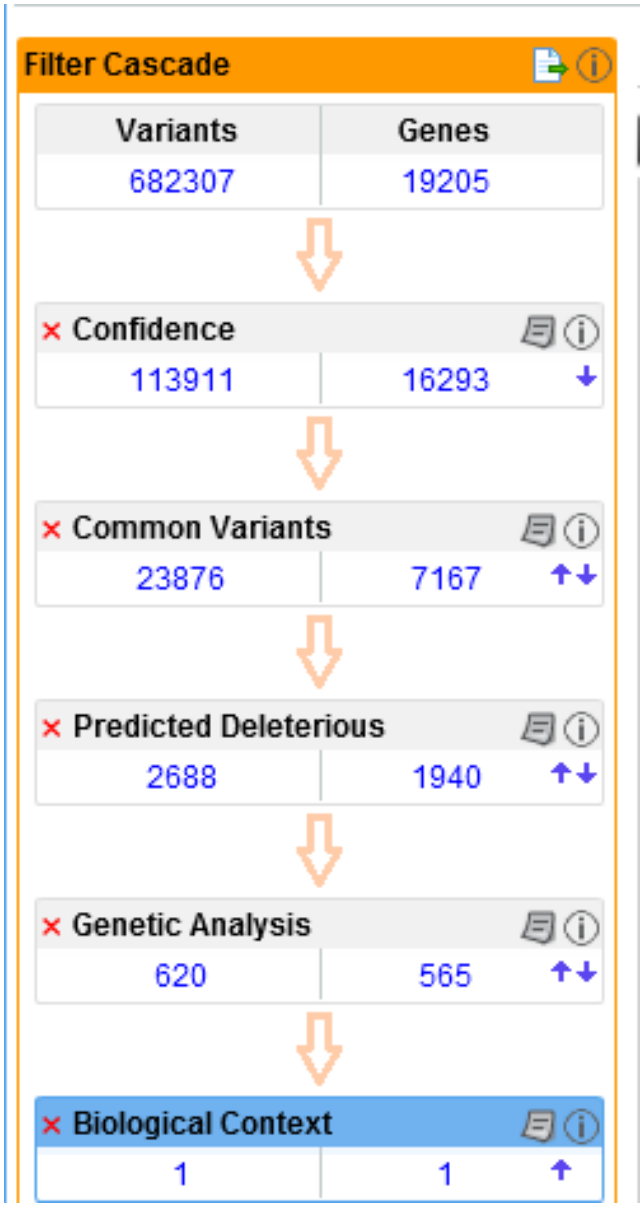
Filter Cascade
Variants
Genes
682307
19205
Confidence
113911
16293
Common Variants
23876
7167
Predicted Deleterious
2688
1940
Genetic Analysis
620
565
Biological Context
1
1

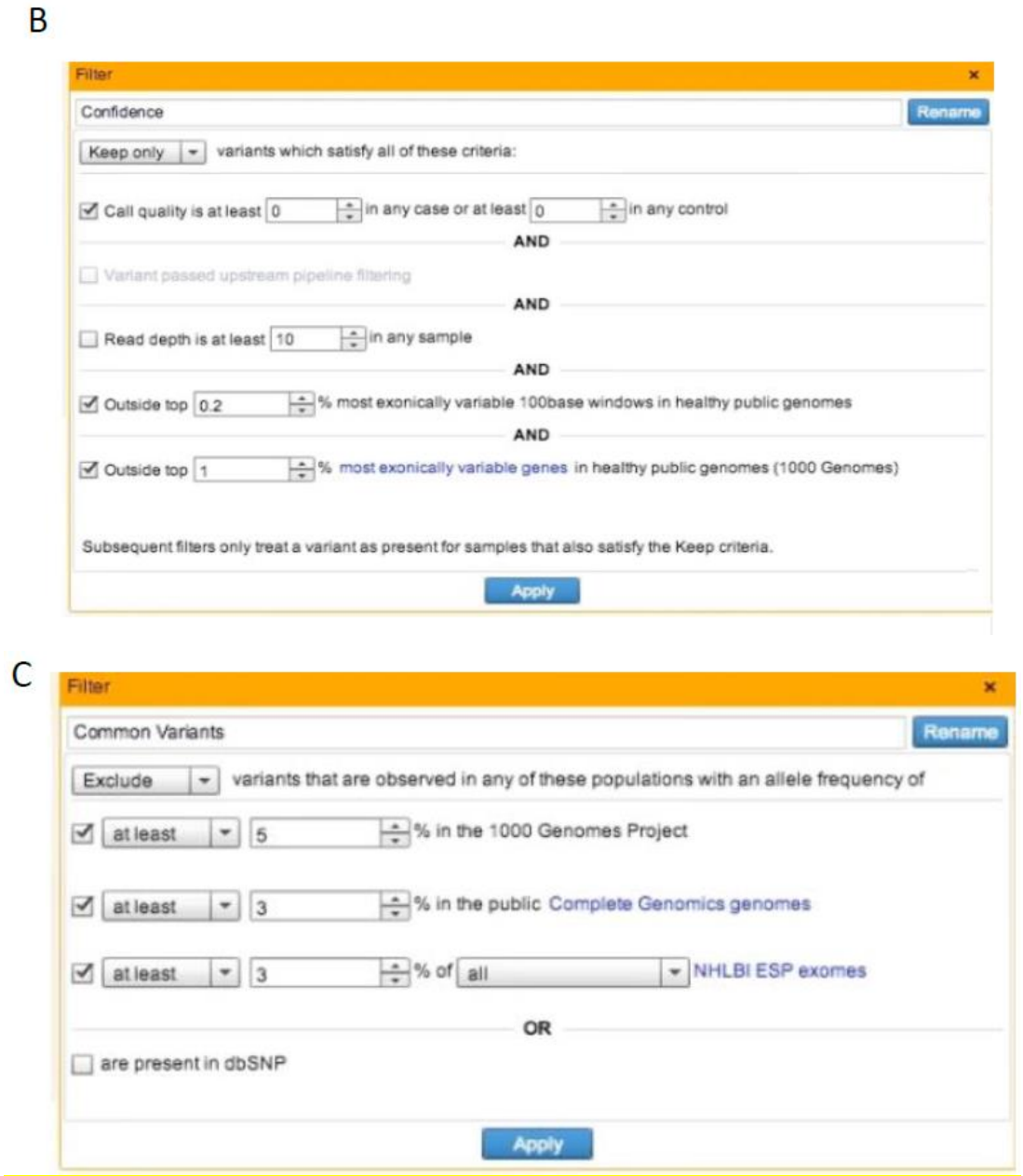

Figure 6.50 Ingenuity Variant Analysis of whole exome sequencing data for the "Atypical progeria" cell line TAG08466, compared to three unaffected family members

A shows a screenshot of the filter cascade and identifying the number of identified variants before and after filters. Filter cascade shows results for TAG08466 analysed at the default confidence. B shows custom setting in Ingenuity Analysis software used to increase the confidence by removing variant where there was a low read depth. C shows the custom filter used to remove common variants based on occurrence in the 1000 Genomes Project and the Public Complete Genomics Genomes.

Ingenuity Variant Analysis software was used to filter through identified variants based on a dominant inheritance pattern, therefore, heterozygous de novo variants were selected. HGPS was entered as a key term and as a result one biologically relevant variant was identified. The variant identified was a deletion in the intronic promoter region of the *LMNA* gene. Figure 6.57 shows the location and description of the *LMNA* variant.

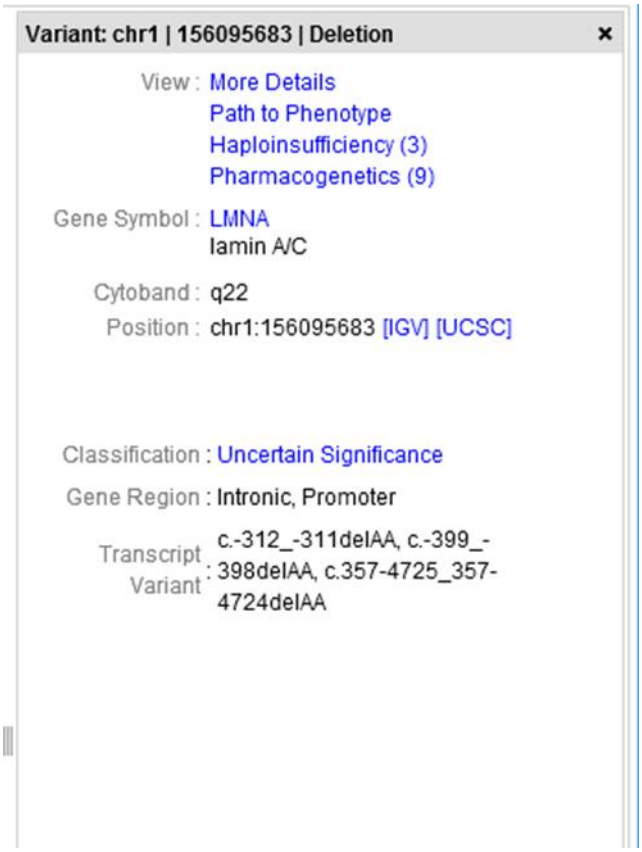

Figure 6.51 Ingenuity Variant Analysis software information on the LMNA variation identified in TAG08466 "Atypical" Progeria cell line

Screenshot showing information on variant position, gene region, classification and transcription variation, created using Ingenuity Variant Analysis software.

The only observed variant, identified as having biological relevance was the *LMNA* variant shown in figure 6.57. This variant was identified under the least stringent filtering parameters and was removed from the filter once the confidence rating was increased. This variant was only covered by a low read depth and is likely an

artefact. It is thought that a variant of this nature would affect lamin A abundance in cells, something which had previously been examined, see figure 4.19 chapter 4.

Analysis of the TAG08466 cell line through saturating PCR revealed lamin A transcripts, but no progerin as predicted for a cell line known not to possess the G608G *LMNA* mutation (personal communication Professor Nico Levy). Despite searching for nuclear membrane proteins and premature ageing disease, no other biologically relevant variants were identified using the ingenuity variant analysis software.
The exome data was specifically searched for variants in genes previously identified in HGPS, such as *BANF1* and *ZMPSTE24*, however, no variants in these genes were present. Using the information gathered from the characterisation of the hTERT immortalised TAG08466 cell line, the exome data was also analysed for variations in proteins linking the nucleus and the cytoskeleton, such as Nesprins, SUN1 and SUN2, however, no variants in these proteins were identified either. A full list of genes and variants identified under 3 separate filter stringencies is available in Appendix iv.

In collaboration with Dr Eric Schirmer's group at the University of Edinburgh, further analysis of the exome sequencing data was performed. These searches identified variants in DNA repair genes, which may have significance in this "Atypical" progeria patient. Several studies have previously identified links between DNA damage and classic HGPS (Liu *et al*, 2005; Liu *et al*, 2006; Mukherjee and Costello, 1998). A heterozygous frameshift variant resulting in an early stop codon in *INO80E* a DNA repair protein was identified. hTERT immortalisation of the AG08466 cell line has resulted in a large amount of genomic instability and suggesting deficiencies in DNA repair and cell cycle progression in this cell line. The early stop codon in *IN080E* may truncate the foot domain of the protein, affecting in particular the ARP8 (Actin-Related Protein) binding module (Tosi *et al*, 2015). The INO80 complex has previously been shown to be recruited to DNA damage sites in an ARP8 dependent manner (Kashiwaba *et al*, 2010; Osakabe *et al*, 2014). To validate this potential candidate gene knowdown experiments using RNAi would identify if loss of this protein causes the "Atypical" progeria-like cell

characterisitcs seen in TAG08466. Complimentation studies coulds also be used whereby functional copies of the mutated gene are introduced into the patient cell line, with the aim of improving cell characterisitcs. If this candidate genes is not found to be causative, one potential next step in the analysis of this data series is to identify any clinically relevant findings in this patient such as the Marfan like features and exploit these as an avenue to search the exome data.

6.3 Discussion

All known genetic causes of progeria are in proteins associated with lamin A, the mutated protein in classic HGPS cases (Eriksson et al, 2003; De Sandre-Giovannoli et al, 2003). These include transcription factor *BANF1* (Puente *et al*, 2011) and lamin processing enzyme *ZMPSTE24* (Shackleton *et al*, 2005). The lamina has a large number of nuclear functions, including nuclear shape and structure, heterochromatin organisation, transcription regulation and cell cycle progression (Zastrow *et al*, 2004; Gruenbaum *et al*, 2005; Starr *et al*, 2010). This creates a great number of lamin A interacting proteins (Kubben *et al*, 2010), which could cause a progeria like syndrome such as that seen in patient AG08466. With such a large scope of potential candidate genes an inclusive approach such as exome sequencing was essential. With an estimated 85% of all disease causing variant being found within exome boundaries, WES is a method for analysing the majority of coding DNA whilst reducing the statistical power required (Wang *et al*, 2013). In this study we have ruled out all previously identified progeria causing mutations (*BANF1* and *ZMPSTE24*), through exome sequencing and protein analysis

Through characterisation of the hTERT immortalised TAG08466 cell line, interesting observations have been made. Unlike the classic HGPS cell line TAG06297 (Chapter 3), the TAG08466 appeared less stable after prolonged growth in the presence of hTERT. This was demonstrated by the increased nuclear shape abnormalities and genomic instability. This again reveals the volatility of progeria cells to hTERT immortalisation and demonstrates their instability in future studies.

The observed effect of hTERT immortalisation were, however, exploited for analysis of the exome sequencing data with candidate genes such as SUN proteins and Nesprins being posed. Despite the corresponding genes not being responsible for APS in patient AG08466, they do pose credible candidates for other case of APS. Considering that normal aged fibroblasts show changes in cell motility linked to Nesprins (Mellard et al, 2011) and the identification of a *LMNA* mutation (Q432X) responsible for a cardiomyopathy/ premature ageing phenotype resulting from changes in lamin A- Nesprin-2 interactions (Yang *et al,* 2013). Changes in chromosome stability were also identified in this cell line, similar to those observed in TAG08466.

When taken in combination, identification of genomic instability in response to hTERT and previously described lamin A-telomere interactions (Wood *et al,* 2014), suggests a role of cell cycle regulation and activation of DNA damage checkpoints in "Atypical" HGPS. Classic HGPS cells have been shown to have constitutively active DNA damage checkpoints and stochastically shortened telomeres (Campisi *et al,* 2001; Decker *et al,* 2009). The inclusion of progerin in nuclear envelope, during mitosis, has been shown to cause lagging chromosome, one possible explanation of aneuploidy in HGPS (Dechat *et al,* 2007).

The identification of a rare, genetic variations in a gene encoding DNA damage repair protein IN080E, in this cell line, is of interest. Further information regarding the phenotype of this patient, in particular any cancer development, would add evidence to the role of DNA repair in this case of HGPS. This would suggest a great deal ofoverlap with the adult premature ageing disease Werners Syndrome, which is characterised by high incidence of cancer, resulting from the mutated WRN protein, a REQ helicase involved in DNA damage repair (Yu *et al,* 1996). Conversely the hTERT immortalisation of WS fibroblasts, was found to reduce levels of genomic instability (Crabbe *et al,* 2006), concluding that genome instability in WS is dependent on telomere dysfuction. Interestingly IN080E has been described as having a role in telomere maintenance and chromosome segregation. The relationship between IN080 complex function, telomeres and cell division, needs to

be further eluicidated, but current knowledge based on this APS cell lines reaction to telomerase does add significance to *IN080E* as a candidate gene for APS.

By identifying further genetic causes of the disease greater understanding of the disease pathology will be achieved. With lamin As involvement in a large number of cellular process, further mutation identification may add more insight into thoses involved in premature ageing. Knowledge about premature ageing disease can also add greater understanding to the processes behind normal human ageing.

7 Discussion

7.1 hTERT immortalisation

The classic disease causing *LMNA* mutation which accounts for approximately 80% of progeria cases has been well characterised since its discovery in 2003 (Eriksson *et al,* 2003; De Sandre-Giovannoli *et al,* 2003). Expression of the mutant lamin A protein progerin, has a dominant negative effect on cell function (Scaffidi and Misteli, 2005), disrupting the numerous roles of lamin A within the nucleus. This includes the appearance of abnormal shaped nuclei (Goldman *et al,* 2004; Bridger & Kill, 2004), increased levels of DNA damage (Mukherjee and Costello, 1998; Liu *et al,* 2005), aberrant transcription (Kubben *et al,* 2012), chromosome re-positioning (Meaburn *et al,* 2007; Mehta *et al,* 2007), loss of heterochromatin anchoring (Goldman *et al,* 2004; Scaffidi and Misteli, 2005; Shumaker *et al,* 2006) and decreased cell motility and mechanical strength (Verstraeten *et al,* 2008; Paradisi *et al,* 2005).

There has been much debate about the implications of hTERT immortalisation on HGPS cells. Cells from classic progeria patients, expressing the mutant protein progerin through activation of a cryptic splice site, have been shown to have shortened replicative potential in culture (Bridger and Kill, 2004). This has been linked to premature senescence thought to occur through stochastic telomere shortening, resulting in activation of DNA damage checkpoints (Allsopp *et al,* 2004; Campisi *et al,* 2001). Increased levels of apoptosis have also been observed in fibroblast cultures (Bridger and Kill, 2004). The effect of exogenous hTERT expression has been postulated to act as an opposing force to progerin (Cao *et al,* 2011), with some studies identifying loss of progeria cell characteristics in response to hTERT immortalisation of HGPS cells (Benson *et al,* 2010; Cao *et al,* 2011).

7.1.1 Progerin

This study aimed to identify if hTERT immortalised cells could provide a useful tool for future research into HGPS. After two years continuous growth the TAG06297

cell line was found to show little resemblance to a classic progeria cell in parameters such as shape, movement and DNA damage (Chapter 3). This suggests that hTERT expression does have long-term effects on progerin, which result in a healthier cell phenotype. It has previously been suggested that this occurs through decrease in progerin expression relative to lamin A (Cao *et al,* 2011). This phenomenon was replicated in this study although to a lesser extent. A two fold reduction in progerin transcripts relative to lamin A is hard to quantify. Preliminary western blot analysis identified a significant reduction in progerin protein. This appeared to be more extensive than the 2 fold decrease in expression suggesting modulation at the protein level. The proteasome degradation of progerin was proposed in response to the proteasome inhibiting drug MG132. Lamin proteins were previously thought to be degraded through autophagy (Graziotto *et al*, 2012).

This suggests that in response to the growth pressure of hTERT immortalisation, clonal expiation has occurred. Through modulation of progerin protein or increased E3 Ubiquitin ligase affinity (Fu *et al,* 2004), a subset of cells within the culture may have become better able to cope with hTERT, resulting in a clonal expansion (van Waarde-Verhagen *et al*, 2005). This supports the theory that hTERT and progerin act as opposing forces in cells and that hTERT immortalisation is not a viable method for gaining cell number in disease characterised by short cell replicative lifespans. This evidence adds weight to the theory that hTERT negates the progerin induced telomere dysfunction that leads to replicative arrest and premature senescence in HGPS cells (Benson *et al,* 2010). Unlike previous findings, however, this study does not provide support for the notion of telomere length being an upstream signal of progerin expression. This study suggests that cells have evolved to cope with increased growth pressure, as a result of the artificial environment. The difficulty in hTERT immortalisation of this cell line may support the argument for clonal evolution. This raises questions about the suitability of hTERT cell lines for the study of a number of diseases which have defects in cell cycle control, DNA damage and genomic stability.

7.1.2 Therapeutic Potential

The successful hTERT immortalisation of progeria cells and resulting clonal expansion has opened up new avenues for therapy. Previously progerin was thought to be broken down via autophagy (Graziotto *et al*, 2012), which led to perspective clinical trial for the autophagy promoting drug rapamycin (Cao *et al*, 2011; Graziotto *et al*, 2012). Studies using fibroblast cultures identified improvements in progeria cell characteristics such as nuclear shape and heterochromatin organisation (Cao *et al*, 2011; Graziotto *et al*, 2012). Identification of a model cell line, which demonstrate preferential breakdown of progerin through the 26S proteasome, resulting in similar improvement in cell phenotype (Chapter 4), may offer a novel target avenue for therapy. To test this a U3 conjugated Nanobody targeted to A type lamins was employed. This demonstrated the ability of Nanobodies to effectively target A type lamins for degradation, all be it not determined if through proteasome or autophagosome. Further use of more specifically target Nanobodies may replicate the effect achieved through prolonged growth in the presence of hTERT. If a reduction in progerin protein is produced this has previously been shown to improve cell phenotype (Scaffidi and Misteli, 2005), a common goal of treatments. This is particularly exciting because Nanobodies are an emerging field, with several clinical trials currently underway (Peyvandi *et al*, 2016).

The development of TAT-Lamin A and TAT-Progerin fusion proteins may prove valuable in determining the effectiveness of therapy. Through hTERT immortalisation a significant reduction in progerin abundance and distribution has been observed (Chapter 4). It is not known what level of progerin is tolerated by cells, with some studies identifying a role of progerin in normal human ageing (Scaffidi and Misteli, 2006). Through concentration dependent studies a proper investigation into the level of progerin toxicity could be performed, adding evidence to that Chojnowski *et al*, 2015 described a threshold of progerin toxicity. With current treatments estimated to extend life-expectancey by only 1.6 years (Gordon *et al*, 2014), new stratergies for HGPS are essential.

TAT proteins may also be used to increase our understanding of lamin A and progerin interacting partners, through pulldown studies (Kubben *et al,* 2010). This could add insight into the Lamina fuctions most associated with premature ageing, which could aid in futher APS gene discovery and identify new therapeutic targets. These proteins can also be used to evaluate nuclear entry, whether it is using the NLS (Wu *et al,* 2014) or farnesylation. This would help determine the need for farnesylation (Smallwood and Shackleton, 2010) and add further insight to the use of FTIs as current progeria treatment (Servick, 2014).

7.1.3 Atypical Progeria

20% of cases of progeria are not caused by the well characterised *LMNA* mutation (Hennekam, 2006). These patients demonstrate a more diverse spectrum of characteristics which is represented by the underlying cell phenotype (Hennekam, 2006). To date only two other genes have been shown to cause progeria and one of those is a lamin post-translational modification protein (*ZMPSTE24)* (Shackleton *et al,* 2005). With atypical patients showing overlap with other disease as well as normal human ageing (McKenna *et al,* 2013), the addition of more genes would help paint a more detailed picture. In this study we described the use of exome sequencing to search for the mutated gene. With the identification of DNA repair gene *IN080E* as a potential candidate, this study suggests a link between telomere function and cell cycle control in this case of APS. A recent study by Professor Wendy Bickmore has, however, suggested that DNA damage is not a mechanism for progeria related cell ageing (Deniaud *et al,* 2016). With this in mind more information about the clinical presentation of the patient, in particular a cancer phenotype, may add insight into DNA damage in this patient or highlight other lamin A processes to target in the WES data.

7.1.4 Normal ageing

Progerin expression and protein have been observed in several studies in cells and tissues from healthy individuals (Scaffidi & Misteli, 2006; Rodrigue *et al,* 2009; Cao *et al,* 2011; McClintock *et al,* 2007; Olive *et al,* 2010). Thus has led to the belief that

progerin build up as impact on normal human ageing (Scaffidi and Misteli, 2006), potentially through telomere interactions (Decker *et al,* 2009). The novel QPCR designed by Dr Evgeny Makarov, Brunel University London and implemented in this study (Chapter 4) offers the opportunity to more accurately quantify progerin involvement in normal human ageing.

7.2 Key Findings

7.2.1 Future work

Key work to be carried out following this study includes further characterisation of the reduction of progerin within the TAG06297 Late cells, in particular the proposed proteasomal degradation in response to hTERT immortalisation. This could be achieved through analysis using other proteasome/Ubiquitin Ligase inhibiting drugs clasto-Lactacystin β-Lactone an inhibitor of the 20S proteasome, Epoxomicin an inhibitor of Z catalytic subunits of the proteasome), as well as panels to identify E2/E3 ubiquitin ligases (Fu *et al,* 2004, Marblestone *et al,* 2013).

Identifying specific changes in the hTERT immortalised cell line to understand how they cured themselves. This will involve *LMNA* sequence analysis and even micro-array expression profiling. Could also analyse changes to miRNA expression profiles, as other nuclear envelope disease and laminopathies have been linked to changes in miRNA, which have an adverse effect on cell cycle progression (Malhas *et al,* 2010; Sylvius *et al,* 2011). MiRNA 9 expression been shown to regulate changes in lamin and progerin in neuronal tissue, suggested to be neuro protective, no ageing associated neurological impairments in HGPS patients (Nissan, 2012). It could be interesting to identify changes in miRNA expression in response to hTERT to identify new targets for therapy.

Continued development of Nanobodies targeted to progerin is an exciting potential therapy. Once a more specific Nanobody has been developed the impact on cell phenotype can be examined.

Further mining of the exome data will allow potential discovery of a progeria causing gene. The addition of new disease causing genes increases understanding of progeria pathology, and allows further comparisons to normal human ageing. This is particularly exciting as hTERT cell characterisation suggests the involvement of genes involved in cell cycle control or telomere interactions.

7.3 Conclusion

This study has identified several phenotypical changes in response to hTERT immortalisation, concluding that hTERT immortalisation does not yield an effective tool for studying HGPS. This work has, however, identified a potential new therapeutic approach using proteasomal degradation through Nanobody targeting and raised questions about telomere and cell cycle control in a specific case of atypical progeria. Finally, this study has also employed a novel method for QPCR and suggest this would be useful for further examination of progerin in normal human ageing.

8 References

Aebi, U., Cohn, J., Buhle, L. and Gerace, L. (1986) 'The nuclear lamina is a meshwork of intermediate-type filaments.', *Nature,* 323(6088), pp. 560-564.

Aliper, A.M., Csoka, A.B., Buzdin, A., Jetka, T., Roumiantsev, S., Moskalev, A. and Zhavoronkov, A. (2015) 'Signaling pathway activation drift during aging: Hutchinson-Gilford Progeria Syndrome fibroblasts are comparable to normal middle-age and old-age cells.', *Aging,* 7(1), pp. 26-37.

Allsopp, R.C., Vaziri, H., Patterson, C., Goldstein, S., Younglai, E.V., Futcher, A.B., Greider, C.W. and Harley, C.B. (1992) 'Telomere length predicts replicative capacity of human fibroblasts.', *Proceedings of the National Academy of Sciences of the United States of America,* 89(21), pp. 10114-10118.

Anderson, M.J. and Stanbridge, E.J. (1993) 'Tumor suppressor genes studied by cell hybridization and chromosome transfer', *FASEB Journal,* 7(10), pp. 826-833.

Anderson, R. (2010)'Multiplex Fluorescence in situ Hybridization (M-FISH). Protocols and Applications.' In: Bridger, J.M. and Volpi, E.V. Methods in Molecular Biology Volume 659. Heidelberg: Springer, pp. 83-97.

Barrowman, J., Hamblet, C., George, C.M. and Michaelis, S. (2008) 'Analysis of prelamin A biogenesis reveals the nucleus to be a CaaX processing compartment.', *Molecular biology of the cell,* 19(12), pp. 5398-5408.

Beard, G.S., Bridger, J.M., Kill, I.R. and Tree, D.R. (2008) 'Towards a Drosophila model of Hutchinson-Gilford progeria syndrome.', *Biochemical Society transactions,* 36(Pt 6), pp. 1389-1392.

Becker-Hapak, M., McAllister, S.S. and Dowdy, S.F. (2001) 'TAT-mediated protein transduction into mammalian cells', *Methods (Duluth),* 24(3), pp. 247-256.

Bjedov, I., Toivonen, J.M., Kerr, F., Slack, C., Jacobson, J., Foley, A. and Partridge, L. (2010) 'Mechanisms of life span extension by rapamycin in the fruit fly Drosophila melanogaster.', *Cell Metabolism,* 11(1), pp. 35-46.

Belzile, J., Richard, J., Rougeau, N., Xiao, Y. and Cohen, E.A. (2010) 'HIV-1 Vpr induces the K48-linked polyubiquitination and proteasomal degradation of target cellular proteins to activate ATR and promote G2 arrest.', *Journal of virology,* 84(7), pp. 3320-3330.

Benson, E.K., Lee, S.W. and Aaronson, S.A. (2010) 'Role of progerin-induced telomere dysfunction in HGPS premature cellular senescence.', *Journal of cell science,* 123(Pt 15), pp. 2605-2612.

Bodnar, A.G., Ouellette, M., Frolkis, M., Holt, S.E., Chiu, C.P., Morin, G.B., Harley, C.B., Shay, J.W., Lichtsteiner, S. and Wright, W.E. (1998) 'Extension of life-span by introduction of telomerase into normal human cells.', *Science,* 279(5349), pp. 349-352.

Bonello-Palot, N., Simoncini, S., Robert, S., Bourgeois, P., Sabatier, F., Levy, N., Dignat-George, F. and Badens, C. (2014) 'Prelamin A accumulation in endothelial cells induces premature senescence and functional impairment.', *Atherosclerosis,* 237(1), pp. 45-52.

Brandt, A., Krohne, G. and Grosshans, J. (2008) 'The farnesylated nuclear proteins KUGELKERN and LAMIN B promote aging-like phenotypes in Drosophila flies.', *Aging Cell,* 7(4), pp. 541-551.

Bridger, J.M., Kill, I.R., O'Farrell, M. and Hutchison, C.J. (1993) 'Internal lamin structures within G1 nuclei of human dermal fibroblasts.', *Journal of cell science,* 104(Pt 2), pp. 297-306.

Bridger, J.M., Eskiw, C.H., Makarov, E.M., Tree, D. and Kill, I.R. (2011) 'Progeria Research Day at Brunel University', *Nucleus (Calcutta),* 2(6), pp. 517-522.

Bridger, J.M. and Kill, I.R. (2004) 'Aging of Hutchinson-Gilford progeria syndrome fibroblasts is characterised by hyperproliferation and increased apoptosis.', *Experimental gerontology,* 39(5), pp. 717-724.

Broers, J.L., Machiels, B.M., van Eys, G.J., Kuijpers, H.J., Manders, E.M., van Driel, R. and Ramaekers, F.C. (1999) 'Dynamics of the nuclear lamina as monitored by GFP-tagged A-type lamins.', *Journal of cell science,* 112(Pt 20), pp. 3463-3475.

Brown, W.T. (1992) 'Progeria: a human-disease model of accelerated aging', *American Journal of Clinical Nutrition,* 55(6 Suppl), pp. 1222S-1224S.

Bustin, S.A., Benes, V., Garson, J.A., Hellemans, J., Huggett, J., Kubista, M., Mueller, R., Nolan, T., Pfaffl, M.W., Shipley, G.L., Vandesompele, J. and Wittwer, C.T. (2009) 'The MIQE guidelines: minimum information for publication of quantitative real-time PCR experiments.', *Clinical chemistry,* 55(4), pp. 611-622.

Campisi, J., Kim, S.H., Lim, C.S. and Rubio, M. (2001) 'Cellular senescence, cancer and aging: the telomere connection', *Experimental gerontology,* 36(10), pp. 1619-1637.

Cao, K., Capell, B.C., Erdos, M.R., Djabali, K. and Collins, F.S. (2007) 'A lamin A protein isoform overexpressed in Hutchinson-Gilford progeria syndrome interferes with mitosis in progeria and normal cells.', *Proceedings of the National Academy of Sciences of the United States of America,* 104(12), pp. 4949-4954.

Cao, K., Graziotto, J.J., Blair, C.D., Mazzulli, J.R., Erdos, M.R., Krainc, D. and Collins, F.S. (2011) 'Rapamycin reverses cellular phenotypes and enhances mutant protein clearance in Hutchinson-Gilford progeria syndrome cells.', *Science Translational Medicine*, 3(89), pp. 89ra58.

Cao, K., Blair, C.D., Faddah, D.A., Kieckhaefer, J.E., Olive, M., Erdos, M.R., Nabel, E.G. and Collins, F.S. (2011) 'Progerin and telomere dysfunction collaborate to trigger cellular senescence in normal human fibroblasts.', *Journal of Clinical Investigation*, 121(7), pp. 2833-2844.

Capell, B.C. and Collins, F.S. (2006) 'Human laminopathies: nuclei gone genetically awry', *Nature Reviews Genetics*, 7(12), pp. 940-952.

Capell, B.C., Erdos, M.R., Madigan, J.P., Fiordalisi, J.J., Varga, R., Conneely, K.N., Gordon, L.B., Der, C.J., Cox, A.D. and Collins, F.S. (2005) 'Inhibiting farnesylation of progerin prevents the characteristic nuclear blebbing of Hutchinson-Gilford progeria syndrome.', *Proceedings of the National Academy of Sciences of the United States of America*, 102(36), pp. 12879-12884.

Cau, P., Navarro, C., Harhouri, K., Roll, P., Sigaudy, S., Kaspi, E., Perrin, S., De Sandre-Giovannoli, A. and Levy, N. (2014) 'Nuclear matrix, nuclear envelope and premature aging syndromes in a translational research perspective', *Seminars in cell & developmental biology*, 29, pp. 125-147.

Cenni, V., Capanni, C., Columbaro, M., Ortolani, M., D'Apice, M.R., Novelli, G., Fini, M., Marmiroli, S., Scarano, E., Maraldi, N.M., Squarzoni, S., Prencipe, S. and Lattanzi, G. (2011) 'Autophagic degradation of farnesylated prelamin A as a therapeutic approach to lamin-linked progeria', *European Journal of Histochemistry*, 55(4), pp. e36.

Chen, L., Lee, L., Kudlow, B.A., Dos Santos, H.G., Sletvold, O., Shafeghati, Y., Botha, E.G., Garg, A., Hanson, N.B., Martin, G.M., Mian, I.S., Kennedy, B.K. and Oshima, J. (2003) 'LMNA mutations in atypical Werner's syndrome.', *Lancet*, 362(9382), pp. 440-445.

Chen, M., Rockel, T., Steinweger, G., Hemmerich, P., Risch, J. and von Mikecz, A. (2002) 'Subcellular recruitment of fibrillarin to nucleoplasmic proteasomes: implications for processing of a nucleolar autoantigen.', *Molecular biology of the cell*, 13(10), pp. 3576-3587.

Choi, S., Wang, W., Ribeiro, A.J.S., Kalinowski, A., Gregg, S.Q., Opresko, P.L., Niedernhofer, L.J., Rohde, G.K. and Dahl, K.N. (2011) 'Computational image analysis of nuclear morphology associated with various nuclear-specific aging disorders.', *Nucleus (Calcutta)*, 2(6), pp. 570-579.

Chojnowski, A., Ong, P.F., Wong, E.S.M., Lim, J.S.Y., Mutalif, R.A., Navasankari, R., Dutta, B., Yang, H., Liow, Y.Y., Sze, S.K., Boudier, T., Wright, G.D., Colman, A., Burke, B., Stewart, C.L. and Dreesen, O. (2015) 'Progerin reduces LAP2alpha-telomere association in Hutchinson-Gilford progeria.', *eLife*, 4.

Couzin-Frankel, J. (2012) 'Medicine. Drug trial offers uncertain start in race to save children with progeria.', *Science*, 337(6102), pp. 1594-1595.

Crabbe, L., Jauch, A., Naeger, C.M., Holtgreve-Grez, H. and Karlseder, J. (2007) 'Telomere dysfunction as a cause of genomic instability in Werner syndrome.', Proceedings of *the National Academy of Sciences of the United States of America*, 104(7), pp. 2205-2210.

Csoka, A.B., Cao, H., Sammak, P.J., Constantinescu, D., Schatten, G.P. and Hegele, R.A. (2004) 'Novel lamin A/C gene (LMNA) mutations in atypical progeroid syndromes.', *Journal of medical genetics*, 41(4), pp. 304-308.

Cuthbert, A.P., Trott, D.A., Ekong, R.M., Jezzard, S., England, N.L., Themis, M., Todd, C.M. and Newbold, R.F. (1995) 'Construction and characterization of a highly stable human: rodent monochromosomal hybrid panel for genetic complementation and genome mapping studies.', *Cytogenetics & Cell Genetics*, 71(1), pp. 68-76.

Dayton, A.I., Sodroski, J.G., Rosen, C.A., Goh, W.C. and Haseltine, W.A. (1986) 'The trans-activator gene of the human T cell lymphotropic virus type III is required for replication.', *Cell*, 44(6), pp. 941-947.

De Sandre-Giovannoli, A., Bernard, R., Cau, P., Navarro, C., Amiel, J., Boccaccio, I., Lyonnet, S., Stewart, C.L., Munnich, A., Le Merrer, M. and Levy, N. (2003) 'Lamin a truncation in Hutchinson-Gilford progeria.', *Science*, 300(5628), pp. 2055.

Dechat, T., Adam, S.A., Taimen, P., Shimi, T. and Goldman, R.D. (2010) 'Nuclear lamins', *Cold Spring Harbor perspectives in biology*, 2(11), pp. a000547.

Dechat, T., Korbei, B., Vaughan, O.A., Vlcek, S., Hutchison, C.J. and Foisner, R. (2000) 'Lamina-associated polypeptide 2alpha binds intranuclear A-type lamins.', *Journal of cell science*, 113(Pt 19), pp. 3473-3484.

Dechat, T., Shimi, T., Adam, S.A., Rusinol, A.E., Andres, D.A., Spielmann, H.P., Sinensky, M.S. and Goldman, R.D. (2007) 'Alterations in mitosis and cell cycle progression caused by a mutant lamin A known to accelerate human aging.', *Proceedings of the National Academy of Sciences of the United States of America*, 104(12), pp. 4955-4960.

Dechat, T., Pfleghaar, K., Sengupta, K., Shimi, T., Shumaker, D.K., Solimando, L. and Goldman, R.D. (2008) 'Nuclear lamins: major factors in the structural organization and function of the nucleus and chromatin', *Genes & development*, 22(7), pp. 832-853.

Decker, M.L., Chavez, E., Vulto, I. and Lansdorp, P.M. (2009) 'Telomere length in Hutchinson-Gilford progeria syndrome.', *Mechanisms of Ageing & Development*, 130(6), pp. 377-383.

Deniaud, E., Boyle, S. and Bickmore, W. (2016) 'Expression of progerin does not result in an increased mutation rate', *bioRxiv*, .

Dikic, I., Wakatsuki, S. and Walters, K.J. (2009) 'Ubiquitin-binding domains - from structures to functions', *Nature Reviews Molecular Cell Biology,* 10(10), pp. 659-671.

Dino Rockel, T. and von Mikecz, A. (2002) 'Proteasome-dependent processing of nuclear proteins is correlated with their subnuclear localization.', *Journal of structural biology,* 140(1-3), pp. 189-199.

Dittmer, T.A. and Misteli, T. (2011) 'The lamin protein family', *Genome biology,* 12(5), pp. 222.

Doh, Y.J., Kim, H.K., Jung, E.D., Choi, S.H., Kim, J.G., Kim, B.W. and Lee, I.K. (2009) 'Novel LMNA gene mutation in a patient with Atypical Werner's Syndrome.', *Korean Journal of Internal Medicine,* 24(1), pp. 68-72.

Dowdy, S.F., Scanlon, D.J., Fasching, C.L., Casey, G. and Stanbridge, E.J. (1990) 'Irradiation microcell-mediated chromosome transfer (XMMCT): the generation of specific chromosomal arm deletions.', *Genes, chromosomes & cancer,* 2(4), pp. 318-327.

Elliott, G. and O'Hare, P. (1997) 'Intercellular trafficking and protein delivery by a herpesvirus structural protein.', *Cell,* 88(2), pp. 223-233.

Eriksson, M., Brown, W.T., Gordon, L.B., Glynn, M.W., Singer, J., Scott, L., Erdos, M.R., Robbins, C.M., Moses, T.Y., Berglund, P., Dutra, A., Pak, E., Durkin, S., Csoka, A.B., Boehnke, M., Glover, T.W. and Collins, F.S. (2003) 'Recurrent de novo point mutations in lamin A cause Hutchinson-Gilford progeria syndrome.', *Nature,* 423(6937), pp. 293-298.

Essafi, M., Baudot, A.D., Mouska, X., Cassuto, J., Ticchioni, M. and Deckert, M. (2011) 'Cell-penetrating TAT-FOXO3 fusion proteins induce apoptotic cell death in leukemic cells.', *Molecular Cancer Therapeutics,* 10(1), pp. 37-46.

Fawell, S., Seery, J., Daikh, Y., Moore, C., Chen, L.L., Pepinsky, B. and Barsoum, J. (1994) 'Tat-mediated delivery of heterologous proteins into cells.', *Proceedings of the National Academy of Sciences of the United States of America,* 91(2), pp. 664-668.

Fisher, A.G., Feinberg, M.B., Josephs, S.F., Harper, M.E., Marselle, L.M., Reyes, G., Gonda, M.A., Aldovini, A., Debouk, C. and Gallo, R.C. (1986) 'The trans-activator gene of HTLV-III is essential for virus replication.', *Nature,* 320(6060), pp. 367-371.

Flajnik, M.F., Deschacht, N. and Muyldermans, S. (2011) 'A case of convergence: why did a simple alternative to canonical antibodies arise in sharks and camels?.', *Plos Biology,* 9(8), pp. e1001120.

Flanagan, J.M., Healey, S., Young, J., Whitehall, V., Trott, D.A., Newbold, R.F. and Chenevix-Trench, G. (2004) 'Mapping of a candidate colorectal cancer tumor-suppressor gene to a 900-kilobase region on the short arm of chromosome 8.', *Genes, chromosomes & cancer,* 40(3), pp. 247-260.

Fong, L.G., Frost, D., Meta, M., Qiao, X., Yang, S.H., Coffinier, C. and Young, S.G. (2006) 'A protein farnesyltransferase inhibitor ameliorates disease in a mouse model of progeria.', *Science,* 311(5767), pp. 1621-1623.

Fong, L.G., Ng, J.K., Lammerding, J., Vickers, T.A., Meta, M., Cote, N., Gavino, B., Qiao, X., Chang, S.Y., Young, S.R., Yang, S.H., Stewart, C.L., Lee, R.T., Bennett, C.F., Bergo, M.O. and Young, S.G. (2006) 'Prelamin A and lamin A appear to be dispensable in the nuclear lamina.', *Journal of Clinical Investigation,* 116(3), pp. 743-752.

Fong, L.G., Vickers, T.A., Farber, E.A., Choi, C., Yun, U.J., Hu, Y., Yang, S.H., Coffinier, C., Lee, R., Yin, L., Davies, B.S.J., Andres, D.A., Spielmann, H.P., Bennett, C.F. and Young, S.G. (2009) 'Activating the synthesis of progerin, the mutant prelamin A in Hutchinson-Gilford progeria syndrome, with antisense oligonucleotides.', *Human molecular genetics,* 18(13), pp. 2462-2471.

Fournier, R.E. and Ruddle, F.H. (1977) 'Microcell-mediated transfer of murine chromosomes into mouse, Chinese hamster, and human somatic cells.', *Proceedings of the National Academy of Sciences of the United States of America,* 74(1), pp. 319-323.

Frankel, A.D. and Pabo, C.O. (1988) 'Cellular uptake of the tat protein from human immunodeficiency virus.', *Cell,* 55(6), pp. 1189-1193.

Fu, X., Richards, D.E., Fleck, B., Xie, D., Burton, N. and Harberd, N.P. (2004) 'The Arabidopsis mutant sleepy1gar2-1 protein promotes plant growth by increasing the affinity of the SCFSLY1 E3 ubiquitin ligase for DELLA protein substrates.', *Plant Cell,* 16(6), pp. 1406-1418.

Fukuchi, K., Katsuya, T., Sugimoto, K., Kuremura, M., Kim, H.D., Li, L. and Ogihara, T. (2004) 'LMNA mutation in a 45 year old Japanese subject with Hutchinson-Gilford progeria syndrome.', *Journal of medical genetics,* 41(5), pp. e67.

Furukawa, K. and Hotta, Y. (1993) 'cDNA cloning of a germ cell specific lamin B3 from mouse spermatocytes and analysis of its function by ectopic expression in somatic cells.', *EMBO Journal,* 12(1), pp. 97-106.

Garavelli, L., D'Apice, M.R., Rivieri, F., Bertoli, M., Wischmeijer, A., Gelmini, C., De Nigris, V., Albertini, E., Rosato, S., Virdis, R., Bacchini, E., Dal Zotto, R., Banchini, G., Iughetti, L., Bernasconi, S., Superti-Furga, A. and Novelli, G. (2009) 'Mandibuloacral dysplasia type A in childhood.', *American Journal of Medical Genetics.Part A,* 149A(10), pp. 2258-2264.

Georgatos, S.D., Stournaras, C. and Blobel, G. (1988) 'Heterotypic and homotypic associations between the nuclear lamins: site-specificity and control by phosphorylation.', *Proceedings of the National Academy of Sciences of the United States of America*, 85(12), pp. 4325-4329.

Gilford, H. 'On a condition of mixed premature and immature development.', *Medico-Chirurgical Transactions*, 80, pp. 17-45.

Gilford, H. (1904a) 'Progeria: a form of senilism.', *Practitioner*, 73, pp. 188-217.

Gilford, H. (1904b) 'Ateliosis and progeria: contniuous youth and premature old age.', *Br Med J*, 2, pp. 914-918.

Gingold, H. and Pilpel, Y. (2011) 'Determinants of translation efficiency and accuracy', *Molecular Systems Biology*, 7, pp. 481.

Glynn, M.W. and Glover, T.W. (2005) 'Incomplete processing of mutant lamin A in Hutchinson-Gilford progeria leads to nuclear abnormalities, which are reversed by farnesyltransferase inhibition.', *Human molecular genetics*, 14(20), pp. 2959-2969.

Godwin, L.S. (2010) 'The role of lamin A and emerin in mediating genome organization'. PhD Thesis, Brunel University.

Goldman, A.E., Moir, R.D., Montag-Lowy, M., Stewart, M. and Goldman, R.D. (1992) 'Pathway of incorporation of microinjected lamin A into the nuclear envelope.', *Journal of Cell Biology*, 119(4), pp. 725-735.

Goldman, R.D., Gruenbaum, Y., Moir, R.D., Shumaker, D.K. and Spann, T.P. (2002) 'Nuclear lamins: building blocks of nuclear architecture', *Genes & development*, 16(5), pp. 533-547.

Goldman, R.D., Shumaker, D.K., Erdos, M.R., Eriksson, M., Goldman, A.E., Gordon, L.B., Gruenbaum, Y., Khuon, S., Mendez, M., Varga, R. and Collins, F.S. (2004) 'Accumulation of mutant lamin A causes progressive changes in nuclear architecture in Hutchinson-Gilford progeria syndrome.', *Proceedings of the National Academy of Sciences of the United States of America*, 101(24), pp. 8963-8968.

Gordon, L.B., Kleinman, M.E., Miller, D.T., Neuberg, D.S., Giobbie-Hurder, A., Gerhard-Herman, M., Smoot, L.B., Gordon, C.M., Cleveland, R., Snyder, B.D., Fligor, B., Bishop, W.R., Statkevich, P., Regen, A., Sonis, A., Riley, S., Ploski, C., Correia, A., Quinn, N., Ullrich, N.J., Nazarian, A., Liang, M.G., Huh, S.Y., Schwartzman, A. and Kieran, M.W. (2012) 'Clinical trial of a farnesyltransferase inhibitor in children with Hutchinson-Gilford progeria syndrome.', *Proceedings of the National Academy of Sciences of the United States of America*, 109(41), pp. 16666-16671.

Gordon, L.B., McCarten, K.M., Giobbie-Hurder, A., Machan, J.T., Campbell, S.E., Berns, S.D. and Kieran, M.W. (2007) 'Disease progression in Hutchinson-Gilford progeria syndrome: impact on growth and development.', *Pediatrics,* 120(4), pp. 824-833.

Gordon, L.B., Rothman, F.G., Lopez-Otin, C. and Misteli, T. (2014) 'Progeria: a paradigm for translational medicine.', *Cell,* 156(3), pp. 400-407.

Graziotto, J.J., Cao, K., Collins, F.S. and Krainc, D. (2012) 'Rapamycin activates autophagy in Hutchinson-Gilford progeria syndrome: implications for normal aging and age-dependent neurodegenerative disorders', *Autophagy,* 8(1), pp. 147-151.

Green, M. and Loewenstein, P.M. (1988) 'Autonomous functional domains of chemically synthesized human immunodeficiency virus tat trans-activator protein.', *Cell,* 55(6), pp. 1179-1188.

Grossman, E., Medalia, O. and Zwerger, M. (2012) 'Functional architecture of the nuclear pore complex', *Annual review of biophysics,* 41, pp. 557-584.

Gruenbaum, Y., Margalit, A., Goldman, R.D., Shumaker, D.K. and Wilson, K.L. (2005) 'The nuclear lamina comes of age', *Nature Reviews Molecular Cell Biology,* 6(1), pp. 21-31.

Haithcock, E., Dayani, Y., Neufeld, E., Zahand, A.J., Feinstein, N., Mattout, A., Gruenbaum, Y. and Liu, J. (2005) 'Age-related changes of nuclear architecture in Caenorhabditis elegans.', *Proceedings of the National Academy of Sciences of the United States of America,* 102(46), pp. 16690-16695.

Hamers-Casterman, C., Atarhouch, T., Muyldermans, S., Robinson, G., Hamers, C., Songa, E.B., Bendahman, N. and Hamers, R. (1993) 'Naturally occurring antibodies devoid of light chains.', *Nature,* 363(6428), pp. 446-448.

Hansen, M., Taubert, S., Crawford, D., Libina, N., Lee, S.J. and Kenyon, C. (2007) 'Lifespan extension by conditions that inhibit translation in Caenorhabditis elegans.', *Aging Cell,* 6(1), pp. 95-110.

Haque, F., Lloyd, D.J., Smallwood, D.T., Dent, C.L., Shanahan, C.M., Fry, A.M., Trembath, R.C. and Shackleton, S. (2006) 'SUN1 interacts with nuclear lamin A and cytoplasmic nesprins to provide a physical connection between the nuclear lamina and the cytoskeleton.', *Molecular & Cellular Biology,* 26(10), pp. 3738-3751.

Haque, F., Mazzeo, D., Patel, J.T., Smallwood, D.T., Ellis, J.A., Shanahan, C.M. and Shackleton, S. (2010) 'Mammalian SUN protein interaction networks at the inner nuclear membrane and their role in laminopathy disease processes.', *Journal of Biological Chemistry,* 285(5), pp. 3487-3498.

Harborth, J., Elbashir, S.M., Bechert, K., Tuschl, T. and Weber, K. (2001) 'Identification of essential genes in cultured mammalian cells using small interfering RNAs.', *Journal of cell science,* 114(Pt 24), pp. 4557-4565.

Harrison, D.E., Strong, R., Sharp, Z.D., Nelson, J.F., Astle, C.M., Flurkey, K., Nadon, N.L., Wilkinson, J.E., Frenkel, K., Carter, C.S., Pahor, M., Javors, M.A., Fernandez, E. and Miller, R.A. (2009) 'Rapamycin fed late in life extends lifespan in genetically heterogeneous mice.', *Nature,* 460(7253), pp. 392-395.

Hawiger, J. (1999) 'Noninvasive intracellular delivery of functional peptides and proteins', *Current opinion in chemical biology,* 3(1), pp. 89-94.

Hennekam, R.C.M., 2006. Hutchinson-Gilford progeria syndrome: review of the phenotype. American Journal of medical genetics. 140, pp. 2603-24.

Herrmann, H., Kreplak, L. and Aebi, U. (2004) 'Isolation, characterization, and in vitro assembly of intermediate filaments.', Methods in cell biology, 78, pp. 3-24.

Heyn, H., Moran, S., Hernando-Herraez, I., Sayols, S., Gomez, A., Sandoval, J., Monk, D., Hata, K., Marques-Bonet, T., Wang, L. and Esteller, M. (2013) 'DNA methylation contributes to natural human variation.', Genome research, 23(9), pp. 1363-1372.

Hisama, F.M., Kubisch, C., Martin, G.M. and Oshima, J. (2012) 'Clinical utility gene card for: Werner syndrome.', *European Journal of Human Genetics,* 20(5).

Hisama, F.M., Lessel, D., Leistritz, D., Friedrich, K., McBride, K.L., Pastore, M.T., Gottesman, G.S., Saha, B., Martin, G.M., Kubisch, C. and Oshima, J. (2011) 'Coronary artery disease in a Werner syndrome-like form of progeria characterized by low levels of progerin, a splice variant of lamin A.', *American Journal of Medical Genetics.Part A,* 155A(12), pp. 3002-3006.

Huang, S., Chen, L., Libina, N., Janes, J., Martin, G.M., Campisi, J. and Oshima, J. (2005) 'Correction of cellular phenotypes of Hutchinson-Gilford Progeria cells by RNA interference.', *Human genetics,* 118(3-4), pp. 444-450.

Hutchinson, J. (1886a) 'A case of congenital absence of hair with atrophic condition of the skin and its appendages.', *Lancet,* 1:923.

Hutchinson, J. (1886b) 'Case of congenital absence of hair, with atrophic condition of the skin and its appendages, in a boy whose mother had been almost wholly bald from alopecia areata from the age of six.', *Transactions of the Medico-Chirurgical Society of Edinburgh*, 69, pp. 473-477.

Jiang, X.R., Jimenez, G., Chang, E., Frolkis, M., Kusler, B., Sage, M., Beeche, M., Bodnar, A.G., Wahl, G.M., Tlsty, T.D. and Chiu, C.P. (1999) 'Telomerase expression in human somatic cells does not induce changes associated with a transformed phenotype.', *Nature genetics,* 21(1), pp. 111-114.

Kashiwaba, S., Kitahashi, K., Watanabe, T., Onoda, F., Ohtsu, M. and Murakami, Y. (2010) 'The mammalian INO80 complex is recruited to DNA damage sites in an ARP8 dependent manner.', Biochemical & Biophysical Research Communications, 402(4), pp. 619-625.

Kane, M.S., Lindsay, M.E., Judge, D.P., Barrowman, J., Ap Rhys, C., Simonson, L., Dietz, H.C. and Michaelis, S. (2013) 'LMNA-associated cardiocutaneous progeria: an inherited autosomal dominant premature aging syndrome with late onset.', *American Journal of Medical Genetics.Part A*, 161A(7), pp. 1599-1611.

Kill, I.R. (1996) 'Localisation of the Ki-67 antigen within the nucleolus. Evidence for a fibrillarin-deficient region of the dense fibrillar component.', *Journal of cell science*, 109(Pt 6), pp. 1253-1263.

King, C.R., Lemmer, J., Campbell, J.R. and Atkins, A.R. (1978) 'Osteosarcoma in a patient with Hutchinson-Gilford progeria.', *Journal of medical genetics*, 15(6), pp. 481-484.

Kirchhofer, A., Helma, J., Schmidthals, K., Frauer, C., Cui, S., Karcher, A., Pellis, M., Muyldermans, S., Casas-Delucchi, C.S., Cardoso, M.C., Leonhardt, H., Hopfner, K. and Rothbauer, U. (2010) 'Modulation of protein properties in living cells using nanobodies.', *Nature Structural & Molecular Biology*, 17(1), pp. 133-138.

Kirschner, J., Brune, T., Wehnert, M., Denecke, J., Wasner, C., Feuer, A., Marquardt, T., Ketelsen, U.P., Wieacker, P., Bonnemann, C.G. and Korinthenberg, R. (2005) 'p.S143F mutation in lamin A/C: a new phenotype combining myopathy and progeria.', *Annals of Neurology*, 57(1), pp. 148-151.

Kubben, N., Adriaens, M., Meuleman, W., Voncken, J.W., van Steensel, B. and Misteli, T. (2012) 'Mapping of lamin A- and progerin-interacting genome regions.', *Chromosoma*, 121(5), pp. 447-464.

Kubben, N., Voncken, J.W., Demmers, J., Calis, C., van Almen, G., Pinto, Y. and Misteli, T. (2010) 'Identification of differential protein interactors of lamin A and progerin.', *Nucleus (Calcutta*), 1(6), pp. 513-525.

Kudlow, B.A., Stanfel, M.N., Burtner, C.R., Johnston, E.D. and Kennedy, B.K. (2008) 'Suppression of proliferative defects associated with processing-defective lamin A mutants by hTERT or inactivation of p53.', *Molecular biology of the cell*, 19(12), pp. 5238-5248.

Lai, C., Yeh, Y., Hsieh, W., Kuo, C., Wang, W., Chu, C., Hung, C., Cheng, C., Tsai, H., Lee, J., Tang, C. and Hsu, L. (2013) 'Whole-exome sequencing to identify a novel LMNA gene mutation associated with inherited cardiac conduction disease.', *PLoS ONE [Electronic Resource]*, 8(12), pp. e83322.

Larrieu, D., Britton, S., Demir, M., Rodriguez, R. and Jackson, S.P. (2014) 'Chemical inhibition of NAT10 corrects defects of laminopathic cells.', *Science*, 344(6183), pp. 527-532.

Lattanzi, G., Marmiroli, S., Facchini, A. and Maraldi, N.M. (2012) 'Nuclear damages and oxidative stress: new perspectives for laminopathies', *European Journal of Histochemistry*, 56(4), pp. e45.

Lee, K.M., Nguyen, C., Ulrich, A.B., Pour, P.M. and Ouellette, M.M. (2003) 'Immortalization with telomerase of the Nestin-positive cells of the human pancreas.', *Biochemical & Biophysical Research Communications*, 301(4), pp. 1038-1044.

Lin, BY. And Kao, MC. (2015) 'Therapeutic applications of the TAT-mediated protein transduction system for complex I deficiency and other mitochondrial diseases.', *Annals of the New York Academy of Sciences*, 1350, pp. 17-28.

Liu, B., Wang, J., Chan, K.M., Tjia, W.M., Deng, W., Guan, X., Huang, J.D., Li, K.M., Chau, P.Y., Chen, D.J., Pei, D., Pendas, A.M., Cadinanos, J., Lopez-Otin, C., Tse, H.F., Hutchison, C., Chen, J., Cao, Y., Cheah, K.S., Tryggvason, K. and Zhou, Z. (2005) 'Genomic instability in laminopathy-based premature aging.', *Nature medicine*, 11(7), pp. 780-785.

Liu, Y., Rusinol, A., Sinensky, M., Wang, Y. and Zou, Y. (2006) 'DNA damage responses in progeroid syndromes arise from defective maturation of prelamin A.', *Journal of cell science*, 119(Pt 22), pp. 4644-4649.

Lobrich, M., Shibata, A., Beucher, A., Fisher, A., Ensminger, M., Goodarzi, A.A., Barton, O. and Jeggo, P.A. (2010) 'gammaH2AX foci analysis for monitoring DNA double-strand break repair: strengths, limitations and optimization.', *Cell Cycle*, 9(4), pp. 662-669.

Luo, Y., Mitrpant, C., Adams, A.M., Johnsen, R.D., Fletcher, S., Mastaglia, F.L. and Wilton, S.D. (2014) 'Antisense oligonucleotide induction of progerin in human myogenic cells.', *PLoS ONE [Electronic Resource]*, 9(6), pp. e98306.

Machwe, A., Xiao, L. and Orren, D.K. (2004) 'TRF2 recruits the Werner syndrome (WRN) exonuclease for processing of telomeric DNA.', *Oncogene*, 23(1), pp. 149-156.

Malhas, A., Saunders, N.J. and Vaux, D.J. (2010) 'The nuclear envelope can control gene expression and cell cycle progression via miRNA regulation.', *Cell Cycle*, 9(3), pp. 531-539.

Mallampalli, M.P., Huyer, G., Bendale, P., Gelb, M.H. and Michaelis, S. (2005) 'Inhibiting farnesylation reverses the nuclear morphology defect in a HeLa cell model for Hutchinson-Gilford progeria syndrome.', *Proceedings of the National Academy of Sciences of the United States of America*, 102(40), pp. 14416-14421.

Mansharamani, M. and Wilson, K.L. (2005) 'Direct binding of nuclear membrane protein MAN1 to emerin in vitro and two modes of binding to barrier-to-autointegration factor.', *Journal of Biological Chemistry*, 280(14), pp. 13863-13870.

Marblestone, J.G., Butt, S., McKelvey, D.M., Sterner, D.E., Mattern, M.R., Nicholson, B. and Eddins, M.J. (2013) 'Comprehensive ubiquitin E2 profiling of ten ubiquitin E3 ligases.', *Cell Biochemistry & Biophysics,* 67(1), pp. 161-167.

Marino, G., Ugalde, A.P., Fernandez, A.F., Osorio, F.G., Fueyo, A., Freije, J.M. and Lopez-Otin, C. (2010) 'Insulin-like growth factor 1 treatment extends longevity in a mouse model of human premature aging by restoring somatotroph axis function.', *Proceedings of the National Academy of Sciences of the United States of America,* 107(37), pp. 16268-16273.

Markiewicz, E., Dechat, T., Foisner, R., Quinlan, R.A. and Hutchison, C.J. (2002) 'Lamin A/C binding protein LAP2alpha is required for nuclear anchorage of retinoblastoma protein.', *Molecular biology of the cell,* 13(12), pp. 4401-4413.

Mazereeuw-Hautier, J., Wilson, L.C., Mohammed, S., Smallwood, D., Shackleton, S., Atherton, D.J. and Harper, J.I. (2007) 'Hutchinson-Gilford progeria syndrome: clinical findings in three patients carrying the G608G mutation in LMNA and review of the literature', *British Journal of Dermatology,* 156(6), pp. 1308-1314.

McClintock, D., Ratner, D., Lokuge, M., Owens, D.M., Gordon, L.B., Collins, F.S. and Djabali, K. (2007) 'The mutant form of lamin A that causes Hutchinson-Gilford progeria is a biomarker of cellular aging in human skin.', *PLoS ONE [Electronic Resource],* 2(12), pp. e1269.

McKenna, T., Baek, JH. And Eriksson, M. (2013). Laminopathies, Genetic Disorders, Prof. Maria Puiu (Ed.), InTech, DOI: 10.5772/53793. Available from: http://www.intechopen.com/books/genetic-disorders/laminopathies

Meaburn, K.J., Cabuy, E., Bonne, G., Levy, N., Morris, G.E., Novelli, G., Kill, I.R. and Bridger, J.M. (2007) 'Primary laminopathy fibroblasts display altered genome organization and apoptosis.', *Aging Cell,* 6(2), pp. 139-153.

Meaburn, K.J., Parris, C.N. and Bridger, J.M. (2005) 'The manipulation of chromosomes by mankind: the uses of microcell-mediated chromosome transfer', *Chromosoma,* 114(4), pp. 263-274.

Mehta, I.S., Bridger, J.M. and Kill, I.R. (2010) 'Progeria, the nucleolus and farnesyltransferase inhibitors.', *Biochemical Society transactions,* 38(Pt 1), pp. 287-291.

Mehta, I.S., Figgitt, M., Clements, C.S., Kill, I.R. and Bridger, J.M. (2007) 'Alterations to nuclear architecture and genome behavior in senescent cells', *Annals of the New York Academy of Sciences,* 1100, pp. 250-263.

Mehta, I.S., Eskiw, C.H., Arican, H.D., Kill, I.R. and Bridger, J.M. (2011) 'Farnesyltransferase inhibitor treatment restores chromosome territory positions and active chromosome dynamics in Hutchinson-Gilford progeria syndrome cells.', *Genome biology,* 12(8), pp. R74.

Meinke, P., Mattioli, E., Haque, F., Antoku, S., Columbaro, M., Straatman, K.R., Worman, H.J., Gundersen, G.G., Lattanzi, G., Wehnert, M. and Shackleton, S. (2014) 'Muscular dystrophy-associated SUN1 and SUN2 variants disrupt nuclear-cytoskeletal connections and myonuclear organization.', *PLoS Genetics*, 10(9), pp. e1004605.

Mellad, J.A., Warren, D.T. and Shanahan, C.M. (2011) 'Nesprins LINC the nucleus and cytoskeleton', *Current opinion in cell biology*, 23(1), pp. 47-54.

Meng, L., Mohan, R., Kwok, B.H., Elofsson, M., Sin, N. and Crews, C.M. (1999) 'Epoxomicin, a potent and selective proteasome inhibitor, exhibits in vivo antiinflammatory activity.', *Proceedings of the National Academy of Sciences of the United States of America*, 96(18), pp. 10403-10408.

Merideth, M.A., Gordon, L.B., Clauss, S., Sachdev, V., Smith, A.C.M., Perry, M.B., Brewer, C.C., Zalewski, C., Kim, H.J., Solomon, B., Brooks, B.P., Gerber, L.H., Turner, M.L., Domingo, D.L., Hart, T.C., Graf, J., Reynolds, J.C., Gropman, A., Yanovski, J.A., Gerhard-Herman, M., Collins, F.S., Nabel, E.G., Cannon, R.O.3., Gahl, W.A. and Introne, W.J. (2008) 'Phenotype and course of Hutchinson-Gilford progeria syndrome.', *New England Journal of Medicine*, 358(6), pp. 592-604.

Miller, R.A., Harrison, D.E., Astle, C.M., Baur, J.A., Boyd, A.R., de Cabo, R., Fernandez, E., Flurkey, K., Javors, M.A., Nelson, J.F., Orihuela, C.J., Pletcher, S., Sharp, Z.D., Sinclair, D., Starnes, J.W., Wilkinson, J.E., Nadon, N.L. and Strong, R. (2011) 'Rapamycin, but not resveratrol or simvastatin, extends life span of genetically heterogeneous mice.', *Journals of Gerontology Series A-Biological Sciences & Medical Sciences*, 66(2), pp. 191-201.

Moiseeva, O., Lessard, F., Acevedo-Aquino, M., Vernier, M., Tsantrizos, Y.S. and Ferbeyre, G. (2015) 'Mutant lamin A links prophase to a p53 independent senescence program.', *Cell Cycle*, 14(15), pp. 2408-2421.

Mok, Q., Curley, R., Tolmie, J.L., Marsden, R.A., Patton, M.A. and Davies, E.G. (1990) 'Restrictive dermopathy: a report of three cases.', *Journal of medical genetics*, 27(5), pp. 315-319.

Morales, C.P., Holt, S.E., Ouellette, M., Kaur, K.J., Yan, Y., Wilson, K.S., White, M.A., Wright, W.E. and Shay, J.W. (1999) 'Absence of cancer-associated changes in human fibroblasts immortalized with telomerase.', *Nature genetics*, 21(1), pp. 115-118.

Moulson, C.L., Fong, L.G., Gardner, J.M., Farber, E.A., Go, G., Passariello, A., Grange, D.K., Young, S.G. and Miner, J.H. (2007) 'Increased progerin expression associated with unusual LMNA mutations causes severe progeroid syndromes.', *Human mutation*, 28(9), pp. 882-889.

Muchir, A., Massart, C., van Engelen, B.G., Lammens, M., Bonne, G. and Worman, H.J. (2006) 'Proteasome-mediated degradation of integral inner nuclear membrane protein emerin in fibroblasts lacking A-type lamins.', *Biochemical & Biophysical Research Communications*, 351(4), pp. 1011-1017.

Mukherjee, A.B. and Costello, C. (1998) 'Aneuploidy analysis in fibroblasts of human premature aging syndromes by FISH during in vitro cellular aging.', *Mechanisms of Ageing & Development*, 103(2), pp. 209-222.

Muyldermans, S. (2013) 'Nanobodies: natural single-domain antibodies', *Annual Review of Biochemistry*, 82, pp. 775-797.

Nissan, X., Blondel, S., Navarro, C., Maury, Y., Denis, C., Girard, M., Martinat, C., De Sandre-Giovannoli, A., Levy, N. and Peschanski, M. (2012) 'Unique preservation of neural cells in Hutchinson- Gilford progeria syndrome is due to the expression of the neural-specific miR-9 microRNA.', *Cell Reports*, 2(1), pp. 1-9.

Olive, M., Harten, I., Mitchell, R., Beers, J.K., Djabali, K., Cao, K., Erdos, M.R., Blair, C., Funke, B., Smoot, L., Gerhard-Herman, M., Machan, J.T., Kutys, R., Virmani, R., Collins, F.S., Wight, T.N., Nabel, E.G. and Gordon, L.B. (2010) 'Cardiovascular pathology in Hutchinson-Gilford progeria: correlation with the vascular pathology of aging.', *Arteriosclerosis, Thrombosis & Vascular Biology*, 30(11), pp. 2301-2309.

Orzechowska, E.J., Kozlowska, E., Czubaty, A., Kozlowski, P., Staron, K. and Trzcinska-Danielewicz, J. (2014) 'Controlled delivery of BID protein fused with TAT peptide sensitizes cancer cells to apoptosis.', *BMC Cancer*, 14, pp. 771.

Osakabe, A., Takahashi, Y., Murakami, H., Otawa, K., Tachiwana, H., Oma, Y., Nishijima, H., Shibahara, K., Kurumizaka, H. and Harata, M. (2014) 'DNA binding properties of the actin-related protein Arp8 and its role in DNA repair.', PLoS ONE [Electronic Resource], 9(10), pp. e108354.

Ouellette, M.M., McDaniel, L.D., Wright, W.E., Shay, J.W. and Schultz, R.A. (2000) 'The establishment of telomerase-immortalized cell lines representing human chromosome instability syndromes.', *Human molecular genetics*, 9(3), pp. 403-411.

Ozaki, T., Saijo, M., Murakami, K., Enomoto, H., Taya, Y. and Sakiyama, S. (1994) 'Complex formation between lamin A and the retinoblastoma gene product: identification of the domain on lamin A required for its interaction.', *Oncogene*, 9(9), pp. 2649-2653.

Palm-Apergi, C., Lonn, P. and Dowdy, S.F. (2012) 'Do cell-penetrating peptides actually "penetrate" cellular membranes?.', *Molecular Therapy: the Journal of the American Society of Gene Therapy*, 20(4), pp. 695-697.

Panza, P., Maier, J., Schmees, C., Rothbauer, U. and Sollner, C. (2015) 'Live imaging of endogenous protein dynamics in zebrafish using chromobodies.', *Development,* 142(10), pp. 1879-1884.

Paradisi, M., McClintock, D., Boguslavsky, R.L., Pedicelli, C., Worman, H.J. and Djabali, K. (2005) 'Dermal fibroblasts in Hutchinson-Gilford progeria syndrome with the lamin A G608G mutation have dysmorphic nuclei and are hypersensitive to heat stress.', *BMC Cell Biology,* 6, pp. 27.

Peters, J.M., Franke, W.W. and Kleinschmidt, J.A. (1994) 'Distinct 19 S and 20 S subcomplexes of the 26 S proteasome and their distribution in the nucleus and the cytoplasm.', *Journal of Biological Chemistry,* 269(10), pp. 7709-7718.

Peyvandi, F., Scully, M., Kremer Hovinga, J.A., Cataland, S., Knobl, P., Wu, H., Artoni, A., Westwood, J., Mansouri Taleghani, M., Jilma, B., Callewaert, F., Ulrichts, H., Duby, C., Tersago, D. and TITAN Investigators (2016) 'Caplacizumab for Acquired Thrombotic Thrombocytopenic Purpura.', *New England Journal of Medicine,* 374(6), pp. 511-522.

Pirzio, L.M., Freulet-Marriere, M., Bai, Y., Fouladi, B., Murnane, J.P., Sabatier, L. and Desmaze, C. (2004) 'Human fibroblasts expressing hTERT show remarkable karyotype stability even after exposure to ionizing radiation.', *Cytogenetic & Genome Research,* 104(1-4), pp. 87-94.

Plasilova, M., Chattopadhyay, C., Pal, P., Schaub, N.A., Buechner, S.A., Mueller, H., Miny, P., Ghosh, A. and Heinimann, K. (2004) 'Homozygous missense mutation in the lamin A/C gene causes autosomal recessive Hutchinson-Gilford progeria syndrome.', *Journal of medical genetics,* 41(8), pp. 609-614.

Powers, R.W.,3rd, Kaeberlein, M., Caldwell, S.D., Kennedy, B.K. and Fields, S. (2006) 'Extension of chronological life span in yeast by decreased TOR pathway signaling.', *Genes & development,* 20(2), pp. 174-184.

Puente, X.S., Quesada, V., Osorio, F.G., Cabanillas, R., Cadinanos, J., Fraile, J.M., Ordonez, G.R., Puente, D.A., Gutierrez-Fernandez, A., Fanjul-Fernandez, M., Levy, N., Freije, J.M. and Lopez-Otin, C. (2011) 'Exome sequencing and functional analysis identifies BANF1 mutation as the cause of a hereditary progeroid syndrome.', *American Journal of Human Genetics,* 88(5), pp. 650-656.

Ramos, F.J., Chen, S.C., Garelick, M.G., Dai, D., Liao, C., Schreiber, K.H., MacKay, V.L., An, E.H., Strong, R., Ladiges, W.C., Rabinovitch, P.S., Kaeberlein, M. and Kennedy, B.K. (2012) 'Rapamycin reverses elevated mTORC1 signaling in lamin A/C-deficient mice, rescues cardiac and skeletal muscle function, and extends survival.', *Science Translational Medicine,* 4(144), pp. 144ra103.

Reddel, C.J. and Weiss, A.S. (2004) 'Lamin A expression levels are unperturbed at the normal and mutant alleles but display partial splice site selection in Hutchinson-Gilford progeria syndrome.', *Journal of medical genetics,* 41(9), pp. 715-717.

Reunert, J., Wentzell, R., Walter, M., Jakubiczka, S., Zenker, M., Brune, T., Rust, S. and Marquardt, T. (2012) 'Neonatal progeria: increased ratio of progerin to lamin A leads to progeria of the newborn.', *European Journal of Human Genetics,* 20(9), pp. 933-937.

Richards, S.A., Muter, J., Ritchie, P., Lattanzi, G. and Hutchison, C.J. (2011) 'The accumulation of un-repairable DNA damage in laminopathy progeria fibroblasts is caused by ROS generation and is prevented by treatment with N-acetyl cysteine.', *Human molecular genetics,* 20(20), pp. 3997-4004.

Rivera-Torres, J., Acin-Perez, R., Cabezas-Sanchez, P., Osorio, F.G., Gonzalez-Gomez, C., Megias, D., Camara, C., Lopez-Otin, C., Enriquez, J.A., Luque-Garcia, J.L. and Andres, V. (2013) 'Identification of mitochondrial dysfunction in Hutchinson-Gilford progeria syndrome through use of stable isotope labeling with amino acids in cell culture.', *Journal of Proteomics,* 91, pp. 466-477.

Rober, R.A., Weber, K. and Osborn, M. (1989) 'Differential timing of nuclear lamin A/C expression in the various organs of the mouse embryo and the young animal: a developmental study.', *Development,* 105(2), pp. 365-378.

Rodriguez, S., Coppede, F., Sagelius, H. and Eriksson, M. (2009) 'Increased expression of the Hutchinson-Gilford progeria syndrome truncated lamin A transcript during cell aging.', *European Journal of Human Genetics,* 17(7), pp. 928-937.

Rodriguez, S. and Eriksson, M. (2010) 'Evidence for the involvement of lamins in aging', *Current Aging Science,* 3(2), pp. 81-89.

Roll, P. (2015) 'microRNA deregulation in Hutchinson-Gilford Progeria', Orphanet *Journal of Rare Diseases*, 10(2), pp. 1-1.

Roncarati, R., Viviani Anselmi, C., Krawitz, P., Lattanzi, G., von Kodolitsch, Y., Perrot, A., di Pasquale, E., Papa, L., Portararo, P., Columbaro, M., Forni, A., Faggian, G., Condorelli, G. and Robinson, P.N. (2013) 'Doubly heterozygous LMNA and TTN mutations revealed by exome sequencing in a severe form of dilated cardiomyopathy.', *European Journal of Human Genetics,* 21(10), pp. 1105-1111.

Rothbauer, U., Zolghadr, K., Muyldermans, S., Schepers, A., Cardoso, M.C. and Leonhardt, H. (2008) 'A versatile nanotrap for biochemical and functional studies with fluorescent fusion proteins.', *Molecular & Cellular Proteomics,* 7(2), pp. 282-289.

Rothbauer, U., Zolghadr, K., Tillib, S., Nowak, D., Schermelleh, L., Gahl, A., Backmann, N., Conrath, K., Muyldermans, S., Cardoso, M.C. and Leonhardt, H. (2006) 'Targeting and tracing antigens in live cells with fluorescent nanobodies.', *Nature Methods,* 3(11), pp. 887-889.

Sakaki, M., Koike, H., Takahashi, N., Sasagawa, N., Tomioka, S., Arahata, K. and Ishiura, S. (2001) 'Interaction between emerin and nuclear lamins.', *Journal of Biochemistry,* 129(2), pp. 321-327.

Scaffidi, P. and Misteli, T. (2006) 'Lamin A-dependent nuclear defects in human aging.', *Science,* 312(5776), pp. 1059-1063.

Scaffidi, P. and Misteli, T. (2005) 'Reversal of the cellular phenotype in the premature aging disease Hutchinson-Gilford progeria syndrome.', *Nature medicine,* 11(4), pp. 440-445.

Schwarze, S.R., Hruska, K.A. and Dowdy, S.F. (2000) 'Protein transduction: unrestricted delivery into all cells?', *Trends in cell biology,* 10(7), pp. 290-295.

Servick, K. (2014) 'Unorthodox Study Claims Drug Prolongs Lives of Children With Premature Aging Disease.', Science, 8 May 2014.

Shackleton, S., Smallwood, D.T., Clayton, P., Wilson, L.C., Agarwal, A.K., Garg, A. and Trembath, R.C. (2005) 'Compound heterozygous ZMPSTE24 mutations reduce prelamin A processing and result in a severe progeroid phenotype.', *Journal of medical genetics,* 42(6), pp. e36.

Shalev, S.A., De Sandre-Giovannoli, A., Shani, A.A. and Levy, N. (2007) 'An association of Hutchinson-Gilford progeria and malignancy.', *American Journal of Medical Genetics.Part A,* 143A(16), pp. 1821-1826.

Shumaker, D.K., Dechat, T., Kohlmaier, A., Adam, S.A., Bozovsky, M.R., Erdos, M.R., Eriksson, M., Goldman, A.E., Khuon, S., Collins, F.S., Jenuwein, T. and Goldman, R.D. (2006) 'Mutant nuclear lamin A leads to progressive alterations of epigenetic control in premature aging.', *Proceedings of the National Academy of Sciences of the United States of America,* 103(23), pp. 8703-8708.

Smallwood, D.T. and Shackleton, S. (2010) 'Lamin A-linked progerias: is farnesylation the be all and end all?.', *Biochemical Society transactions,* 38(Pt 1), pp. 281-286.

Smigiel, R., Jakubiak, A., Esteves-Vieira, V., Szela, K., Halon, A., Jurek, T., Levy, N. and De Sandre-Giovannoli, A. (2010) 'Novel frameshifting mutations of the ZMPSTE24 gene in two siblings affected with restrictive dermopathy and review of the mutations described in the literature.', *American Journal of Medical Genetics.Part A,* 152A(2), pp. 447-452.

Stanbridge, E.J. (1992) 'Functional evidence for human tumour suppressor genes: chromosome and molecular genetic studies', *Cancer surveys*, 12, pp. 5-24.

Starr, D.A. and Fridolfsson, H.N. (2010) 'Interactions between nuclei and the cytoskeleton are mediated by SUN-KASH nuclear-envelope bridges', *Annual Review of Cell & Developmental Biology*, 26, pp. 421-444.

Sullivan, T., Escalante-Alcalde, D., Bhatt, H., Anver, M., Bhat, N., Nagashima, K., Stewart, C.L. and Burke, B. (1999) 'Loss of A-type lamin expression compromises nuclear envelope integrity leading to muscular dystrophy.', *Journal of Cell Biology*, 147(5), pp. 913-920.

Sylvius, N., Bonne, G., Straatman, K., Reddy, T., Gant, T.W. and Shackleton, S. (2011) 'MicroRNA expression profiling in patients with lamin A/C-associated muscular dystrophy.', *FASEB Journal*, 25(11), pp. 3966-3978.

Tan, J.M.M., Wong, E.S.P., Kirkpatrick, D.S., Pletnikova, O., Ko, H.S., Tay, S., Ho, M.W.L., Troncoso, J., Gygi, S.P., Lee, M.K., Dawson, V.L., Dawson, T.M. and Lim, K. (2008) 'Lysine 63-linked ubiquitination promotes the formation and autophagic clearance of protein inclusions associated with neurodegenerative diseases.', *Human molecular genetics*, 17(3), pp. 431-439.

Tindall, K.R., Glaab, W.E., Umar, A., Risinger, J.I., Koi, M., Barrett, J.C. and Kunkel, T.A. (1998) 'Complementation of mismatch repair gene defects by chromosome transfer', *Mutation research*, 402(1-2), pp. 15-22.

Torvaldson, E., Kochin, V. and Eriksson, J.E. (2015) 'Phosphorylation of lamins determine their structural properties and signaling functions.', *Nucleus (Calcutta)*, 6(3), pp. 166-171.

Tosi, A., Haas, C., Herzog, F., Gilmozzi, A., Berninghausen, O., Ungewickell, C., Gerhold, C.B., Lakomek, K., Aebersold, R., Beckmann, R. and Hopfner, K. (2013) 'Structure and subunit topology of the INO80 chromatin remodeler and its nucleosome complex.', Cell, 154(6), pp. 1207-1219.

Toth, J.I., Yang, S.H., Qiao, X., Beigneux, A.P., Gelb, M.H., Moulson, C.L., Miner, J.H., Young, S.G. and Fong, L.G. (2005) 'Blocking protein farnesyltransferase improves nuclear shape in fibroblasts from humans with progeroid syndromes.', *Proceedings of the National Academy of Sciences of the United States of America*, 102(36), pp. 12873-12878.

Towbin, H., Staehelin, T. and Gordon, J. (1979) 'Electrophoretic transfer of proteins from polyacrylamide gels to nitrocellulose sheets: procedure and some applications.', *Proceedings of the National Academy of Sciences of the United States of America*, 76(9), pp. 4350-4354.

van Waarde-Verhagen,M A W H., Kampinga, H.H. and Linskens, M.H.K. (2006) 'Continuous growth of telomerase-immortalised fibroblasts: how long do cells remain normal?.', *Mechanisms of Ageing & Development*, 127(1), pp. 85-87.

Varela, I., Pereira, S., Ugalde, A.P., Navarro, C.L., Suarez, M.F., Cau, P., Cadinanos, J., Osorio, F.G., Foray, N., Cobo, J., de Carlos, F., Levy, N., Freije, J.M. and Lopez-Otin, C. (2008) 'Combined treatment with statins and aminobisphosphonates extends longevity in a mouse model of human premature aging.', *Nature medicine,* 14(7), pp. 767-772.

Vergnes, L., Peterfy, M., Bergo, M.O., Young, S.G. and Reue, K. (2004) 'Lamin B1 is required for mouse development and nuclear integrity.', *Proceedings of the National Academy of Sciences of the United States of America,* 101(28), pp. 10428-10433.

Verstraeten, V.L., Ji, J.Y., Cummings, K.S., Lee, R.T. and Lammerding, J. (2008) 'Increased mechanosensitivity and nuclear stiffness in Hutchinson-Gilford progeria cells: effects of farnesyltransferase inhibitors.', *Aging Cell,* 7(3), pp. 383-393.

Villa-Bellosta, R., Rivera-Torres, J., Osorio, F.G., Acin-Perez, R., Enriquez, J.A., Lopez-Otin, C. and Andres, V. (2013) 'Defective extracellular pyrophosphate metabolism promotes vascular calcification in a mouse model of Hutchinson-Gilford progeria syndrome that is ameliorated on pyrophosphate treatment.', *Circulation,* 127(24), pp. 2442-2451.

Viteri, G., Chung, Y.W. and Stadtman, E.R. (2010) 'Effect of progerin on the accumulation of oxidized proteins in fibroblasts from Hutchinson Gilford progeria patients.', *Mechanisms of Ageing & Development,* 131(1), pp. 2-8.

Vlcek, S. and Foisner, R. (2007) 'Lamins and lamin-associated proteins in aging and disease', *Current opinion in cell biology,* 19(3), pp. 298-304.

von Mikecz, A. (2006) 'The nuclear ubiquitin-proteasome system', *Journal of cell science,* 119(Pt 10), pp. 1977-1984.

Vyas, P.M., Tomamichel, W.J., Pride, P.M., Babbey, C.M., Wang, Q., Mercier, J., Martin, E.M. and Payne, R.M. (2012) 'A TAT-frataxin fusion protein increases lifespan and cardiac function in a conditional Friedreich's ataxia mouse model.', *Human molecular genetics,* 21(6), pp. 1230-1247.

Wadia, J.S. and Dowdy, S.F. (2005) 'Transmembrane delivery of protein and peptide drugs by TAT-mediated transduction in the treatment of cancer', *Advanced Drug Delivery Reviews,* 57(4), pp. 579-596.

Wadia, J.S., Stan, R.V. and Dowdy, S.F. (2004) 'Transducible TAT-HA fusogenic peptide enhances escape of TAT-fusion proteins after lipid raft macropinocytosis.', *Nature medicine,* 10(3), pp. 310-315.

Wallis, C.V., Sheerin, A.N., Green, M.H., Jones, C.J., Kipling, D. and Faragher, R.G. (2004) 'Fibroblast clones from patients with Hutchinson-Gilford progeria can senesce despite the presence of telomerase.', Experimental gerontology, 39(4), pp. 461-467.

Wang, Z., Liu, X., Yang, B. and Gelernter, J. (2013) 'The role and challenges of exome sequencing in studies of human diseases', Frontiers in genetics, 4.

Winter-Vann, A.M. and Casey, P.J. (2005) 'Post-prenylation-processing enzymes as new targets in oncogenesis', *Nature Reviews.Cancer*, 5(5), pp. 405-412.

Wood, A.M., Rendtlew Danielsen, J.M., Lucas, C.A., Rice, E.L., Scalzo, D., Shimi, T., Goldman, R.D., Smith, E.D., Le Beau, M.M. and Kosak, S.T. (2014) 'TRF2 and lamin A/C interact to facilitate the functional organization of chromosome ends.', *Nature communications*, 5, pp. 5467.

Wu, D., Flannery, A.R., Cai, H., Ko, E. and Cao, K. (2014) 'Nuclear localization signal deletion mutants of lamin A and progerin reveal insights into lamin A processing and emerin targeting.', *Nucleus (Calcutta)*, 5(1), pp. 66-74.

Wu, X., Hawse, J.R., Subramaniam, M., Goetz, M.P., Ingle, J.N. and Spelsberg, T.C. (2009) 'The tamoxifen metabolite, endoxifen, is a potent antiestrogen that targets estrogen receptor alpha for degradation in breast cancer cells.', *Cancer research*, 69(5), pp. 1722-1727.

Wyllie, F.S., Jones, C.J., Skinner, J.W., Haughton, M.F., Wallis, C., Wynford-Thomas, D., Faragher, R.G. and Kipling, D. (2000) 'Telomerase prevents the accelerated cell ageing of Werner syndrome fibroblasts.', *Nature genetics*, 24(1), pp. 16-17.

Xiong, ZM., Choi, J.Y., Wang, K., Zhang, H., Tariq, Z., Wu, D., Ko, E., LaDana, C., Sesaki, H. and Cao, K. (2016) 'Methylene blue alleviates nuclear and mitochondrial abnormalities in progeria.', *Aging Cell*, 15(2), pp. 279–290.

Yang, S.H., Meta, M., Qiao, X., Frost, D., Bauch, J., Coffinier, C., Majumdar, S., Bergo, M.O., Young, S.G. and Fong, L.G. (2006) 'A farnesyltransferase inhibitor improves disease phenotypes in mice with a Hutchinson-Gilford progeria syndrome mutation.', *Journal of Clinical Investigation*, 116(8), pp. 2115-2121.

Yang, S.H., Andres, D.A., Spielmann, H.P., Young, S.G. and Fong, L.G. (2008) 'Progerin elicits disease phenotypes of progeria in mice whether or not it is farnesylated.', *Journal of Clinical Investigation*, 118(10), pp. 3291-3300.

Yang, S.H., Chang, S.Y., Ren, S., Wang, Y., Andres, D.A., Spielmann, H.P., Fong, L.G. and Young, S.G. (2011) 'Absence of progeria-like disease phenotypes in knock-in mice expressing a non-farnesylated version of progerin.', Human molecular genetics, 20(3), pp. 436-444.

Yang, L., Munck, M., Swaminathan, K., Kapinos, L.E., Noegel, A.A. and Neumann, S. (2013) 'Mutations in LMNA modulate the lamin A--Nesprin-2 interaction and cause LINC complex alterations.', *PLoS ONE [Electronic Resource*], 8(8), pp. e71850.

Yassaee, V.R., Khojaste, A., Hashemi-Gorji, F., Ravesh, Z. and Toosi, P. (2016) 'A novel homozygous LMNA mutation (p.Met540Ile) causes mandibuloacral dysplasia type A.', *Gene,* 577(1), pp. 8-13.

Ye, Q. and Worman, H.J. (1995) 'Protein-binding partners between human nuclear lamins expressed in yeast.', *Experimental cell research,* 219(1), pp. 292-298.

Yoshida, K., Ishio, I., Nagakawa, E., Yamamoto, Y., Yamamoto, M. and Fujita, Y. (2000) 'Systematic study of gene expression and transcription organization in the gntZ-ywaA region of the Bacillus subtilis genome.', *Microbiology,* 146(Pt 3), pp. 573-579.

Yu, C.E., Oshima, J., Fu, Y.H., Wijsman, E.M., Hisama, F., Alisch, R., Matthews, S., Nakura, J., Miki, T., Ouais, S., Martin, G.M., Mulligan, J. and Schellenberg, G.D. (1996) 'Positional cloning of the Werner's syndrome gene.', *Science,* 272(5259), pp. 258-262.

Zastrow, M.S., Vlcek, S. and Wilson, K.L. (2004) 'Proteins that bind A-type lamins: integrating isolated clues', *Journal of cell science,* 117(Pt 7), pp. 979-987.

Zheng, R., Ghirlando, R., Lee, M.S., Mizuuchi, K., Krause, M. and Craigie, R. (2000) 'Barrier-to-autointegration factor (BAF) bridges DNA in a discrete, higher-order nucleoprotein complex.', *Proceedings of the National Academy of Sciences of the United States of America,* 97(16), pp. 8997-9002.

Zirn, B., Kress, W., Grimm, T., Berthold, L.D., Neubauer, B., Kuchelmeister, K., Muller, U. and Hahn, A. (2008) 'Association of homozygous LMNA mutation R471C with new phenotype: mandibuloacral dysplasia, progeria, and rigid spine muscular dystrophy.', *American Journal of Medical Genetics.Part A,* 146A(8), pp. 1049-1054

Appendices

Appendix I. pMM45-1 and pMM46-2

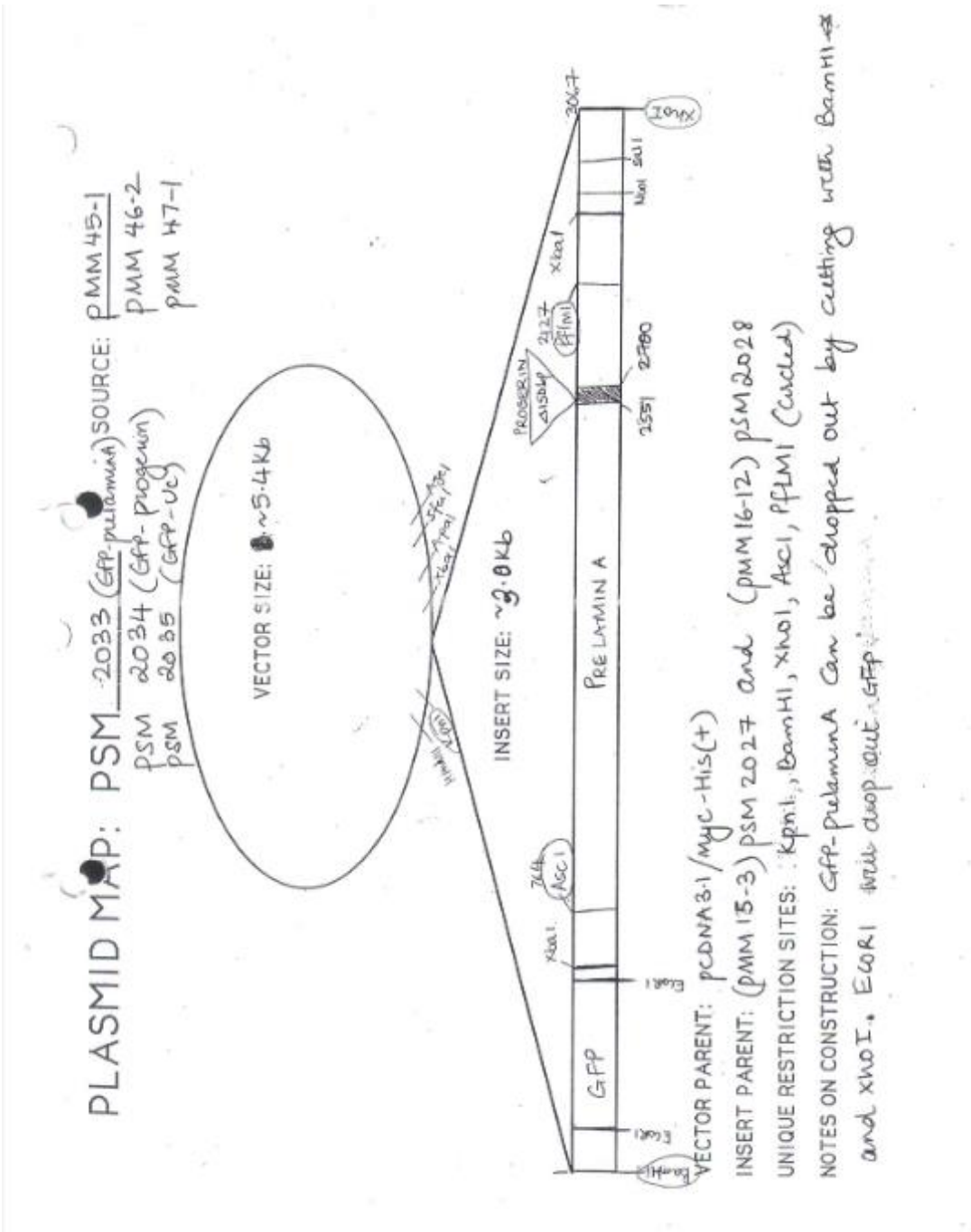

Appendix I. TAT Sequences

3L Sequence

TAT Sequence 3L - Page 1

TAT Sequence 3L - Page 2

TAT Sequence 3L - Page 3

TAT 6L Sequence

TAT Sequence 6L - Page 1

TAT Sequence 6L - Page 2

TAT 4P Sequence

TAT Sequence 4P - Page 1

TAT Sequence 4P - Page 2

TAT 8P Sequence

TAT Sequence 8P - Page 1

TAT Sequence 8P - Page 2

Appendix III.M-FISH karyotypes of TAG08466 cel

Table 10 M-FISH karyotypes of TAG08466 cells

Cell number	Karyotype
0001	61,XXX,del(Xp),der(1)t(1;17),-2,-3,-3,-4,-4,del(4p),-5,del(5p),-6,-6,-7,-8, ,-9,del(9q),-10,-11,-11,-12,-13,-13,del(13q),del(13q),-14,-14,der(15)t(8;15),-15,-15,-16,-16,-17,-18,-18,-19,-20,-21,-22,-22,+2mar
0002	62,XXXY,-1,der(1)t(1;13),der(1)t(1;17),ace(1p),-3,del(3p),-4,-5,-5,-5,del(5p),-6,-7,-8,-8, -9,-9,der(9)t(1;9),-10,-10,-10,-11,-11,-12,-13,-13,-14,der(15)t(8;15),-16,-17,der(17)(1;17),del(18q),-19,-19,-20,-20,der(22)t(18;22),-22
0005	79,XXX,der(X)t(X;18),der(1)t(14;1;17),ins(1;14),del(1q),der(2)t(1;2),del(3p),-4,-5,der(6)t(6;19),der(7)t(7;21),-9,-12,-13,der(14)t(10;14),ace(14;21),-15,-15, der(15)t(8;15),-20,-21,+2mar
0011	76,X,-X,-X,-X,ins(1;14),der(1)t(1;18),del(1q),-2,der(2)t(2;15),del(3p),-4,del(5p),del(5q),der(6)t(6;19),-7,-7,-8,der(12)t(12;20), -13,-14,der(14)t(10;14), der(15)t(8;15),del(15q),-17,-18,-19,-21,-22+3mar
0013	78,XXX,der(X)t(X;18),der(1)t(14;1;17),ins(1;14), der(1)(1;14),del(1q),der(2)t(1;2),del(3p),-4,-5,del(5p),-6,der(6)t(6;10),del(7q),-9,del(9q),-11,-13,-14,der(14)(10;14),der(15)t(8;15),-16,-18,del(18q),-19,-20,-20,-21
0018	66,XXX,der(X)t(X;1),der(1)t(14;1;17),der(1)t(1;18),del(1p),der(1)ins(15;1;X),del(2p),-3,del(3p),der(4)t(4;19),del(5p),del(5q),-6,-6,-6,-6,-7,-7,-9,-10,-11,-11,-12,-13,-13,-14,der(15)t(8;15),del(15q) ,-18,der(18)t(17;18) ,-20,-20,-20,-21,-21,-21,-22,-22
0019	85,XXX,der(X)t(X;18),del(Xq),ins(1;14),der(1)t(14;1;17),der(2)t(1;2),del(3p),-4,del(5p),der(6)t(6;13),der(7)t(7;21),dic(8;17)+ace(8q),-9,-12,-13,-14,der(14)t(10;14),-17,der(18)t(18;20),-19,-21
0020	79,XXX,der(X)t(X;18),ins(1;14),der(2)t(1;2),-3,-4,del(5p),del(5p),-6,der(7)t(7;21),-9,-12,-12,-13,-14,der(14)t(10;14),der(15)t(8;15),-17,del(18p),-19,del(20p)+del(20q),-20,-22,+mar
0021	83,XXX,t(X;1),ins(1;14),der(1)t(14;1;17),del(2p),del(3p),der(4)t(4;19),der(5)t(5;10),del(5p),-6,der(7)t(7;21),-13,-14,der(14)t(10;14),-15,der(15)t(8;15),-16,del(17q)
0025	79,XXX,der(X)t(X;18),ins(1;14),der(1)t(14;1;17), der(2)t(1;2), del(3p),-4,-5,del(5p), der(6)t(6;19), der(7)t(7;21),-8,-9,-11,der(14)t(10;14),del(14q), der(15)t(8;15),-16,-20,-22,-22
0029	86,XXX,t(X;1),ins(1;14),der(1)t(14;1;17),der(1)(1;17),der(1)t(1;18),del(2p),del(3p),der(4)t(4;19), del(5p),-6,der(7)t(7;21),-13,-14,der(14)t(10;14),der(15)t(8;15),ace(15p),-16,der(16)t(14;16),+del(18p)+del(18q),-20,-22,del(22q)+ace(22q)
0030	71,XXX,del(Xp),der(1)t(1;17),ace(1;17),ace(1q),ace(1p),der(1)t(1;13),der(3)t(3;10),-4,-4,del(5p),-6,der(7)t(2;7),-8,del(9p),-10,-14,-15,der(15)t(8;15),-16,-16,-17,-18,-18,-19,-19,-20,-20,-22,-22

0034	73,XXX,der(X)t(X;18),ins(1;14),der(1)t(14;1;17),der(2)t(1;2),del(3p),-4,del(5p),del(5p),-6,-7,-9,-9,-10,-11,-12,-13,-14,der(14)t(10;14),-15,der(15)t(8;15),del(18p),-19,-20,der(20)t(18;20),-21
0041	81,XXX,t(X;1),ins(1;14),der(1)t(14;1;17),del(1p),del(1q),del(2p),del(2q),-3,del(4p),del(5p),-6,der(7)t(7;21),-12,-13,-14,-15,der(15)t(8;15),ace(15p),-17,der(17)t(Y;17),der(18)t(18;21),-19,+mar
0046	81,XXX,der(X)t(X;18),ins(1;14),der(1)t(14;1;17),der(2)t(1;2),der(3)t(3;22),-4,del(5p),-6,der(7)t(7;21),-9,-12,-13,-14,der(14)t(10;14),-15,der(15)t(8;15),-19,der(20)t(18;20),+mar
0049	75,X,-X,-X,t(X;1),ins(1;14),der(1)t(14;1;17),x2ace(1q),-2,del(2p),-3,del(3p),der(4)t(4;19),-5,-6,der(7)t(7;21),-8,-9,-12,-12,-13,-13,-14,der(14)t(10;14),-15,-15,-16,der(16)t(16;?),der(17)t(X;17),del(17q),-19,-19,der(20)t18;20),-22,+2mar
0051	70,XXX,der(X)t(X;18),-1,ins(1;14),der(1)t(1;14),der(1)t(1;18),der(2)t(1;2),-4,-5,-5,-5,-6,-6,der(6)t(6;19),-7,-9,-12,-13,-13,-14,der(14)t(10;14),der(15)t(8;15),-16,-16,-17,-17,del(18p),-20,-21,-22,del(22q)+ace(22q),+mar

Table 11 Occurrence of structural rearrangements in TAG08466 cells

	Observed in cell number																	Number of cells
	1	**2**	**5**	**11**	**13**	**18**	**19**	**20**	**21**	**25**	**29**	**30**	**34**	**41**	**46**	**49**	**51**	
t(Xcen;1)									X		X			X		X		4
der(X)t(Xcen;1)						X												1
der(X)t(Xcen;18?cen)			X		X		X	X		X			X		X		X	8
der(1)t(1cen;13)		X										X						2
der(1)t(1cen;14)					X												X	2
ins(1?cen;14)			X	X	X		X	X		X	X		X	X	X	X	X	12
der(1)ins(15;1;X)						X												1
der(1)t(1;17)	X	X									X	X						4
der(1)t(14;1cen;17)			X		X	X	X		X	X	X		X	X	X	X		11
ace(1;17)												X						1
der(1)t(1cen;18)				X		X					X						X	4
der(2)t(1?cen;2cen)			X		X		X	X		X			X		X		X	8
der(2)t(2pter;15)				X														1
der(3)t(3;10)												X						1
der(3)t(3cen;22)															X			1
der(4)t(4cen;19)	X					X			X		X					X		5
der(5)t(5;10)									X									1
der(6)t(6cen;13)							X											1
der(6)t(6cen;19)			X	X						X							X	4
der(7)t(2;7)												X						1
der(7)t(7?qter;21)			X				X	X	X	X	X			X	X	X		9
dic(8cen;17)							X											1
der(9)t(1;9)		X																1

der(12)t(12cen;20)				X														1
der(14)t(10;14cen)			X	X	X		X	X	X	X	X		X		X	X	X	12
ace(14;21)			X															1
der(15)t(8;15)	X	X	X	X	X	X		X	X	X	X	X	X	X	X		X	15
der(16)t(14;16cen)											X							1
der(16)t(16;?)																X		1
der(17)t(X;17cen)																X		1
der(17)t(Y;17)														X				1
der(17)(?1;17)		X																1
der(18)t(5;18)											X							1
der(18)t(17;18cen)						X												1
der(18)t(18cen;20)							X											1
der(18)t(18cen;21)														X				1
der(20)t(18;20cen)													X		X			2
der(22)t(18;22cen)		X																1

Table 12 Occurrence of structural deletions in TAG08466 cells

	Observed in cell number																	Number of cells
	1	**2**	**5**	**11**	**13**	**18**	**19**	**20**	**21**	**25**	**29**	**30**	**34**	**41**	**46**	**49**	**51**	
del(Xp)	X											X						2
del(Xcenq)							X											1
ace(1p)		X										X						2
ace(1q)												X				X		2
ace(1q)																X		1
del(1q)			X	X	X													3
del(1cenq)						X								X				2
del(2cenp)						X			X		X			X		X		5
del(2cenq)														X				1
del(3p)		X	X	X	X	X	X		X	X	X		X			X		11
del(4cenp)														X				1
del(5cenp)	X	X		X	X	X	X	X	X	X	X	X	X	X	X			14
del(5cenq)				X		X												2
del(7q)					X													1
ace(8q)							X											1
del(9cenp)	X											X						2
del(9q)					X													1
del(13q)	X																	1
del(13q)	X																	1
del(14cenq)										X								1
ace(15p)											X			X				2
del(15q)				X		X												2
del(17q)									X							X		2
del(18cenp)								X			X		X				X	4

del(18cenq)		X			X						X							3
del(20cenq)								X										1
del(22q)											X						X	2
ace(22q)											X						X	2

Table 13 Occurrence of numerical aberrations TAG08466 cells

	Observed in cell number																	Number of cells
	1	**2**	**5**	**11**	**13**	**18**	**19**	**20**	**21**	**25**	**29**	**30**	**34**	**41**	**46**	**49**	**51**	
-1		X															X	2
-2	X			X												X		3
-3	X	X				X		X						X		X		6
-3	X																	1
-4	X	X	X	X	X		X	X		X		X	X		X		X	12
-4	X											X						2
-5	X	X	X		X					X						X	X	7
-5		X															X	2
-5		X															X	2
-6	X	X			X	*X*		X	X		X	X	X	X	X	X	X	13
-6	X					X											X	3
-6						X												1
-6						X												1
-7	X	X		X		X							X				X	6
-7				X		X												2
-8	X	X		X						X		X				X		6
-8		X																1
-9	X	X	X		X	X	X	X		X			X		X	X	X	12
-9		X											X					2
-10	X	X				X						X	X					5
-10		X																1
-10		X																1
-11	X	X			X	X				X			X					6
-11	X	X				X												3
-12	X	X	X			X	X	X					X	X	X	X	X	11

-12								X								X		2
-13	X	X	X	X	X	X		X	X		X		X	X	X	X	X	14
-13	X	X				X	X									X	X	6
-14	X	X		X	X	X	X	X	X		X	X	X	X	X	X	X	14
-14	X																	1
-15	X		X						X		X	X	X	X	X	X		9
-15	X		X													X		3
-16	X	X			X				X	X	X	X				X	X	9
-16	X											X					X	3
-17	X	X		X			X	X				X		X			X	8
-17																	X	1
-18	X			X	X	X						X						5
-18	X											X						2
-19	X	X		X	X		X	X				X	X	X	X	X		11
-19		X										X				X		3
-20	X	X	X		X	X		X			X	X	X			X	X	11
-20		X			X	X				X		X						5
-20						X												1
-21	X		X	X	X	X	X						X				X	8
-21						X												1
-21						X												1
-22	X	X		X		X		X		X	X	X				X	X	10
-22	X					X				X		X						4
-X				X												X		2
-X				X												X		2
-X				X														1
+22					X													1

Table 14 Occurrence of clonal structural rearrangements in TAG08466 cells

	Observed in cell number																	Number of cells
	1	**2**	**5**	**11**	**13**	**18**	**19**	**20**	**21**	**25**	**29**	**30**	**34**	**41**	**46**	**49**	**51**	
t(X;1)									X		X			X		X		4
der(X)t(X;18)			X		X		X	X		X			X		X		X	8
der(1)t(1;13)		X										X						2
der(1)t(1;14)					X												X	2
ins(1;14)			X	X	X		X	X		X	X		X	X	X	X	X	12
der(1)t(1;17)	X	X									X	X						4
der(1)t(14;1;17)			X		X	X	X		X	X	X		X	X	X	X		11
der(1)t(1;18)				X		X					X						X	4
der(2)t(1;2)			X		X		X	X		X			X		X		X	8
der(4)t(4;19)	X					X			X		X					X		5
der(6)t(6;19)			X	X						X							X	4
der(7)t(7;21)			X				X	X	X	X	X			X	X	X		9
der(14)t(10;14)			X	X	X		X	X	X	X	X		X		X	X	X	12
der(15)t(8;15)	X	X	X	X	X	X		X	X	X	X	X	X	X	X		X	15
der(20)t(18;20)													X			X		2

Table 15 Occurrence of clonal structural deletions in TAG08466 cells

	Observed in cell number																	Number of cells
	1	**2**	**5**	**11**	**13**	**18**	**19**	**20**	**21**	**25**	**29**	**30**	**34**	**41**	**46**	**49**	**51**	
del(Xp)	X											X						2
ace(1p)		X										X						2
ace(1q)												X				X		2
del(1q)			X	X	X													3
del(1cenq)						X								X				2
del(2cenp)						X			X		X			X		X		5
del(3p)		X	X	X	X	X	X		X	X	X		X			X		11
del(5cenp)	X	X		X	X	X	X	X	X	X	X	X	X	X	X			14
del(5cenq)				X		X												2
del(9cenp)	X											X						2
ace(15p)											X			X				2
del(15q)				X		X												2
del(17q)									X							X		2
del(18cenp)								X			X		X				X	4
del(18cenq)		X			X						X							3
del(22q)											X						X	2
ace(22q)											X						X	2

Table 16 Occurrence of clonal numerical aberrations in TAG08466 cells

	Observed in cell number																	Number of cells
	1	**2**	**5**	**11**	**13**	**18**	**19**	**20**	**21**	**25**	**29**	**30**	**34**	**41**	**46**	**49**	**51**	
-2	X			X												X		3
-3	X	X				X		X						X		X		6
-4	X	X	X	X	X		X	X		X		X	X		X		X	12
-5	X	X	X		X					X						X	X	7
-6	X	X			X	X		X	X		X	X	X	X	X	X	X	13
-6	X					X											X	3
-7	X	X		X		X							X				X	6
-8	X	X		X						X		X				X		6
-9	X	X	X		X	X	X	X		X			X		X	X	X	12
-10	X	X				X						X	X					5
-11	X	X			X	X				X			X					6
-11	X	X				X												3
-12	X	X	X			X	X	X					X	X	X	X	X	11
-13	X	X	X	X	X	X		X	X		X		X	X	X	X	X	14
-13	X	X				X	X									X	X	6
-14	X	X		X	X	X	X	X	X		X	X	X	X	X	X	X	14
-15	X		X						X		X	X	X	X	X	X		9
-15	X		X													X		3
-16	X	X			X				X	X	X	X				X	X	9
-16	X											X					X	3
-17	X	X		X			X	X				X		X			X	8
-18	X			X	X	X						X						5
-19	X	X		X	X		X	X				X	X	X	X	X		11
-19		X										X				X		3
-20	X	X	X		X	X		X			X	X	X			X	X	11

-20		X			X	X				X		X						5
-21	X		X	X	X	X	X						X				X	8
-22	X	X		X		X		X		X	X	X				X	X	10
-22	X					X				X		X						4

Appendix IV. Refined Search

Table 17 Refind Search

Name	#Variants	#Cases	#Controls
NBPF10 (includes others)	4	1	0
IRF2BPL	3	1	0
MUC2	3	1	0
MUC3A	3	1	0
ANKRD36	2	1	0
ARMCX4	2	1	0
ATXN1	2	1	0
ATXN7	2	1	0
CHD3	2	1	0
FAM157A/FAM157B	2	1	0
IGFN1	2	1	0
LENG9	2	1	0
LOR	2	1	0
LURAP1L	2	1	0
mir-3150	2	1	0
MUC6	2	1	0
NKX1-1	2	1	0
OR2A1/OR2A42	2	1	0
POTEG (includes others)	2	1	0
PRAMEF1 (includes others)	2	1	0
PRSS48	2	1	0
REC8	2	1	0
SLC35G4	2	1	0
SOCS7	2	1	0
TTN	2	1	0
ZNF714	2	1	0
ACSS2	1	1	0
ALMS1	1	1	0
ANKLE1	1	1	0
APOB	1	1	0
ARHGEF17	1	1	0
ARHGEF26	1	1	0
ASCL1	1	1	0
ATAD3B	1	1	0
ATAD5	1	1	0
ATMIN	1	1	0
ATP6V1C2	1	1	0
ATXN3	1	1	0

AUTS2	1	1	0
BAIAP2L2	1	1	0
C11orf95	1	1	0
C20orf96	1	1	0
C6orf132	1	1	0
C7orf49	1	1	0
CACNA1A	1	1	0
CACNA1I	1	1	0
CACNB2	1	1	0
CAMKK2	1	1	0
CBWD3/CBWD6	1	1	0
CCER2	1	1	0
CCL3L1	1	1	0
CCL3L3	1	1	0
CDC42EP1	1	1	0
CDKL4	1	1	0
CEBPB	1	1	0
CELA1	1	1	0
CFAP44	1	1	0
CGA	1	1	0
CHD7	1	1	0
CKAP4	1	1	0
CLSPN	1	1	0
CNTN4	1	1	0
COL18A1	1	1	0
COPZ2	1	1	0
CPXM2	1	1	0
DCHS2	1	1	0
DDX31	1	1	0
DDX56	1	1	0
DMGDH	1	1	0
DMRTA2	1	1	0
DNHD1	1	1	0
DOK3	1	1	0
DPP9-AS1	1	1	0
DSE	1	1	0
EGR1	1	1	0
EIF4E2	1	1	0
EMC7	1	1	0
ENGASE	1	1	0
ESRP2	1	1	0
FAM117B	1	1	0
FAM86B1	1	1	0
FAM98C	1	1	0

FBN1	1	1	0
FBXO24	1	1	0
FBXW10	1	1	0
FHOD3	1	1	0
FIGNL2	1	1	0
FIP1L1	1	1	0
FLG2	1	1	0
FOXF2	1	1	0
FOXN3	1	1	0
FOXO3	1	1	0
FREM2	1	1	0
FSCB	1	1	0
GHDC	1	1	0
GIGYF2	1	1	0
GJC2	1	1	0
GNL3	1	1	0
GPRIN2	1	1	0
GSPT1	1	1	0
GTF3C4	1	1	0
GXYLT1	1	1	0
HEG1	1	1	0
HELQ	1	1	0
HERC2	1	1	0
HERC3	1	1	0
HMGB4	1	1	0
HNRNPC	1	1	0
HOXD11	1	1	0
HRC	1	1	0
HSP90B1	1	1	0
HTT	1	1	0
IFI27	1	1	0
IGDCC4	1	1	0
IGFBP2	1	1	0
IGSF10	1	1	0
INO80E	1	1	0
IQSEC2	1	1	0
JMJD8	1	1	0
JPH3	1	1	0
KANSL3	1	1	0
KBTBD7	1	1	0
KCNJ12	1	1	0
KCNJ18	1	1	0
KCNN3	1	1	0
KDM6B	1	1	0

KIF1A	1	1	0
KLHL40	1	1	0
KLRC2	1	1	0
KRT3	1	1	0
KRT39	1	1	0
KRTAP4-6	1	1	0
KRTAP9-4	1	1	0
LEPREL2	1	1	0
LFNG	1	1	0
LILRA6	1	1	0
LILRB3	1	1	0
LMTK3	1	1	0
LOC729159	1	1	0
LRP5	1	1	0
LRRIQ1	1	1	0
LSR	1	1	0
MAN2A1	1	1	0
MAP3K7	1	1	0
MAPK8IP2	1	1	0
MCM9	1	1	0
MDFIC	1	1	0
MED15	1	1	0
MEGF9	1	1	0
MEOX2	1	1	0
mir-181	1	1	0
mir-663	1	1	0
mir-6859	1	1	0
MIR8078	1	1	0
MMP17	1	1	0
MPL	1	1	0
MROH8	1	1	0
MST1L	1	1	0
MUC12	1	1	0
MUC16	1	1	0
MUC20	1	1	0
MUC5B	1	1	0
MYRIP	1	1	0
NADK	1	1	0
NAP1L2	1	1	0
NAV1	1	1	0
NKD2	1	1	0
NOTCH2	1	1	0
NOTCH4	1	1	0
NPIPB4 (includes others)	1	1	0

NXNL2	1	1	0
OR1M1	1	1	0
OR2B11	1	1	0
OR2T27	1	1	0
OR2T33	1	1	0
OR4C45	1	1	0
OR5P2	1	1	0
OR6C6	1	1	0
OR9G1	1	1	0
OR9G9	1	1	0
OTUD4	1	1	0
PADI2	1	1	0
PALD1	1	1	0
PASD1	1	1	0
PAXBP1	1	1	0
PCDH12	1	1	0
PCDHGB4	1	1	0
PCLO	1	1	0
PCMTD1	1	1	0
PDZD7	1	1	0
PFKFB2	1	1	0
PGBD4	1	1	0
PKD1L3	1	1	0
PKP2	1	1	0
PLCL1	1	1	0
PLEKHM3	1	1	0
PLXNA2	1	1	0
PLXNA4	1	1	0
PNPLA8	1	1	0
POMZP3	1	1	0
POTEE/POTEF	1	1	0
PPM1E	1	1	0
PRAMEF11	1	1	0
PRAMEF14	1	1	0
PRAMEF4 (includes others)	1	1	0
PRR18	1	1	0
PRX	1	1	0
PTPN13	1	1	0
PVRL2	1	1	0
QRICH2	1	1	0
RASA4	1	1	0
RASA4B	1	1	0
RBM10	1	1	0
RBMXL3	1	1	0

RGPD4 (includes others)	1	1	0
RHPN2	1	1	0
RPL14	1	1	0
RRAGD	1	1	0
RRN3	1	1	0
RSPH6A	1	1	0
RTTN	1	1	0
RXFP1	1	1	0
SERF2	1	1	0
SERINC2	1	1	0
SH3PXD2A	1	1	0
SKIDA1	1	1	0
SMTNL2	1	1	0
SORCS3	1	1	0
SPATA31A6 (includes others)	1	1	0
SPHKAP	1	1	0
SPIRE2	1	1	0
SSC5D	1	1	0
SSUH2	1	1	0
SUPT20H	1	1	0
SYNRG	1	1	0
TBC1D8B	1	1	0
TBP	1	1	0
TDRD6	1	1	0
TDRP	1	1	0
TET2	1	1	0
TIGD1	1	1	0
TMEM109	1	1	0
TMEM163	1	1	0
TMEM229A	1	1	0
TMEM52	1	1	0
TMTC2	1	1	0
TNRC18	1	1	0
TPSAB1/TPSB2	1	1	0
TRIOBP	1	1	0
TSC22D1	1	1	0
TSPYL1	1	1	0
TTC34	1	1	0
UBXN11	1	1	0
UBXN2B	1	1	0
UNC93B1	1	1	0
UQCR10	1	1	0
UTF1	1	1	0

VCX2 (includes others)	1	1	0
VPS13A	1	1	0
VPS45	1	1	0
VWDE	1	1	0
WASH1	1	1	0
WASL	1	1	0
WDHD1	1	1	0
WNK1	1	1	0
YTHDC1	1	1	0
ZBED6	1	1	0
ZBTB33	1	1	0
ZBTB47	1	1	0
ZC3H10	1	1	0
ZDHHC16	1	1	0
ZFHX4	1	1	0
ZMAT5	1	1	0
ZNF598	1	1	0
ZNF705G	1	1	0
ZNF792	1	1	0

Appendix V. Strict Search

Table 18 Strict Search

Name	#Variants	#Cases	#Controls
NBPF10 (includes others)	4	1	0
MUC2	3	1	0
ANKRD36	2	1	0
ARID1B	2	1	0
ATXN1	2	1	0
CHD3	2	1	0
CKAP4	2	1	0
COL18A1	2	1	0
FAM157A/FAM157B	2	1	0
IRF2BPL	2	1	0
LOR	2	1	0
MUC5B	2	1	0
MUC6	2	1	0
REC8	2	1	0
SOCS7	2	1	0
ACSM2A	1	1	0
ALMS1	1	1	0
ANKLE1	1	1	0
APOB	1	1	0
ARHGEF17	1	1	0
ATAD5	1	1	0
ATXN3	1	1	0
BAIAP2L2	1	1	0
BET1L	1	1	0
C19orf33	1	1	0
C20orf96	1	1	0
C5orf60	1	1	0
C6orf132	1	1	0
CACNA1I	1	1	0
CACNB2	1	1	0
CAMKK2	1	1	0
CCDC144NL	1	1	0
CCER2	1	1	0
CD3EAP	1	1	0
CDC27	1	1	0
CDC42EP1	1	1	0
CELA1	1	1	0
CLSPN	1	1	0

CNTNAP3B	1	1	0
CPXM2	1	1	0
DCHS2	1	1	0
DEFB126	1	1	0
DNHD1	1	1	0
DOK3	1	1	0
DSE	1	1	0
E2F4	1	1	0
ERCC1	1	1	0
FAM155B	1	1	0
FAM58A	1	1	0
FAM86B1	1	1	0
FBN1	1	1	0
FCGBP	1	1	0
FHOD3	1	1	0
FOXN3	1	1	0
FOXO3	1	1	0
GIGYF2	1	1	0
GJC2	1	1	0
GPRIN2	1	1	0
GRIN2C	1	1	0
GSPT1	1	1	0
GXYLT1	1	1	0
HEG1	1	1	0
HELQ	1	1	0
HRC	1	1	0
HTT	1	1	0
IFI27	1	1	0
IGFBP2	1	1	0
IGFN1	1	1	0
IGSF10	1	1	0
IST1	1	1	0
KCNN3	1	1	0
KIAA1549	1	1	0
KIZ	1	1	0
KLHL40	1	1	0
KLRC2	1	1	0
KRT3	1	1	0
KRTAP4-6	1	1	0
KRTAP9-6	1	1	0
LENG9	1	1	0
LFNG	1	1	0
LMTK3	1	1	0
LOC729159	1	1	0

LRP8	1	1	0
LRRIQ1	1	1	0
LSR	1	1	0
LURAP1L	1	1	0
MAN2A1	1	1	0
MAPK8IP2	1	1	0
MED15	1	1	0
MEGF9	1	1	0
MEOX2	1	1	0
mir-3150	1	1	0
mir-663	1	1	0
MIR3131	1	1	0
MMP12	1	1	0
MMP17	1	1	0
MOGAT1	1	1	0
MPL	1	1	0
MST1L	1	1	0
MUC12	1	1	0
MUC16	1	1	0
MUC3A	1	1	0
NADK	1	1	0
NAP1L2	1	1	0
NCOR2	1	1	0
NKD2	1	1	0
NOTCH2	1	1	0
NOTCH4	1	1	0
OR13C5	1	1	0
OR2B11	1	1	0
OR2T27	1	1	0
OR2T33	1	1	0
OR4C3	1	1	0
OTUD4	1	1	0
PAXBP1	1	1	0
PCDH12	1	1	0
PCDHGB4	1	1	0
PCLO	1	1	0
PDZD7	1	1	0
PKD1L3	1	1	0
POTEG (includes others)	1	1	0
PPM1E	1	1	0
PRSS48	1	1	0
PRX	1	1	0
QRICH2	1	1	0
RASA4	1	1	0

RASA4B	1	1	0
RBM10	1	1	0
RBMXL3	1	1	0
RHPN2	1	1	0
RIC8A	1	1	0
RPL14	1	1	0
RRAGD	1	1	0
RRN3	1	1	0
RTTN	1	1	0
RXFP1	1	1	0
SART3	1	1	0
SEMA3B	1	1	0
SERINC2	1	1	0
SGK223	1	1	0
SLC35G4	1	1	0
SNRPF	1	1	0
SSC5D	1	1	0
SSUH2	1	1	0
SYNRG	1	1	0
TBP	1	1	0
TCHH	1	1	0
TDRD6	1	1	0
TDRP	1	1	0
TMEM229A	1	1	0
TNRC18	1	1	0
TRIOBP	1	1	0
TSC22D1	1	1	0
TSPYL1	1	1	0
TTC34	1	1	0
TTN	1	1	0
UBXN11	1	1	0
USP37	1	1	0
UTF1	1	1	0
VPS13A	1	1	0
VPS45	1	1	0
WASL	1	1	0
YIF1B	1	1	0
YTHDC1	1	1	0
YY1	1	1	0
ZBTB33	1	1	0
ZBTB40	1	1	0
ZFHX4	1	1	0
ZNF705G	1	1	0
ZNF792	1	1	0